University of Strathclyde

Department of Electronic and Electrical Engineering

Control Design and Stability Assessment of VSC-HVDC networks for Large-Scale Offshore Wind Integration

Giddani Osman Addalan Kalcon

BTech, MSc

A thesis presented in fulfilment of the requirement for the degree of Doctor of Philosophy

September 2011

The copyright of this thesis belongs to the author under terms of United Kingdom copyright acts as qualified by University of Strathclyde Regulation 3.51. Due acknowledgement must always be made of the use of any material in, or, derived form of this thesis.

Acknowledgements

First of all, I would like to express all my thanks to Allah for his great help in completing this thesis.

I would also like to express my sincerest thanks to my supervisors Dr. Olimpo Anaya-Lara and Prof. K. L. Lo for accepting me as a PhD student. I would like to give my special thanks to Dr. Olimpo Anaya-Lara for his useful guidance, patience, keen interest and efforts at every time.

Also, I would like to thank Dr. Grain P. Adam for his technical and moral support during my PhD studies.

Finally, I express my deep thanks to my family for their prayers and support.

Dedication

To my family, my wife (Rehab) and daughter (Nazik)

Table of Contents

		Page No.
	Copyright	II
	Acknowledgment	III
	Dedication	IV
	Table of Contents	V
	Abstract	XI
	List of symbols and Abbreviations	XII
	Chapter One: Introduction	
1-1	Background	1
1-2	Voltage source converter HVDC systems	2
1-3	Wind power in power systems	2
1-4	Research Motivation	3
1-5	Objectives and Scope of the research	4
1-6	Thesis Contributions	5
1-7	Thesis organization	6
1-8	Publication	7
	Chapter Two: High-voltage direct current transmission system base on Current source converter (CSC-HVDC) systems	
2-1	Introduction	11
2-2	CSC-HVDC transmission systems	13
2-3	HVDC Transmission System Configurations	15
2-4	CSC Converter configurations	17
	2-4-1 Line-commutated converter	17
	2-4-2 Capacitor-commutated converter	17
2-5	Line-commutated converter operation	18
	2-5-1 Rectifier operation without commutation angle	19
	2-5-2 Rectifier operation with commutation angle	20
	2-5-3 Inverter operation	22
2-6	Commutation failure	24
2-7	The ac and dc harmonics	25
2-8	Line-commutated converter-HVDC system Control	29

2-9 Control system design 31
2-10 Steady-state and transient behaviour of LCC- HVDC systems 32
2-10-1 System behavior during a step in active Power 33
2-10-2 System behavior during DC fault 35
2-10-3 System behavior during a three-phase fault at the inverter side 36
2-11 The environmental effect and the limitation of HVDC systems 38
2-12 Summary 39

Chapter Three: High-voltage direct current transmission systems based on Voltage Source Converter (VSC-HVDC)

3-1 Introduction 43
3-2 Principle of Voltage Source Converter Operation 44
3-3 Components of VSC-HVDC 46
3-4 VSC-HVDC steady-state model 48
3-5 The two-level voltage source converter 51
3-6 The three-level voltage source converter 54
3-7 Voltage source converter conversion losses 57
3-7-1 The Conduction losses 58
3-7-2 Switching losses estimation 59
3-8 VSC-HVDC Transmission System Dynamic Model 59
3-9 Control of the VSC-HVDC 62
3-9-1 The inner controller design 63
3-9-2 The outer controller design 65
3-10 Steady-state and transient behavior of the three-level VSC-HVDC 66
system 68
3-10-1 Case I: Active power step and provision of reactive power 70
3-10-2 System behaviour during three-phase ac fault at the receiving end 71
3-10-3 System behaviour during a dc fault at the midpoint of the dc link
3-11 Application of VSC-HVDC systems 72
3-12 Summary 73

Chapter Four: Multi-terminal high-voltage dc transmission systems based on voltage source converter

4-1 Introduction 77
4-2 Configurations of multi-terminal dc transmission systems 78

4-2-1 Multi-terminal VSC-HVDC systems for wind farm integration 79
4-2-2 Multi-terminal VSC-HVDC for transnational dc network (SuperGrid) 79
4-2-3 Multi-terminal VSC-HVDC systems for distribution networks in urban areas 80
4-2-4 Multi-terminal VSC-HVDC systems for oil and gas platforms 81
4-3 Power Management of multi-terminal dc transmission systems 82
4-4 MTDC system behavior during a sudden loss of converter/dc link cable 86
4-5 Multi-terminal VSC-HVDC for creation of a regional dc network (SuperGrid) 88
4-6 VSC-HVDC network for regional dc network and renewable energy integration 91
4-6-1 The dc network control strategy 92
4-6-2 System protection 93
4-6-3 Multi-terminal VSC-HVDC network power trading 95
4-6-4 Multi-terminal dc system performance during loss of a converter station 97
4-7 Summary 99

Chapter Five: High voltage dc transmission system based on voltage source converter (VSC-HVDC) for offshore wind farms integration

5-1 Introduction 103
5-2 Requirements for wind farm integration 105
5-2-1 Voltage and reactive power control 105
5-2-2 Fault ride-through capability 106
5-2-3 Frequency control 107
5-3 Offshore Wind Farms integration options 108
5-3-1 High-voltage alternating-current transmission (HVAC) 108
5-3-2 CSC-HVDC transmission system 109
5-3-3 VSC-HVDC transmission system for offshore wind farms integration 111
5-4 Control system strategies for VSC-HVDC system integrating FSIG wind farms 112
5-5 VSC-HVDC system integrating FSIG wind farm without power 112

command
5-6 Performance evaluation of VSC-HVDC connecting an FSIG wind farm operating without power command 114
5-6-1 Scenario I: System performance during wind speed variations 116
5-6-2 System performance during a solid three-phase fault at the grid side 119
5-7 VSC-HVDC system integrating FSIG wind farm with power command 120
5.7.1 Control system design of FSIG wind farm and VSC-HVDC system 121
5-7-2 FSIG and VSC-HVDC response during power demand change 125
5-7-3 System performance during solid three-phase fault at the grid side 126
5-8 Features of FSIG and VSC-HVDC system 127
5-9 Multi-terminal VSC-HVDC System for FSIG wind Farm Integration 128
5-10 VSC-HVDC system for integration of other wind farm technologies 130
5-11 Summary 134
Chapter Six: Small-signal stability of multi-terminal VSC-HVDC connecting wind farms
6-1 Introduction 139
6-2 State-space model of multi-terminal VSC-HVDC connecting wind farms 141
6-3 Grid-side VSC Converter Model 142
6-4 Synchronous Generator, AVR, and governor-turbine models 145
6-5 Onshore network model 146
6-6 DC link circuit model 147
6-7 Wind farm-side VSC Converter Model 148
6-8 Wind farm state-space model 151
6-9 The complete state-space model of interconnected ac/dc system 153
6-10 The initial values of the interconnected ac/dc system 154
6-11 Small-signal stability analysis of the dc/ac interconnected system 155
6-12 Impact of grid-side VSC current controllers on system stability 156
6-13 Impact of grid-side VSC converter ac voltage controllers on system stability 158
6-14 Impact of the grid-side VSC dc voltage controllers on system stability 160

6-15	The effect of synchronous machine rating on system stability	162
6-16	Summary	163
	Chapter Seven: Network Reinforcement of 400kV the Scottish-English Interconnectors using VSC-HVDC Transmission systems	
7-1	Introduction	166
7-2	Scotland-England interconnectors	168
7-3	Using FACTS devices for reinforcement of the interconnectors	171
7-4	VSC converter reactive power capability to provide voltage provision	173
7-5	Reinforcement of Scotland-England interconnectors using VSC-HVDC system	174
	7-5-1 Frequency regulation at the Scottish network in decoupling operation	175
	7-5-2 Simulation results to demonstrate ability of VSC-HVDC systems to provide frequency regulation in the Scottish network	177
	7-5-3 Isolating of Scottish network from disturbances in English network	182
7-6	Scotland-England interconnectors reinforcement using parallel HVAC-HVDC links	185
7-7	Simulation results of using parallel operation	189
7-8	Summary	192
	Chapter Eight: Conclusions and Recommendations	
8-1	General conclusions	196
8-2	Research Finding	199
8-3	Suggestions for future research	200
	Appendix A: Fourier analysis of a LCC converter ac input current	
A-1	Harmonic analysis of a 6-pulse converter with star/star transformer	201
A-2	Harmonic analysis of a 6-pulse converter with star/delta transformer	202
A-3	Harmonic analysis of a 12-pulse converter	202
	Appendix B: Pulse Width Modulation (PWM)	
B-1	Sinusoidal PWM Modulation	204
B-2	Third harmonic injection and Switching Frequency Optimal PWM techniques	206
B-3	Multi-level carrier-based PWM	207

Appendix C: Analytical method for calculation the VSC converter conversion losses

C-1 Analytical method to calculate conversion losses in two-level converters 209

C-2 Analytical method to calculate conversion losses in three-level converters 210

Appendix D: Fixed Speed Wind Turbine Model

D-1 Wind Turbine Aerodynamic System 213

D-2 Mechanical System 214

D-3 Squirrel cage induction generator 215

Appendix E: Participation factor matrix 217

Appendix F: List of Figures and Tables

F-1 List of Figures 219

F-2 List of Tables 223

Abstract

This thesis investigates the use of voltage source converter high-voltage direct current (VSC-HVDC) transmission systems for large-scale integration of offshore wind farms into the Scottish power network, and reinforcement or replacement of the existing high-voltage ac links between Scotland and England to increase transmission capacity, without affecting the power and voltage stability of both networks. To achieve these objectives, several multi-tasking controllers for VSC-HVDC transmission that use neutral-point clamped converter are developed as a platform in Simulink, and used throughout the research work presented in the thesis. The main controllers implemented in this thesis are, active power, dc voltage, ac current in synchronous reference frame, ac voltage and frequency control.

Regarding the use of VSC-HVDC for offshore wind farm integration, two control approaches for the offshore-side converter were investigated. In the first approach, the wind farm-side converter injects all the wind power into the dc side without assigning a direct power command and establishes a stiff ac bus at the wind farm network main hub (bus). In the second approach, the wind farm-side converter uses an assigned power command to inject the wind power into the dc side while the wind turbines use their pitch control to regulate active power production so as to guarantee power balance between the offshore ac network and the dc side. The advantages and shortcomings of both approaches are highlighted and their influence on network stability assessed. Two possible HVDC configurations were investigated to accommodate future offshore wind power into Scottish networks without significantly compromising the overall system stability and reliability, paying special attention to Grid Code compliance. The two configurations investigated are two independent point-to-point HVDC networks and a multi-terminal HVDC network. The viability of the both configurations is evaluated in steady-state and transient conditions. This evaluation includes flexibility of power dispatch, provision of ancillary services to Scottish networks and potential improvement in system stability. For completeness of the work, the small-signal stability of the multi-terminal HVDC network configuration when used to connect offshore wind farms was explored using eigenvalue Techniques.

This thesis also investigated two possible connection scenarios to increase the transmission capacity of the links between England and Scotland, by reinforcing the existing HVAC links with parallel HVDC links (hybrid connection), or replacement of the current HVAC links by two independent point-to-point HVDC links. The benefits and drawbacks of both connection scenarios are highlighted. These include the benefits to frequency control in the Scottish network in the event o severe disturbance in the English network. The impact of both connection scenarios on the network stability were assessed during steady-state and transient conditions.

List of symbols and abbreviations

List of symbols

A	state matrix
B	Input matrix
f	System Frequency
f^*	Frequency reference of the frequency controller
$f(\omega t)$	Fourier analysis series
H_c	Effective dc inertia constant
i_{av}	Mean average current
i_{rms}	Root mean square current
i_{sd}, i_{sq}	Direct and quadrature axis currents at converter ac side
I_{dc}	dc link current
i_{dw}	Direct axis current at wind side converter
i_{qw}	quadrature axis current at wind side converter
i^*_{sd}	Direct current axis reference point of the current controller
i^*_{sq}	Quadrature axis current reference point of the current controller
i^*_{dw}	Direct axis voltage reference point of the current controller of wind side converter
i^*_{qw}	Quadrature axis voltage reference point of the current controller of wind side converter
i^*_{core}	The correction signal
k_{pi}, k_{ii}	Proportional and integral gain of the current controller
k_{pac}, k_{iac}	Proportional and integral gain of the ac voltage controller
k_{dcp}, k_{dci}	Proportional and integral gain of the dc voltage controller
k_{fp}, k_{fi}	Proportional and integral gain of the frequency controller
i^*_{core}	The correction signal
P_{sw}	Switching losses in converter
P_{dc}	dc link power
P	ac side power
P_C	Conduction losses in converter
P^*	Active power reference of the active power controller
Q	ac side reactive power
r_f	Device forward resistance

$v_{ab,}, v_{bc,} v_{ca}$	Line-to-line voltage at converter terminals
$v_{az,} v_{bz,} v_{cz}$	Line-to-natural voltage at converter terminals
$v_{sd,}$ v_{sq}	Direct and quadrature axis voltages at point of common coupling
$v_{cd,}$ v_{cq}	Direct and quadrature axis voltages at converter ac side terminal
v_{dw}	Direct axis voltages at wind side converter
v_{qw}	quadrature axis voltages at wind side converter
V_{ac}	ac voltage
V_{dc}	dc link voltage
V_f	Device forward current
V^*_{ac}	ac voltage reference point of the ac voltage controller
V^*_{dc}	dc voltage reference point of the dc voltage controller
v^*_{dw}	Direct axis voltage reference point of the ac voltage controller of wind side converter
v^*_{qw}	Quadrature axis voltage reference point of the ac voltage controller of wind side converter
λ	Eigenvalue
γ	extinction angle
Δx	state vector
Δu	input vector
β	Turbine blade angle
ΔP_{dc}	the change on the dc transmitted power
ΔP_L	the load change
ω_{TUR}	Turbine rotor speed
τ	Time constant

List of abbreviations

AVR	Automatic voltage regulator
CC	Constant current control
CO_2	Carbon dioxide
CIA	Constant-ignition angle control
CSC	Current source converter
CSC-HVDC	HVDC base on current source converter

DFIG	Doubly-fed induction generator
ESCR	Effective Short-Circuit Ratio
FACTS	Flexible ac transmission devices
FSIG	Fixed-speed induction generator
FRT	Fault Ride-Through capability
FWD	Forward wheeling diode
GB	Great Britain
HVAC	High voltage alternative current
HVDC	High voltage direct current
IEEE	Institute of Electrical and Electronics Engineers
IGBT	Insulated gate bipolar transistor
LCC	Line commutated converter
MTDC	Multi-terminal dc system
NGET	National Grid Electricity Transmission
PCC	Point of common coupling
PMSG	Permanent magnetic synchronous generator
PWM	Pulse width modulation
SCR	Short-Circuit Ratio
SFO-PWM	Switching Frequency Optimal pulse width modulation
SG	Synchronous generator
SHETL	Scottish Hydro Electric Transmission Ltd
SPT	Scottish Power Transmission
SSSC	Static synchronous series compensator
STATCOM	static synchronous compensator
SVC	Static voltage compensator
TCSC	thyristor-controlled series compensation
THD	Total harmonic distortion
TL	Transmission line
TSSC	thyristor-switched series compensation
UPFC	Unified power flow controller
VSC	Voltage source converter
VSC-HVDC	HVDC base on voltage source converter
XLPE	Cross linked polyethylene insulated power cable

Chapter One

Introduction

1-1 Background

Nowadays, alternating current (ac) systems are dominant in electrical power networks regarding generation, transmission and distribution of the electricity supply. Due to the rapid increase in electricity demand, the need arises for the interconnection of power networks distributed in different areas to increase supply reliability, and to facilitate power exchange between areas. The interconnection of separated networks results in a large power system expanding hundreds and even thousands of kilometres. In this large power system, high-voltage alternating current lines (HVAC) are used to accommodate the power over long distances between the different networks. HVAC lines have proven to be effective in transmission and distribution of electrical power but this creates challenges for power system operators such as the following [1]:

- In systems based on HVAC the automatic generation control of the individual units is coordinated using power and frequency signals in the tie-lines. The problem with coordinated control is the presence of large frequency oscillations, which may lead to frequent tripping, fault level increase, and disturbance propagation from one network to another.
- Long-distance transmission requires special arrangements to keep the voltage at rated value, whilst reducing transmission losses. Reactive power devices are used to overcome voltage stability problems and the distance limitation of transmission lines.
- Non-synchronized grids operation is not possible.
- Offshore wind farms integration: the high capacitance of ac submarine cables causes a large charging current, which reduces the power transfer capacity of the cable, increases power losses, and hence limits the transmission distance of the cable [2].

High-voltage direct current (HVDC) transmission has been extensively researched over the last six decades as an alternative to conventional HVAC transmission systems. The main component of an HVDC system is the conversion station which converts from ac to dc and vice versa. HVDC systems address most of the challenges associated with HVAC facilitating power transmission over long distances, prevention of disturbance propagation, connection of non-synchronized grids, and long submarine cable transmission [3-4]. The first generation of

HVDC converters is based on current-commutated converters with naturally-commutated thyristors (CSC-HVDC). The thyristors need an active ac voltage source to commutate, therefore CSC-HVDC systems transfer the power between two active systems. CSC-HVDC cannot be used to connect offshore wind farms without the aid of start-up generators or synchronous compensators. Also, given that the converter operates only with lagging power factor, reactive power compensation is required at the converter stations.

HVDC systems based on voltage source converter (VSC-HVDC) are the latest development in dc transmission, manufactured by ABB with the name of HVDC-light and by Siemens under the name of HVDC-plus. This technology becomes possible thanks to the development in IGBT devices which can switch ON/OFF the current. VSC-HVDC systems can address the challenges associated with both HVAC and CSC-HVDC systems.

1-2 Voltage source converter HVDC systems

VSC-HVDC operation is based on self-commutated devices which can turn ON/OFF the current, i.e. there is no need for a commutation voltage source at neither of the inter-connected ac networks. This development enables VSC-HVDC systems to operate with *dead* networks (with no generation), islanded networks, industrial remote areas and wind farms [4-5]. Also, VSC-HVDC systems can operate with lagging or leading power factor, that is, they can provide reactive power support to the ac system during steady-state, transient and dynamic conditions. The incorporation of vector control and pulse-width modulation in VSC-HVDC systems facilitates the independent control of active and reactive power flows.

Features of HVDC transmission such as fast response, precise power flow control, and reactive power capability make of VSC-HVDC transmission a suitable solution for many applications and concepts, which previously have not been considered due to technical and economical limitations. These applications include transmission of bulk power over long distances, multi-terminal operation, wind farm integration, transnational super-grid development, and reinforcement of transmission lines [3, 6].

1-3 Wind power in power systems

The recent increase of wind power penetration in electrical power systems is due to the intention of governments to mitigate the negative environmental impacts of conventional electrical power plants. In the past, wind farms were small-size installations connected to the distribution level of electrical networks, with a small overall contribution to the total generation capacity [7]. They were treated as small embedded generators of negligible

importance from a power system point of view, and were not required to contribute to voltage and frequency regulation. Also, their installation requirements were very few, and disconnection of the wind farm from the grid in the events of disturbances was a common practice. However, due to the massive increase in installed wind generation capacity, and bearing in mind the unpredictable nature of the wind resource, wind farms are nowadays treated as independent power plants with similar impact on power system operation as that of conventional synchronous generation. New wind turbine technologies and different wind farm connection scenarios are being developed to cope with new requirements issued by power companies for large-scale wind power integration (i.e. Grid Codes). The need arises for new connection requirements to mitigate the negative impacts of wind farms on power system stability due to the wind variability. At present, one of the main concerns is the power balancing in the system during wind power variations, which affects frequency stability. Power electronics devices installed within the wind farms or in the system may assist conventional plant to achieve the power levelling in the network.

Since large-scale wind farms are usually installed in remote locations, enhancement of transmission lines is necessary to enable the connection of additional wind power and its transfer to major load centres. This can be done either by building new lines or reinforcing the existing ones.

1-4 Research Motivation

With the increased penetration in recent years of wind power into the GB system and other European power networks, several technical and operational challenges have emerged. Some of these challenges are related to power and voltage stability, provision of ancillary services, and power dispatch. Other challenges associated with connection of far-located offshore wind farms using HVAC are increased losses (due to the ac cable charging current), need for expensive reactive power compensation devices, fault ride-through capabilities issues, and Grid Code compliance. Also, variation of power generation due to wind intermittency represents a major challenge regarding the power balance in the network. High-response technologies may be required to address this challenge.

Grid integration of large-scale offshore wind farms using voltage source converter HVDC links may address the shortcomings of synchronous connections and provide additional functionalities to offshore and mainland ac networks [10-11]. These functionalities include black-start capability of the offshore network, provision of voltage support at both networks, decoupling of wind farm dynamics from the onshore grid in the event of disturbances, and

limited frequency support to the onshore ac grid. However, the vulnerability of HVDC transmission to dc-side faults limits at present its applications to point-to-point connections.
In the context of the GB network, the expected installation of large-scale offshore wind farms in Scotland may require significant expansion of the existing network in order to accommodate and transmit the additional power to load centres in England [12]. This may necessitate reinforcement of the existing links between Scotland and England to increase their transmission capacity and power flow controllability. At the present, there are many options proposed for reinforcement of these links, including ac reinforcement using a combination of new ac lines and FACTS devices, conversion of the existing HVAC links into HVDC links, or installation of new HVDC links in parallel with the existing HVAC links (Hybrid connection) [12-13].
The use of HVDC links instead of HVAC may facilitate decoupling the Scottish network from the English one. This may improve the resilience of the Scottish network to large ac disturbances in the English power system, increase transmission capacity, enable provision of voltage support to both power networks, facilitate precise power flow control, and provide frequency support in the Scottish network.
From the above discussion, the main motivation of this thesis is then to explore the potential benefits that may be achieved by using VSC-HVDC point-to-point and multi-terminal networks for integration of large-scale wind farms into the Scottish power system, and to assess the applicability of VSC-HVDC transmission to reinforce the interconnectors between Scotland and England. In addition to assessing the benefits, the influence on steady-state and transient stability are also investigated. The ability of VSC-HVDC systems to cope with network disturbances in interconnected systems is among the questions this thesis attempts to answer.

1-5 Objectives and Scope of the Research

This thesis investigates the use of voltage source converter HVDC as an enabling technology for large-scale integration of future large-scale offshore wind power plants into the Scottish power network. The potential applicability of VSC-HVDC transmission for reinforcement of the existing transmission links between Scotland and England networks is also investigated. An assessment is conducted on how such reinforcement may increase the transmission capacity without affecting power and voltage stability of both networks. In order to achieve these objectives the following tasks are carried out:

- ❖ Suitable controllers for VSC-HVDC systems are developed and validated. This includes basic controllers such active power, dc link voltage and ac voltage. In some cases, additional controllers such as frequency control are incorporated in the active power loop. These controllers are usable with both point-to-point and multi-terminal HVDC networks. Power management in the HVDC network is achieved using active power/dc voltage droop control when the wind farms are integrated to the grid without a direct power command.

- ❖ In this thesis, two approaches are used to control the wind farm-side voltage source converters. In the first approach, the wind farm-side converter is controlled to establish a stiff ac bus for the wind farm and to ensure injection of all the wind power generated into the dc side without a direct power command. In the second approach, the wind farm-side converters and wind turbines generators are controlled in order to inject the approximate assigned power command given to the converters.

- ❖ The impact of large-scale integration of offshore wind farms using VSC-HVDC on the operation of the Scottish network is assessed using small-signal and transient stability analyses. In both studies, all the necessary controllers are incorporated during the modelling and simulation process.

- ❖ The benefits of using VSC-HVDC transmission for reinforcement of the Scottish-English interconnectors are assessed regarding steady-state and transient stability, provision of voltage and frequency support and increased transmission capacity in the existing power corridors.

- ❖ The technical and economical feasibility of decoupling the Scottish and English networks by means of VSC-HVDC transmission are comprehensively explored and discussed.

1-6 Thesis Contributions

Since the main objective of the thesis is to investigate the potential use of VSC-HVDC transmission for large-scale integration of wind generation into the Scottish network and reinforcement of the existing transmission links between Scotland and England, the following points highlight the main contributions of this thesis:

- ➢ Implementation of multi-task control for the VSC-HVDC systems, which facilitate the power management, frequency regulation and provision of independent voltage/reactive power control at the point of common coupling.

- Implementation of control strategies for the dc transnational grid that may facilitate effective power dispatch and trading between interdependent ac networks, including frequency support.
- Implementation of a frequency controller that may enable the offshore/onshore wind farms to provide support to the short- and long-term frequency regulation and power levelling in the onshore grid.
- Development of a state-space model that facilitate the investigation of the small-signal stability of a multi-terminal VSC-HVDC network connected to offshore wind farms and conventional ac systems. In this approach all basic converter stations and conventional synchronous plants controllers were incorporated.
- Investigation of the reinforcement of the existing Scottish-English interconnectors using two different scenarios namely, two point-to-point VSC-HVDC systems, and two hybrid links (VSC-HVDC in parallel with HVAC link). An assessment of the potential benefits that the decoupling of the Scottish network from the English one by means of VSC-HVDC transmission is also included.

1-7 Thesis organization

The thesis is organized to cover the research objectives discussed earlier. The thesis includes eight chapters summarized as follows:

- Chapter one gives a brief introduction to the thesis and highlights the objectives of the research.
- Chapter two focuses on HVDC systems based on current source converters. Simulation and theoretical analyses are carried out to determine the limitations and shortenings of CSC-HVDC systems.
- In Chapter three, the steady-state and dynamic models of the VSC-HVDC are presented. Based on these models, multi-task control systems are designed for the converters in order to achieve the VSC-HVDC purposes. The transient stability of the VSC-HVDC is investigated during major load changes to assess the robustness of the system. The assessment is conducted during power step changes, three-phase faults and faults in the dc link.
- Chapter four concentrates on the multi-terminal operation of the VSC-HVDC systems. The multi-terminal dc system is an attractive solution to increase system controllability and supply reliability. In this Chapter, a multi-terminal dc system is presented to create a

transnational super grid to maximize wind power utilization and to accommodate the power between the national grids.

- Chapter five highlights the use of VSC-HVDC systems for large-scale offshore wind integration and its benefits. The control system of the wind farm-side converter is designed considering two scenarios: the first is to transmit the wind power without assigning a power command, and the second is to transmit the wind power with a power command. The VSC-HVDC ability to meet the Grid Code requirements and the operational functionality for both scenarios are investigated.
- In Chapter six, the small-signal stability of multi-terminal dc systems integrating offshore wind farms is studied. The effect of the grid-side converter on system stability is assessed so as to choose the converters control parameters that ensure network stability in the event of both small and large perturbations.
- Chapter seven focuses on the use of VSC-HVDC transmission in the reinforcement of the interconnectors between the Scottish and English networks. Two scenarios are investigated to increase controllability and capacity of these interconnectors either by conversion of the HVAC links to VSC-HVDC or by the parallel operation of the existing HVAC with additional VSC-HVDC links.
- Chapter eight presents the conclusions of the thesis and discusses some suggestions for future work.

1-8 Publications

The following publications were produced during the development of the research presented in this thesis:

1- **O. A. Giddani**, G. P. Adam, O. Anaya-Lara, K. L. Lo, "Grid integration of a large offshore wind farm using VSC-HVDC in parallel with an AC submarine cable," in *Universities Power Engineering Conference (UPEC), 2009 Proceedings of the 44th Iternational*, 03/09/2009, Glasgow, UK.

2- **O. A. Giddani,** G. P. Adam, O. Anaya-Lara, K. L. Lo, "Efficiency evaluation of a DC transmission system based on voltage source converters," in *Power Electronics, Machines and Drives (PEMD 2010), 5th IET International Conference on*, 20/05/2010, Brighton, UK.

3- **O. A. Giddani,** G. P. Adam, O. Anaya-Lara, K. L. Lo "Grid integration of offshore wind farms using multi-terminal DC transmission systems (MTDC)," in *Power Electronics, Machines and Drives (PEMD 2010), 5th IET International Conference on*, 20/05/2010, Brighton, UK.

4- **O. A. Giddani,** G. P. Adam, O. Anaya-Lara, G. Burt and K. L. Lo, "Control strategies of VSC-HVDC transmission system for wind power integration to meet GB grid code requirements," in *Power Electronics Electrical Drives Automation and Motion (SPEEDAM), 2010 International Symposium on*, 21/6/2010, Pisa, Italy.

5- **O. A. Giddani**, G. P. Adam, O. Anaya-Lara, G. Burt and K. L. Lo, "Enhanced performance of FSIG wind farms for grid code compliance," in *Power Electronics Electrical Drives Automation and Motion (SPEEDAM), 2010 International Symposium on*, 21/06/2010, Pisa, Italy.

6- **O. A. Giddani**, G. P. Adam, O. Anaya-Lara, G. Burt and K. L. Lo, "Potential benefits of decoupling the Scotland-England network using VSC-HVDC," in *AC and DC Power Transmission, 2010. ACDC. 9th IET International Conference on*, 20/10/2010, London, UK.

7- **O. A. Giddani,** G. P. Adam, O. Anaya-Lara, G. Burt and K. L. Lo ,HVDC Network: Wind Power Integration and Creation of Super Grid," *10th International Conference on Environment and Electrical Engineering 2011, 8-11 May, 2011,* Rome, Italy.

8- **O. A. Kalcon,** G. P. Adam, O. Anaya-Lara and G. Burt, "Frequency Stability of Future Power Systems with High Penetration of Renewable Power and Distributed Storage systems," CIGRE Conference on Power Systems, Halifax, Canada, September 2011.

9- G. P. Adam, **O. A. Kalcon,** S. J. Finney, D. Holliday, O. Anaya-lara and B.W. Williams, "HVDC Network: dc fault ride-through improvement," CIGRE Conference on Power Systems, Halifax, Canada, September 2011.

10- **O. A. Kalcon**, G. P. Adam, O. Anaya-Lara, G. Burt, K. L. Lo, "Analytical Efficiency Evaluation of Two and Three level VSC-HVDC Transmission System," submitted to International Journal of Electrical Power & Energy Systems, under review.

11- **O. A. Kalcon**, G. P. Adam, O. Anaya-Lara, K. L. Lo, and K. Uhlen, "Small-Signal Stability Analysis of Multi-terminal VSC-based DC Transmission Systems," Submitted to the IEEE Transactions on Power Systems. First submission accepted with modifications, second resubmission currenlty under review.

12- G. P. Adam, **O. A. Kalcon**, O. Anaya-Lara, and S. J. Finney, "Static Synchronous Compensator based on the Three-level H-Bridge Voltage Source Converter (3L-HB-VSC)" submitted to International Journal of Electrical Power & Energy Systems, under review.

13- **O. A. Giddani**, Grain P. Adam, Olimpo Anaya-Lara" Multi-task Control for VSC-HVDC Power Management and Frequency Control" submitted to International Journal of Electrical Power & Energy Systems, under review

References

[1] K. R. Padiyar, *HVDC power transmission systems: technology and system interactions*. New Delhi: New Age International (P) Limited, Publishers, 2005.

[2] O. A. Giddani, *et al.*, "Grid integration of a large offshore wind farm using VSC-HVDC in parallel with an AC submarine cable," in *Universities Power Engineering Conference (UPEC), 2009 Proceedings of the 44th International*, 2009, pp. 1-5.

[3] N. Flourentzou, *et al.*, "VSC-Based HVDC Power Transmission Systems: An Overview," *IEEE Trans on Power Electronics,*, vol. 24, pp. 592-602, 2009.

[4] M. P. Bahrman and B. K. Johnson, "The ABCs of HVDC transmission technologies," *Power and Energy Magazine, IEEE,* vol. 5, pp. 32-44, 2007.

[5] D. Cuiqing, *et al.*, "A New Control Strategy of a VSC-HVDC System for High-Quality Supply of Industrial Plants,," *Power Delivery, IEEE Transactions on,* vol. 22, pp. 2386-2394, 2007.

[6] S. Cole and R. Belmans, "Transmission of bulk power," *Industrial Electronics Magazine, IEEE,* vol. 3, pp. 19-24, 2009.

[7] I. M. Alegri, *et al.*, "Connection requirements for wind farms: A survey on technical requirements and regulation," *Renewable and Sustainable Energy Reviews Volume 11, Issue 8, October 2007, Pages 1858-1872.*

[8] S. Chondrogiannis, *et al.*, "Modelling and GB Grid Code Compliance Studies of Offshore Wind Farms with Doubly-Fed Induction Generators," in *Power Electronics, Machines and Drives, 2006. The 3rd IET International Conference on*, 2006, pp. 22-26.

[9] K. Moslehi and R. Kumar, "Smart Grid - a reliability perspective," in *Innovative Smart Grid Technologies (ISGT), 2010*, 2010, pp. 1-8.

[10] P. Bresesti, *et al.*, "HVDC Connection of Offshore Wind Farms to the Transmission System," *Energy Conversion, IEEE Transactions on,* vol. 22, pp. 37-43, 2007.

[11] O. A. Giddani, *et al.*, "Control strategies of VSC-HVDC transmission system for wind power integration to meet GB grid code requirements," in *Power Electronics Electrical Drives Automation and Motion (SPEEDAM), 2010 International Symposium on*, 2010, pp. 385-390.

[12] "OUR ELECTRICITY TRANSMISSION NETWORK: A VISION FOR 2020," *A Report by the Electricity Networks Strategy Group, avialable at webarchive.nationalarchives.gov.uk/...uk/.../1696-01-ensg_vision2020.pdf, March 2009*.

[13] C. Bayfield, *et al.*, "Planning for the integration of on-shore renewable generation for the GB transmission system," *CIGRÉ 2006 Session in Paris, avialable at http://www.labplan.ufsc.br/congressos/cigre06/DATA/C1_114.PDF*.

Chapter Two

High-voltage direct current transmission system base on Current source converter (CSC-HVDC) systems

2-1 Introduction

The rapid and continuous growth of electrical power consumption has led to an increase in the generation and transmission facilities to meet the increase in demand. Due to environmental consideration or availability of energy resources, most electrical power plants are placed in remote locations, some times hundreds of kilometers from the load centers, so the need is rising for effective transmission lines capable to transmit large amounts of power with higher technical benefits, at reasonable economic cost.

High-Voltage Alternating Current transmission systems (HVAC) have proven to be effective in transmission and distribution of electrical energy but there are some performance limitations to HVAC systems in long distance-high power transmission. With the re-evaluation and the development in power electronic semiconductors capable to operate at higher voltages and larger currents, high voltage direct current transmission (HVDC) became possible by using a converter at each end of the line (ac/dc/ac).

The choice between a high voltage ac or dc transmission system is usually made based on economical and technical considerations such as, transmission distance, transmission medium (overhead line or cable), fault levels and purpose of the line [1]. Fig. 2.1 shows the economic related choice between the ac and the dc transmission system. The break-even distance for an overhead line is in the order of 800-1000km, excluding the cost of compensation equipment, while the break-even distance for submarine cables is much shorter, around 50km. As a result, HVDC remains the only feasible solution in cases where the transmission line crosses the sea with a distance of more than 50km [1],[2],[3].

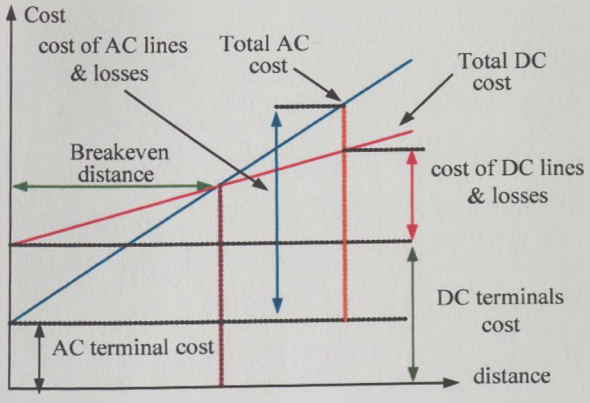


Fig. 2.1: HVAC and HVDC transmission cost versus distance [1]-[4],[5].

The main problems with HVAC transmission when used to transmit bulk power over long distance are [1]-[6],[7]:

- The high stray capacitance of an ac submarine cable (in environments where only underground or submarine cables can be used), causes a large charging current to flow in the cable and this reduces the line load-carrying capability and increases the I^2R losses.
- Due to the high capacitance of the cable, resonances may occur in the system.
- The ac cable transmission system requires complex and expensive reactive power compensation at both ends of the line to avoid voltage problems, and this increases the overall cost of the line.
- ac transmission systems do not allow the input of additional power at any point in the ac network with a low short circuit ratio, without causing power and voltage stability problems.
- In synchronous connections as in ac systems, the operation of the tie-line may cause power oscillations; moreover the fault in part of the network will propagate and affect the whole system. This increases the risk of blackout and other stability problems as each network loses autonomy.
- The high ground impedance (zero sequence) in ac system may not only affect efficient power transfer but also cause communication interference.

High-Voltage Direct Current transmission systems (HVDC) have several advantages over ac transmission systems when it comes to power transmission over long distances. These advantages can be summarized as follow [1],[3], [8]:

- Low net transmission losses for the same power capacity.
- HVDC transmission can carry up to 2.5 times the capacity of an ac line of similar voltage.
- Lack of technical limitations on the length of a submarine cable (long distance water crossing.
- Asynchronous connection of two ac systems.
- Reduces the dependency on the short circuit ratio (SCR), which is critical in the connection of ac systems with low short circuit ratios, such as offshore wind farms.
- Power flow is fully controlled (magnitude and direction).
- Provides frequency and voltage regulation to the ac network through active and reactive power modulation.
- Decouples and improves the stability of the ac power system (as the ac fault in one network will not be seen by the other network).

- Does not change the fault level at the point of connection and contributes limited current to any AC fault.
- The environmental impact is more favourable with dc lines because less right of way is required.

HVDC transmission systems in operation installed worldwide have been built using two different converter types:

- Current Source Converter (CSC), which uses line-commutated switching devices (thyristors).
- Voltage Source Converter (VSC), which uses self-commutated switching devices such as IGBT, MOSFET, and GTO.

2-2 CSC-HVDC transmission systems

The classic current source converter (CSC) approach is the most effective solution for bulk, long distance power transmission. Most existing dc transmission systems are based on this technology [9]. Table 2.1 summarizes the most recent projects using CSC-HVDC technology. The first classic HVDC transmission link was installed in 1954. It used line-commutated current-source converters (LCC) with mercury-arc valves. The next development was in the 1960's by replacing the mercury-arc valves with semiconductor thyristor valves. Semiconductor thyristor converters have now become the standard equipment for dc current source converter stations. The turn on of a thyristor is controlled by a gate signal and needs an ac voltage source in order to commutate, therefore it is only capable to transfer electrical power between active ac networks. The current source converter always absorbs reactive power either in rectifier or conversion operation; therefore, reactive power compensation is always required.

The operation of a current source converter depends on the power network strength, as this has great influence during system abnormal operation. For a strong system, any disturbance does not produce significant change in the voltage and angle in the power system. In weak systems even small disturbances cause changes in the operational conditions of the system.

Table 2.1: Examples of existing (and under construction) HVDC transmission systems using current source converter technology [10], [11].

Project	Rating (MW)	DC voltage (KV)	Distance (km)	Commissioning year
Sumatra-Java (Indonesia)	3000	±500	700 (cable)	2013
Madeira (Brazil)	3150	±600	2500 (Overhead line)	2012
Xianjiaba- Shanghai (China)	6400	±800	2071 (Overhead line)	2011
SAPEI (Italy)	1000	±500	435 (Overhead line)	2010
Outaouais (Canada)	1250	±175	0	2009
NorNed (Norway -Netherlands)	600	±500	2X580	2008
Neptune (USA)	660	±550	105 (cable)	2007
Three Gorges- Shanghai (china)	3000	±500	1060 (Overhead line)	2006
Vizag II (India)	500	±88	0	2005
Rapid city (USA)	200	±13	0	2003
Moyle (USA)	500	2X250	700 (cable)	2001
SwePol (Sweden-Poland)	600	±450	245 (cable)	2000
Welch Monticello (USA)	600	450	0	1998
Chandrapur-Ramagundum	1000	2X205	0	1997
Kontek (Denmark-Germany)	600	400	119(Overhead line)+52 (cable)	1995
Sakuma (Japan)	300	±125	0	1993
Hydro Quebec(Canada-USA)	2250	±450	1100 (Overhead line)	1991
Vindhyachal (India)	500	2X69.7	0	1989
Zhoushan (china)	50	100	12(Overhead line)+42 (cable)	1987
Cross Channel 2(UK- France)	2000	±450	72 (cable)	1986
Highgate (USA)	200	±56	0	1985
Chateauguay (Canada –USA)	1000	2X140	0	1984

The operation of a conventional HVDC transmission system is mainly affected by the network strength since the HVDC can be considered as a special load with a voltage and load angle. The strength of the system can be measured using the short circuit ratio (SCR) or the equivalent impedance at the busbar. According to the IEEE Standard 1204-1997 [12], the system Short-Circuit Ratio (SCR) and Effective Short-Circuit Ratio (ESCR) are defined as follow:

$$SCR = \frac{S}{P_{dc}} \tag{2-1}$$

$$ESCR = \frac{S - Q_C}{P_{dc}} \tag{2-2}$$

where S is the ac system three-phase symmetrical short-circuit level in mega volt-ampere (MVA) at the converter terminals (ac bus), calculated at rated terminal voltage (1.0 pu), P_{dc} is the rated dc power of the terminals in megawatts (MW), and Q_C is the three-phase fundamental MVAr at rated P_{dc} and rated terminal voltage. This includes ac filters and shunt capacitors. The system strength is classified as follow:

- System is strong if SCR>3 or $ESCR$>2.5
- System is weak if 3> SCR >2 or 2.5> $ESCR$ >1.5
- System is very weak (very low SCR) if SCR <2 or $ESCR$ <1.5

2-3 HVDC Transmission System Configurations

Depending on the function and location of the converter stations, various HVDC configurations can be identified. These configurations are generic and applicable to both, current source and voltage source converter schemes [13],[14].

a. Monopolar HVDC system

In the monopolar configuration, two converters are connected by a single pole line and a positive or a negative dc voltage is used. In Fig. 2.2(a) there is only one insulated transmission conductor installed and the ground or sea provides the path for the return current. Alternatively, a metallic return conductor may be used as the return path.

b. Bipolar HVDC system

The bipolar configuration consists of two monopolar systems, one with positive polarity and the other with negative polarity, as shown in Fig. 2.2(b). Each terminal has two converters of equal rated voltage connected in series on the dc side. Normally the currents in the two poles are equal and there is negligible ground current. A bipolar scheme is the most commonly used configuration in applications where overhead lines are used to transmit power, as it is economically attractive to install an additional pole conductor. In case of failure of one pole, power transmission can continue on the other pole (increasing system reliability).

c. Homopolar HVDC system

In the homopolar configuration, shown in Fig. 2.2(c), two or more conductors have the negative polarity and can be operated with ground or a metallic return. With two poles operated in parallel, the homopolar configuration reduces the insulation costs, but the earth return current is the major disadvantage.

d. Back-to-back HVDC system

This is the common configuration for connecting two asynchronous ac systems. Two converter stations are located at the same site and a transmission line or cable is not needed. A block diagram of a back-to-back HVDC system is shown in Fig. 2.2(d). The two interconnected ac systems may have the same or different nominal frequencies.

e. Multi-terminal HVDC system

In this configuration there are more than two terminals, typically between three and five, but in practice no scheme has so far been operated with more than three terminals. Multi-terminal systems are generally divided into series and parallel systems as shown in Fig. 2.2(e) and 2.2(f). The multi-terminal configuration imposes a significant complexity to achieve the control and communication between different converter substations, especially in the case of current source converter schemes.

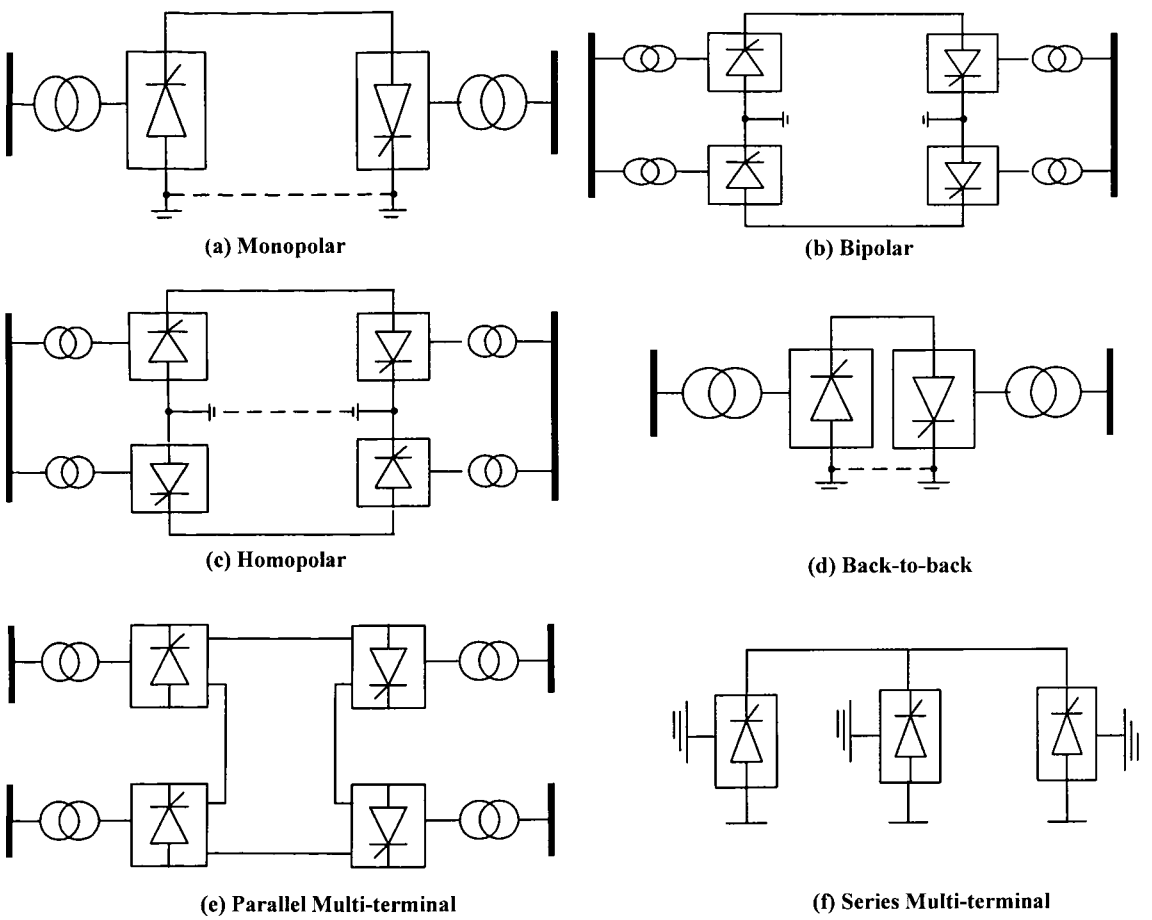


Fig. 2.2: Schematic diagrams of different HVDC circuit arrangements.

2-4 CSC Converter configurations

In general HVDC transmission systems based on current source converter technology can be built as line-commutated converters (LCC) or capacitor-commutated converters (CCC).

2-4-1 Line-commutated converter

The current source converter is capable to transfer the current only in one direction and the power flow reversal is achieved by dc voltage polarity reversal. A large dc inductor is connected in series at the dc terminals to get a smoother dc current. The current source converter can operate as rectifier and the firing angle of the converter is less than 90°, or as inverter and the firing angle is more a 90°. The basic building block of the converter station is the well-known six-pulse thyristor bridge or the 12-pulse thyristor configuration. With a six-pulse bridge the lowest order current harmonics are the 5^{th} and 7^{th}, and the 11^{th} and 13^{th} for the12-pulse converter [15], [16]. Fig 2.3a shows the schematic of a line-commuted converter.

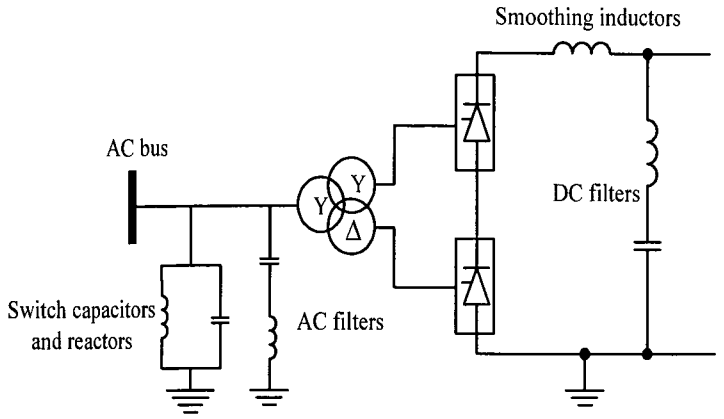


Fig. 2.3: Line-commutated converter station.

2-4-2 Capacitor-commutated converter

The capacitor-commutated converter was developed by ABB with the objective to extend the application of CSC-HVDC transmission to systems with low short-circuit ratio. Fig 2.4 shows the schematic of a capacitor-commuted converter. The capacitor is connected in series with the converter transformer to reduce the commutation impedance of the converter, which in turn reduces the reactive power requirement of the converter. Increasing the size of the series capacitor can furthermore even allow operation at leading power factor [17],[18]. Other advantages over the LCC-HVDC include the ability to operate with weaker ac systems, and to deliver more power than an LCC-HVDC of similar size and cost. The negative impact of reduced commutation impedance is that additional stresses are imposed on the valves and converter transformers (higher di/dt).

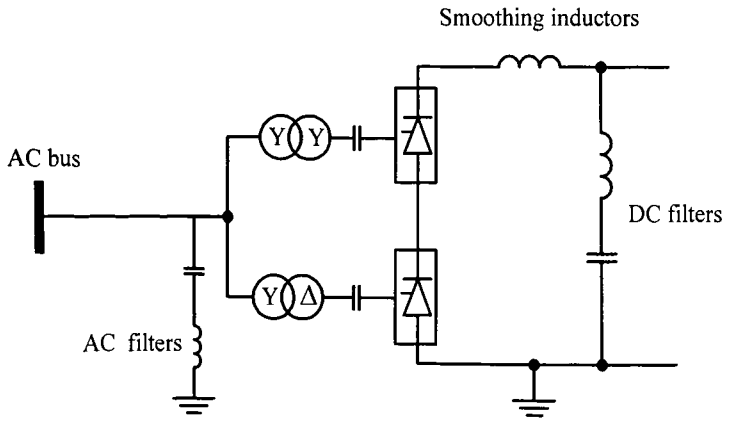


Fig. 2.4: Capacitor-commutated converter station.

2-5 Line-commutated converter operation

The standard bridge or converter connection is double way connection with six thyristor valves connected as shown in Fig. 2.5a. The converter transformer may be wound as star-star, star-delta, or delta-star, or delta-delta. The output of each of these connections are the same but phase-shifted by 30° with respect to each other. To obtain a smooth output waveform, two bridges, one connected as star-star and the other connected as star-delta are connected together to give the twelve-pulse bridge as shown in Fig. 2.5b.

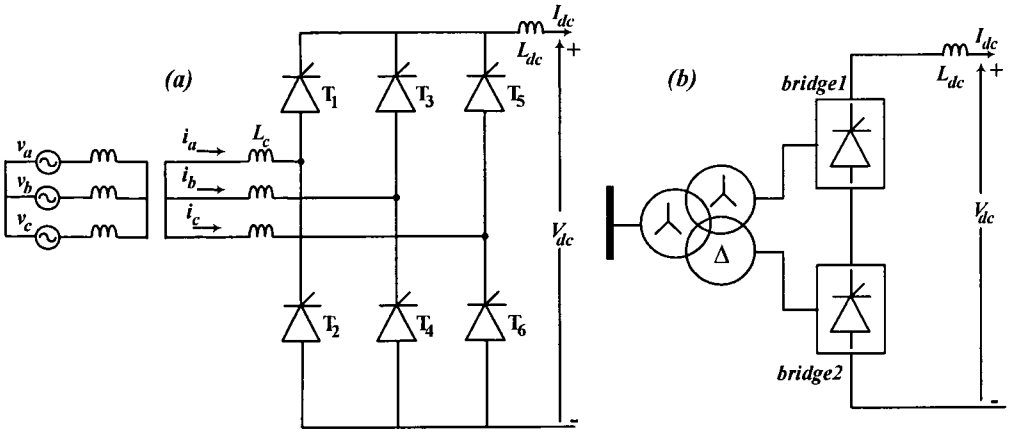


Fig. 2.5: Converter arrangements: (a) six pulse connection, (b) twelve pulse connection.

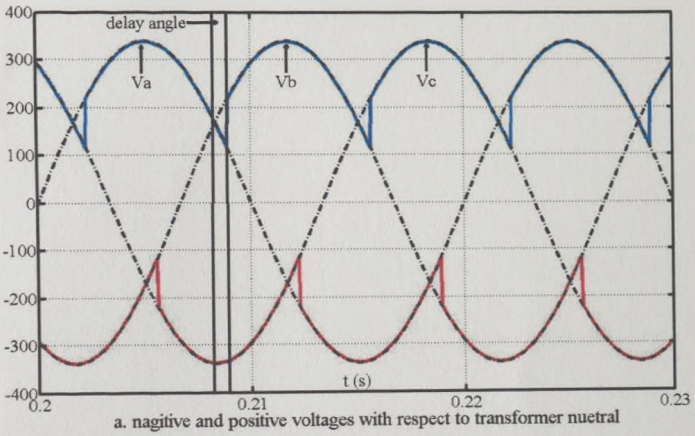
The analysis of the six-pulse converter operation is explained with a number of reasonable assumptions to simplify the derivation of the conversion steady-state equations. The assumptions are [11]-[15]:

- The converter valves are considered as ideal switches, when calculating the power losses the valve resistance is added to the dc transmission resistance.
- The ac side is infinitely strong and consists of balanced and sinusoidal voltages, the commutation reactance is equal in every phase and its resistance is neglected.

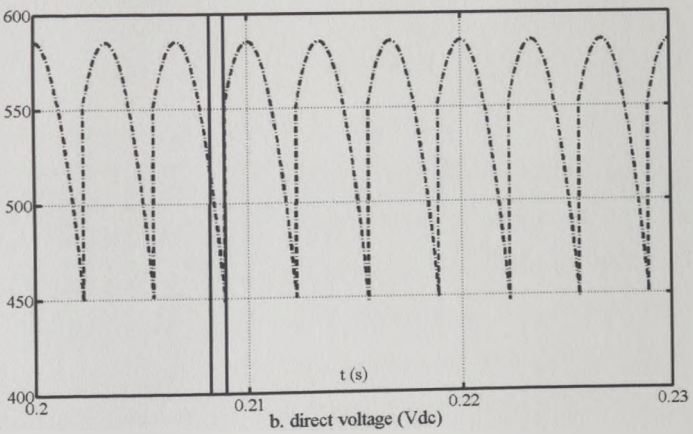
- The dc current I_d is constant with a smoothing infinite reactance L_d.
- Only two or three valves conduct simultaneously, which means that two simultaneous commutations are not considered.

2-5-1 Rectifier operation without commutation angle

If the commutation reactance L_c is neglected the transfer of the current between thyristor valves on the same side occurs instantaneously. The rectified voltage waveforms across the thyristors are shown in Fig.2.6a. The top waveforms are the positive-pole direct voltage produced by thyristor valves (T_1,T_3,T_5), while the bottom waveforms are the negative-pole direct voltage produced by thyristor valves (T_2,T_4,T_6), with respect to the transformer neutral. The dc average output voltage (positive-pole with respect to negative-pole V_{dc}) is shown in Fig. 2.6b. The dc average output voltage contains harmonics which can be eliminated by using a large smoothing reactor on the dc side. The ac line currents I_{abc} are shown in Fig. 2.6c.



a. nagitive and positive voltages with respect to transformer nuetral



b. direct voltage (Vdc)

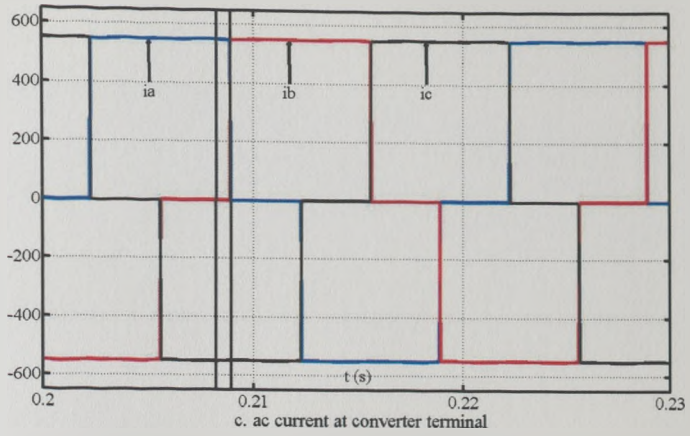


Fig. 2.6: Rectifier operation without commutation angle.

At any instant, one valve of the upper commutation group and one of the lower row are conducting. Therefore, the instantaneous direct voltage at any time equals one of the six line-to-line voltages. The instant at which the direct voltage changes to another line-to-line voltage is controlled via the firing angle α. The mean direct voltage output is calculated by [15]:

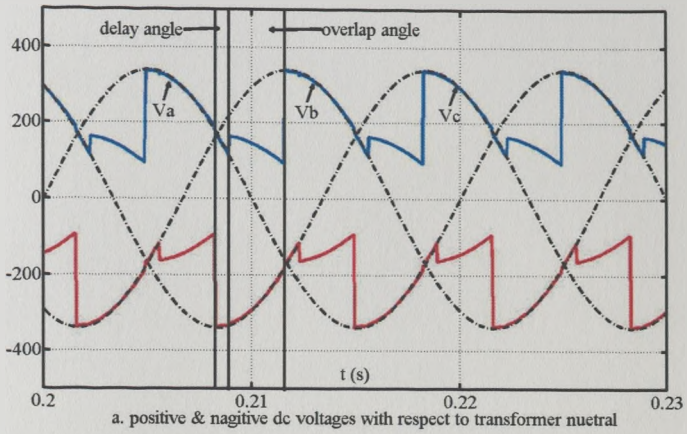
$$V_{dc} = \frac{2V_{max}}{2/3\pi} \int_{-\pi/3+\alpha}^{\pi/3+\alpha} \cos \omega t \, d\omega t = \frac{3\sqrt{2}}{\pi} V_{l-l} \cos \alpha \qquad (2\text{-}3)$$

where V_{max} is the peak phase voltage at the transformer secondary side, and $V_{l\text{-}l}$ is the rms line-to-line secondary voltage.

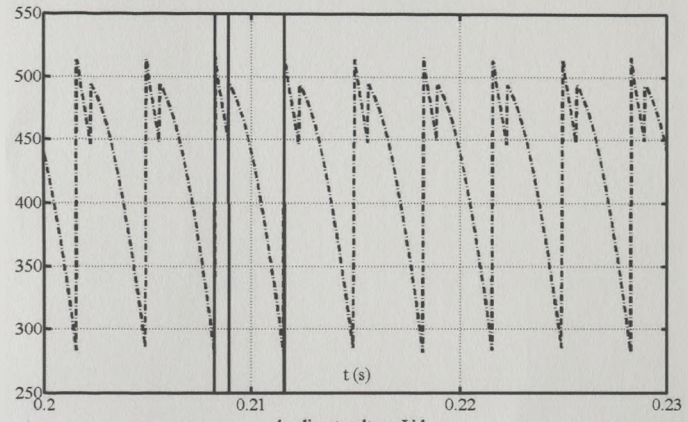
2-5-2 Rectifier operation with commutation angle

In practice, the transfer of current between two consecutive valves in the same side is not instantaneous. The current requires finite time to transfer from one valve to another, this phenomena is known as overlap period. In Fig. 2.7 each valve will switch ON when it receives a firing pulse and its forward bias voltage becomes more positive than the forward bias of the conducting valve. The current passing through the conducting valve does not change immediately as it commutates to another valve because of the commutation reactance. The commutation ends when i_a becomes zero and i_b has taken over the whole dc current. During commutation, two valves conduct at a time, which means that there is an instantaneous short circuit between the two voltages participating in the process. As the inductances of each phase are the same, the current i_c produces the same voltage drop in each

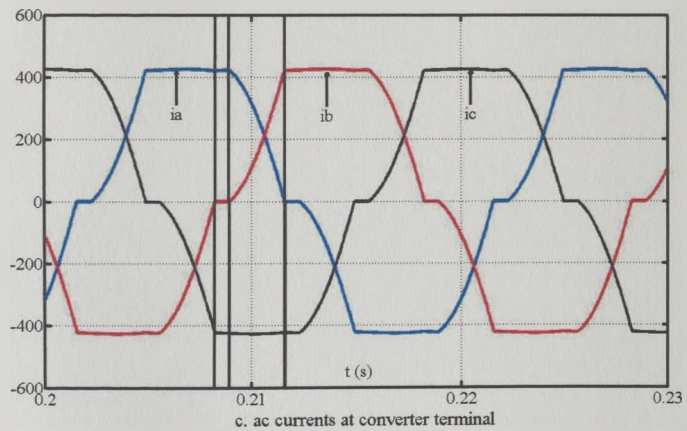
L_c but with opposite sign because this current flows in reverse direction in each inductance. The phase with the higher instantaneous voltage suffers a voltage drop and the phase with the lower voltage suffers a voltage increase.



a. positive & nagitive dc voltages with respect to transformer nuetral



b. direct voltage Vd



c. ac currents at converter terminal

Fig. 2.7: Rectifier operation with commutation angle.

After analyzing the commutation circuit, the expression for the dc current I_{dc} is given as [11]-[15]:

$$I_{dc} = \frac{v_{ab}}{\sqrt{2}\omega L_c}\left(cos\alpha - cos(\alpha + \mu)\right) \tag{2-4}$$

The voltage drop during commutation is:

$$\Delta V_d = \frac{3v_{ab}}{\pi\sqrt{2}}\left(cos\alpha - cos(\alpha + \mu)\right) \tag{2-5}$$

And the mean direct output voltage V_{dc} is:

$$V_{dc} = \frac{3\sqrt{2}}{\pi}V_{l-l}\cos\alpha - \frac{3I_{dc}\omega L_c}{\pi} = \frac{3\sqrt{2}}{\pi}V_{l-l}\left(\cos\alpha + \cos(\alpha + \mu)\right) \tag{2-6}$$

2-5-3 Inverter operation

Referring to equation (2.3), the average dc voltage becomes smaller when the delay angle increases; when α=90° the average dc voltage is zero. When the delay angle exceeds 90° the V_{dc} becomes negative and the converter operates as inverter driving the current in the same direction, in opposition to the induced e.m.f in the converter transformer. The three necessary conditions for inverter operation are:

1- Three-phase ac voltage to provide the commutation voltages.

2- Delay angle greater than 90°.

3- dc power supply.

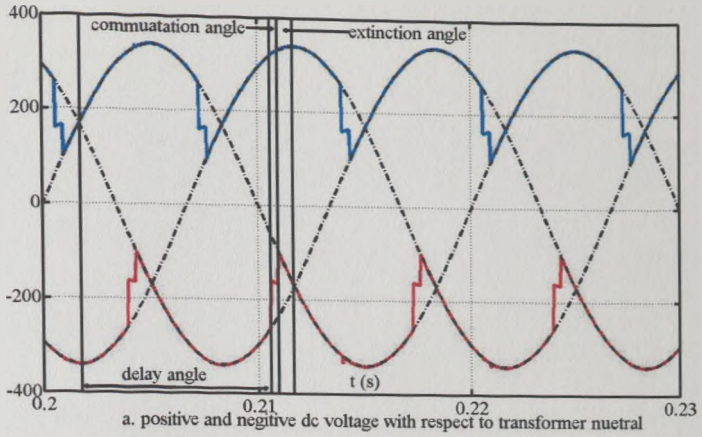
The commutation from valve T_1 to valve T_2 in Fig. 2.8 is only possible if phase b is positive with respect to phase a, and if there is enough extinction angle for valve T_1, which has just stop conducting, to reestablish its blocking capability. Fig. 2.8 shows the key waveforms when the converter operates as the inverter.

The maximum power inversion occurs with α=180°, but this is not possible because there is not enough time for the commutation. The delay angle is limited to $\alpha=\pi-(\mu+\gamma_o)$, where γ_o is the minimum extinction angle. For the inverter operation the equations are expressed in term of the angle of advance β, or the extinction angle γ. The mean dc voltage is expressed by the following equation [15]-[19]:

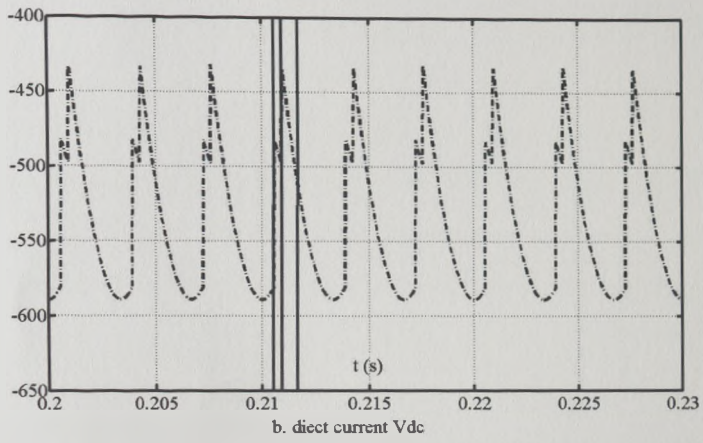
$$V_{dc} = \frac{3\sqrt{2}}{\pi}V_{l-l}\cos\gamma - \frac{3I_{dc}\omega L_c}{\pi} = \frac{3\sqrt{2}}{\pi}V_{l-l}\cos\beta + \frac{3I_{dc}\omega L_c}{\pi}$$

$$V_{dc} = \frac{3}{\sqrt{2}\pi}V_{l-l}\left(\cos\beta + \cos\gamma\right) \tag{2-7}$$

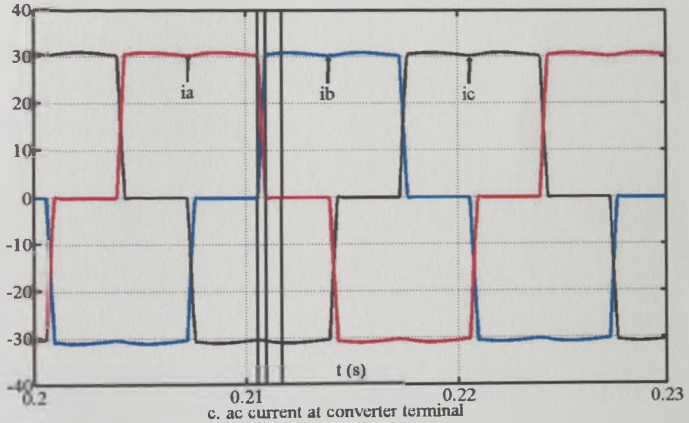
where $\beta = \pi - \alpha,\ \gamma = \beta - \mu$



a. positive and negitive dc voltage with respect to transformer nuetral



b. diect current Vdc



c. ac current at converter terminal

Fig. 2.8: Inverter operation

If the rectifier is assumed lossless, the power balance between its ac and dc sides can be expressed as:

$$\sqrt{3}V_{l-l}I_{ac}\cos\theta = \frac{3\sqrt{2}}{\pi}V_{l-l}\left(\cos\alpha+\cos(\alpha+\mu)\right)*I_{dc} \qquad (2\text{-}8)$$

where θ is the phase angle at which the current lags the ac voltage and I_{ac} is the fundamental amplitude of the ac current. After using Fourier analysis of the ac current waveform, I_{ac} could be expressed as $\frac{2\sqrt{3}}{\pi} I_{dc}$ .Therefore the expression for the power factor after rearranging equation (2.8) is [19]:

$$\cos\theta = \frac{1}{2}\left(\cos\alpha + \cos(\alpha + \mu)\right) \tag{2-9}$$

And for the inverter:

$$\cos\theta = \frac{1}{2}\left(\cos\gamma + \cos(\beta)\right) \tag{2-10}$$

2-6 Commutation failure

Commutation failure is the inability to complete commutation before the commutation voltage reverses; this occurs due to conditions in the system. Commutation failure is more common in the inverter and occurs during disturbances such as higher dc current or low ac voltage; sometimes the commutation failure occurs in the rectifier if the firing angle fails. At the inverter, a valve will turn OFF when its forward current commutates to zero and the voltage across the valve remains negative. The period for which the valve stays negatively biased is the extinction angle γ. All valves require removal of the internal stored charges produced during the forward conducting period before the valve can successfully establish its ability to block a forward bias. The inverter therefore requires a minimum period of negative bias or minimum extinction angle γ_o for forward-blocking to be successful.
Commutation failure at a converter bridge operating as an inverter is caused by any of the following reasons [15]-[20]:

1- Any increase in the dc inverter current leads to an increase in the overlap angle μ. The extinction angle γ will reduce and may reach the point where the valve is unable to maintain forward-blocking. Increasing the dc inductance and commutating reactance reduces the rate-of-change of the dc current and reduces the risk of commutation failure.

2. When the magnitude of the ac side voltage on one or more phases reduces or is distorted causing the extinction angle to be inadequate as commutation is attempted.

3. A phase angle shift in the ac commutating voltage can cause commutation failure.

4. The value of the normal operation extinction angle γ affects the sensitivity of the inverter to commutation failure. A value of $\gamma = 18°$ is commonly used for most inverters. Increasing γ to values of 25° or higher will reduce the possibility of commutation failure, but this will increase the reactive power demand of the inverter.

2-7 The ac and dc harmonics

The ac input current waveform of a 6-pulse converter has harmonic frequency components. The ac input current waveform of the converter fed via a star-star transformer is shown in (Fig. 2.9a) and described as:

$$\begin{cases} i = 0, & 0 < \omega t < \pi/6 \\ i = I_{dc}, & \pi/6 < \omega t < 5\pi/6 \\ i = -I_{dc}, & 7\pi/6 < \omega t < 11\pi/6 \\ i = 0, & 11\pi/6 < \omega t < 2\pi \end{cases}$$

The Fourier analysis for the current waveform is [15], [16]:

$$i = \frac{2\sqrt{3}I_{dc}}{\pi}\left(\cos\omega t - \frac{1}{5}\cos 5\omega t - \frac{1}{7}\cos 7\omega t + \frac{1}{11}\cos 11\omega t + \frac{1}{13}\cos 13\omega t + ...\right) \qquad (2\text{-}11)$$

If the converter is fed via a star/delta or delta/star transformer then the ac input current waveform is that shown in Fig. 2.9b and described as:

$$\begin{cases} i = I_{dc}/\sqrt{3}, \ (0 < \omega t < \pi/3) & i = 2I_{dc}/\sqrt{3}, \ (\pi/3 < \omega t < 2\pi/3) \\ i = I_{dc}/\sqrt{3}, \ (2\pi/3 < \omega t < \pi) & i = -I_{dc}/\sqrt{3}, \ (\pi < \omega t < 4\pi/3) \\ i = -2I_{dc}/\sqrt{3}, \ (4\pi/3 < \omega t < 5\pi/3) & i = -I_{dc}/\sqrt{3}, \ (5\pi/3 < \omega t < 2\pi) \end{cases}$$

And the Fourier analysis for the current is (Fig. 2.28c):

$$i = \frac{2\sqrt{3}I_{dc}}{\pi}\left(\cos\omega t + \frac{1}{5}\cos 5\omega t + \frac{1}{7}\cos 7\omega t + \frac{1}{11}\cos 11\omega t + \frac{1}{13}\cos 13\omega t + ...\right) \qquad (2\text{-}12)$$

The harmonic spectrum obtained using equations (2.11) and (2.12) shows the following:

1- The Fourier series includes only odd harmonics.

2- The absence of triple harmonics.

3- The harmonics orders are $6k\pm1$, where k is integer number.

4- The rms magnitude is $I_1 = \frac{\sqrt{6}I_{dc}}{\pi}$ for the fundamental and $\frac{I_1}{n}$ for n^{th} harmonic.

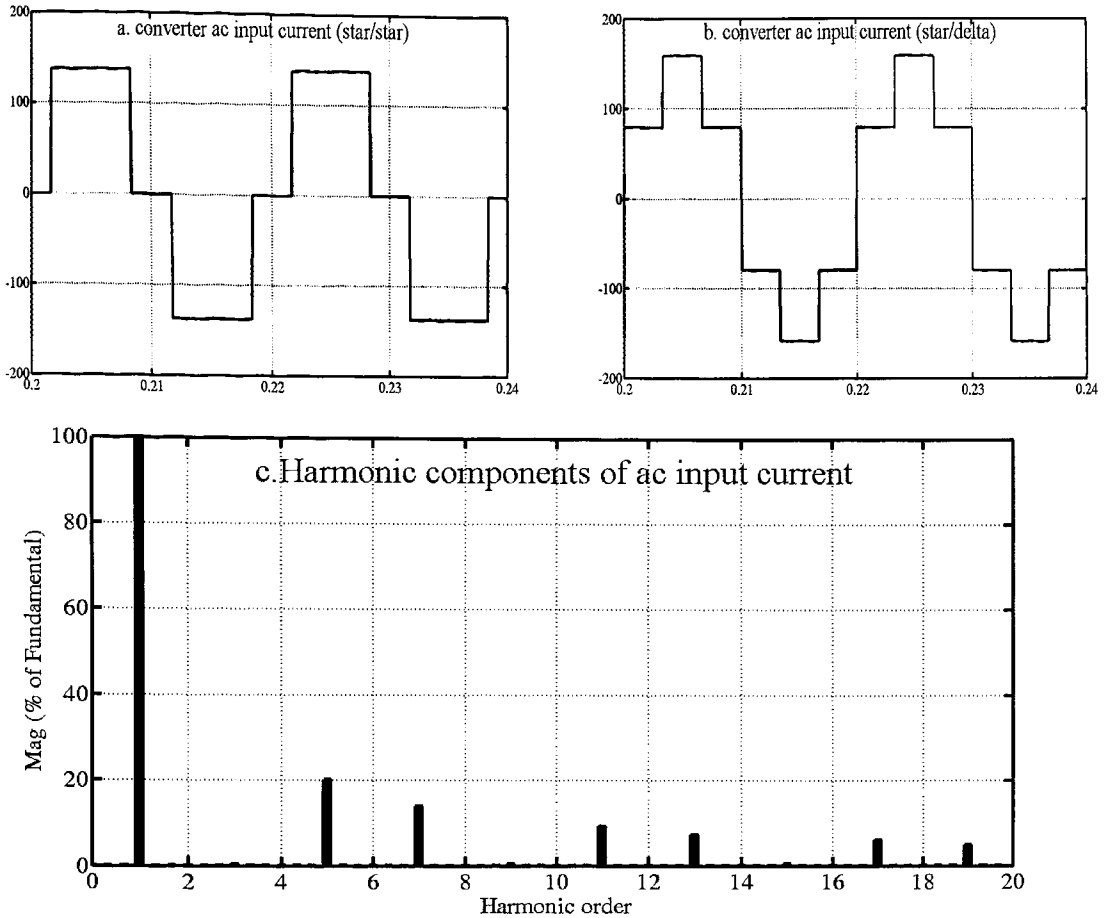


Fig. 2.9: ac Harmonic analysis of a 6-pulse converter.

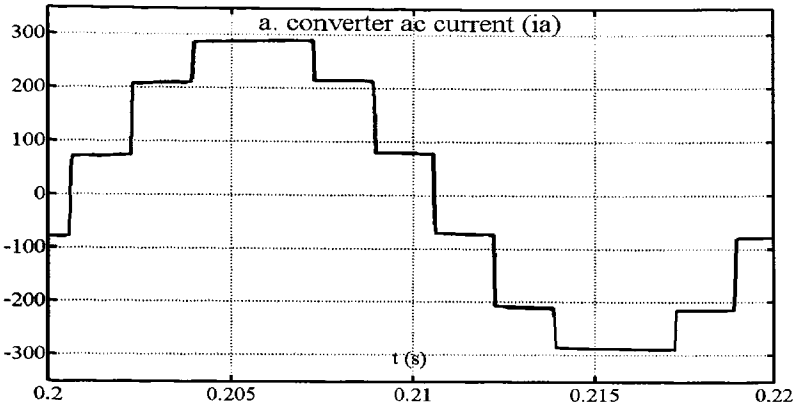
To reduce the amount of ac harmonics a 12-pulse converter configuration is used. The 12-pluse converter comprises two parallel 6-pulse converters. The first one is connected via a star/star transformer while the second one is connected via a star/delta transformer. The ac input current waveform in a 12-pulse converter is shown in Fig. 2.10a, and described as:

$$\begin{cases} i = I_{dc}/2\sqrt{3}, (0 < \omega t < \pi/6) & i = I_{dc}/2\sqrt{3} + I_{dc}/2, \ (\pi/6 < \omega t < \pi/3) \\ i = I_{dc}/\sqrt{3} + I_{dc}/2, \ (\pi/3 < \omega t < 2\pi/3) & i = I_{dc}/2\sqrt{3} + I_{dc}/2, \ (2\pi/3 < \omega t < 5\pi/6) \\ i = I_{dc}/2\sqrt{3}, \ (5\pi/6 < \omega t < \pi) & i = -I_{dc}/2\sqrt{3}, \ (\pi < \omega t < 7\pi/6) \\ i = -I_{dc}/2\sqrt{3} - I_{dc}/2, \ (7\pi/6 < \omega t < 4\pi/3) & i = -I_{dc}/\sqrt{3} - I_{dc}/2, \ (4\pi/3 < \omega t < 5\pi/3) \\ i = -I_{dc}/2\sqrt{3} - I_{dc}/2, \ (5\pi/3 < \omega t < 11\pi/6) & i = -I_{dc}/2\sqrt{3}, \ (11\pi/6 < \omega t < 2\pi) \end{cases}$$

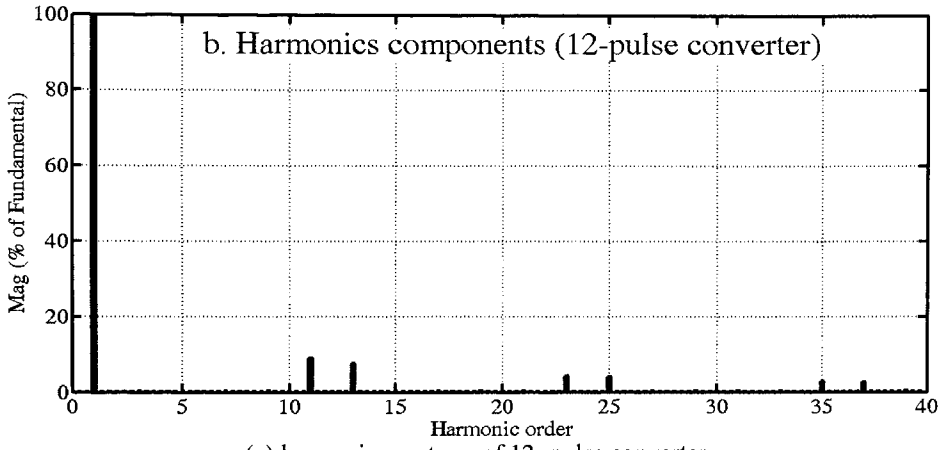
And the Fourier analysis for the current waveform is [15],[16]:

$$i = \frac{4\sqrt{3}I_{dc}}{\pi}\left(\cos\omega t + \frac{1}{11}\cos 11\omega t + \frac{1}{13}\cos 13\omega t + \frac{1}{23}\cos 23\omega t + \frac{1}{25}\cos 25\omega t + ...\right) \qquad (2\text{-}13)$$

The waveform only contains harmonics of order $12k\pm1$. Harmonic currents of order $6k\pm1$ with k odd (5^{th}, 7^{th}, 17^{th}, 19^{th} ...) circulate between the two converters transformer but do not appear in the output current waveform. The line current waveform shown in Fig. 2.10a is closer to a sinusoidal than the one obtained with the six-pulse converter configuration.



a. the converter ac current



(a) harmonic spectrum of 12- pulse converter

Fig. 2.10: ac Harmonic analysis of a 12-pulse converter

If an 18-pulse converter (three 6-pulse converter bridges in parallel) is used, the input current will have harmonic components of order $18k\pm1$ at the following multiples of the fundamental frequency (17^{th}, 19^{th}, 35^{th}, 37^{th}, 53^{th}, 55^{th}...). In multiple-pulse configuration, the configuration includes multiple converters connected together. The harmonics generated by one converter is cancel by harmonics generated by the other converters. Certain harmonics related to the number of converters are eliminated from the multiple-pulse converter ac input line current [21]. Any further increase in the number of converters will reduce further the harmonics in the converter ac input current.

The dc output voltage is not purely constant. It contains harmonics as shown in Fig. 2.7b and Fig.2.8b. The Fourier analysis of the dc voltage waveform produced by a 6-pulse converter shows that it contains harmonics of order 6k (6^{th}, 12th, 18^{th}...). In the 12-pluse converter the harmonic orders in the dc voltage waveform are the 12k (12^{th}, 24^{th}, 36^{th}...). The 6^{th}, 18^{th}, 30th... will be canceled in a 12-pulse bridge. The magnitude of the voltage harmonics depend on the operating α, a higher α produces a higher harmonic level. In multiple converter, the generated harmonics in the dc voltage are in order nk. Where k is the number of individual converter units and n is a positive integer number. For example (18^{th}, 36^{th}, 54^{th}...), if 18 pulse converter is used. The harmonic spectrum of the DC voltage waveforms for 6 and 12 pulse converters are shown in Fig. 2.11.

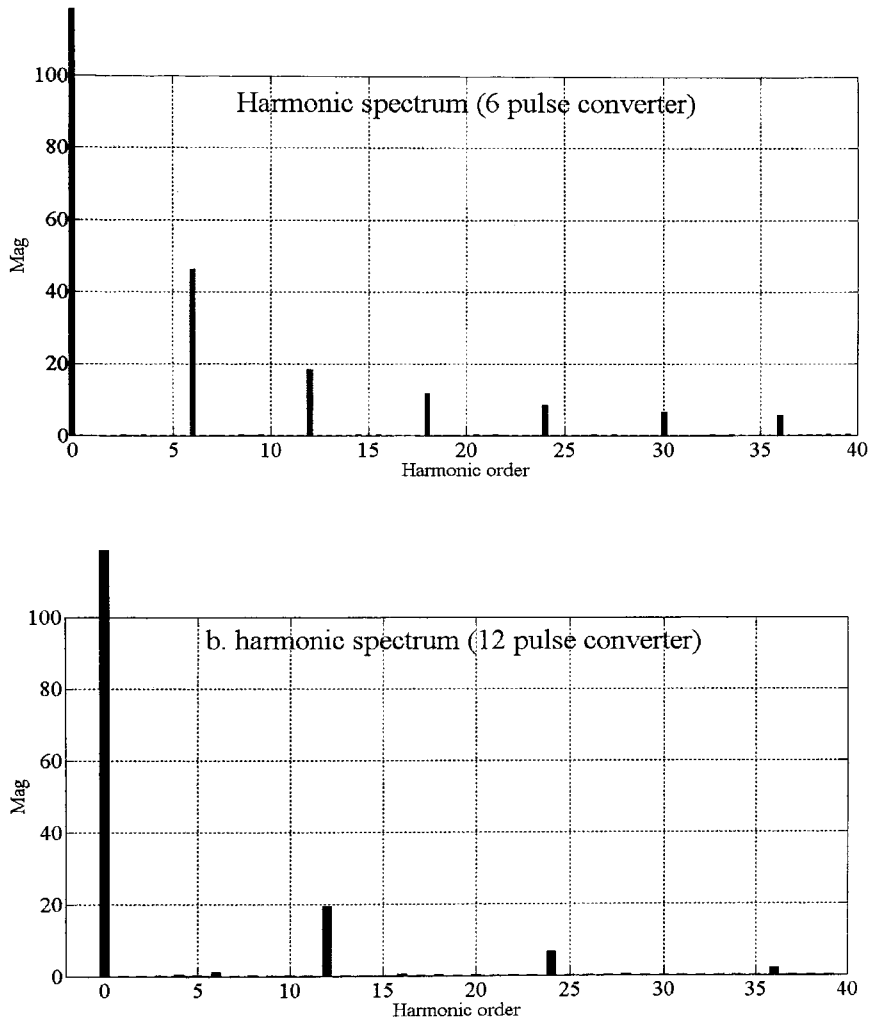


Fig. 2.11: Harmonic spectrum of the dc voltage for 6 -pulse and 12 -pulse converters.

2-8 Line-commutated converter-HVDC system Control

The main functions of the control system in an LCC-HVDC transmission system are to control the power flow between the sending and receiving end converters, and to protect the equipment against over-current and voltage stress. The basic desired features of an LCC-HVDC control system are [11]-[15]:

1. Limit maximum dc current: using constant-current control in the rectifier to protect the converter valves.
2. Maintain maximum dc voltage: using constant voltage control in the inverter to reduce the losses in transmission line and converter valves.
3. Keep the ac reactive power demand low at either converter terminal. That is means keeping the operating angles at the converters at the lower level possible by using minimum firing angle.
4. Prevent commutation failures at the inverter hence improving the stability of the power transmission.

The best way to understand the control principles of HVDC transmission is to study the voltage-current characteristics (Fig. 2.12) [15]. These characteristics are used to illustrate the relationship between the dc voltage and current in steady state during power flow control on a dc line.

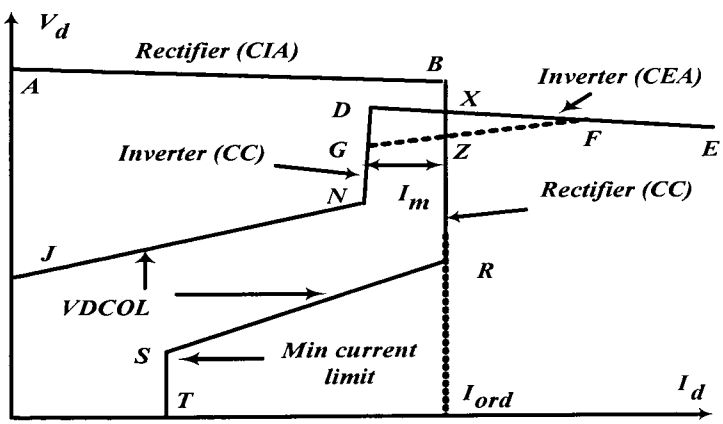


Fig. 2.12. V_d-I_d characteristics for a two terminal LCC-HVDC system [15].

Under steady-state condition the control system of the inverter is designed to maintain the dc voltage by keeping constant extinction angle (γ). In this case the dc voltage droop increases as the dc current increases, as indicated by line DXFE and equation (2.14):

$$V_{dc} = \frac{3\sqrt{2}}{\pi} V_{l-l} \cos\gamma - \frac{3 I_{dc} \omega L_c}{\pi} \tag{2-14}$$

The inverter can operate with constant dc voltage as indicated by line GF meaning that the extinction angle must increase beyond its minimum limit (always set as 18°). If the inverter is operated at either constant voltage or constant extinction angle then line BXZR is normal operation of the rectifier, where the delay angle α is varied in order to keep the dc current constant. The delay angle α cannot be below its minimum set point (α_{min} always set as 5°). If α reaches its minimum point then the rectifier will operate at minimum constant ignition angle which is indicated by line AB, and defined as:

$$V_{dc} = \frac{3\sqrt{2}}{\pi} V_{l-l} \cos\alpha - \frac{3 I_{dc} \omega L_c}{\pi} \tag{2-15}$$

The rectifier valves have limited thermal capability and cannot carry large current; hence a maximum current limit is used in the control system to protect the valves. I_{dc} minimum is defined in the rectifier such as to ensure a minimum dc current to avoid the possibility of dc current extinction caused by the valve current dropping below the hold-on thyristor current. The operating point of the HVDC system is represented by points X or Z (the intersection of the rectifier and inverter characteristics). The operating point is achieved with the help of the converter transformer tap-changers. For the rectifier, the transformer tap-changer is used to keep the delay angle α at its normal operating range to meet the constant current setting I_{ref}. For inverter operation, the tap-changer is adjusted to meet the desired level extinction angle control.

Another possible operating mode for the inverter is the constant current mode line DGN. The current demanded by the inverter is usually less than the current demanded by the rectifier by a current margin I_m that is typically about 10%. The current margin is chosen so large to prevent the interaction between rectifier and inverter constant current modes due to current harmonics in the dc current. The current control at the inverter is activated when α reaches its minimum point. If for any reason such as low commutation voltage the line AB falls below either point X or Z, the operating point will shift to somewhere along line DGN, then the inverter will control the dc current and the rectifier will control the dc voltage.

During low voltage conditions, it is not possible to maintain the dc current. The low ac voltage will result in an increase in the reactive power consumption and in a low dc voltage, therefore increasing the risk of commutation failure. A voltage-dependant current-order limit (VDCOL) is used to reduce the dc current order when the voltage drops below a

predetermined value. VDCOL is represented by line RST in the rectifier and line JN in the inverter. To prevent the inverter from operating in the rectifier region, and hence having power reversal, a minimum alpha limit is imposed, typically about 100-110°.

2-9 Control system design

The control of power flow in an LCC-HVDC system is achieved by synchronizing the firing pulses generated by the trigger unit [22]. There are many control techniques but all of them use a voltage-controlled oscillator (VCO), and a ring counter to decouple the firing pulses from the commutation voltage. The rectifier during normal operation is operating at constant current control (CC) by changing the delay angle until α is less than the minimum limit, then the rectifier will operate at constant-ignition angle (CIA).

Fig. 2.13 shows the block diagram of the rectifier control system. The actual dc current flowing in the dc link is compared with the reference value I_{ord}. The resultant error signal I_e is then passed through a PI controller, the output of the PI controller is the alpha order α_{ord} which controls the frequency output of the VCO. The train of pulses generated by the VCO is fed to the ring counter which has six or twelve stages (according to converter type). Only one stage is ON at any time, therefore a complete set of 6 or 12 pulses is generated by the ring counter at equal intervals in one full cycle. A limit is used to prevent the dc current from exceeding the specific value to provide over-current protection to converter valves.

The problems of using a PI controller are:

- It uses fixed gains, although some possibility for gain scheduling exists.
- Difficult to select optimal gains, and even then, they are optimal over a limited range only, while the plant system is varying continually.

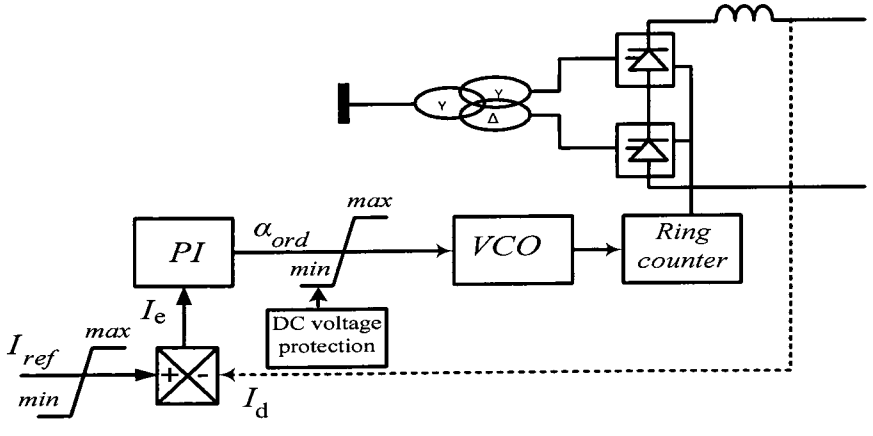


Fig. 2.13: Rectifier control system layout.

The control system of the inverter comprises of a dc voltage controller, extinction angle control, and current regulator. A control angle selector is placed to choose the desired control signal from the above controllers. The control system is similar to the rectifier control system including the comparing loop, PI controller, VCO, and counter ring. The schematic block diagram of the inverter control system is shown in Fig. 2.14.

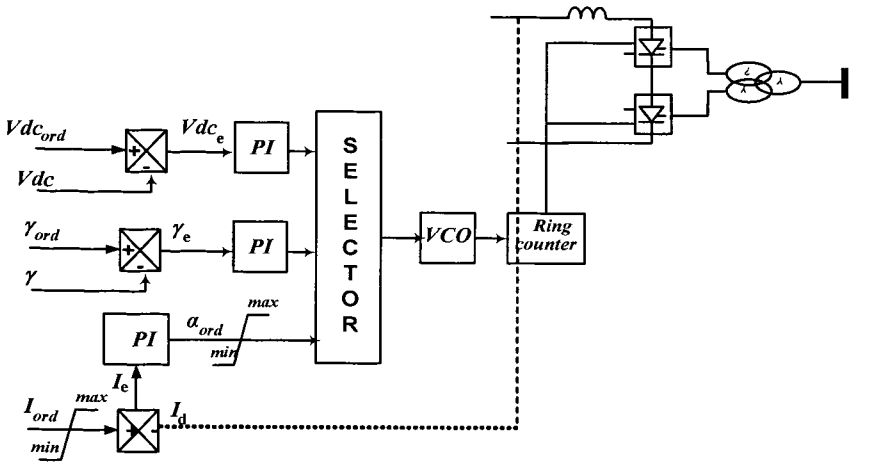


Fig. 2.14: inverter control system layout

2-10 Steady-state and transient behaviour of LCC- HVDC systems

The steady-state and transient behavior of the LCC-HVDC transmission system is investigated using a complete 12-pulse converter model. The investigation includes: system behavior during ac faults and sudden changes in active power. The key results are illustrated together with supplementary details. The studied system is shown in Fig. 2.15 and the system parameters are listed in Table 2.2. The control strategies are implemented to control the current at the rectifier and to control either the voltage or the extinction angle at the inverter.

Table 2.2: LCC-HVDC parameters (obtained from Matlab simulink library)

Rectifier circuit	Three-winding transformer data (500/200/200 kV, 1000MVA, 60Hz, transformer reactance are: 0.24, 0.12, 0.12 pu, transformer resistance are: 0.0025, 0.00125, 0.00125 pu, 600MVA ac filter, and delay angle of 25°.
dc circuit	Dc voltage V_{dc}=500kV, rated dc power, P_{dc}= 1000MW, DC reactor L_{dc}=0.75H, dc cable resistance R_{dc}= 0.015Ω/km, dc cable length= 250km,
Inverter circuit	Three-winding transformer data (500/200/200 kV, 1000MVA, 60Hz, the reactance are: 0.24, 0.12, 0.12 pu, the resistance are: 0.0025, 0.00125, 0.00125 pu, 600MVA ac filter, and delay angle is 145°.

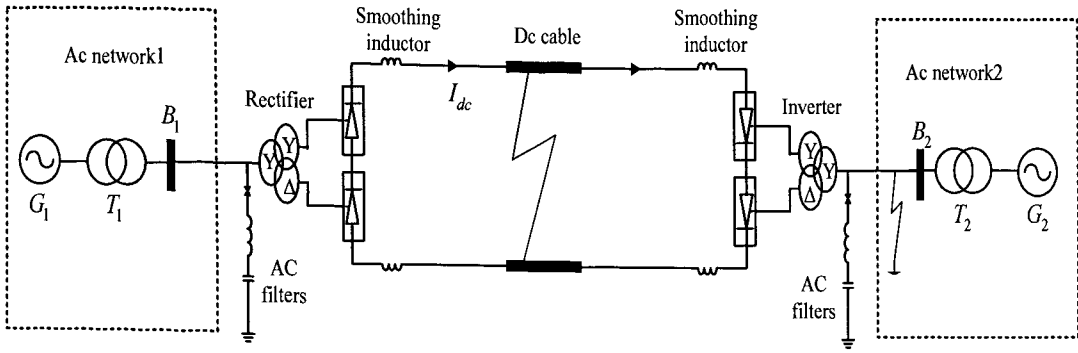


Fig. 2.15: 12 pulse LCC-HVDC connecting two ac networks.

2-10-1 System behavior during a step in active Power

The dc link power can be increased or decreased using power run-up and run-down controls in response to local or remote disturbances. The step power change is achieved by adjusting the current reference value. The dc system behavior during a sudden power change is shown in Fig. 2.16. The current reference value is stepped down at t=1s from 1.0pu to 0.80pu gradually with a slope during 0.2s, and then at t=1.8s, it steps up to 1.2pu during 0.2s. The dc voltage at the inverter is kept at constant value by inverter controller resulting in constant dc voltage at the rectifier side as shown in Fig. 2.16c. The rectifier delay angle (α_r) is increased during power step-down and decreased during power step-up as shown in Fig 2.16d. Since the dc voltage is kept constant and $P_{dc} = V_{dc} * I_{dc}$, then the dc current is adjusted by varying the rectifier delay angle in order to change the transmitted dc power (Fig. 2.16b). The ac voltage at the inverter side is varied proportionally to the change in the transmitted power and this can be explained using the power balance equation:

$$P = \sqrt{3} V_{l-l} I_{ac} \cos\theta = \frac{3\sqrt{2}}{\pi} V_{l-l} \left(\cos\alpha + \cos(\alpha + \mu)\right).I_{dc} \qquad (2\text{-}16)$$

The ability of an LCC-HVDC transmission system to control the active power flow can be utilized to provide frequency regulation in the ac network. In this case the power control is activated when significant change in system frequency occurs. Therefore the transmitted power is varied to match the new power demand; the fast change of power achieved by dc control can improve the ac system transient stability and damping of electromechanical oscillations from nearby generators. One practical example of fast power command changes is the Pacific Intertie system where power command changes could be initiated at either the inverter or rectifier end and completed within 50 ms [23].

The disadvantages which limit the application of LCC-HVDC systems, especially to interconnect renewable energy systems are:

1- The converter cannot provide reactive power control at the PCCs as shown in Fig. 2.16f.

2- Low-order harmonics filter is required to eliminate the 5^{th} and 7^{th} harmonics from the ac currents and voltage as shown in Fig. 2.16e.

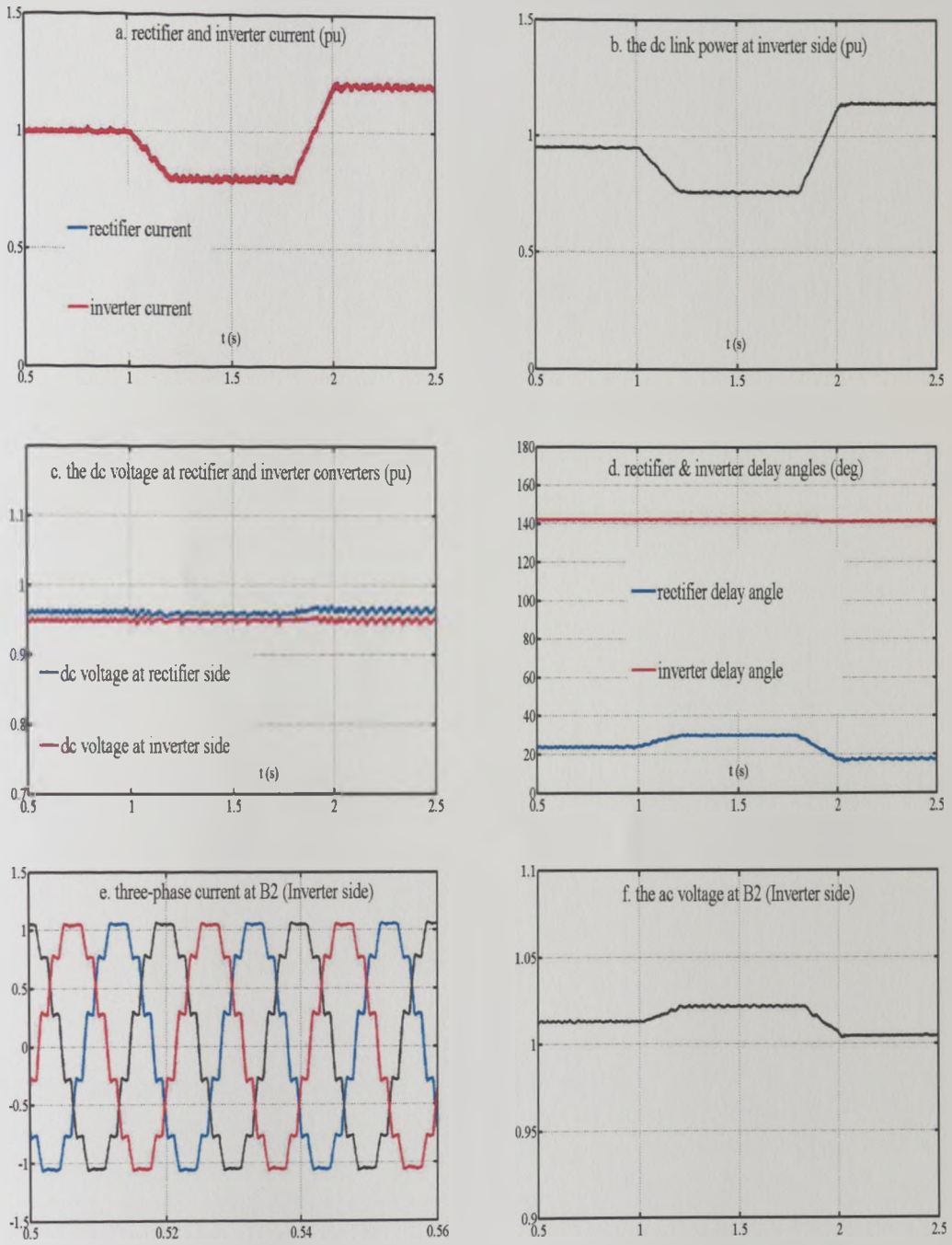


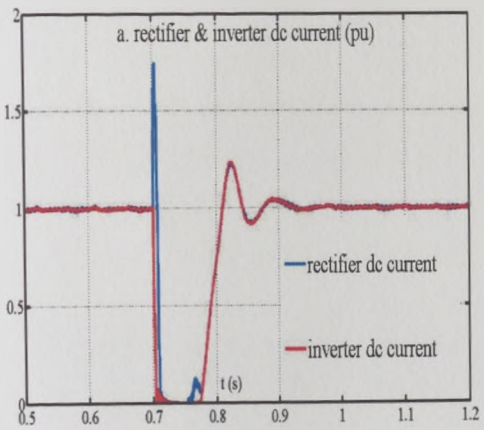
Fig. 2.16: LCC-HVDC behavior during current step (power step).

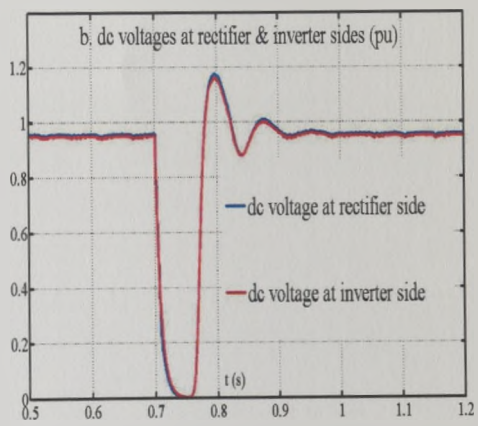
2-10-2 System behavior during dc fault:

Normally the fault at the dc side of a LCC-HVDC system is extinguished by pushing the energy away from the fault. Both converters are operated in inversion mode until the arc is cleared. In this situation the dc fault will not draw any fault current from the ac side due to uni-directional characteristics of the thyristor unit.

In Fig. 2.17 a temporary solid pole-to-pole short-circuit is applied at the end of the dc link close to the inverter at t=0.7s and cleared after 0.05s. The dc line fault leads to temporary loss of the transmitted dc power in-feed to the receiving ac system. When the fault happens the dc voltage and dc current collapse (Figs. 2.17a and b) resulting in elimination of the dc power (which is the product of dc voltage and dc current). The rectifier current tends to increase and the inverter current tends to decrease. The increase in the dc link current is limited by the large smoothing reactor. The delay angle at the rectifier is forced by the protection system to rapidly increase to the maximum limit (166°). The rectifier is operated in inversion mode and the dc voltage is reversed to push the energy away from the fault location.

It is very important to bring the current to zero to extinguish the dc fault and this is achieved by driving the two converters into inversion mode to clear the energy stored in the dc circuit as fast as possible. A limit above 92° to 95° is set in the inverter side to prevent rectifier operation. The total time for fault clearing and return to rated power transfer for intermittent faults is reported to be in the order of 200ms to 300ms [23]. For permanent faults the system is shut down completely until the fault has completely extinguished.





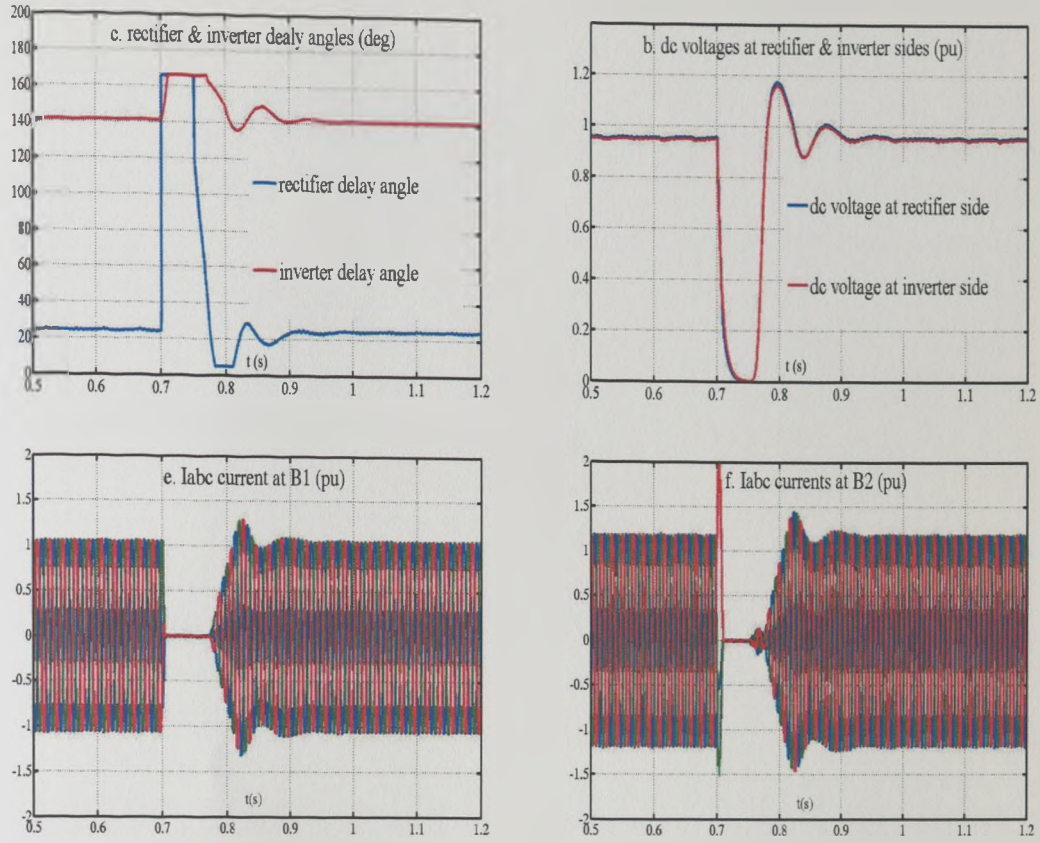


Fig. 2.17: LCC-HVDC behavior during a dc fault.

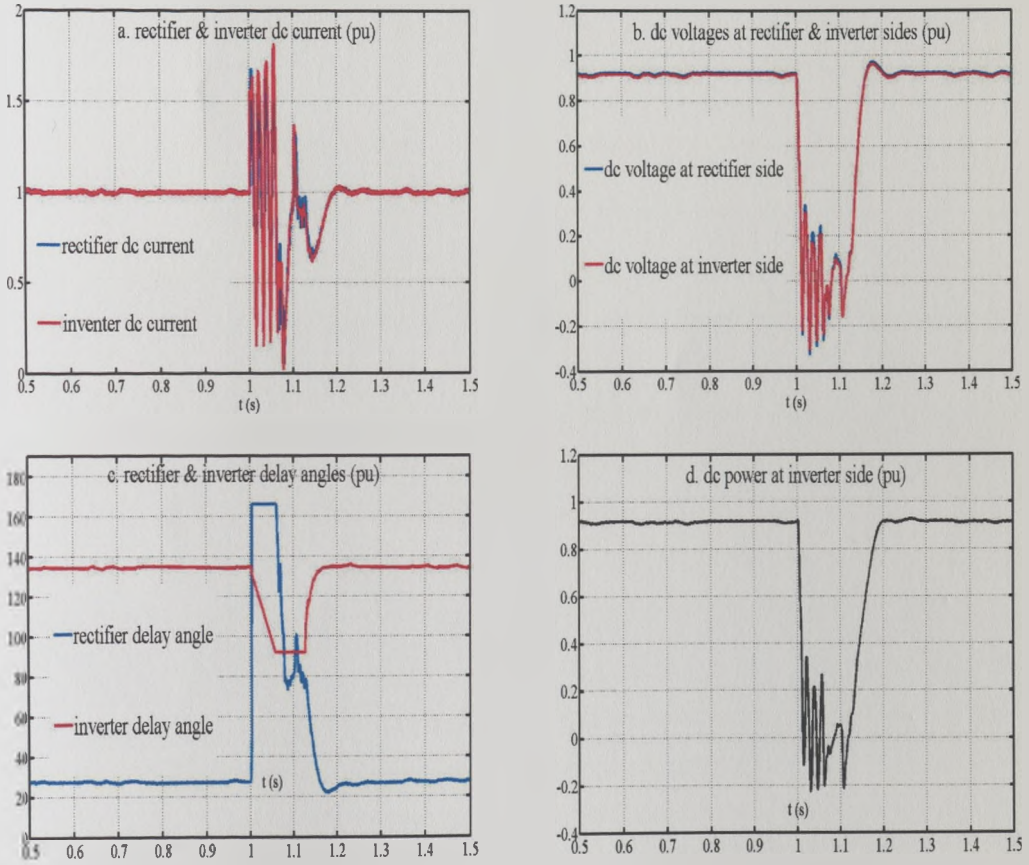
2-10-3 System behavior during a three-phase fault at the inverter side

An ac fault at the rectifier side will lead to temporary lose of the dc power in-feed to the receiving ac system. Depending on the ac system strength, an overvoltage may occur in the converters due to the reactive power compensation devices connected at the point of common coupling. If the fault occurs at the inverter side, commutation failure may be associated with the loss of the dc transmitted power.

At time t=2s a solid three-phase fault-to-ground is applied close to B_2 at the ac side with a fault duration of 5 cycles (100ms for 50Hz). The results obtained from this scenario are presented in Fig. 2.18. When the ac fault occurs at the inverter side the inverter depressed terminal voltage will either reduce further or terminate the transmitted dc power, since $P_{dc} = V_{dc} . I_{dc}$, then both the dc voltages and dc currents will be affected by the fault. The V_{dc} and I_{dc} are altered during the fault period and recover after fault clearance (Fig. 2.18a and b). The protection system forces the delay angle at the rectifier to increase and convert the operation mode to inversion (see Fig. 2.18c) when detecting a negative dc voltage caused by

voltage reversal at the inverter side. Therefore the storage energy will discharge and the fault will be extinguished. The dc system current contribution to the three-phase short-circuits current is limited due to the dc system current rating, and no additional current is injected to the fault location compared to an ac interconnection. The short-circuit current level will depend mainly on the short circuit ratio of the ac system. Fig. 2.18h shows the ac current measured at bus B_2. In a practical LCC-HVDC system the time for the dc system to recover to 90% of its pre-fault power following ac fault clearing is typically in the range of 25 ms to 500 ms [23].

It was observed that in LCC-HVDC transmission system any disturbance in the receiving-end side will affect the sending-end side which results in non-decoupled operation of the two ac networks. This is explained by Fig. 2.18g, the voltage at B_1 is affected by the ac fault at B_2, this feature limits the use of LCC-HVDC systems for wind farm integration because the wind farm may be affected by the fault and open its breakers, and this may lead to black-out unless enough reserve generation is available.



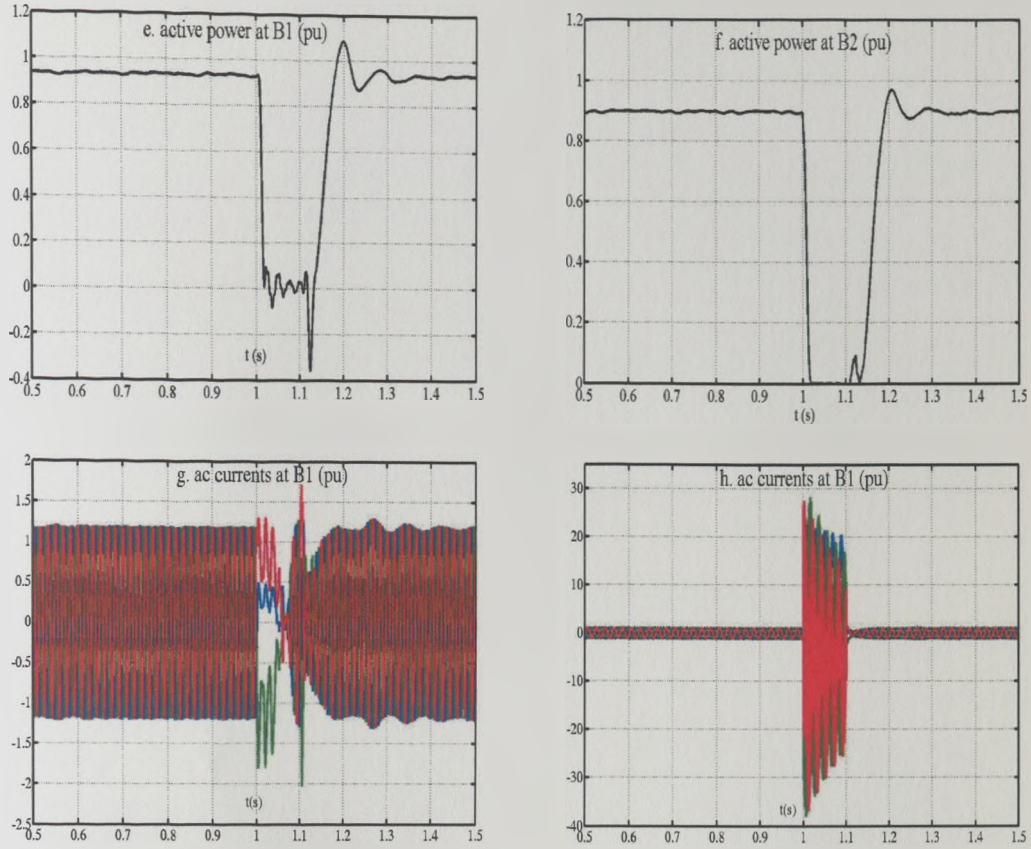


Fig. 2.18: LCC-HVDC behavior during three-phase fault at B2.

2-11 The environmental effect and the limitation of HVDC systems

The electrical environmental effects from HVDC transmission systems can be characterized by the magnetic field, ion effects, and corona effects; the magnetic field is produced by dc current flowing through the conductors and air ions produced by HVDC lines form clouds which drift away from the line when blown by the wind and may come in contact with humans, animals and plants outside the transmission line right-of-way or corridor. The corona effects may produce low levels of radio interference, audible noise and ozone generation. The environmental impact associated with the construction of new HVDC transmission systems are [24], [25]:

- The magnetic field levels generated by the HVDC converters and the dc cables are not harmful for human and marine life in the case of submarine cables.
- Converter stations generate audible noise. This can be minimized using an indoor converter station.

- Visual impact can be minimized using oil-free underground or sub-sea cable.
- The use of oil-free polymeric extruded cables eliminates the risk of pollution as a result of oil leakage.
- Improves transmission efficiency by 25% in applications necessitating the use of submarine cable. This significantly reduces CO_2 emission and defers construction of new transmission systems and power plant.
- Low space requirements and short delivery time may encourage local authorities to ease issuing of planning permissions, and may also reduce public opposition for its construction.
- The corona effects of dc transmission lines lead to a small contribution of ozone production.

The main disadvantages and limitations associated with LCC-HVDC transmission systems are [6]-[26]:

- Requires large reactive power for filtering purposes and to aid thyristor commutation. As a result, the converter station may be bulky and have a large footprint.
- Can not be used to transfer the wind power without the aid of start-up generators or synchronous compensators devices which provide the necessary commutation voltage and reactive power compensation.
- Produce large amount of harmonics and this make the use of harmonics filters obligatory.
- Do not provide independent active and reactive power control.
- The power reversal necessitates the dc link voltage polarity to be reversed [15]-[27].
- There is a theoretical minimum power flow of 10% in the dc link to guarantee satisfactory operation.
- Only suitable for connection of ac networks with a high short circuit ratio.
- Suffers from commutation failure.
- Requires complex control strategies to achieve a multi-terminal configuration; as a result the number of terminals is limited.

2-12 Summary

This chapter presented a comprehensive comparison of ac and dc transmission systems and investigated the advantages of HVDC system over HVAC systems. The LCC converter operation was analyzed at rectifier and inverter operation with simulation results as validation.

The control system design of a LCC-HVDC system was investigated using the V_d-I_d characteristics and hence the overall control system was implemented with the dc system.

The steady-state and transient performance of an LCC-HVDC system was investigated during several operating conditions including: active power step changes, three-phase solid fault at inverter side and dc link fault.

From simulation results it can be concluded that the LCC-HVDC cannot improve the ac fault ride-through capability, the dc converter could just consume the reactive power and can not provide reactive power compensation; low-order harmonic filtering is required to eliminate the harmonics in the ac output voltage and current. All this limit its applications especially with regards to the connection of renewable energy sources.

References

[1] D. M. Larruskain, "Transmission and Distribution Networks: AC versus DC," *IEEE Power Engineering Society General Meeting, 24-28 June 2007, pp. 1-5.*

[2] T. J. Hammons, *et al.*, "Role of HVDC transmission in future energy development," *Power Engineering Review, IEEE,* vol. 20, pp. 10-25, 2000.

[3] P. Jiuping, *et al.*, "AC Grid with Embedded VSC-HVDC for Secure and Efficient Power Delivery," in *Energy 2030 Conference, 2008. ENERGY 2008. IEEE*, 2008, pp. 1-6.

[4] R. Rudervall, *et al.*, "High Voltage Direct Current (HVDC) Transmission Systems Technology Review Paper," *presented at Energy 2000, Washington, D.C, USA, 7-8 March, 2000,* 7-8 March 2000.

[5] V. K. S. Chan-Ki Kim, Gil-Soo Jang,Seong-Joo Lim, Seok-Jin Lee *HVDC Transmission: Power Conversion Application in Power System*: John Wiley & Sons (Asia), Publication, 2009, Singapore.

[6] P. Bresesti, *et al.*, "HVDC Connection of Offshore Wind Farms to the Transmission System," *Energy Conversion, IEEE Transactions on,* vol. 22, pp. 37-43, 2007.

[7] X. Lie, *et al.*, "Power Electronics Options for Large Wind Farm Integration: VSC-Based HVDC Transmission," in *Power Systems Conference and Exposition, 2006. PSCE '06. 2006 IEEE PES*, 2006, pp. 760-767.

[8] K. R. Padiyar, *HVDC power transmission systems: technology and system interactions*. New Delhi: New Age International (P) Limited, Publishers, 2005.

[9] J. Arrillaga, *et al.*, *Flexible Power Transmission Systems-The HVDC Options*: John Wiley & Sons, Publication, 2007.

[10] V. K.Sood, *HVDC and FACTS Controllers Application of Static Converter in Power System*: Kluwar Academic Publisher, 2004.

[11] M. H. Rashid, *Power Electronics Handbook*: Academic Press, 2001.

[12] "IEEE Guide for Planning DC Links Terminating at AC Locations Having Low Short-Circuit Capacities," *IEEE Std 1204-1997,* p. i, 1997.

[13] V. G. Agelidis, *et al.*, "Recent Advances in High-Voltage Direct-Current Power Transmission Systems," in *Industrial Technology, 2006. ICIT 2006. IEEE International Conference on*, 2006, pp. 206-213.

[14] N. Flourentzou, *et al.*, "VSC-Based HVDC Power Transmission Systems: An Overview," *IEEE Trans on Power Electronics,*, vol. 24, pp. 592-602, 2009.

[15] P. Kundur, *Power System Stability and Control*: Electric Power Research Institute, Power System Engineering Series, 1994.

[16] J. Arrillaga, *High Voltage Direct Current Transmission*, 2nd Edition ed.: The Institution of Electrical Engineers, 1998.

[17] *Article: CCC-Capacitor Commutated Converters, Available at online at ABB website.*

[18] M. Meisingset and A. M. Gole, "A comparison of conventional and capacitor commutated converters based on steady-state and dynamic considerations," in *AC-DC Power Transmission, 2001. Seventh International Conference on (Conf. Publ. No. 485)*, 2001, pp. 49-54.

[19] O. Wasynczuk, "Modeling and Dynamic Performance of a Line-Commutated Photovoltaic Inverter System," *Power Engineering Review, IEEE,* vol. 9, pp. 35-36, 1989.

[20] L. Lingxue, *et al.*, "Studies of Commutation Failures in HVDC System Based on Hypersim," in *Power System Technology, 2006. PowerCon 2006. International Conference on*, 2006, pp. 1-7.

[21] D. Paice, *Multipulse Methods for Clean Power*: IEEE PRESS, 1999, 1999.

[22] Y. Iwatta, *et al.*, "Simulation Study Of A Hybrid Hvdc System Composed Of A Self-commutated Converter And A Line-commutated Converter," in *Sixth International Conference on AC and DC Power Transmission,* , 1996, pp. 381-386.

[23] *Review of HVDC Link Technology Issues, Electricity Network Investment (ENI), March 2009.*

[24] W. Shu, *et al.*, "Economic assessment of HVDC project in deregulated energy markets," in *Electric Utility Deregulation and Restructuring and Power Technologies, 2008. DRPT 2008. Third International Conference on*, pp. 18-23.

[25] A. Gustafsson, *et al.*, "Light, Safe and Effective: HVDC Light Cable System are the Future of Power Transmission," *ABB Review 2008, available online at ABB website.*

[26] Z. Chengyong, *et al.*, "A Novel HVDC Transmission System with Parallel Large Capacitor Connected in the DC Side of the Rectifier and Its Technical Feasibility," in *Transmission and Distribution Conference and Exhibition: Asia and Pacific, 2005 IEEE/PES*, 2005, pp. 1-5.

[27] Y. Isayama, *et al.*, "The polarity reversal properties of power cable," in *Dielectric Liquids, 1999. (ICDL '99) Proceedings of the 1999 IEEE 13th International Conference on*, 1999, pp. 408-413.

Chapter Three

High-voltage direct current transmission systems based on Voltage Source Converter (VSC-HVDC)

3-1 Introduction

High-voltage dc transmission systems based on voltage source converters (VSC-HVDC) were developed to address the shortcomings associated with the CSC-HVDC systems. VSC converters use semiconductor switching devices which can be switched ON and OFF at any time such as IGBT, GTO, and IGCT. Hence, in VSCs, the current can be made to lead or lag the ac voltage, and so the converter can consume or supply reactive power to the connected ac network eliminating the need for reactive power compensation devices. The advantages of the voltage source converter technology are [1-3]:

- In VSC-HVDC schemes the converter is controlled using a Pulse Width Modulation (PWM) switching strategy that allows independent control of the magnitude and phase angle of the ac-side voltage. This makes it possible to control the real and reactive power independently
- The use of PWM with a switching frequency in the range of 1 to 2 kHz is sufficient to separate the fundamental voltage from the sidebands, and suppress the harmonic components around and beyond the switching frequency components. This significantly reduces filtering requirements.
- Power flow can be reversed instantaneously without the need to reverse the polarity of the dc link voltage.
- As the voltage source converter is capable of generating leading and lagging reactive power, the converter station can be used to provide voltage support to the ac network whilst transmitting the active power.
- Since the voltage source converter actively controls the output current, the VSC-HVDC contribution to the fault current during ac faults is limited to rated current or less, and the converter can remain in operation to provide voltage support to the ac networks, provided the ac network remains stable.
- Black-start capability is provided, which is the ability to start/or restore power to a dead network. This feature eliminates the need for a start-up generator in applications where footprint is critical or expensive such as with offshore wind farms.

- In cases where there is no need to transmit active power between the two ends, a VSC-HVDC can operate in sleep mode (zero active power), and both converter stations operate as two independent STATCOMs to regulate the ac network voltages.
- VSC-HVDC can be controlled to provide fast frequency/or damping support to the ac networks through active power modulation. This feature can be used to stabilize future power systems with high penetration of renewable energy.

A comparison of the characteristics of the voltage source converter and current source converter is shown in Table 3-1.

Table 3.1: Voltage source converter (VSC) and current source converter (CSC) comparison [4-5].

	CSC	VSC
On ac side	▪ Acts as constant voltage source ▪ Capacitor is the energy storage device ▪ Requires large ac harmonic filter ▪ Requires reactive power compensation	▪ Acts as constant current source ▪ Inductor is the energy storage device ▪ Requires small ac harmonic filter ▪ A converter acts as reactive power compensator
On dc side	▪ Acts as constant current source ▪ Inductor is the energy storage device ▪ Requires dc filter ▪ Provides inherent fault current limiting features	▪ Acts as constant voltage source ▪ Capacitor is the energy storage device ▪ The energy storage capacitor acts as dc filter ▪ Problematic for dc faults as the charged capacitor will discharge into the fault
Switches	▪ Line-commutated switches. ▪ Switching occurs at system frequency ▪ Lower switching losses	▪ Self-commutated switches ▪ Switching occurs at higher frequency ▪ Higher switching losses

3-2 Principle of Voltage Source Converter Operation

Consider a converter connected to an ac system through a lossless reactor as shown in Fig. 3.1a. The VSC can be represented by equivalent ac and dc circuits as shown in Fig. 3.1b, the VSC is modeled as a controlled voltage source at the ac side and as controlled current source at the dc side [6]. The output waveform of the VSC is given by the following equation [7-8]

$$v_c = \frac{V_{dc}}{2} M \sin(\omega t + \delta) \tag{3-1}$$

where M is the modulation index, V_{dc} the dc voltage, ω is the system frequency, and δ is the phase shift of the output voltage. The VSC controller can adjust the variables M, and δ to give any combination of voltage and phase shift and hence, control the active and reactive power flows.

The current source is calculated based on the power balance at the ac and dc side of the converter. The current balance equation on the dc side of the converter is:

$$I_{dc} = C\frac{dV_{dc}}{dt} + I_{cc} \tag{3-2}$$

The power balance equation (with converter losses neglected) is:

$$P_{ac} = \sqrt{3} v_c I_s \cos\theta = P_{dc} = V_{dc} I_{dc} \tag{3-3}$$

where θ is the phase angle of the ac side. Therefore, the controlled current source value is:

$$I_{ac} = P_{ac} / V_{dc} \tag{3-4}$$

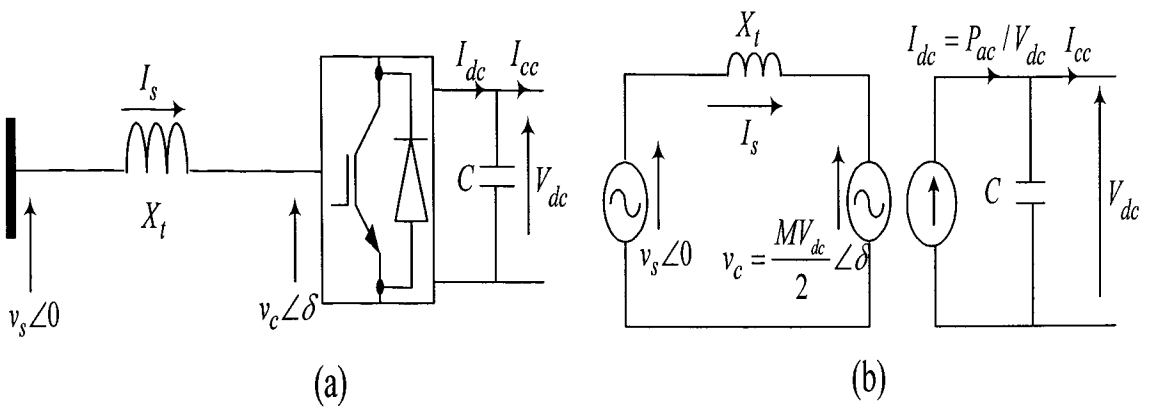


Fig. 3.1: (a) VSC connected to an ac system; (b) equivalent ac and dc circuits.

The active and reactive power flows between the VSC and the ac network can be expressed respectively as [9-10]:

$$P = \frac{v_c * v_s \sin(\delta)}{X_t} \tag{3-5}$$

$$Q = \frac{v_c * v_s \cos(\delta)}{X_t} - \frac{V_c^2}{X_t} \tag{3-6}$$

With respect to equations (3-5) and (3-6), the following observations can be drawn:

1. The active power flow is controlled by the phase angle δ. If $\delta > 0$ the active power flow is from the converter to the ac system otherwise the power flow is in the opposite direction.

2. The reactive power flow is controlled by the ac source voltage v_s, and the VSC converter voltage v_c. The converter generates reactive power if $v_c > v_s$ and consumes it for $v_c < v_s$.

The reactive power generation or consumption can be used to control the ac voltage of the network. In this case the VSC acts as a static reactive power compensator with instantaneous response because the VSC has no inertia. The ac current and voltage of the VSC can have any phase relationship, and the converter can act as a rectifier or an inverter with leading or lagging reactive power. Fig. 3.2 shows the active-reactive power characteristics (P-Q diagram) of VSC converter [3].

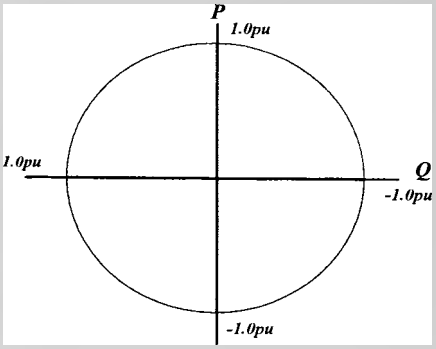


Fig. 3.2: *PQ* diagram of VSC converter.

3-3 Components of VSC-HVDC

The schematic of a typical VSC- HVDC system is shown in Fig. 3.3 [2, 11]

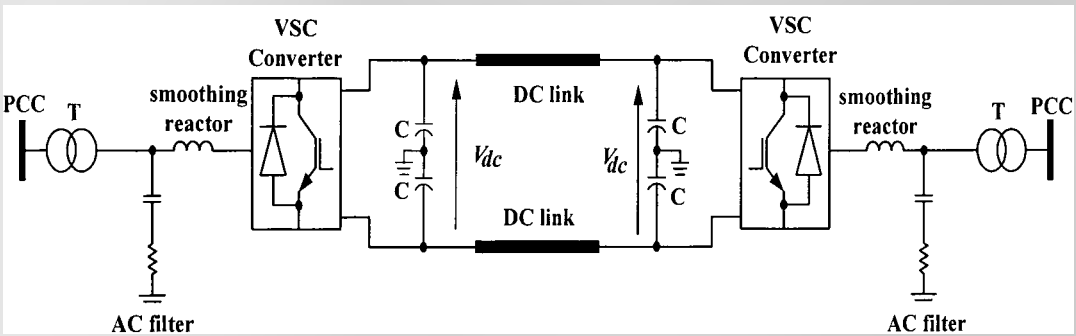


Fig. 3.3: Schematic of a typical VSC-HVDC system.

3-3-1 VSC Converter

A VSC uses IGBTs with anti-parallel freewheeling diode as switching devices. To achieve the required ratings of HVDC transmission, a number of switches are connected in series to build a single unit. For instance, 3.3 kV valves are typically used in HVDC systems. The number of series-connected IGBTs required to withstand the converter rating is increased to provide a suitable redundancy if any sudden failure occurs in some of the IGBT switches.

The VSC switching devices can be connected in many ways to build different types of converter configurations such as: two-level converter, three-level converter or multi-level converter (more than three levels), as shown in Fig. 3.4.

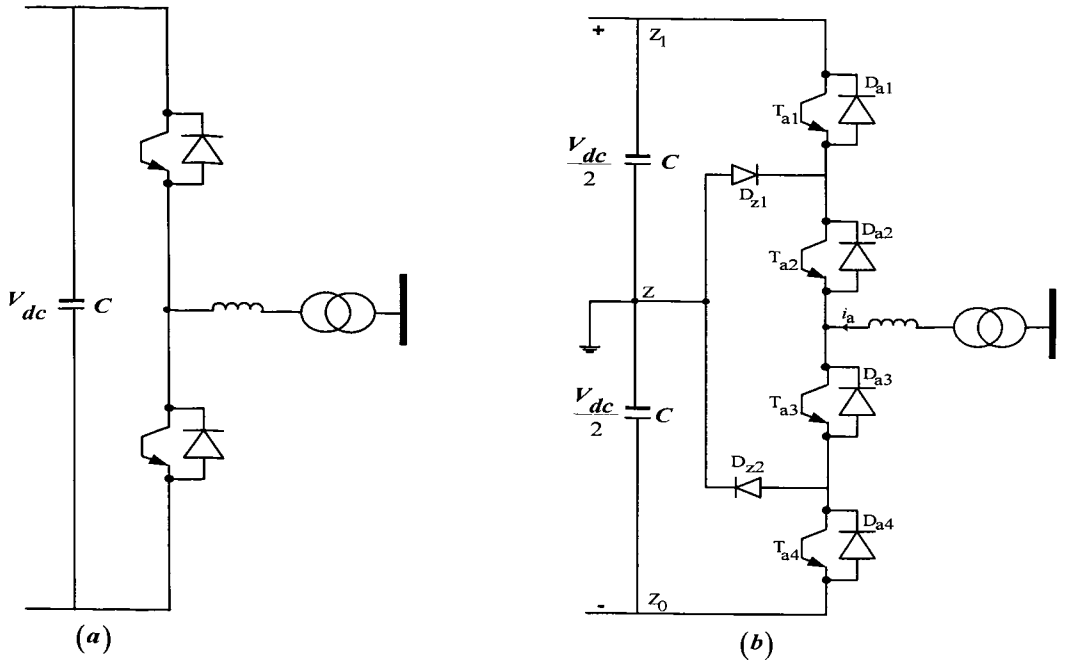


Fig. 3.4: VSC converter: (a) two-level converter; (b) three-level converter.

3-3-2 Coupling Transformers

In a VSC-HVDC system, the ac filters are installed between the smoothing reactor and the transformer. The transformer is not exposed to harmonics or dc voltages like transformers in a conventional HVDC system. Hence, a normal transformer without special arrangement/specifications is used. In general, the functions of the transformers are:

- To transform the voltage of the ac system to a level suitable for the converter.
- Provide a reactance between the converter and the ac system to limit and control the ac current.

3-3-3 Smoothing reactors

The smoothing reactor facilitates controlling the active and reactive power flow by regulating the currents through them. Additional functions are: act as harmonic filters to reduce the harmonics in voltage and current waveforms, and to limit the short-circuit current.

3-3-4 ac harmonic filters

The switching of the IGBTs using high-frequency PWM technique produces only high-order harmonic components around and beyond the switching frequency components. Hence, passive high-pass filters are only needed to eliminate high-order harmonic components to prevent them from causing malfunction of the ac system equipment, or from generating radio and telecommunication disturbances.

3-3-5 dc capacitors

Two capacitors with the same size are located at the end of the dc sides. The main objective of the dc capacitors is to keep the power balance during transient conditions and to reduce the harmonics on the dc side. Equation (3-7) is used to calculate the dc capacitor size [12]:

$$\tau = \frac{0.5CV_{dc}^2}{S_n} \tag{3-7}$$

Where τ is the time constant, C is the dc capacitor, V_{dc} is the dc voltage and S_n is the nominal power of the converter. The time constant is equal to the time needed to charge the capacitor from zero to the rated voltage V_{dc} if the converter is supplied with a constant active power equal to S_n. To obtain a smooth and sinusoidal voltage waveform, the dc voltage must be greater than 2.0 times the ac voltage (rms value) for PWM, and greater than 1.74 for PWM with third-harmonic injection [13].

3-3-6 dc cables

The dc cables are typically XLPE (Cross-Linked Poly-Ethylene) polymer extruded cables. Polymeric cables are the best choice for HVDC transmission because of their mechanical strength, flexibility and low weight. The insulation system is triple-extruded, i.e. the conductor screen, the insulation and the insulation screen are all extruded simultaneously [4] [14].

The economic and environmental benefits of the dc cable compensate for the cost of the VSC converters [15]:

- For example, the capacitive nature of ac submarine cables requires installation of reactive power compensation devices for transmission distances greater than 50km.
- The losses in ac cables due to the charging current are higher than in dc cables.
- The investment cost for installation of only one dc cable is less than that for installing three ac cables.
- The generation of magnetic fields and the corona effects of a dc cable lead to a small contribution of ozone production.

3-4 VSC-HVDC steady-state model

The equivalent ac/dc/ac circuit of a VSC-HVDC, as that in Fig. 3.3, is shown in Fig. 3.5 (the ac harmonics filter is neglected). To simplify the description, the interface transformers are represented with their leakage reactance (X_T) in series with the winding resistance (R_T), while the smoothing reactor is represented with its reactance (X_F). v_c is the VSC converter output

voltage and v_s is the terminal voltage of the ac network. V_{dc} is the converter dc voltage; (R_{dc}) and (L_{dc}) are the resistance and inductance of the dc link.

The ac system voltage and current relationships at the sending and receiving-ends are shown in the vector diagrams of Fig. 3.6. In these diagrams δ is the phase angle difference between the ac system voltage and the VSC converter voltage, θ_s is the phase angle difference between the ac system voltage and the ac current flowing from or into the converter, while θ_c is the phase angle difference between the VSC converter voltage and the ac current. The subscripts "1" and "2" represent the variable associated to the sending-end and receiving-end stations, respectively.

The following expressions apply to the active and reactive powers at the sending and receiving ends of the link at fundamental frequency:

$$P_1 = \frac{v_{s1}v_{c1}}{X_{T1}+X_{F1}} sin\delta_1 \tag{3-8}$$

$$P_2 = \frac{v_{s2}v_{c2}}{X_{T2}+X_{F2}} sin\delta_2 \tag{3-9}$$

$$Q_{sc1} = \frac{v_{s1}(v_{s1} - v_{c1}cos\delta_1)}{X_{T1}+X_{F1}} \tag{3-10}$$

$$Q_{sc2} = \frac{v_{s2}(v_{s2} - v_{c2}cos\delta_2)}{X_{T2}+X_{F2}} \tag{3-11}$$

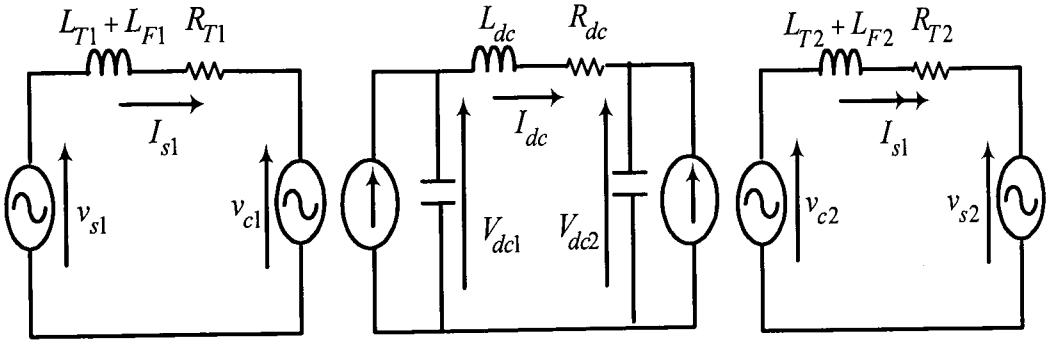


Fig. 3.5: Equivalent circuit of a VSC-HVDC transmission system.

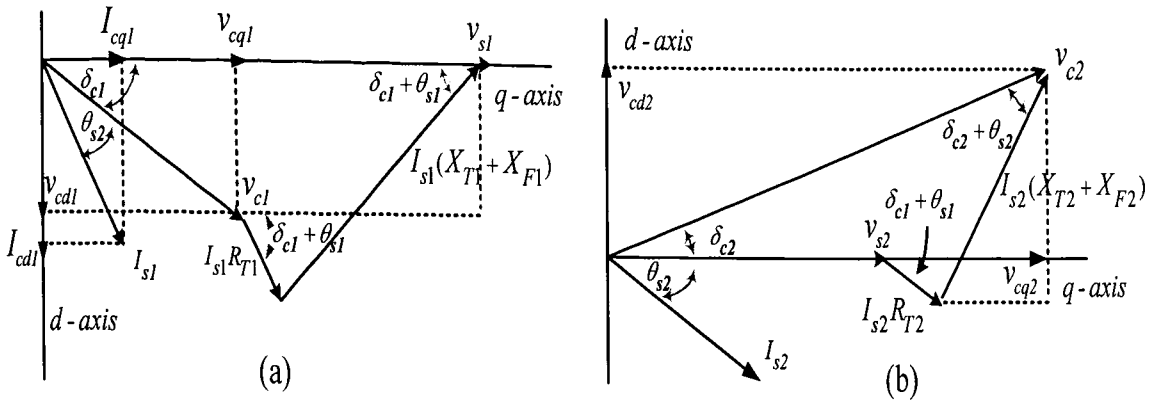


Fig. 3.6: Vector diagram representation of a VSC-HVDC System: (a) sending end; (b) receiving end.

If the system in Fig. 3.5 is operating in steady-state mode then all variables in the system are either constant or sinusoidal with time. The following relationships are obtained from the vector diagram in Fig. 3.6a (the sending-end VSC converter acting as rectifier):

The voltage at the VSC converter terminal is:

$$V_{c1}\cos\delta_1 = V_{s1} - I_{s1}R_{T1}\cos(\theta_1+\delta_1) - I_{s1}X_{T1}sin(\theta_1+\delta_1) \tag{3-12}$$

From the vector diagram, the following relation is derived:

$$I_{s1}X_{T1}\cos(\theta_1+\delta_1) - I_{s1}R_{T1}\sin(\theta_1+\delta_1) = V_{c1}\sin\delta_1 \tag{3-13}$$

Using trigonometric equations and making some arrangements the load angle is

$$tan\delta_1 = \frac{I_{s1}X_{T1}cos\theta_1 - I_{s1}R_{T1}sin\theta_1}{v_{c1} + I_{s1}X_{T1}sin\theta_1 + I_{s1}R_{T1}cos\theta_1} \tag{3-14}$$

The *dq* components of the voltage and current at the VSC converter terminal are:

$$I_{sd1} = -I_{s1}\sin(\delta_1+\theta_1) \quad \& \quad I_{sq1} = I_{s1}\cos(\delta_1+\theta_1) \tag{3-15}$$

$$v_{cd1} = -V_{c1}\sin\delta_1 \quad \& \quad v_{cq1} = V_{c1}\cos\delta_1 \tag{3-16}$$

Similarly, the relationship for the receiving-end (VSC acting as inverter) is derived from Fig. 3.6b:

The voltage at the VSC terminals is:

$$V_{c2}\cos\delta_2 = V_{s2} + I_{s2}R_{T2}\cos(\theta_2+\delta_2) + I_{s2}X_{T2}sin(\theta_2+\delta_2) \tag{3-17}$$

The load angle is expressed as:

$$tan\delta_2 = \frac{I_{s2}X_{T2}cos\theta_2 - I_{s2}R_{T2}sin\theta_2}{v_{c2} + I_{s2}X_{T2}sin\theta_2 + I_{s2}R_{T2}cos\theta_2} \tag{3-18}$$

3-5 The two-level voltage source converter

Fig. 3.7a shows the circuit diagram of a three-phase two-level VSC converter which consists of three legs, one for each phase. Each converter leg is composed of two IGBTs switches, T_1 and T_2, with corresponding anti-parallel free-wheeling diodes, D_1 and D_2,. The midpoint of the capacitors, n, is used as a reference for the ac output voltage.

There are four possible current paths in a single-phase two-level converter as shown in Fig. 3.7b [11, 16]. When the upper switch is ON, the output voltage is $+V_{dc}$ and the current flows through the upper free-wheeling diode if the current is negative or it flows through the upper IGBT if the current is positive. When the lower switch is ON, the output voltage is $-V_{dc}$ and the current flows through the lower IGBT if the current is negative or through the lower free-wheeling diode if the current is positive. Table 3.2 shows the possible condition paths in one leg of the two-level converter (leg A).

If the two switches are turned ON at the same time this would create a short circuit of the dc capacitors, therefore before one switch is turned ON, the opposite switch must be turned OFF. This causes a small blanking period where none of the switches are ON and the current path is via the free-wheeling diodes [11]

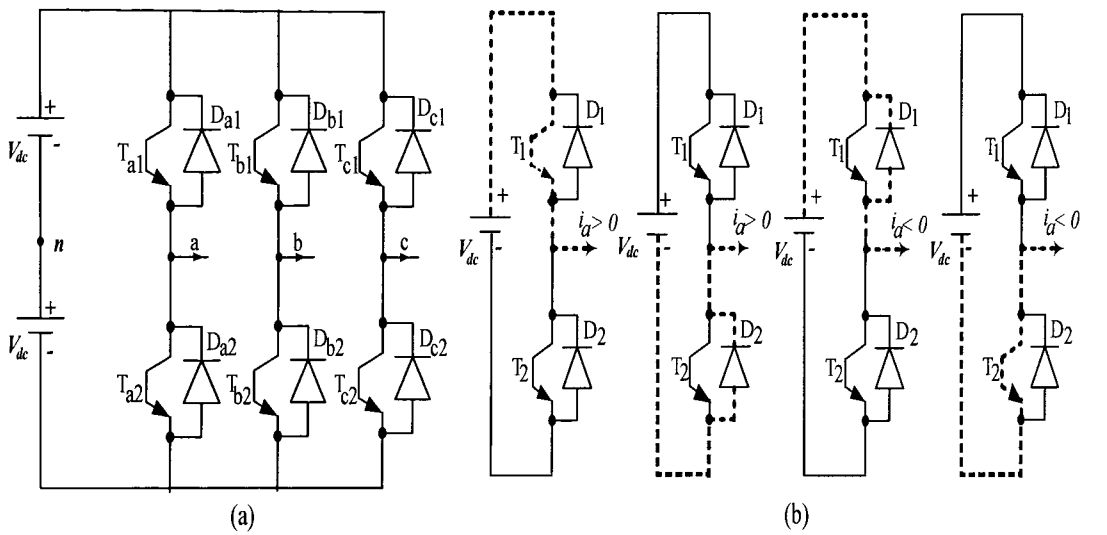


Fig. 3.7: Two-level voltage source converter and the possible conduction current paths in one leg.

Table 3.2: Switching states of a 2-level voltage source converter.

Conducting devices		Switching conditions		Terminal voltage
$i_a > 0$	$i_a < 0$	T_{a1}	T_{a2}	
T_{a1}	D_{a1}	ON	OFF	V_{dc}
D_{a2}	T_{a2}	OFF	ON	$-V_{dc}$

Fig. 3.8 shows the SPWM of a three-phase, two-level converter, where v_{az}, v_{bz}, and v_{cz} are the sinusoidal reference waveforms displaced in time by 120°.

$$v_{az} = V_m sin\omega t = V_{dc} M sin\omega t \tag{3-19}$$

$$v_{bz} = V_m sin(\omega t - \frac{2\pi}{3}) = V_{dc} M sin(\omega t - \frac{2\pi}{3}) \tag{3-20}$$

$$v_{bz} = V_m sin(\omega t - \frac{4\pi}{3}) = V_{dc} M sin(\omega t - \frac{4\pi}{3}) \tag{3-21}$$

The three-phase, line-to-line output voltages are given as:

$$v_{ab} = v_{az} - v_{bz} = M\sqrt{3}\, V_{dc} sin(\omega t + \frac{\pi}{6}) \tag{3-22}$$

$$v_{ab} = v_{bz} - v_{cz} = M\sqrt{3}\, V_{dc} sin(\omega t - \frac{\pi}{2}) \tag{3-23}$$

$$v_{ca} = v_{cz} - v_{az} = M\sqrt{3}\, V_{dc} sin(\omega t + \frac{5\pi}{6}) \tag{3-24}$$

The phase and line output voltages for a three-phase, two-level converter operating with M_a=0.85, M_f=15, f=50Hz and f_{cr}=900Hz are shown in Fig. 3.8.

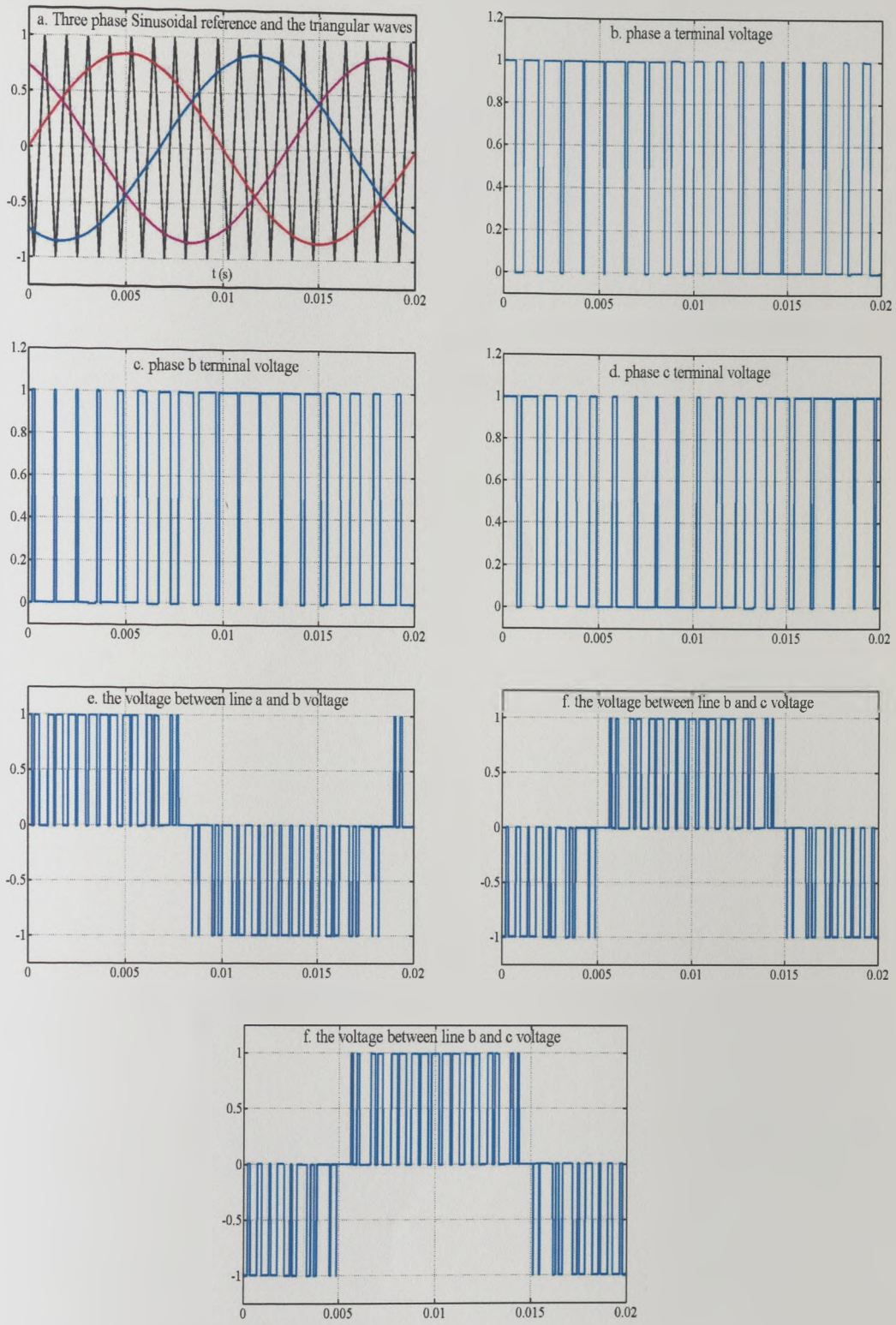


Fig. 3.8: SPWM of a three-phase two-level converter.

3-6 The three-level voltage source converter

Fig. 3.9 shows the simplified circuit diagram of a three-level NPC converter. The converter leg A is composed of four IGBTs switches, T_{a1} to T_{a4}, with four anti-parallel diodes D_{a1} to D_{a4}. On the dc side of the converter, the dc bus capacitor is split into two, providing a neutral point, z. The diodes connected to the neutral point, D_{z1} and D_{z2}, are the clamping diodes. When switches T_{a2} and T_{a3} are turned ON, the converter output terminal A is connected to the neutral point through one of the clamping diodes.

The voltage across each of the dc capacitors is $V_{dc}/2$, which is normally equal to half that of the total dc voltage. With a finite value for C_{a1} and C_{a2}, the capacitors can be charged/discharged by the neutral current i_{az}, causing neutral-point voltage unbalance.

Fig. 3.10 and Table 3.3 summarise all the possible power paths and switching states in the NPC three-level converter. Switching state 'P' denotes that the upper two switches in leg A are ON and the VSC terminal voltage v_{az}, which is the voltage at terminal A with respect to the neutral point z, is $+V_{dc}/2$, whereas 'N' indicates that the lower two switches conduct, leading to $v_{az} = -V_{dc}/2$. Switching state 'O' means that the inner two switches T_2 and T_3 are ON and v_{az} is clamped to zero through the clamping diodes.

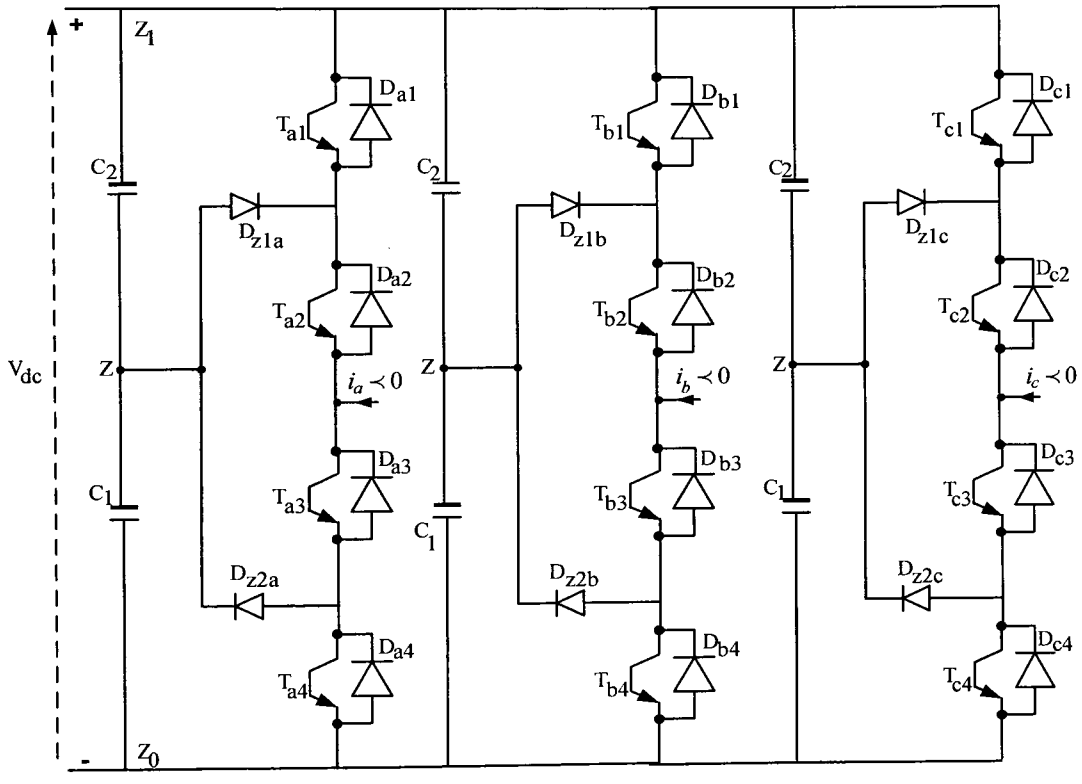
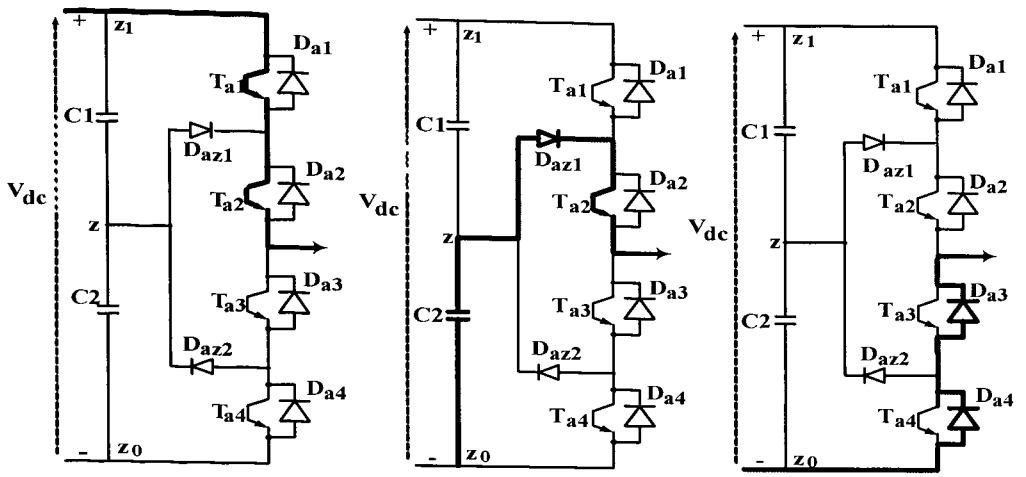
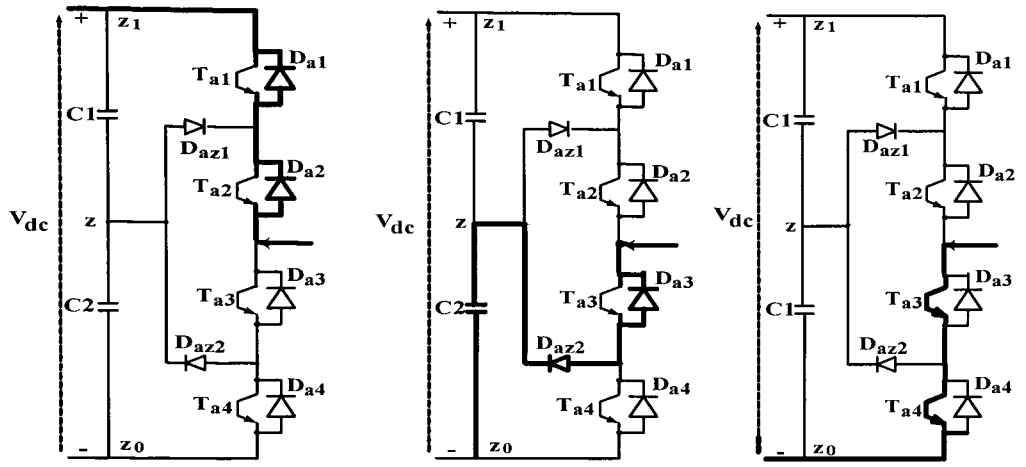


Fig. 3.9: Three-level Neutral-Point Clamped (NPC) voltage source converter.



Conducting devices for $i_a > 0$



Conducting devices for $i_a < 0$

Fig. 3.10: Power paths in one leg of a three-level NPC converter.

Table 3.3: Switching states of a 3-level diode clamped voltage source converter [16-17].

Switching Symbols	Switching conditions				Terminal voltage (v_{az})
	T1	T2	T3	T4	
P	ON	ON	OFF	OFF	$V_{dc}/2$
0	OFF	ON	ON	OFF	0
N	OFF	OFF	ON	ON	$-V_{dc}/2$

Depending on the direction of the load current i_a, one of the two clamping diodes is turned ON. For instance, a positive load current ($i_a > 0$) forces D_{z1} to turn ON and the terminal A is connected to the neutral point z through the conduction of D_{z1} and T_2. It can be observed from Table 3.3 that switches T_1 and T_3 operate in a complementary manner. With one switched ON, the other must be OFF. Similarly, T_2 and T_4 is also a complementary pair.

Fig. 3.11 shows the SPWM of the three-level converter and the corresponding terminal line and phase voltages. The phase waveform for v_{az} has three voltage levels, + $V_{dc}/2$, 0, and – $V_{dc}/2$, based on which the converter is referred to as a three-level converter. The converter line voltages v_{az}, v_{bz}, and v_{cz} are three-phase balanced with a phase shift of $2\pi/3$ between each other. The line-to-line voltage v_{ab} can be found from $v_{ab} = v_{AZ} - v_{bz}$, which contains five voltage levels ($+V_{dc}$, + $V_{dc}/2$, 0, – $V_{dc}/2$, and – V_{dc}).

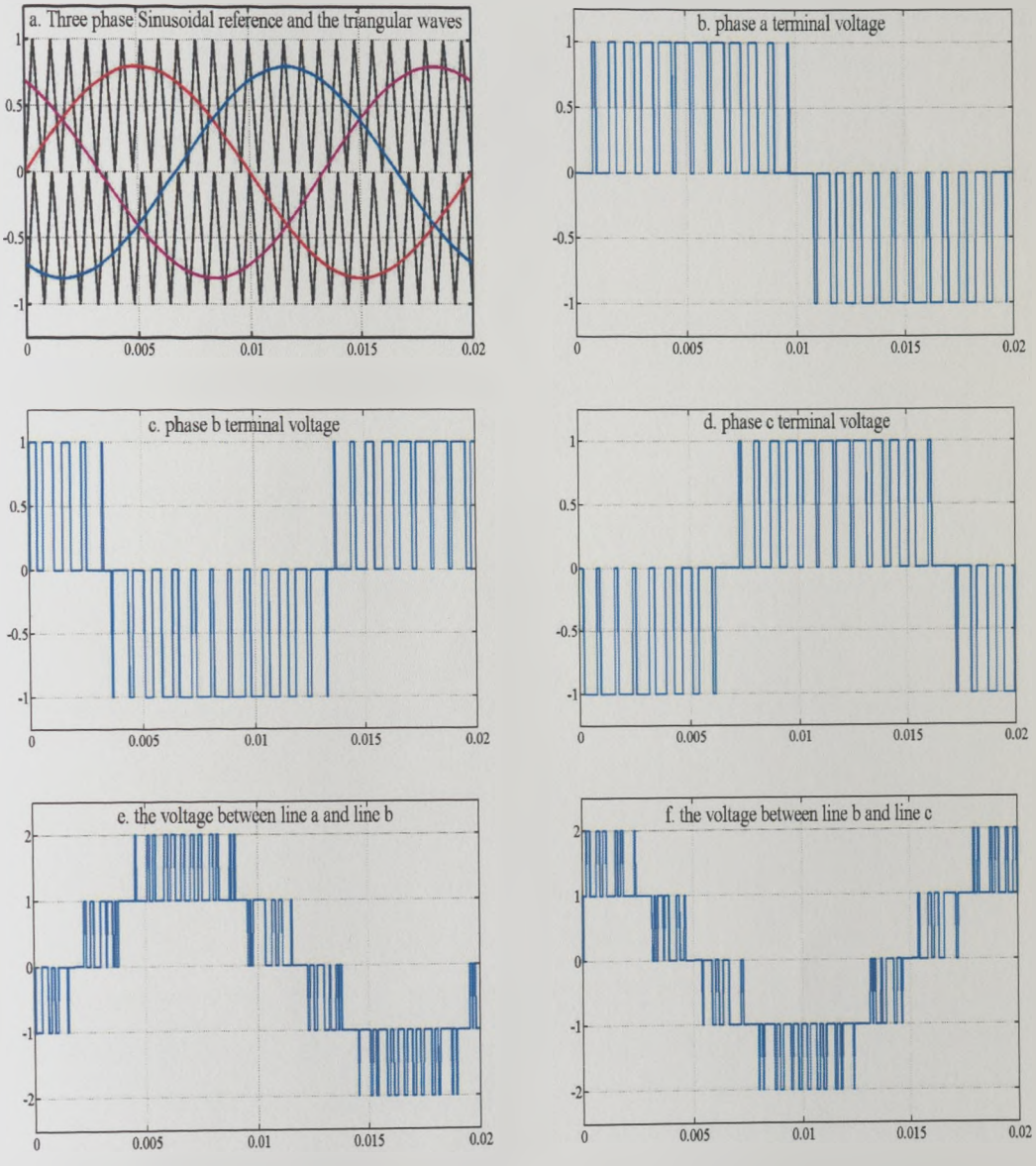


Fig. 3.11: SPWM of the three-level NPC converter.

3-7 Voltage source converter conversion losses

Currently, there are two established approaches for the construction of a VSC-HVDC system. The first approach uses a standard two-level converter or a neutral-point clamped converter with forced-commutated devices such IGBTs. This approach imposes a high insulation requirement on the interfacing transformer due to the high *dv/dt* that results from switching high voltage with relatively low switching frequencies. This arrangement also requires fairly large filters at the output to attenuate the switching frequency components from the output voltage at the point of common coupling.

The second approach uses a two-switch modular multilevel converter with medium voltage devices such as 4.5kV IGBTs [18]. This approach produces lower *dv/dt* (allowing the use of a transformer with standard insulation requirements) and significantly lowers voltage harmonic distortion. This approach requires however, a large number of switching devices and capacitors, and a relatively complex modulation strategy compared to the first approach.

Both approaches produce higher conversion losses compared to the classic HVDC system based on line-commutated or capacitor-commutated current source converters. Estimation of the power losses during the design stage of the VSC-HVDC is essential, because it allows the designers to optimize the overall system performance through a compromise of several design indices. It also helps in the selection of heat-sinking equipment and cooling system for the converters. In general the conversion losses of the VSC converter are composed of conduction and switching losses. There are many methods to calculate and evaluate the losses in a VSC converter such as [19-20]:

a. Practical measure:

In this method the input power and the output power at each component of the VSC-HVDC is measured and the difference are the losses inside the component. This method is reasonably reliable at low voltage and low power transmission.

b. Software method

The VSC converter model is built using the physical and mathematical relationship in every component with reasonable considerations and assumptions. The voltages and currents in converter components are found to calculate the conversion losses. The accuracy of conversion losses calculation depends on how accurate the model is.

c. Analytical method

This method is used during the early stage of converter design to estimate the conversion losses and the cooling system requirements. In this method a numerical relation for power losses is derived for each component (see Appendix B).

3-7-1 The Conduction losses

The conduction losses occur due to the voltage drop across the switching devices during the conduction period [21]. The average conduction losses are computed by averaging the average conduction losses in each switching cycle as follow:

$$P_C = \frac{1}{T}\int_0^T V_f(\omega t) i(\omega t) d\omega t \tag{3.25}$$

Where P_c is the device conduction losses, T is the switching period, $V_f(\omega t)$ is the device forward voltage, $i(\omega t)$ is the current flow through the device in the conduction period. The value of $V_f(\omega t)$ is calculated as follow [22-23]:

$$V_f = V_{f0} + r_f i(t) \tag{3.26}$$

where V_{f0} is the device forward voltage at no load, and r_f is the device forward resistance. The values of V_{f0} and r_f are calculated using the datasheet of device characteristics provided by manufacturing companies as shown in Fig. 3.12. The r_f is the ratio between the Collector-Emitter voltage difference and the collector current difference $\left(r_f = {}^{\Delta V_{CE}}\!/_{\Delta I_C}\right)$, while V_{f0} is the value in the curve corresponding to the actual collector current flow in the device.

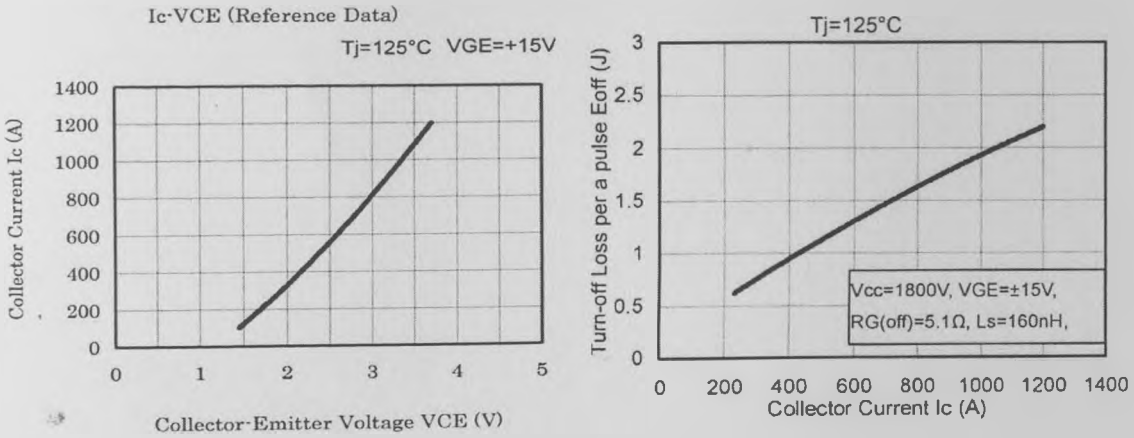


Fig. 3.12: IGBT datasheet.

Substituting equation (3.26) into equation (3.25) gives:

$$P_C = V_f I_{av} + r_f I_{rms}^2 \tag{3-27}$$

Where I_{av} and I_{rms} are the average and the *rms* current through the device in the conduction period respectively, and are calculated as follow:

$$i_{av} = \frac{1}{T_s}\int_0^{T_s} i_a(t)d \tag{3-28}$$

$$i_{rms}^2 = \frac{1}{T_s}\int_0^{T_s} i_a^2(t)d\omega \tag{3-29}$$

3-7-22 Switching losses estimation

The switching losses are the total sum of ON-state switching losses and turn-OFF switching losses, and they depend on the device characteristics, switching frequency, and device current. The switching energy can be expressed as a function of the device current as follow:

$$P_{sw} = \frac{f_S}{2\pi}\int_0^{T_s} k_1 i d\omega t \tag{3-30}$$

where k_1 is the switching resistance obtained from the device datasheet (see Fig. 3.12).

3-8 VSC-HVDC Transmission System Dynamic Model

Fig. 3.13 shows the typical basic structure of a VSC-HVDC transmission system. The ac source voltages denoted by (v_{sa},v_{sb},v_{sc}) are three ideal sinusoidal waveforms displaced by 120° in the time domain. The three-phase current denoted by (i_{sa},i_{sb}, i_{sc}) are source currents flowing from the ac source to the VSC converter or in the reverse direction. The voltages and currents at the VSC terminal are denoted by (v_{ca},v_{cb}, v_{cc}) and (i_{ca},i_{cb}, i_{cc}) respectively; R_t and L_t are the resistance and inductance of the coupling transformer, R_F and L_F are the resistance and inductance of the coupling reactor. The dc side is modeled as a series inductive (L_{dc}) and resistive (R_{dc}) circuit, while C, V_{dc} and I_{dc} are the dc link capacitor, dc link voltage, and dc link current respectively. In Fig. 3.13 the left converter (VSC_1) is assumed to operate as rectifier transforming the power from the ac source side to the VSC dc side. The right converter (VSC_2) is operated as inverter and transforms the power from the VSC dc side to the ac side. The subscripts "*1*" and "*2*" represent the variable belonging to the sending-end station and receiving-end station, respectively.

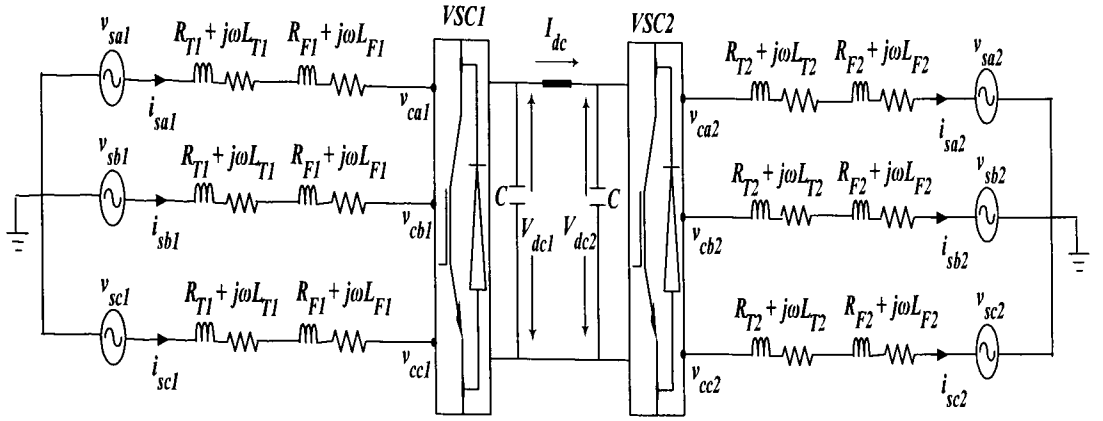


Fig. 3.13: VSC-HVDC Transmission System.

Applying Kirchhoff Voltage Laws in Fig. 3.13 and adopting the time t in seconds and all quantities in per unit, the dynamic equations for the rectifier side are:

$$\frac{di_{sabc}}{dt} = -\frac{R_1}{L_1} i_{sabc} + \frac{1}{L_1}\left(v_{sabc} - v_{cabc}\right) \tag{3-31}$$

Where $R_1=R_{T1}+R_{F1}$ and $L_1=L_{T1}+L_{F1}$

The dynamic equations for the inverter station are:

$$\frac{di_{sabc2}}{dt} = -\frac{R_2}{L_2} i_{sabc2} + \frac{1}{L_2}\left(v_{cabc2} - v_{sabc2}\right) \tag{3-32}$$

Where $R_2=R_{T21}+R_{F2}$ and $L_2=L_{T2}+L_{F2}$

To simplify the design of the control system, the three-phase quantities are expressed in the dq reference frame using the Park transformation matrix given in equation (3-33) as:

$$\begin{bmatrix} f_d \\ f_q \\ f_o \end{bmatrix} = \begin{bmatrix} \cos\theta & \cos(\theta - \frac{2\pi}{3}) & \cos(\theta - \frac{4\pi}{3}) \\ \sin\theta & \sin(\theta - \frac{2\pi}{3}) & \sin(\theta - \frac{4\pi}{3}) \\ \frac{1}{2} & \frac{1}{2} & \frac{1}{2} \end{bmatrix} \begin{bmatrix} f_a \\ f_b \\ f_c \end{bmatrix} = [T] \begin{bmatrix} f_a \\ f_b \\ f_c \end{bmatrix} \tag{3-33}$$

And the inverse Park transformation is:

$$\begin{bmatrix} f_a \\ f_b \\ f_c \end{bmatrix} = \begin{bmatrix} \cos\theta & \cos(\theta - \frac{2\pi}{3}) & \cos(\theta - \frac{4\pi}{3}) \\ \sin\theta & \sin(\theta - \frac{2\pi}{3}) & \sin(\theta - \frac{4\pi}{3}) \\ \frac{1}{2} & \frac{1}{2} & \frac{1}{2} \end{bmatrix} \begin{bmatrix} f_d \\ f_q \\ f_o \end{bmatrix} = [T]^{-1} \begin{bmatrix} f_d \\ f_q \\ f_o \end{bmatrix} \tag{3-34}$$

Applying Park's transformation to equations (3-31) and (3-32), the differential equations for the rectifier side in the *dq* reference are:

$$\begin{aligned}\frac{di_{sd1}}{dt} &= -i_{sd1}\frac{R_1}{L_1} + \omega i_{sq1} + \frac{1}{L_1}\left(v_{sd1} - v_{cd1}\right)\\ \frac{di_{sq1}}{dt} &= -i_{sq1}\frac{R_1}{L_1} - \omega i_{sd1} + \frac{1}{L_1}\left(v_{sd1} - v_{cd1}\right)\end{aligned} \tag{3-35}$$

Similarly, for the inverter side:

$$\begin{aligned}\frac{di_{sd2}}{dt} &= -i_{sd2}\frac{R_2}{L_2} + \omega i_{sq2} + \frac{1}{L_2}\left(v_{cd2} - v_{sd2}\right)\\ \frac{di_{sq2}}{dt} &= -i_{sq2}\frac{R_2}{L_2} - \omega i_{sd2} + \frac{1}{L_2}\left(v_{cd2} - v_{sd2}\right)\end{aligned} \tag{3-36}$$

If the converter is assumed lossless, the power balance equation between the dc and ac sides in the rectifier and inverter, respectively, are:

$$\begin{aligned}V_{dc1}I_{dc} &= \frac{3}{2}(v_{cd1}i_{sd1} + v_{cq1}i_{sq1}) - CV_{dc1}\frac{dV_{dc1}}{dt}\\ V_{dc2}I_{dc} &= \frac{3}{2}(v_{cd1}i_{sd1} + v_{cq1}i_{sq1}) + CV_{dc2}\frac{dV_{dc2}}{dt}\end{aligned} \tag{3-37}$$

Equations (3-35), (3-36), and (3-37) are the differential dynamic equations representing the VSC-HVDC transmission system.

In a converter with sinusoidal PWM the relationship between the modulation index M, dc link voltage and the dq components of the ac voltage are given by:

$$v_{cd} = \frac{1}{2}MV_{dc}\cos\delta \tag{3-38}$$

$$v_{cq} = \frac{1}{2}MV_{dc}\sin\delta \tag{3-39}$$

The instantaneous total power in the time domain is expressed as:

$$S(t) = v_a(t)i_a(t) + v_b(t)i_b(t) + v_c(t)i_c(t) \tag{3-40}$$

Applying the park transformation to equation (3-40) yields:

$$p(t) = \frac{3}{2}[v_d(t)i_d(t) + v_q(t)i_q(t)] \tag{3-41}$$

$$q(t) = \frac{3}{2}[-v_d(t)i_q(t) + v_q(t)i_d(t)] \tag{3-42}$$

3-9 Control of the VSC-HVDC

In a VSC, the control of the ac voltage and active and reactive power flow is done by means of PWM technique. With PWM modulation, the VSC controller can adjust the modulation index (M), and converter phase angle (θ) to give any combination of voltage and phase shift and hence, control the active power, reactive power, ac voltage and dc link voltage. Vector control is the most popular technique to modify M and θ to achieve the desired control function. In vector control the three-phase rotating voltage and current are transformed to the dq reference before calculating the modulation index and the phase angle. It is then synchronized with the ac three-phase voltages using a phase-locked-loop (PLL). The controlled variable is forced to follow the reference values to generate the desired values of M and θ and fed their values to the VSC. The control system of the VSC converters is composed of the inner controller and the outer controller. The main function of the inner controller is to control the currents in the complete range of actuation, and to ensure that the converter is not overloaded to protect the converter from transient and to ensure that the converter is not overloaded to protect the converter from transient currents due to system disturbances. The outer controller is responsible for supplying the reference values to the inner controller. Fig 3.14 shows an example of VSC control system including: the inner and outer controller, and phase-locked-loop (PLL).

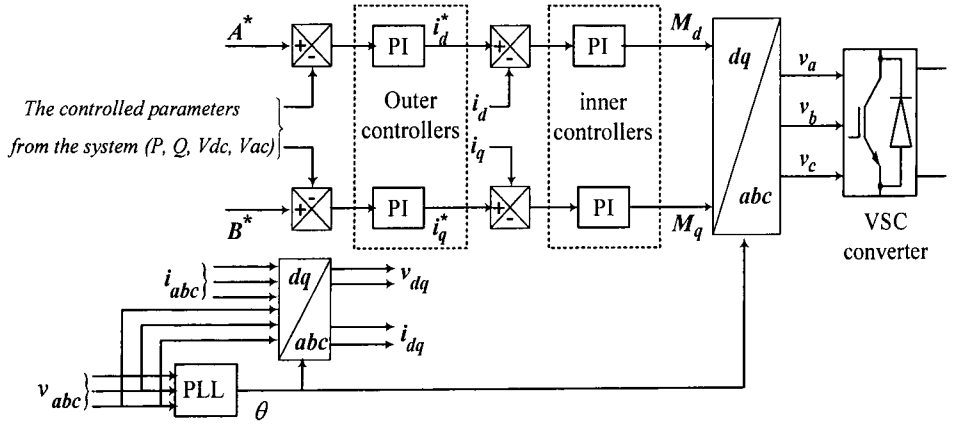


Fig. 3.14: Overall Control of a VSC-HVDC.

There are four possible control modes to be chosen from as outer controller for the control system of the VSC converter [24]:

(1) dc voltage control mode.
(2) Active power control mode.
(3) ac voltage control mode.
(4) Reactive power control mode.

The choice of controller to be added to the VSC converter (not all controllers can be used at the same time), depends on the application of the VSC-HVDC, but in all cases an option for the dc voltage controller is necessary in all applications to ensure the power balance between the sending and receiving converters.

3-9-1 The inner controller design

In order to design an inner current controller the cross-coupling terms in equations (3-35) are decoupled as follow [25-26]:

$$v_{sd1} = u_{d1} - \omega L_1 i_{q1} + v_{d1} \tag{3-43a}$$

$$v_{sq1} = u_{q1} + \omega L_1 i_{d1} + v_{q1} \tag{3-43b}$$

Substituting equation (3.43) into equation (3.35) then

$$\frac{d}{dt}\begin{bmatrix} i_{sd1} \\ i_{sq1} \end{bmatrix} = \begin{bmatrix} -R_1/L_1 & 0 \\ 0 & -R_1/L_1 \end{bmatrix}\begin{bmatrix} i_{sd1} \\ i_{sq1} \end{bmatrix} + \begin{bmatrix} 1/L_1 & 0 \\ 0 & 1/L_1 \end{bmatrix}\begin{bmatrix} u_{d1} \\ u_{q1} \end{bmatrix} \tag{3-44}$$

where u_d and u_q are new variables obtained from the inner controllers which regulate the dq-axis currents. The values of u_d and u_q are defined as:

$$u_{d1} = k_{pi}(i_{d1}^* - i_{d1}) + k_{ii}\int(i_{d1}^* - i_{d1})dt \tag{3-45}$$

$$u_{q1} = k_{pi}(i_{q1}^* - i_{q1}) + k_{ii}\int(i_{q1}^* - i_{q1})dt \tag{3-46}$$

where k_{pi} and k_{ii} are the proportional and integral gains of the current controller, and the superscript * refers to the reference value. The inner current loop for converter VSC_1 is designed according to equation (3-43) and the block diagram of the inner controller is shown in Fig. 3.15.

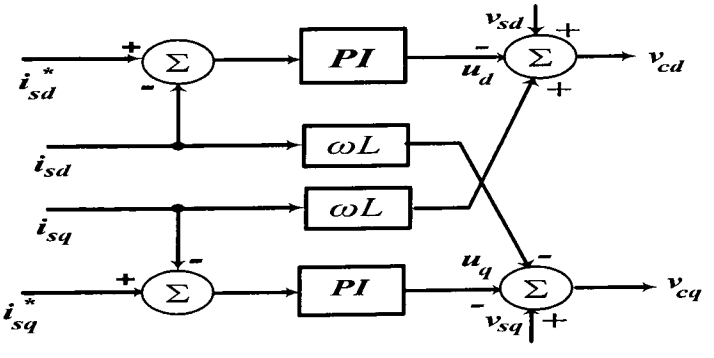


Fig. 3.15: Block diagram of the current control loop.

Replacing the integral part of equations (3-45) and (3-46) by new auxiliary control variables z_d and z_q, the following sets of equations are obtained:

$$u_d = k_{pi}(i_{sd}^* - i_{sd}) + k_{ii} z_d \tag{3-47a}$$

$$u_q = k_{pi}(i_{sq}^* - i_{sq}) + k_{ii} z_q \tag{3-47b}$$

$$\frac{dz_d}{dt} = -i_{sd} + i_{sd}^* \tag{3-47c}$$

$$\frac{dz_q}{dt} = -i_{sq} + i_{sq}^* \tag{3-47d}$$

Substituting equation (3.47) into equation (3.44) then

$$\frac{d}{dt}\begin{bmatrix} i_{sd} \\ z_d \\ i_{sq} \\ z_q \end{bmatrix} = \begin{bmatrix} -(R_1+k_{pi})/L_1 & K_{ii}/L_1 & 0 & 0 \\ -1 & 0 & 0 & 0 \\ 0 & 0 & -(R_1+k_{pi})/L_1 & K_{ii}/L_1 \\ 0 & 0 & -1 & 0 \end{bmatrix} \begin{bmatrix} i_{sd} \\ z_d \\ i_{sq} \\ z_q \end{bmatrix} + \begin{bmatrix} k_{pi}/L_1 & 0 \\ 1 & 0 \\ 0 & k_{pi}/L_1 \\ 0 & 1 \end{bmatrix} \begin{bmatrix} i_{sd}^* \\ i_{sq}^* \end{bmatrix} \tag{3-48}$$

From equation (3-48), the *dq*-currents are defined in the Laplace domain as follow:

$$\begin{bmatrix} i_{sd}(s) \\ z_d(s) \\ i_{sq}(s) \\ z_q(s) \end{bmatrix} = \frac{1}{s^2 + \frac{(R_1+K_{pi})}{L_1}s + \frac{K_{ii}}{L_1}} \begin{bmatrix} s & K_{ii}/L_1 & 0 & 0 \\ -1 & s + (R_1+K_{pi})/L_1 & 0 & 0 \\ 0 & 0 & s & K_{ii}/L_1 \\ 0 & 0 & -1 & s + (R_1+K_{pi})/L_1 \end{bmatrix} \begin{bmatrix} i_{sd}^* \\ i_{sq}^* \end{bmatrix} \tag{3-49}$$

Therefore, the Laplace transfer function of the inner current controller is:

$$G(s) = \frac{\frac{K_{pi}}{L_1}\left(s + \frac{K_{ii}}{K_{pi}}\right)}{s^2 + \frac{(R_1+K_{pi})}{L_1}s + \frac{K_{ii}}{L_1}} \tag{3-50}$$

From the characteristics equation of the current controller in the diameter of equation (3-50), the proportional and integral gains of the current controller are defined as follow [27]:

$$k_{pi} = 2\zeta\omega_n L_1 - R_1 \tag{3-51}$$

$$k_{ii} = \omega_n^2 L_1 \tag{3-52}$$

where, ω_n and ζ are the natural frequency and damping factor, respectively. The obtained values may be quite different from practical values due to stray elements, voltage drop in switches and other circuit elements, heat losses. This theoretical design is necessary to get the

limits that ensure stable operation but the final gains used in the practical systems are obtained by trial and error due to difficulty in representation of system nonlinearities in the control design. For example for $L=0.3$, $R=0.005$, $\omega_n=35$ *and* $\zeta=0.7$ the values of k_{ii} *is* 367.5 and $k_{pi}=14.69$ and the actual used value were 400 and 1.5, respectively.

3-9-2 The outer controller design

As mentioned earlier, the outer controller consists of the dc voltage controller, the ac voltage controller, the active and reactive power controller and the frequency controller. In this section different outer controllers are described.

1. Active and reactive power controller

Based on the *dq* power equations (3-41) and (3-42) the active and reactive powers delivered to the point of common coupling (PCC) are:

$$p(t)=\frac{3}{2}[v_{sd}(t)i_{sd}(t)+v_{sq}(t)i_{sq}(t)] \tag{3-53}$$

$$q(t)=\frac{3}{2}[-v_{sd}(t)i_{sq}(t)+v_{sq}(t)i_{sd}(t)] \tag{3-54}$$

where v_{sd} and v_{sq} are the dq voltages at the PCC. For balanced steady-state operation $v_{sq}=0$, therefore equations (3-53) and (3-54) can be expressed as:

$$p(t)=\frac{3}{2}v_{sd}(t).i_{sd}(t) \tag{3-55}$$

$$q(t)=\frac{-3}{2}v_{d}(t).i_{q}(t) \tag{3-56}$$

Hence the *dq* current reference values are:

$$i_{sd}^{*}=\frac{2P^{*}}{3v_{sd}} \tag{3-57}$$

$$i_{sq}^{*}=\frac{-2Q^{*}}{3v_{sd}} \tag{3-58}$$

Fig. 3.16 shows the schematic block diagram of the active and reactive power controller.

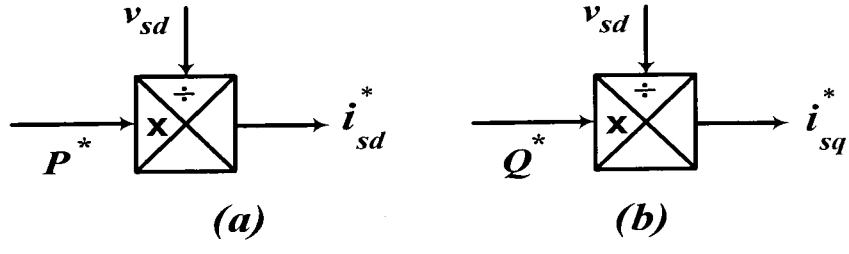


Fig. 3.16: Block diagram of the active and reactive power controller.

2. dc and ac voltage controller

In the dc and ac voltage controllers, the measured voltage is compared with the reference voltage, the error signal between the voltage reference and the measured value is fed to a PI controller to generate the d-axis reference current (i_{sd}^{*}). Equations (3-59) and (5-60) are the mathematical model of the controllers:

$$i_{sd}^{*} = k_{pdc}(V_{dc}^{*} - V_{dc}) + k_{idc}\int(V_{dc}^{*} - V_{dc})dt \tag{3-59}$$

$$i_{sq}^{*} = k_{pac}(V_{ac}^{*} - V_{ac}) + k_{iac}\int(V_{ac}^{*} - V_{ac})dt \tag{3-60}$$

where k_{pdc}, k_{idc}, k_{pac}, k_{iac} are the proportional and integral gains of the dc voltage controller and the ac voltage controller, respectively. Fig. 3.17 shows the schematic block diagram of the dc and ac voltage controller.

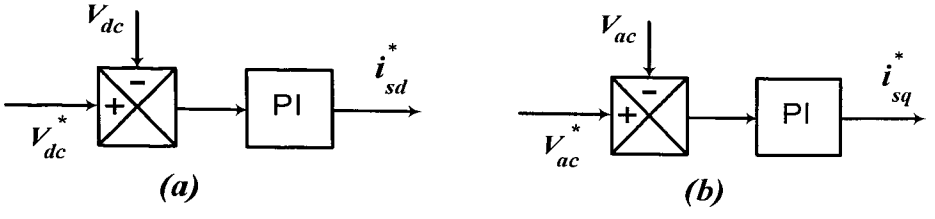


Fig. 3.17: Block diagram of the DC and AC voltage

3-10 Steady-state and transient behavior of the three-level VSC-HVDC system

The performance of the three-level VSC-HVDC connecting two different networks during steady-state and transient conditions is investigated in this section. The test system is shown in Fig. 3.18 and system parameters are given in Table 3.4. The saturation effects in the phase transformer and the phase reactor are neglected. The VSC converters switches are modeled as lumped switches with equivalent internal resistance and forward voltage (turn ON/turn OFF losses are not considered).

Table 3.4: VSC-HVDC parameters (this is not a real system, parameters taken from Matlab library).

SG_1 and SG_2 data	2400MVA, 13.8kV,50Hz, x_d=1.79, $x_d^{'}$= 0.220, $x_d^{''}$=0.193, x_q=1.715,, $x_q^{'}$= 0.243 , $x_q^{''}$=0.243, xl= 0.18 $T_{d0}^{'}$=0.595, $T_{d0}^{''}$=0.035, $T_{q0}^{''}$=0.31, R_s=0.003,H=4.25
ac_1 network	T.L_1 data (R=0.013Ω/km, L=0.934mH/km, 40km length), T_1 (275/132 kV, 500MVA, R_{T1}=0.005pu, L_{T1}=0.2pu), phase reactance (L_{F1}= 0.1pu based on 500MVA&132kV), high pass filter1 (10MVAr, Quality factor=15).
ac_1 network	T.L_2 data (R=0.013Ω/km, L=0.934mH/km, 40km length), T_2 (132/275 kV, 500MVA, R_{T2}=0.005pu, L_{T2}=0.2pu), phase reactance (L_{F2}= 0.1pu based on 500MVA&132kV), high pass filter2 (60MVAr, Quality factor=15).
dc side circuit	V_{dc}=300kV, the capacitor C =1000μF , cable data (0.015Ω/km, 150km)
controllers gains	K_{pi}=1.5, K_{ii}=400, K_{pac}=1.5, K_{iac}=500, K_{pdc}=10, K_{idc}=400

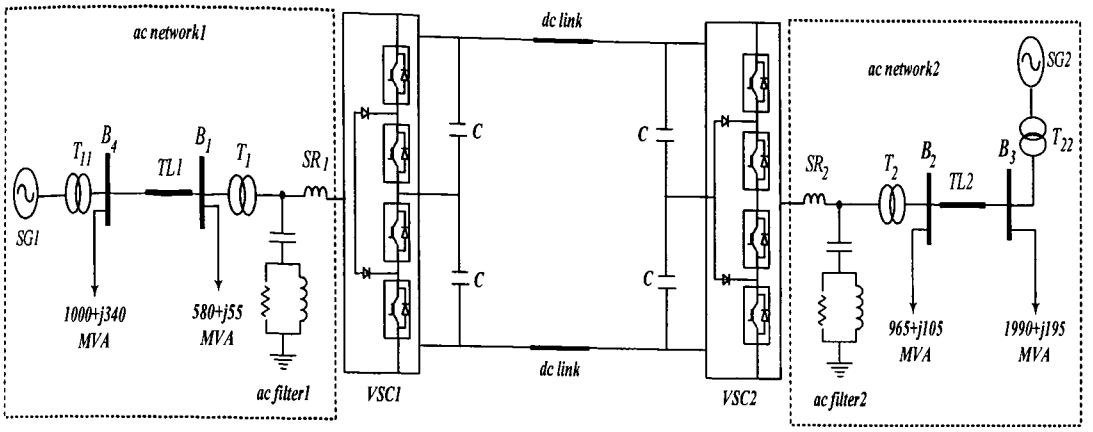


Fig. 3.18: 3-level VSC-HVDC system connecting two ac networks.

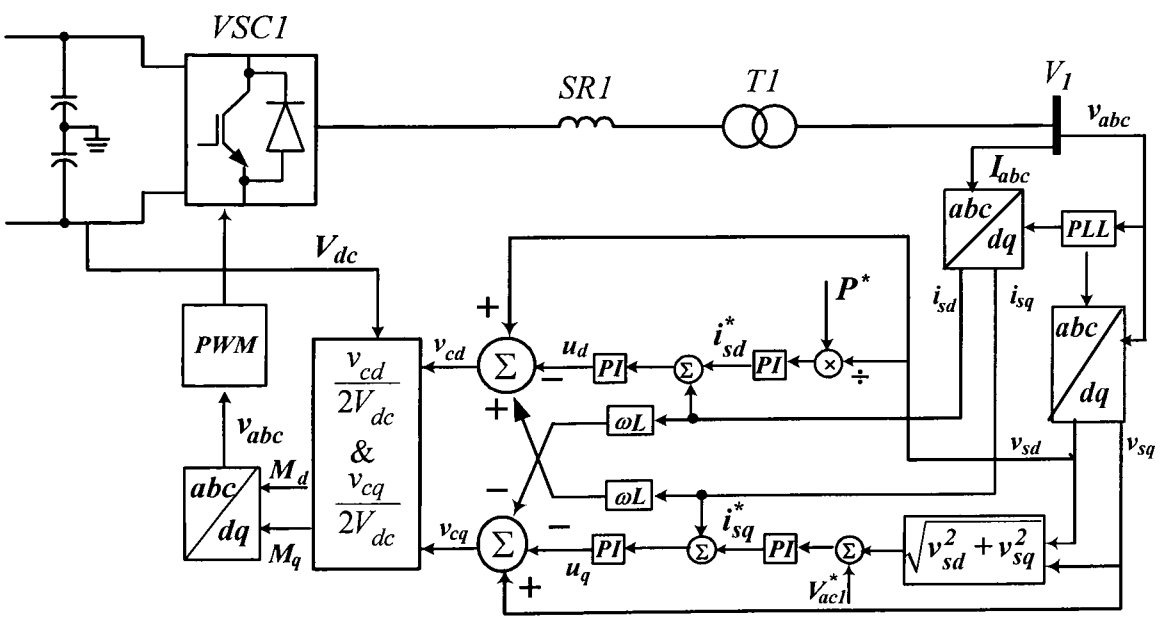
The control modes of the VSC-HVDC system are chosen such that, converter VSC_1 controls the active power flow and the ac voltage at B_1 while VSC_2 is used to control the dc link voltage and ac voltage at B_2. The overall schematic control system of the investigated system is shown in Fig. 3.19. Fig.3.19a is the control system of VSC_1 station, and Fig. 3.19b is the control system of VSC_2 station

The steady-state and transient investigation of the system include:

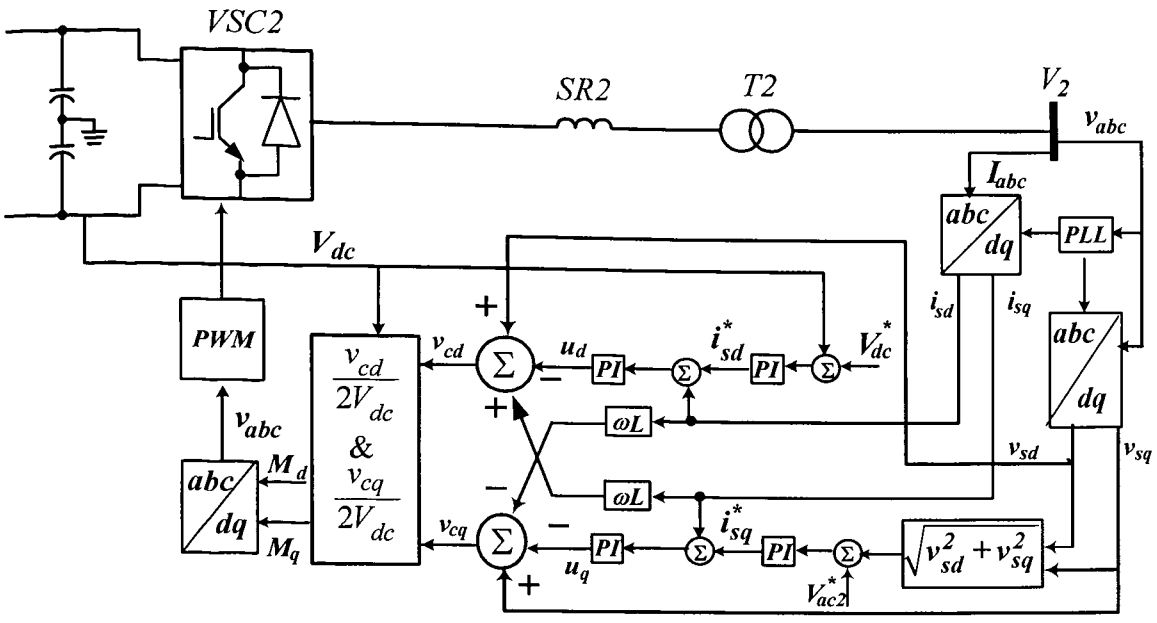
Case I: Active power step and provision of reactive power control.

Case II: Three-phase fault at ac network$_2$

Case III: DC fault at the middle of the dc link cable



(a) Control system of converter VSC_1



(b) Control system of converter VSC_2

Fig. 3.19: Overall schematic control block diagram of a 3-level VSC-HVDC system

3-10-1 Case I: Active power step and provision of reactive power

In order to investigate the dynamic response of the VSC-HVDC during sudden power changes, the active power reference is changed with time during the simulation as follow:

$$\begin{cases} P=1.0 & (0\le t\le 2.0), \quad P=-2t+5 \quad (2.0\le t\le 2.25) \quad P=0.5 \quad (2.25\le t\le 3.25) \\ P=-2t+7 & (3.25\le t\le 3.5) \quad P=0.0 \quad (3.5\le t\le 4.5), \quad P=-2t+9 \quad (4.5\le t\le 4.75), \\ P=-0.5 & (4.75\le t\le 5.75) \quad P=-2t+11 \quad (5.75\le t\le 6.0), \quad P=-1.0 \quad (6.0\le t\le 7.0), \end{cases}$$

The active power change at the sending and receiving ends is shown in Fig. 3.20a and b. According to equation (3.5) the VSC converter angles are changed with the change in power flow as shown in Fig. 3.20d. When the power flow is from the converter to the ac network the angle is positive otherwise the angle will be negative.

The change in the active power transfer at both ends causes a transient on the dc link voltage but the dc link controller manages to return the dc voltage at VSC_2 to the reference value (Fig. 3.20e). When the power direction is from VSC_1 to VSC_2 the dc voltage at VSC_1 is greater than 300kV otherwise it is smaller than 300kV.

Fig. 3.20c indicates that the ac voltage at B_1 and B_2 is kept constant although the buses power and current are changed continuously. According to equation (3.6) the ac voltage controller at both sides controls the reactive power exchange between the converters and the buses to keep constant voltage profile (see Fig. 3.20a and b). In this case the VSC converters act as static

reactive power compensation devices to keep the voltages at the desired values regardless of the power direction or the amount of power. The STATCOM functionality of the VSCs is assessed by switching the dc transmission system to sleep mode (in Fig. 3.20a the power is switched to zero between t=3.5s and t=4.5s).

The capability of the VSC-HVDC system to control the power flow is valuable during load demand changes in the ac systems. The VSC-HVDC system can be controlled to participate in short-term frequency regulation. In this case the power control is activated when significant change in system frequency occurs and hence the dc link transmitted power is adjusted to match the new demand.

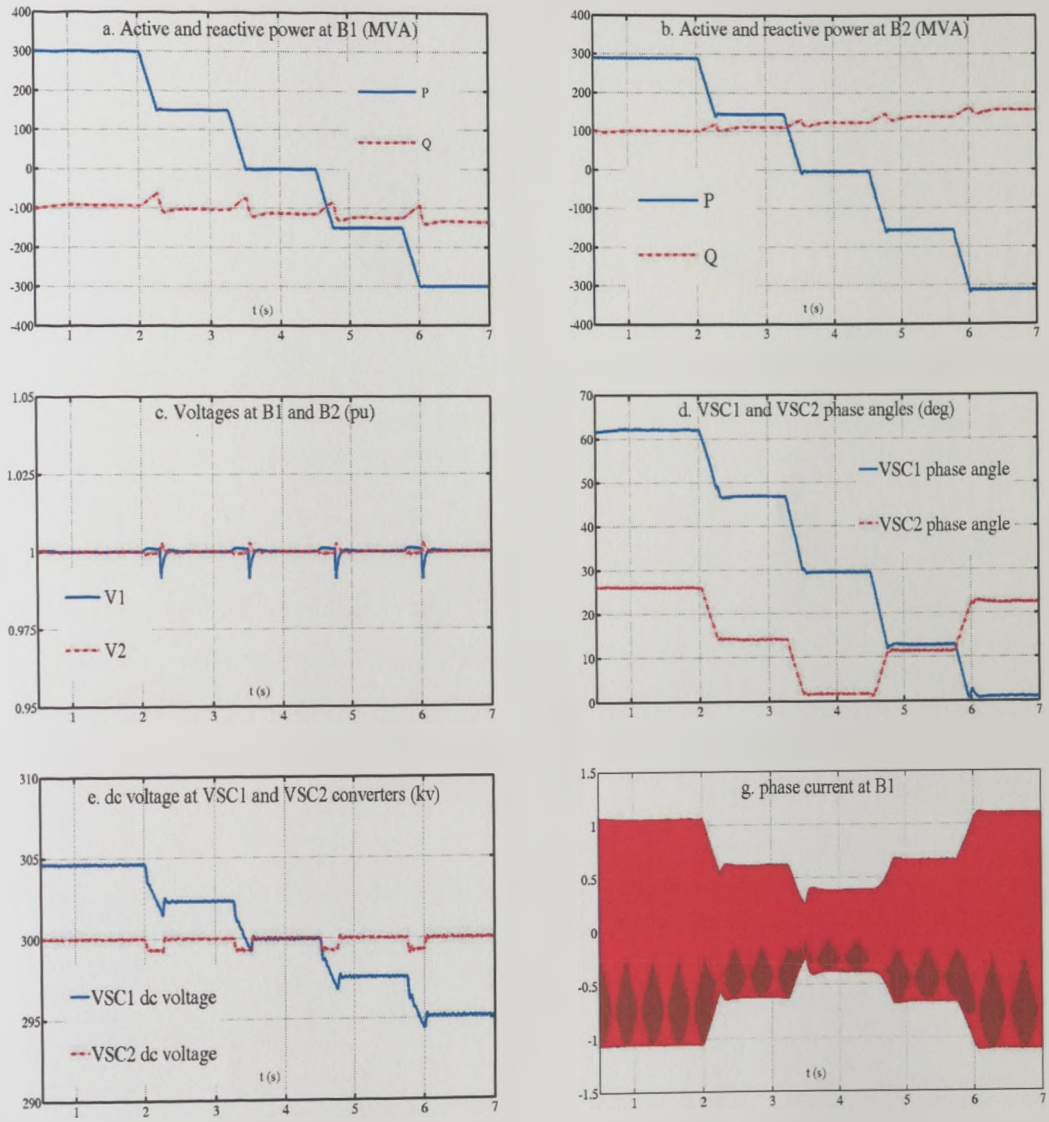


Fig. 3.20: Key simulation results during active power variations.

The Total Harmonic Distortion level (THD) on the ac sides is measured at B_1 and B_2. The results are compared with the harmonic level limit of 1.5% stated in the IEEE Std 519-1992 [28]. The THD in the ac voltage at bus B_1 is 0.593%, whilst the THD in the ac voltage at B_2 is 0.380%. Fig. 3.21 shows the voltage waveforms at B_1 and B_2.

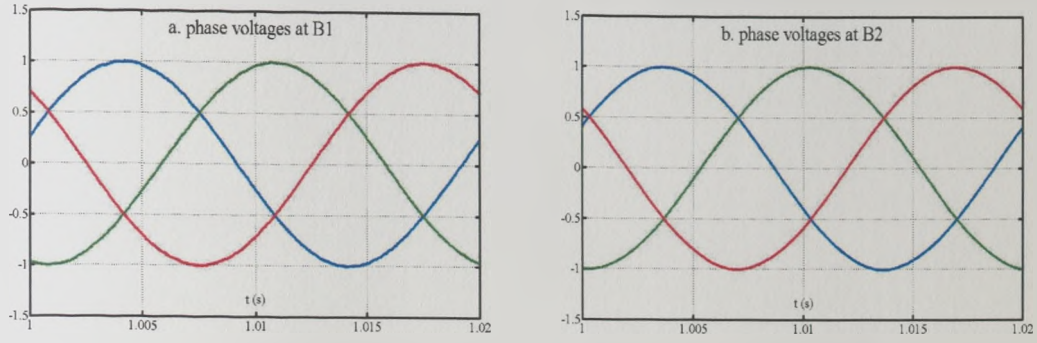


Fig. 3.21: AC voltage waveform at B_1 and B2 with/without ac filter in VSC converter stations.

3-10-2 System behaviour during three-phase ac fault at the receiving end

To demonstrate the transient behaviour of the VSC-HVDC transmission system during abnormal conditions, the system in Fig. 3.18 is subjected to a three-phase fault at bus B_2, at t=1s with duration of 100ms (5 cycles for 50Hz). Fig. 3.22 shows the key waveforms obtained. The voltage at the sending-end side (bus B_1) is less sensitive to the ac fault in the receiving end (Fig. 3.22a), the VSC-HVDC link improves the ac fault ride-through capability of the sending-end by isolating it from the receiving-end (decoupled operation). It can be observed that the ac voltage magnitude at bus B_2 collapses during the fault period and recovers again to the pre-fault value after fault clearance. The ac voltage recovers to a value greater than the pre-fault value, and transient oscillations occur before stabilization because the controllers at the receiving-end attempt to prevent the change in the ac voltage and modulation index (Fig. 3.22a). After fault clearance the ac voltage on the sending-end recovers to 100% within 0.1s (as stated in the Grid Code the voltage must recover to 90% after fault clearance within a time period shorter than 0.5s).

The active power at the receiving-side is decreased to zero when the fault occurs and then raised to double the rated power after fault clearance. The active power at the sending-end is less sensitive to a fault at the receiving-end due to the decoupled operation (Fig. 3.22b). Finally the dc link voltage of the receiving-end converter has increased during the fault to compensate for the adjustment of load angle between the voltage V_2 at B_2 and voltage at converter terminal VSC_2. dc voltage increases may be dangerous to converter equipment

(depending on the insulation breakdown of the converter), hence a dc chopper is required within the dc link circuit. Fig. 3.22d illustrates the three-phase current at B_2.

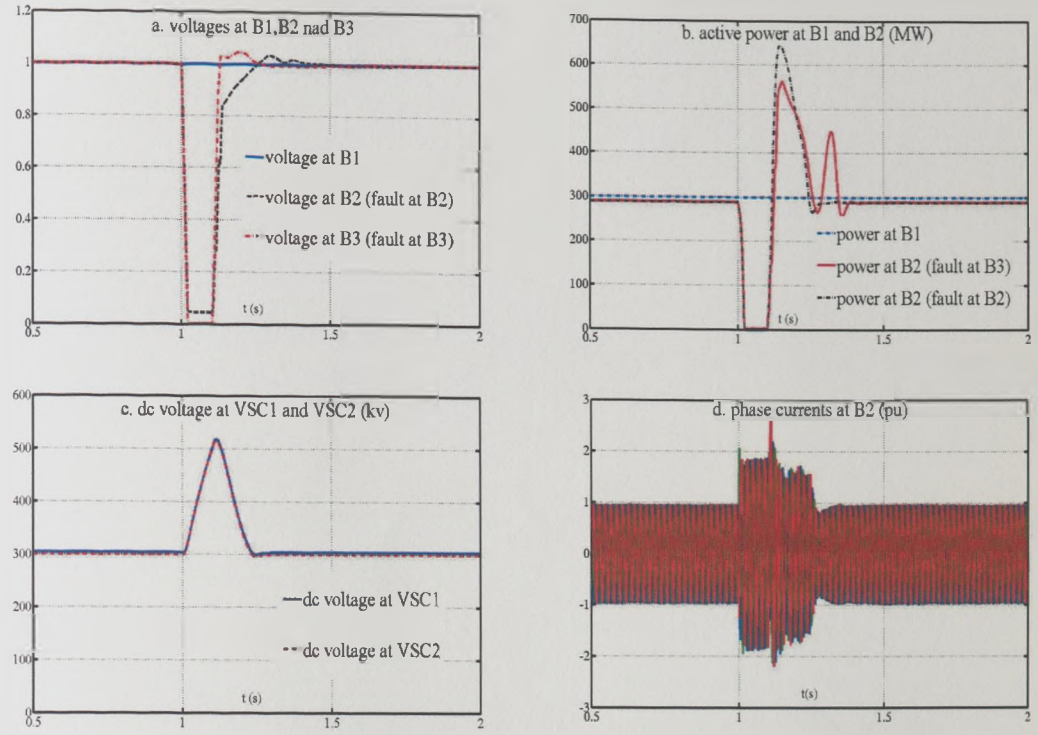


Fig. 3.22: Key simulation results during a three-phase fault at B_2.

3-10-3 System behaviour during a dc fault at the midpoint of the dc link

VSC-HVDC systems are vulnerable to faults occurring in the dc link, this is the weakest point of VSC-HVDC systems. With the absence of the zero crossing point no dc circuit breakers have been manufactured to clear the dc link faults. To protect the VSC converters from the excessive fault current, ac circuit breakers located in the ac sides are used to isolate the dc link circuit until the fault is extinguished.

In order to clear a dc fault, the fault must be starved of the fault current for a period long enough for the plasma to be extinguished and there is no possibility of re-striking when the voltage reappears [29]. Temporary solid pole-to-pole short circuit is applied at the middle of the dc link with duration of 0.05s at t=1.0s. The results obtained are presented in Fig. 3.23.

When the dc fault occurs the dc voltage collapses to zero and recovers to the pre-fault value (Fig. 3.23c). The capacitors rapidly discharge into the fault point, while simultaneously, the ac system will be three-phase, short-circuited through the VSC free-wheeling diodes (FWD)

and the fault point even if the converters are blocked. This means that the ac system will continue to feed power into the fault until the dc fault is cleared.

The ac circuit breaker at the receiving-end side isolates the ac network$_1$ when the dc link fault occurs. In order to reduce the inrush current following the closing of the ac circuit breaker and ensure enough time for the arc extinguishing, the ac circuit breaker isolating time is delayed until t=1.14s [30]. To reduce the effect of the dc fault, a high-impedance grounding system is used to limit the discharging current and to maintain the dc voltage of the capacitors.

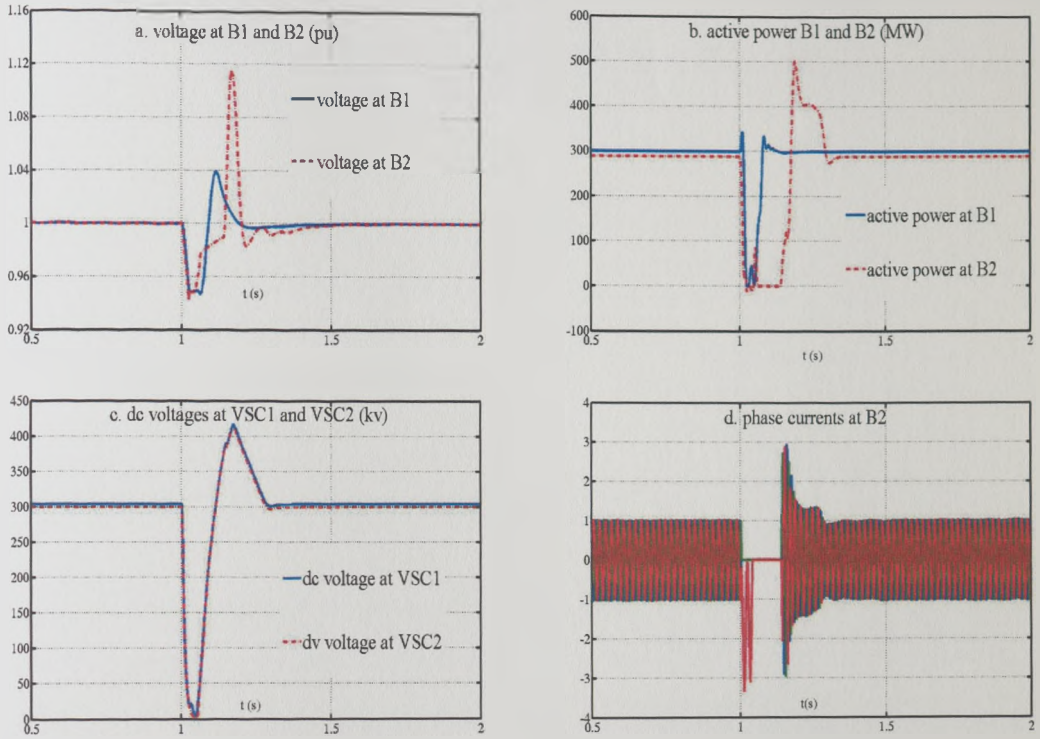


Fig. 3.23: Key simulation results for a dc fault at the mid-point of the dc cable.

3-11 Application of VSC-HVDC systems

The features of HVDC transmission such as fast response, precise power flow control, and reactive power capability have made the VSC-HVDC a suitable solution for many applications and concepts which previously have not been considered due to technical and economical limitations [3, 31].

A. Wind Farms integration

The technical advantages of wind integration via VSC-HVDC are [31]:

- Eliminating the need for start up generator.
- The ability of VSC converter to provide the reactive power control eliminating the need for static reactive power devices, thus reducing the total cost.
- VSC-HVDC has no length restriction like ac submarine cables, and could provide an optimal option for long-distance wind farms offshore connection.

B. Connecting weak and isolated areas

Since the commutation of the voltage source converter do not need external ac voltage, the VSC-HVDC may be used to supply isolated areas such as islands and remote industrial areas [12].

C. Multi-terminal dc system

The structure and controllability of the HVDC system is much simpler with VSC-HVDC than with the conventional HVDC. The flow reversal in conventional HVDC is achieved only by voltage polarity change but in VSC-HVDC systems the power flow direction change is achieved by current direction changes. The control flexibility and power management in multi-terminal VSC-HVDC makes it easy to use any number of VSC converters connected to a DC bus with fixed polarity [32].

D. Provision of Independent Reactive Power Control

The voltage source converter can provide four-quadrant power controllability. The reactive power exchange between the VSC converter and the ac system can be controlled to provide greater flexibility for the AC system, such as stabilizing a particular bus voltage and operating at unity power factor to minimize the transmission current and reduce the transmission losses. A VSC converter at the PCC acts exactly as a synchronous static compensator [11].

3.12 Summary

In this chapter an overview of the VSC-HVDC transmission system has been presented. The function of each component, advantages and applications of the VSC-HVDC have been presented in detail. Moreover, the operation, the steady-state model, and dynamic model of the VSC-HVDC system have been discussed. The two-level and three-level VSC converter operation was discussed in detail; moreover the control system design of the VSC converter

stations and the tuning method for the PI controller to ensure robust system performance were investigated. The steady-state and transient performance of the VSC-HVDC system was investigated during step changes in the active power, balanced ac fault, and dc link fault. From simulation results it can be concluded that the VSC-HVDC can fulfill fast and bi-directional power transfers and ac voltage adjustment.

References

[1] N. Flourentzou, *et al.*, "VSC-Based HVDC Power Transmission Systems: An Overview," *IEEE Trans on Power Electronics,*, vol. 24, pp. 592-602, 2009.

[2] S. Cole and R. Belmans, "Transmission of bulk power," *Industrial Electronics Magazine, IEEE,* vol. 3, pp. 19-24, 2009.

[3] M. P. Bahrman and B. K. Johnson, "The ABCs of HVDC transmission technologies," *Power and Energy Magazine, IEEE,* vol. 5, pp. 32-44, 2007.

[4] V. K. Sood, *HVDC and FACTS Controllers Application of Static Converter in Power System*: Kluwar Academic Publisher, 2004.

[5] M. H. Rashid, *Power Electronics Handbook*: Academic Press, 2001.

[6] L. Xu, *et al.*, "Multi-terminal DC transmission systems for connecting large offshore wind farms," in *Power and Energy Society General Meeting - Conversion and Delivery of Electrical Energy in the 21st Century, 2008 IEEE*, 2008, pp. 1-7.

[7] G. Holmes and T.A.Lio, *Pulse Width Modulation for Power Converters:principles and practice*: IEEE Press, John Wiley & Sons, Publication, 2003.

[8] B. R. Andersen, *et al.*, "Topologies for VSC transmission," in *AC-DC Power Transmission, 2001. Seventh International Conference on (Conf. Publ. No. 485)*, 2001, pp. 298-304.

[9] P. Kundur, *Power System Stability and Control*: Electric Power Research Institute, Power System Engineering Series, 1994.

[10] A. Cetin and M. Ermis, "VSC-Based D-STATCOM With Selective Harmonic Elimination," *Industry Applications, IEEE Transactions on,* vol. 45, pp. 1000-1015, 2009.

[11] J. Arrillaga, *et al.*, *Flexible Power Transmission Systems-The HVDC Options*: John Wiley & Sons, Publication, 2007.

[12] D. Cuiqing, *et al.*, "A New Control Strategy of a VSC-HVDC System for High-Quality Supply of Industrial Plants,," *Power Delivery, IEEE Transactions on,* vol. 22, pp. 2386-2394, 2007.

[13] A. Yazdani and R. Iravani, *Voltage-Sourced Converters in Power Systems: Modeling, Control, and Applications*. Hoboken, New Jersey: John Wiley & Sons, Inc, 2010.

[14] L. Weimers, "New markets need new technology," in *Power System Technology, 2000. Proceedings. PowerCon 2000. International Conference on*, 2000, pp. 873-877 vol.2.

[15] "HVDC Cables Trasmission," *paper available online at ABB website www.abb.com.*

[16] B. Wu, *High-Power Converters and ac Drives*: The Institute of Electrical and Electronics Engineers, Inc., 2006.

[17] W. Qunjing, *et al.*, "Analysis and comparison of conduction losses in neutral-point-clamped three-level inverter with PWM control," in *Electrical Machines and Systems, 2007. ICEMS. International Conference on*, 2007, pp. 143-148.

[18] S. Rohner, *et al.*, "Modulation, Losses, and Semiconductor Requirements of Modular Multilevel Converters," *Industrial Electronics, IEEE Transactions on*, vol. 57, pp. 2633-2642, 2010.

[19] T. Jalakas, *et al.*, "Evaluation of different loss calculation methods for high-voltage IGBT-s under small load conditions," in *Power Electronics and Motion Control Conference, 2008. EPE-PEMC 2008. 13th*, 2008, pp. 1263-1267.

[20] P. Hui, *et al.*, "Evaluation of losses in VSC-HVDC transmission system," in *Power and Energy Society General Meeting - Conversion and Delivery of Electrical Energy in the 21st Century, 2008 IEEE*, 2008, pp. 1-6.

[21] K. S. Oh, "Application Note 9016: IGBT Basics1," *FAIRCHILD Semiconductor, Rev. A2, Febuary 2001*

[22] P. A. Dahono, *et al.*, "Analysis of conduction losses in inverters," *Electric Power Applications, IEE Proceedings -*, vol. 142, pp. 225-232, 1995.

[23] L. K. Mestha and P. D. Evans, "Optimisation of losses in PWM inverters," in *Power Electronics and Variable-Speed Drives, Third International Conference on*, 1988, pp. 394-397.

[24] D. Cuiqing, *et al.*, "Analysis of the control algorithms of voltage-source converter HVDC," in *Power Tech, 2005 IEEE Russia*, 2005, pp. 1-7.

[25] L. Xu, *et al.*, "VSC transmission operating under unbalanced AC conditions - analysis and control design," *Power Delivery, IEEE Transactions on*, vol. 20, pp. 427-434, 2005.

[26] A. Yazdani and R. Iravani, "Dynamic model and control of the NPC-based back-to-back HVDC system," *Power Delivery, IEEE Transactions on,* vol. 21, pp. 414-424, 2006.

[27] S. Douangsyla, *et al.*, "Modeling for PWM voltage source converter controlled power transfer," in *Communications and Information Technology, 2004. ISCIT 2004. IEEE International Symposium on*, 2004, pp. 875-878 vol.2.

[28] "IEEE Guide for Planning DC Links Terminating at AC Locations Having Low Short-Circuit Capacities," *IEEE Std 1204-1997,* p. i, 1997.

[29] Y. Jie, *et al.*, "Characteristics and Recovery Performance of VSC-HVDC DC Transmission Line Fault," in *Power and Energy Engineering Conference (APPEEC), 2010 Asia-Pacific*, 2010, pp. 1-4.

[30] G. P. Adam, *et al.*, "Network fault tolerant voltage-source-converters for high-voltage applications," in *AC and DC Power Transmission, 2010. ACDC. 9th IET International Conference on*, 2010, pp. 1-5.

[31] P. Bresesti, *et al.*, "HVDC Connection of Offshore Wind Farms to the Transmission System," *Energy Conversion, IEEE Transactions on,* vol. 22, pp. 37-43, 2007.

[32] G. P. Adam, *et al.*, "Multi-terminal DC transmission system based on modular multilevel converter," in *Universities Power Engineering Conference (UPEC), 2009 Proceedings of the 44th International*, pp. 1-5.

Chapter Four

Multi-terminal high-voltage dc transmission systems based on voltage source converter

4-1 Introduction

CSC-HVDC or VSC-HVDC transmission can be configured as point-to-point or multi-terminal. Most existing dc schemes have been realized as point-to-point connections, despite the limitations of power exchange between only two converters.

It is noticeable in a multi-terminal system based on a CSC-HVDC system, that the change in operating mode of one of the converters, in order to reverse the power flow, necessitates converter dc link polarity reversal by increasing the firing angle beyond 90° and also a change in the control mode [1]. This example highlights the complications that may arise from the use of CSC-HVDC in multi-terminal dc transmission systems. Due to difficulties associated with power flow control in multi-terminal dc system just only two multi-terminal systems based on CSC-HVDC are in operation now:

1- Italy–Corsica–Sardinia: three terminal HVDC system exchange power between converters in Italian mainland, Corsica and Sardinia. Build in 1965 as a point-to-point system and third terminal was added in 1986 [2].

2- Hydro Quebec-New England (USA/Canada): Four multi-terminal dc system started as 690 MW two-terminal in 1986 between Des Cantons and Comerford, in 1990 the system is extended to deliver 1800MW to converter station located in Sandy Pond and finally the system is extended to deliver 2138MW to fourth terminal located in Montreal [3].

Based on previously discussed advantages of VSC-HVDC technology, it is the most suitable in many applications, including multi-terminal dc systems operation. The active power reversal in multi-terminal based on voltage source converters is achieved by changing the dc current direction without the need to change the dc link voltage polarity and operating mode. This results in instantaneous power reversal without increasing the stress on the dc cable and interfacing transformer, as it occurs in CSC-HVDC. The active power flow between the converters in a multi-terminal HVDC system is controlled using a combination of direct active power control in converters that control active power, and dc voltage droop in the converters used to control the dc link voltage, as demonstrated in references [4-5]. This increases control flexibility of multi-terminal VSC-HVDC systems to respond to any network

alteration resulting from active power imbalance and ac faults (due to add/loss of major load or generation). They also have the capability to participate in the stabilization of ac networks. The ability of multi-terminal VSC-HVDC to fully control the active power flow makes it suitable to reduce network congestion and to extend the steady-state stability limits of an ac network. The inherent reactive power capability within the converter stations of multi-terminal VSC-HVDC transmission improves voltage and power system stability of weak ac networks at no additional cost. It also allows active power injection into any ac networks regardless of their strength. This feature is vital to improve the energy availability at any terminal of any ac network. A reliable coordinated control system is required between the converter stations in addition to robust dc circuit breakers to improve the chance of system recovery from dc faults or loss of converters.

4-2 Configurations of multi-terminal dc transmission systems

The features and advantages of multi-terminal VSC-HVDC transmission systems, which make them more advantageous than point-to-point VSC-HVDC transmission, are [4]:

- Lower investment cost and space requirements: due to continuing growth of electrical demand and the need to upgrade the existing transmission networks. Multi-terminal dc transmission systems can address the issues of scarcity and increasing cost of land for new rights-of-way (and hence reduce the investment needed for network expansion).
- The multi-terminal dc transmission system increases the power flow control flexibility along desired routes.
- The multi-terminal dc transmission system improves system reliability and stability. During the outage of a VSC converter, or loss of a dc link cable, re-routing of the power is available through other parts of the system; therefore the possibility of losing a major generating unit is minimized.
- Suitable for creation of regional-transmission system connecting different ac networks and integrating renewable energy resources. The converter in the dc network could operate as rectifier or inverter to transmit the power to/from a specific point in the dc network [4].

The possible configurations of a multi-terminal VSC-HVDC system, which differs according to their particular application, are described in the following sections.

4-2-1 Multi-terminal VSC-HVDC systems for wind farm integration

VSC-HVDC is being introduced in distribution systems (wind farms, solar energy, photovoltaic, etc.), to decouple the voltage and frequency of the various renewable energy generating sources from the nominally fixed values of conventional grids. Wind farms are geographically dispersed over wide areas and are growing in number and capacity. A multi-terminal VSC-HVDC system is an ideal solution to transmit the offshore wind power into the nearby ac network. There are different configurations for multi-terminal systems for wind farm integration which differ in VSC converter unit number and their arrangement [6].

Fig. 4.1 shows two options for using multi-terminal VSC-HVDC for offshore wind farm integration: double-input single-output, and double-input double-output configurations. The power flow control takes into consideration that the power direction is from the wind farm into the ac grid (no power reversal).

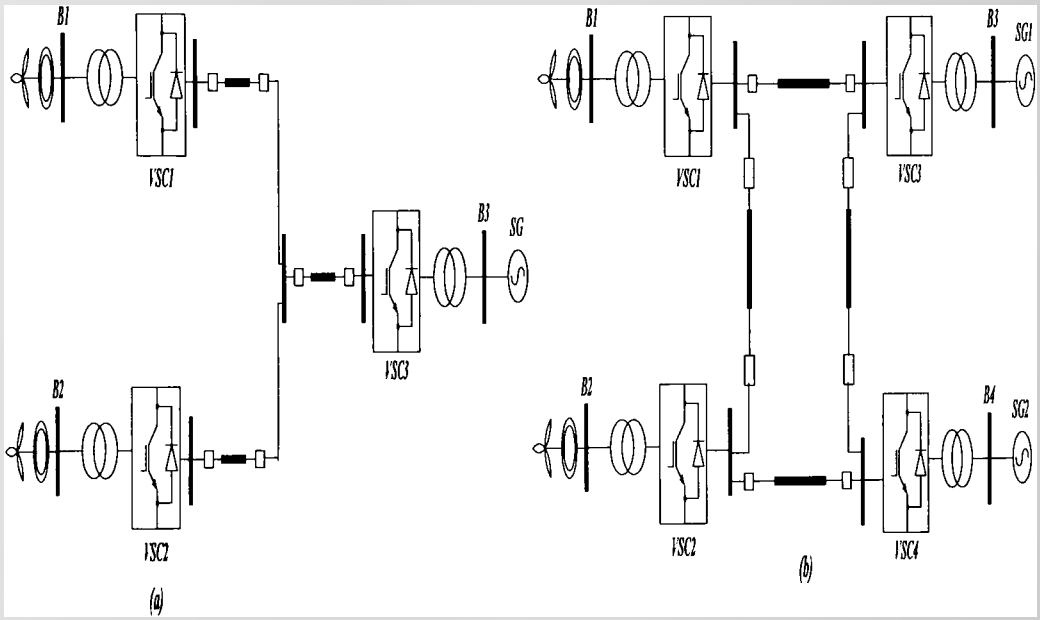


Fig. 4.1: Examples of possible multi-terminal configurations for wind farm integration: (a) double-input single-output configuration; (b) double-input double-output configuration.

4-2-2 Multi-terminal VSC-HVDC for transnational dc network (SuperGrid)

Multi-terminal VSC-HVDC can be used instead of conventional ac transmission to accommodate the power between regional ac networks. In this case the HVDC system is used to create a large power pool that may facilitate the following objectives:

1- Increased connection of renewable power to the ac network without the need for bulky storage systems.

2- Improved resilience of the ac networks attached to this power pool against power and frequency instability problems during local loss of generation or major load.

3- Enable power trading between these regional networks in real time with full control over power flows.

4- Inherent reactive power capability in each converter station enables the converter to provide voltage control at the point of common coupling.

It also provides the flexibility of asynchronous operation; and isolating each network from the abnormal disturbance developing in the other networks, hence reducing the risk of black-out [7]. The active power exchange between the ac networks and the power pool is achieved using active power control. Fig. 4.2 shows the transnational dc network.

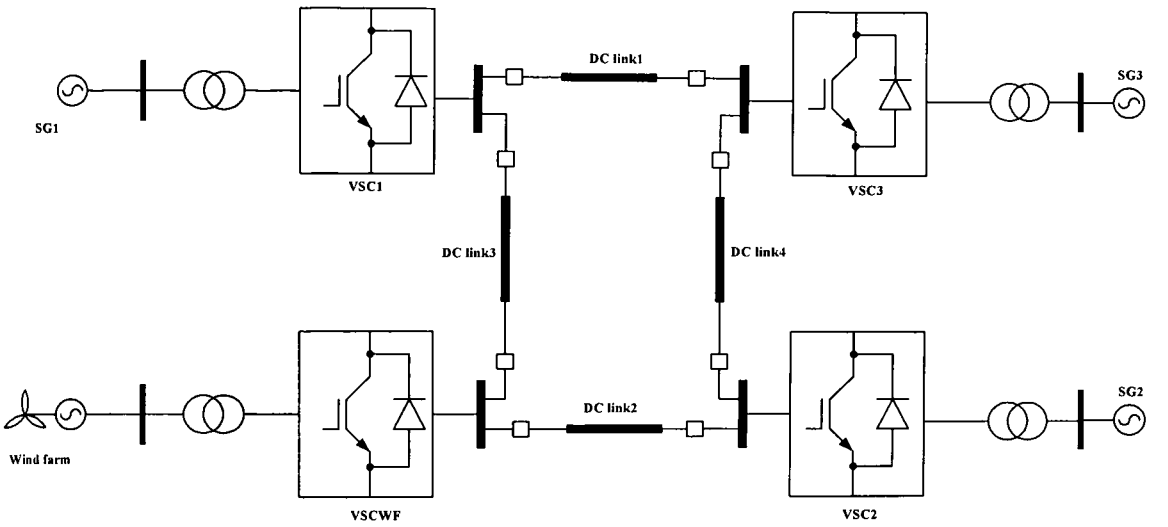


Fig. 4.2: Four-terminal transnational dc network system.

4-2-3 Multi-terminal VSC-HVDC systems for distribution networks in urban areas

In distribution networks, especially in urban and remote industrial areas, the receiving-end systems are purely consumers and there is very limited generation, or even no generation at all. The capabilities of the VSC converter enable the VSC-HVDC systems to feed weak and isolated ac systems, therefore a multi-terminal VSC-HVDC system could be used to replace the conventional ac distribution system, and thus improve the system reliability because abnormal conditions in one area cannot propagate to the rest of the system. The implementation of a multi-terminal HVDC system in an urban area will be based on possible economic benefits, and on the possible better performances compared to the conventional ac system. Fig. 4.3 shows the multi-terminal dc transmission used for an urban area distribution network [8].

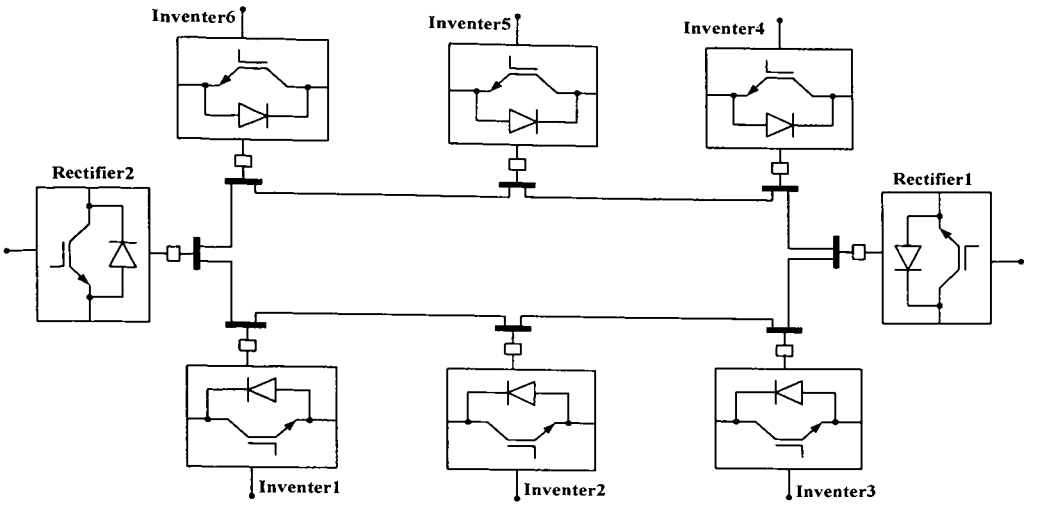


Fig. 4.3: Multi-terminal HVDC system for an urban area distribution network [8].

4-2-4 Multi-terminal VSC-HVDC systems for oil and gas platforms

Offshore oil and gas platforms use electricity generated from gas turbines located at offshore sites. The main disadvantages of gas turbines are their lower efficiency and contribution to emission of greenhouse gases. Multi-terminal VSC-HVDC systems can be used to supply the oil and gas platforms and to transmit the offshore wind power to the onshore ac network. The potential benefits of a multi-terminal dc system configuration are [9]: reduced operational costs, increased system reliability and reduced CO_2 emissions.

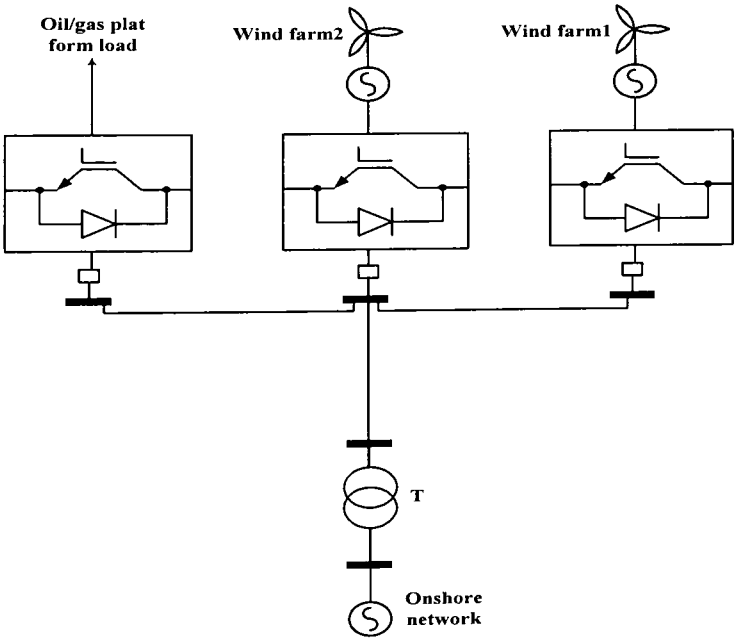


Fig. 4.4: Multi-terminal HVDC system for offshore wind farms, oil/gas platform and onshore network [9].

4-3 Power Management of multi-terminal dc transmission systems

In a multi-terminal VSC-HVDC system with one direction power flow, including converters acting just as rectifier or inverter, without ability to reverse the power direction (wind farm integration, supply of industrial area or supply of isolated island), several VSC converters are connected together. Different power dispatch schemes may be applied among the receiving-end converter (inverter mode) to share the power from the sending-end converters (rectifier mode). In general, there are three different scenarios for power management between receiving-end converters:

1- Equal power sharing: the receiving-end converters share the transmitted power equally and no power flows in the auxiliary cable in normal operation, unless a sudden loss of a receiving-end converter occurs. In this case the dc voltages of the receiving-end converters are kept constant at the same level ($V_{dc1}=V_{dc2}$).

2- Proportional power sharing: the receiving-end converters do not share the power equally. A dc droop controller is used to enable the power sharing between receiving-end converters. The power flow in the auxiliary cable and the dc voltage level is not the same ($V_{dc1}\neq V_{dc2}$).

3- Priority power sharing: one receiving-end converter has the priority to transmit the power to a particular limit while the other converters transmit only the excess power. In this case, a dc droop is also required to ensure the priority power sharing.

The dc droop controller characteristics depend mainly on the dc link setting point and the dc current flow through the auxiliary cable [10-12]. Referring to Fig. 4.6, VSC_1 and VSC_2 control the dc voltage. VSC_2 is equipped with a dc droop controller in addition to the dc voltage controller to enable the power sharing between receiving-end converters. When the dc droop controller increases the dc link voltage of VSC_2 above the setting point, then the current will flow from VSC_2 towards VSC_1, and the power transmitted by VSC_1 is increased; otherwise the current will flow in the opposite direction and the transmitted power by VSC_2 is increased. The voltage-current characteristic of the droop controller is shown in Fig. 4.5.

The current flow in the auxiliary cable in Fig. 4.6 is calculated as:

$$I_{12}=\frac{V_{dc1}-V_{dc2}}{R_{12}} \tag{4-1}$$

The power transmitted through the auxiliary cable is:

$$\Delta P=I_{12}\left(V_{dc1}-V_{dc2}\right)=I_{12}.\Delta V_{dc} \tag{4-2}$$

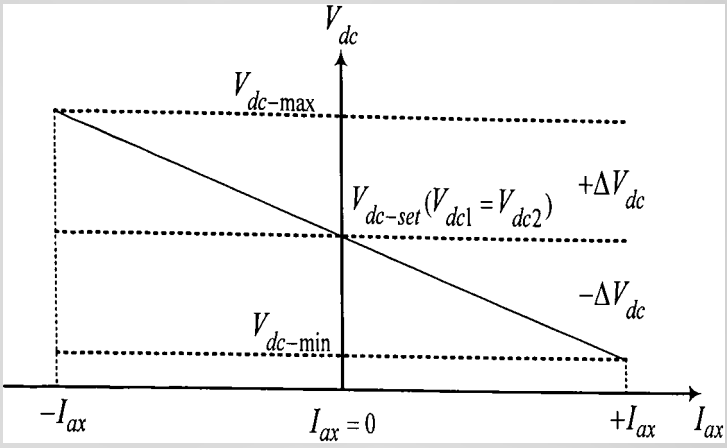


Fig. 4.5: Voltage-current characteristic of the dc droop controller.

The proportional and priority power sharing modes can easily be achieved by proper setting of the dc droop controller. In Fig. 4.6, in the four-terminal VSC-HVDC system connecting two different ac networks, the power sharing between receiving-end converters (VSC_1 and VSC_2) is achieved using a dc droop controller implemented in VSC_2. ac $network_1$ is represented by synchronous generators (SG_1 and SG_2) while ac $network_2$ is represented by a synchronous generator (SG_3), the steady-state conditions of the system are shown in Fig. 4.6 and system parameters are given in Table 4.1. The dc droop characteristics shown in Fig. 4.7 determine the amount and direction of the current flowing in the auxiliary cable if the droop controller is activated.

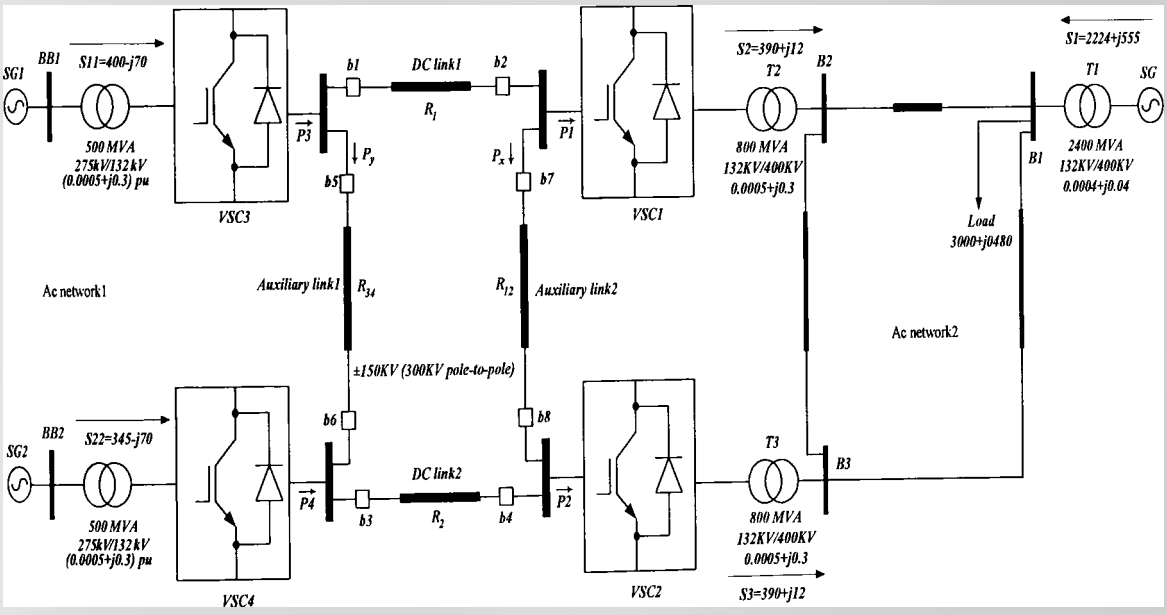


Fig. 4.6: Four-terminal dc transmission system based on voltage source connecting two different grids.

Table 4.1: System parameters (this is not a real system, parameters taken from Matlab library)

ac_1 network	the transformer $T_{3,4}$ (275/132 kV, 300MVA, $R_{T3,4}$=0.0005pu , $L_{T3,4}$=0.3pu), phase reactance ($L_{F3,4}$= 0.3pu based on 300MVA and 132kV)
ac_2 network	The transformer $T_{1,2}$ (132/400 kV, 300MVA, $R_{T1,2}$=0.0005pu, $L_{T1,2}$=0.3pu), phase reactance ($L_{F1,2}$= 0.3pu based on 300MVA and 132kV). SG1 data (2400MVA, 33kV), SG1 transformer (33/400kV), 0.008+j0.008pu)
dc side circuit	V_{dc}=300kV, P_{dc} at $VSC_{1\&2}$=300MW, the dc capacitor C =300μF , DC $link_{1,2}$ data (0.015Ω/km, 150km), dc auxiliary $link_{1,2}$ data (0.25Ω/km, 10km)

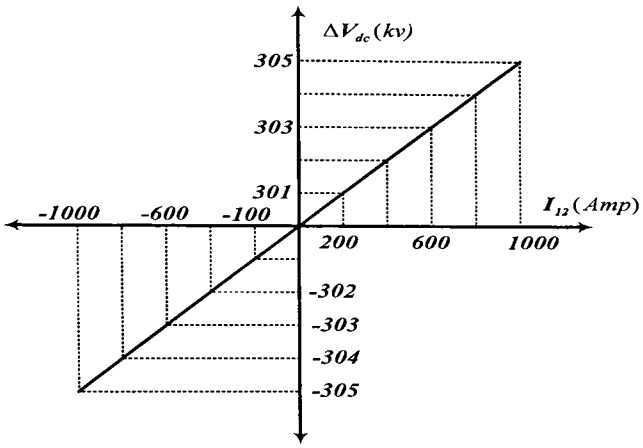


Fig. 4.7: Voltage-current droop controller.

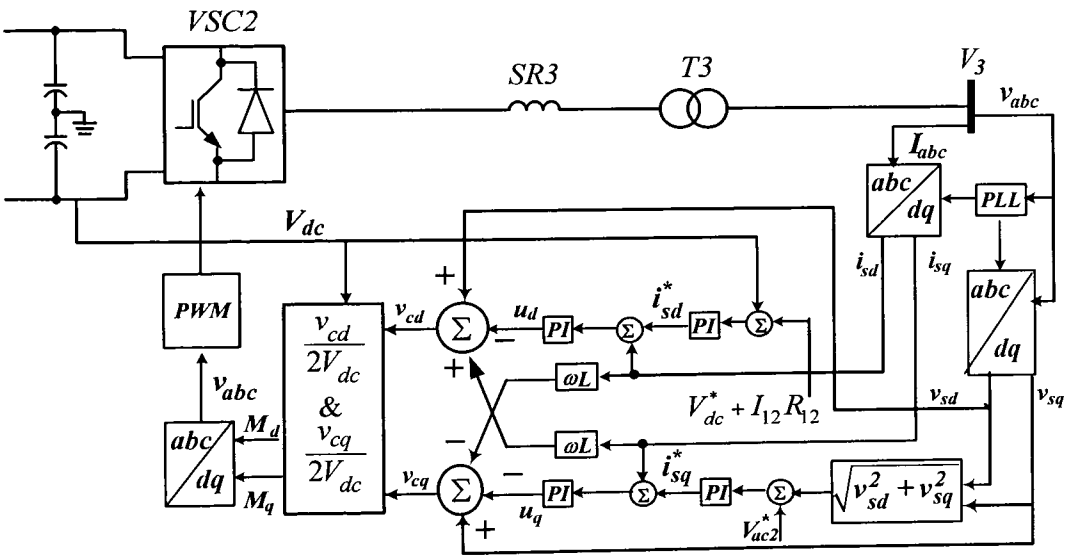


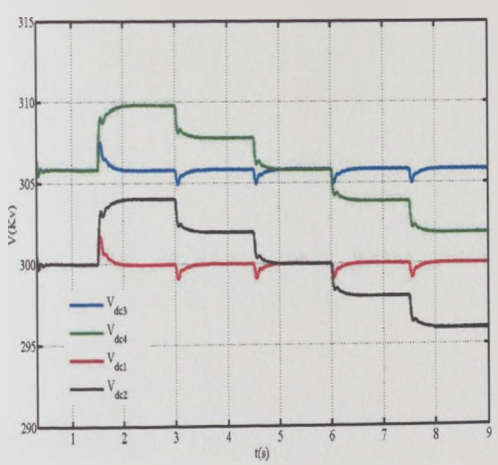
Fig. 4.8: Control system of VSC_2 for power sharing.

Inclusion of the voltage-current characteristics in Fig. 4.7 into the control system of VSC_2 will allow converters VSC_1 and VSC_2 to respond to any power share. The complete control system diagram of VSC_2 including the dc droop controller is shown in Fig. 4.8.

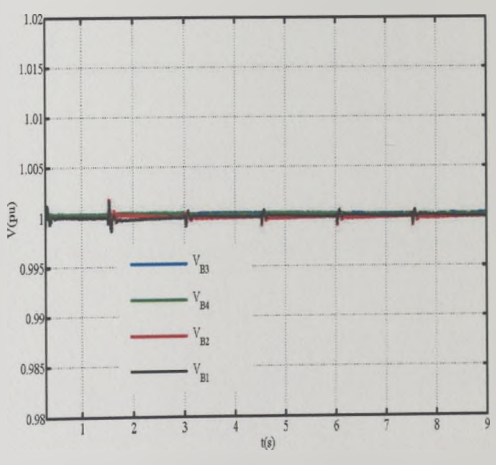
Fig. 4.9c shows the active power sharing between the grid-side converters (VSC_1 and VSC_2). At the start each converter injects 390MW into ac network$_1$ at B_1 and B_2. As expected no power flows in the dc auxiliary cables connecting converters VSC_1-VSC_2 and VSC_3-VSC_4 (P_y and P_x). At time t=1.5s, the droop control is activated to enable converter VSC_1 to inject additional 120MW into B_1. The additional power flow is from VSC_2 to VSC_1 through the auxiliary cable$_2$ and the power injected by VSC_2 to B_2 is reduced by 120MW (if the losses in the auxiliary cable are neglected). At t=3sec the power command has been changed to enable VSC_1 to inject additional 60MW into B_1.

At t=4.5s the dc droop controller is deactivated, each converter is returned to inject 390MW into the ac network$_1$ at B_1 and B_2 and power flows in the auxiliary cable$_2$. At t=6s the situation is changed, now the droop controller is activated to enable VSC_2 to inject 60MW additional power into B_2 at t=6s, and 120MW at t=7.5s. In this case, the power flow in the dc auxiliary cable$_2$ between converters VSC_2-VSC_1 is reversed, and the power delivered by VSC_1 is reduced to match the new situation. The power injected by converters VSC_3 and VSC_4 into the dc network remains constant at 400MW during the entire simulation period.

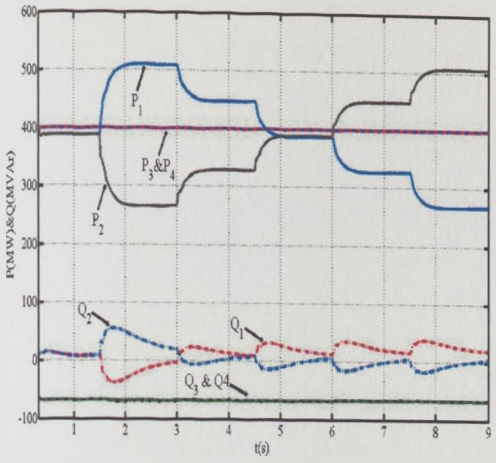
A resistive current limiter is used in the auxiliary cable$_1$ to prevent current flowing between VSC_3-VSC_4 during activation of the dc droop controller. The dc link voltage at VSC_2 is increased by ± 4kV in order to deliver the additional power from VSC_2-to-VSC_1 while the dc link voltage remains constant at 300kV at VSC_1 converter (Fig. 4.9a). The ac voltage at B_1-to-B_4 remains nearly constant during the activation of the dc droop controller (Fig. 4.9b). The reactive power exchange between converters and buses B_1-to-B_4 is manipulated in order to maintain the power at these buses at 1.0pu.



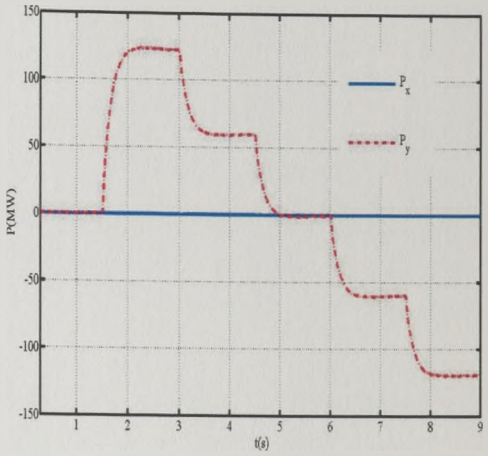
(a) DC voltages at VSC converters (VSC_1-to-VSC_4)



(b) AC voltages at busses B_1-to-B_4



(c) Active and reactive power at busses B_1-to-B_4



(b) Active power in auxiliary cables.

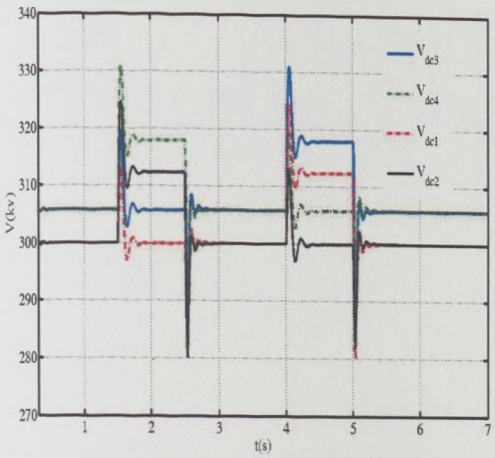
Fig. 4.9: Key simulation results during power management between VSC_1 and VSC_2.

4-4 MTDC system behavior during a sudden loss of converter/dc link cable

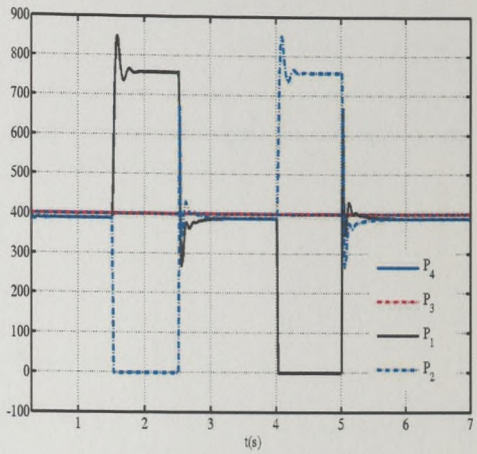
This section investigates the behaviour of multi-terminal VSC-HVDC transmission systems during a sudden loss of a receiving-end converter or a dc link cable, and assesses the potential benefits of multi-terminal dc systems in terms of reliability and security of supply. Firstly, the loss of one grid-side converter is investigated. Fig. 4.10 shows the results obtained during temporary loss of converter VSC_1 and VSC_2. In this case, converter VSC_2 is deliberately disconnected at t=1.5s and reconnected at t=2.5s while VSC_1 is disconnected at t=4s and reconnected again at 5s. It can be observed that during the loss of converter VSC_1 or VSC_2, all the power is delivered to the grid through the other healthy converter, as shown in Fig. 4.10b. To make this case possible, the rating of converters VSC_1 and VSC_2 are increased to twice that of VSC_3 and VSC_4 in order to be able to carry the full power from the ac $network_1$ in case of loss of one of the grid-side converters (from a technical viewpoint this increases the system reliability at the expense of investment cost; optimal operation with capacity constraints may represent another option to avoid increasing VSC rating).

When VSC_2 is suddenly disconnected from the system the power delivered to B_2 by VSC_2 collapses to zero at the same time the dc link voltage at VSC_4 is increased and creates a voltage difference in the auxiliary cables resulting in transfer of the power delivered by the lost converter (VSC_2) through auxiliary cables 1 and 2 into the ac system via VSC_1, the majority of the power is transferred through auxiliary cable 1. The multi-terminal dc system efficiency is reduced during the loss of VSC_1 converter because of the additional power

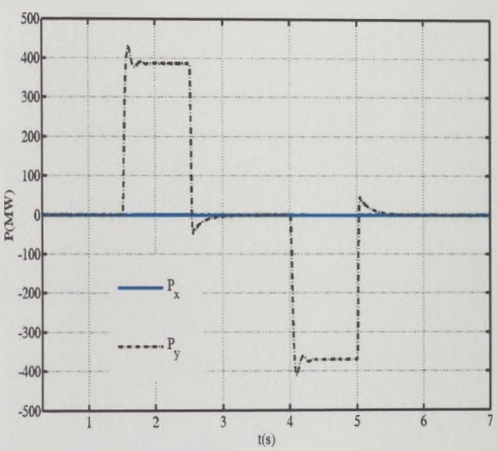
losses occurring during the power flow through the auxiliary cables. The dc voltage stress on the dc cables and the converter is not too high to cause serious operational problems.



(a) DC voltages at VSC converters (VSC_1-to-VSC_4)



(b) Active power in B_1-to-B_4

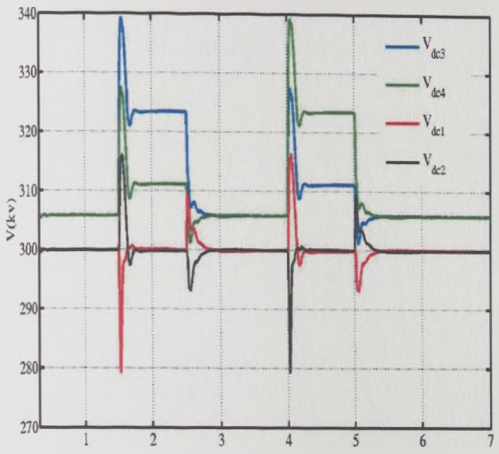


(c) Active power in auxiliary cable.

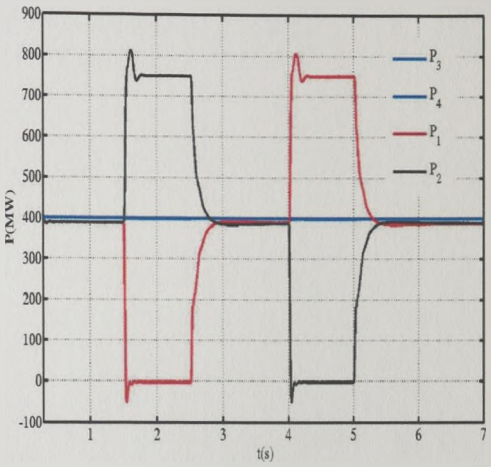
Fig. 4.10: Key simulation results during loss of VSC_1.

Fig. 4.11 shows the results obtained during the temporary loss of dc link $cable_1$ and dc link $cable_2$. The dc link $cable_1$ is suddenly disconnected at t=1.5s and reconnected to the system at t=2.5s, while dc link $cable_2$ is suddenly disconnected at t=4s and reconnected to the system at t=5s. In this case all the power is delivered to the grid through the dc link $cable_2$ as shown in Fig. 4.11b. It is very important to ensure that the rating of the dc cables is increased to twice that of VSC_3 and VSC_4 in order to be able to deliver the total power from the ac $network_1$ in the case of loss of one of the dc link cables (again, the increase of system reliability is achieved with additional investment cost). When the dc link $cable_1$ is disconnected from the system, all the power from the ac $network_1$ is pushed to B_2 by VSC_2, the dc link voltage at VSC_3 is

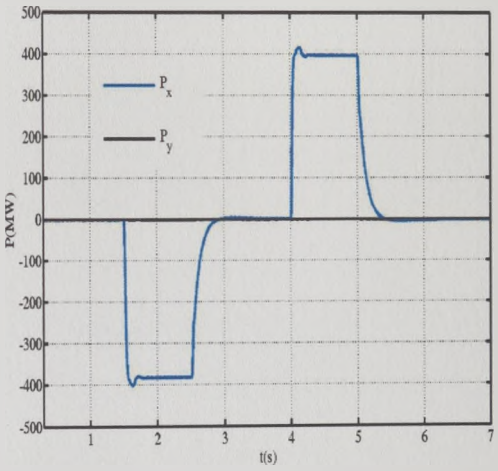
increased and creates a voltage difference in the auxiliary cable$_1$ resulting in pushing of the VSC_3 power through auxiliary cable$_1$ and hence the sum of VSC_3 and VSC_4 power is transmitted through the dc link cable$_2$. The dc voltage stress on VSC_3 and the auxiliary cable$_1$ is more serious in this case because the dc voltage (V_{dc3}) increase is more than that when losing a VSC converter.



(a) DC voltages at VSC converters (VSC_1-to-VSC_4)



(b) Active power in buses B_1-to-B_4



(c) Active power in auxiliary cables.

Fig. 4.11: key simulation results during lost of dc link cable$_1$.

4-5 Multi-terminal VSC-HVDC for creation of a regional dc network (SuperGrid)

The continuous growth of electrical power demand especially in the developed countries has led to large and complex interconnected networks covering part of, or even the whole country [13]. For economical and technical reasons regional power systems are extended to build the national grids which are also extended with the neighbouring countries to create the

transnational supergrids. The largest interconnected power network in Europe is the ENTSO (European Network of Transmission System Operators for Electricity) which uses synchronous connection (HVAC transmission lines) to interconnect 34 countries in Europe.
In general, the potential benefits of the interconnected power system are [13-14]:

- Allows optimum use of available resources.
- Reduction of generation costs by optimal unit commitment.
- Reliable and stable electric power systems.
- Reduction of the necessary reserve capacity in the system.
- Social and environmental advantages.
- Flexibility of building new power plant at favourable locations.

The construction of the backbone of the regional transmission system can be built using the high voltage ac system (HVAC) or high voltage dc system (HVDC). The HVACs are well-known technologies, proven, cheap and reliable but with the increase in the power capacity and the long transmission distance between the regional networks, the HVAC technology face some technical limitations which could reduce the advantages of the interconnected system. These limitations are summarized as follow:

- Reduction of economic advantages due to large transmission distances and insufficient voltage levels.
- Spinning reserve in the system to be transmitted over long distances (additional losses).
- Reactive power compensation is necessary for long distance transmission to avoid voltage problems.
- The operation of the tie-line may cause power oscillations.
- A fault in part of the network propagates and affects the whole system.
- HVAC system did not facilitate the connection of renewable resource especially for long distance transmission.

The conventional CSC-HVDC systems are another possible solution to build the future dc regional networks. The CSC-HVDC system as stated in Chapter 2 cannot be used to transfer the renewable energy without the aid of start-up generators or synchronous compensators devices which provide the necessary commutation voltage, and thus reactive power

compensation devices are required. Another limitation of CSC-HVDC systems is the necessity to reverse the dc voltage polarity in order to achieve power reversal. Complex power control associated with the multi-terminal operation may limit the terminal number.
A VSC-HVDC system is a suitable technology for building the future supergrid dc network. It is easier to control the power flow and build parallel multi-terminal configurations. Simple fixable control system is associated with multi-terminal operation including power management and power reversal. VSC-HVDC facilitates the connection of renewable power plants and isolated islands to the dc network [15-16].

Based on the previous discussion, the multi-terminal VSC-HVDC system can be used to create a large power pool to facilitate the power trading in real time between large regional ac networks, and the integration of renewable energy resources without compromising system reliability and security of supply. This approach, besides the power accommodation between the regional networks, may allow high penetration of renewable power into power systems without the need for energy storage systems for power leveling or other power quality issues.

If HVDC system is used for building of the transnational supergrid, the power pool is comprised of a meshed dc network that includes a group of dc links operated at different dc voltages, where the dc buses are connected to the regional networks via power converters [17]. Presently, there is no specific standard for the dc voltage level. A dc voltage greater than 2 times the ac voltage (rms value) for PWM, or greater than 1.74 for PWM with third-harmonic injection can be used as stated in [18]. The dc converters could operate as rectifier/inverter to inject/withdraw the power into/from the power pool. The power injection or absorption from the power pool is controlled by the converters, while the power flow in the dc links is governed by Kirchhoff voltage law.

The potential benefits of the dc regional supergrid are:

1- It is the ideal solution for the integration of large-scale renewable energy resources such as wind and solar power [19-20]. The supergrid achieves renewable power balancing due to the variation in renewable energy resources output. The connection of widespread wind farms and solar energy projects to a common dc network reduce the possibility of renewable power variability because of correlation of different weather conditions [17].

2- Facilitates power trading between the regional ac networks over long distances with optimum transmission losses. The high voltage in the dc links increases transmission

system efficiency and the power accommodation power in remote locations and load centers.

3- Allows the regional ac networks sharing of back-up power. Any ac network can use the reserve generations in the other ac networks, and this reduces the risk of black-out in the regional ac systems.

4- Allows using underground/submarine cables as transmission medium where only cables can be used. Using cables cause no visual pollution and has less opposition with the licensing [17].

5- The inherent reactive power capabilities of the VSC converter provide the necessary reactive power compensation and limit the overload in the system.

Nine European countries in the border of the north sea agreed in 2010 to build a super HVDC network in the north sea to integrate and accommodate renewable energy (wind, solar and tidal power) between Belgium, Denmark, France, Germany, Ireland, Luxembourg, Netherlands, Norway, and the United Kingdom [21]. Around 100GW offshore wind power are planned to be installed in the North Sea. Norway giant hydropower capacity facilitates the power-demand balancing and stores the massive offshore power and fulfills the system peak load and power stabilization. For example the wind energy generated at night in the UK could be stored in the Norway network and released the following day. The North Sea supergrid will extend to the Sahara desert and connect with the solar power plant in the desert [22].

4-6 VSC-HVDC network for regional dc network and renewable energy integration

Fig. 4.12 shows an HVDC network comprising of four terminals modeled with neutral-point clamped (NPC) converters and controlled using sinusoidal pulse width modulation (SPWM) with 2.05 kHz switching frequency. Each NPC uses two dc link capacitors of 300μF with neutral-point-ground to form bipolar HVDC systems. Converter VSC-WF connects a 400MW wind farm into the dc network. While converters VSC_1 to VSC_3 connect ac networks 1, 2 and 3 into the dc network. The dc grid comprises of four links, each 150km and modeled using a lumped π section. Converters VSC_{WF}, VSC_1 and VSC_2 control the active power and the ac voltage magnitude at B_{WF}, B_1 and B_2. Converter VSC_3 regulates the dc voltage at 300kV pole-to-pole (±150kV) and the ac voltage magnitude at B_3. Further details

on voltage and power levels are depicted in Fig. 4.12, and power flow directions indicated are assumed positive.

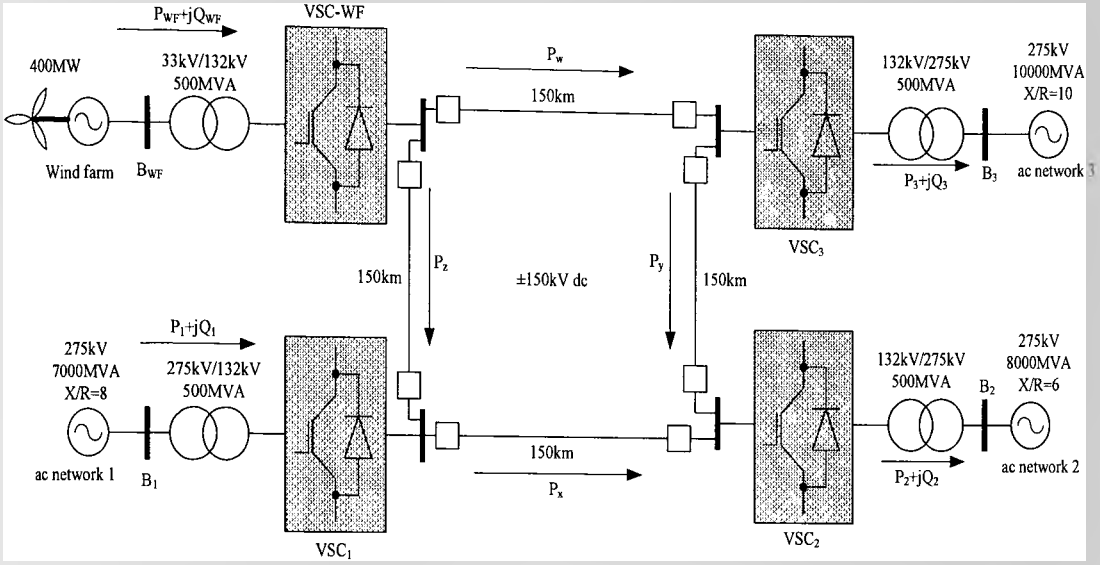


Fig. 4.12: Four-terminal HVDC network used as a test system for grid integration of offshore wind farms, and implementation of a transnational dc grid for power trading with real-time dispatch capability.

4-6-1 The dc network control strategy

All the VSC converters in the proposed dc network system control the active power flow from/into the dc network except converter VSC_3, which is used to control the dc voltage [23]. In this case VSC_3 is considered as the slack bus, which achieves the power balancing in the system. The system connected to the slack bus which acts as the power balancer must have a high reserve power generation and high storage capacity. The power flow in the slack bus is calculated based on the energy balancing law as follows:

$$P_{slack} - P_1 - P_2 - P_{WF} - P_{losses} = 0 \tag{4-3}$$

The power flow in the dc link cables inside the dc network is determined by the voltage difference between the dc voltages at the converters. The dc voltages at the VSC converters are different according to the amount and direction of the power. The dc voltage is higher when the converters injects power into the dc network and lower when the converter absorbs power from the dc network. The VSC converters dc currents are calculated as follows [24]:

$$I_{dci} = \sum_{\substack{j=1 \\ j \neq i}}^{n} \frac{\left(V_{dci} - V_{dcj}\right)}{R_{dcij}} \tag{4-4}$$

A central control system is used to coordinate the power injection/absorption for the VSCs and to set the power references for the VSC converters. dc voltage and the ac voltage control are adopted for the local control in each converter station. Fast and reliable communications to transmit the signals between the converter stations and the central control are required. The power flow re-schedule is achieved by managing the power references in the master control. It is most important that all converter stations have the same ramping speed to avoid unwanted dynamic response.

4-6-2 System protection

The protection system of the multi-terminal system is a major problem especially during a fault in the dc network. The VSC-HVDC system copes well with ac faults with appropriate control and protection methods, but it is vulnerable to faults occurring in the DC link and this has limited its practical application in multi-terminal networks during the last decade. The technology gap in isolation mechanisms of the dc fault and the absence of reliable dc breakers is a real problem facing multi-terminal dc operation. When a short-circuit occurs between the dc links conductors, the capacitors rapidly discharge into the fault point circulating excessive dc fault current (Fig. 4.13). With the absence of the zero crossing point and the excessive fault current no dc circuit breaker has been manufactured to handle the dc link fault.

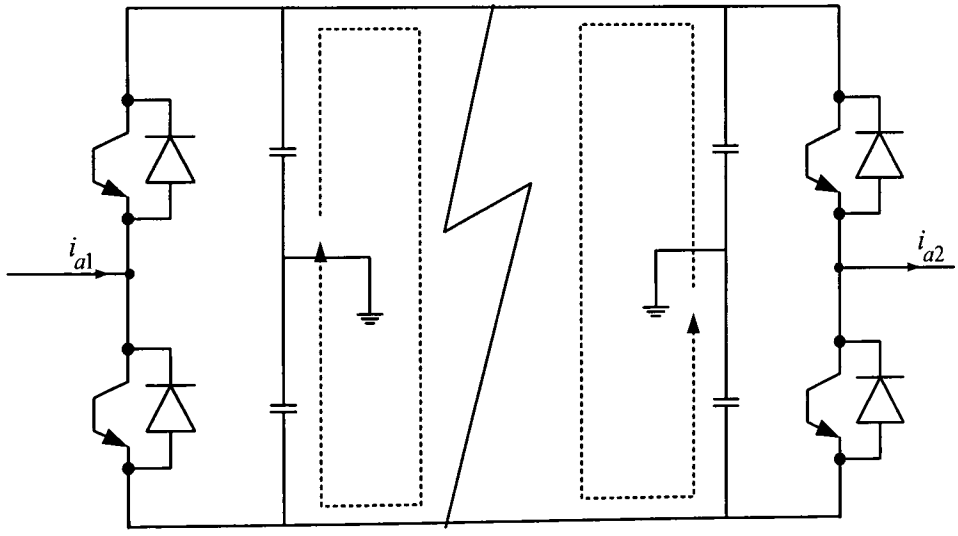


Fig. 4.13: dc fault in the VSC-HVDC system.

Power electronics converters are very sensitive to the overload current and cannot withstand the excessive fault current [25]. Reliable protection system capable to sense, detect the fault location and terminate the fault is required to maintain system stability during dc faults. The

dc fault could be cleared using ac circuit breakers associated with power converter blocking, but this would require all terminals to be isolated, resulting in complete shut-down of the dc system [17, 26].

Several approaches are introduced to address the clearing of the dc fault. AC circuit breakers can be used to eliminate the fault in the dc network. The existing VSC-HVDC systems activate the ac breakers placed on the ac networks to isolate the dc network until the fault is extinguished. Power electronics converters are blocked during the isolation to speed up the clearance time. After fault clearance, the dc system is reconnected again and the converters are unblocked gradually with a ramp function [27]. For the permanent faults the faulty dc cable is totally remove from the dc network after the opening of isolation of the dc network by opening the ac breakers.

IGBT circuit breakers placed between each converter terminal capacitors and the dc network buses are used to protect the dc network against the dc network faults [28]. The limitation of this approach is the unidirectional capability of the IGBT circuit breaker. When the fault occurs on the converter side, the IGBT-CB is blocked-in and no power flows into the dc network until the fault is extinguished. If the fault occurs in the dc network side the fault current flows into the VSC converters through the anti-parallel diodes (Fig 4.14). In this case the blocking of the IGBT-CB is associated with the blocking of the VSC converters. The IGBT-CBs have the same rating of the VSC converter and this increases system transmission losses.

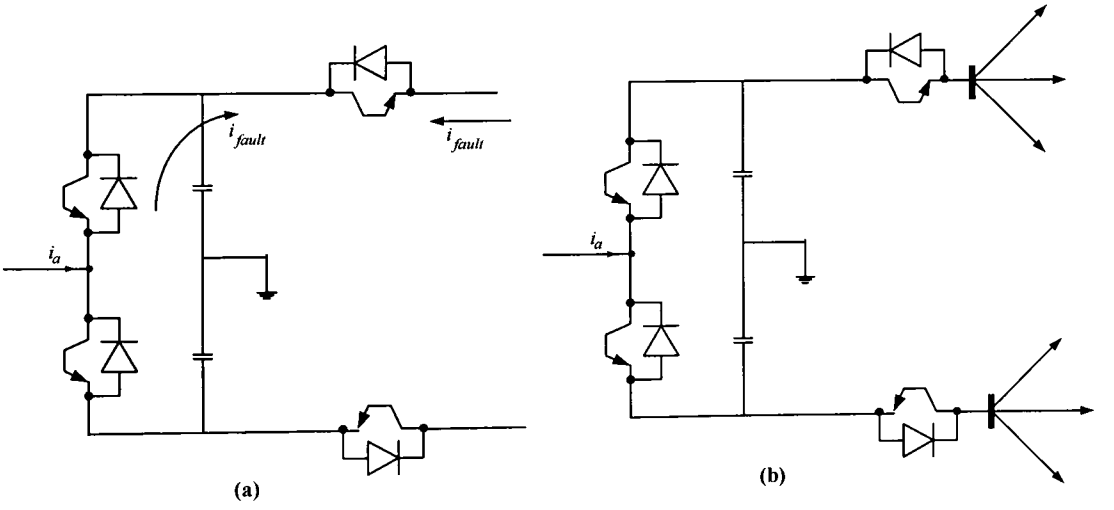


Fig. 4.14: IGBT-circuit breakers.

New technology introduced by ABB is capable to address the dc fault issues. In the two-switch modular multilevel converter, the current magnitude that converter switches may

experience during dc side faults is significantly reduced due to the absence of the dc link capacitors [26].

When the protection system isolates the affected dc cable, the dc network power flow is re-routed through the healthy dc cables. The remaining cables must be capable to withstand the additional power transferred by the faulty cable.

4-6-3 Multi-terminal VSC-HVDC network power trading

In steady state, the multi-terminal system accommodates the power between the system terminals according to the scheduled power curve setting by power system operators. The slack-bus converter is used to achieve the power balance between the ac and the dc networks. If for any reason the power schedule is changed or a converter terminal is lost, the slack-bus converter power will change to match the new situation as shown in Fig. 4.15.

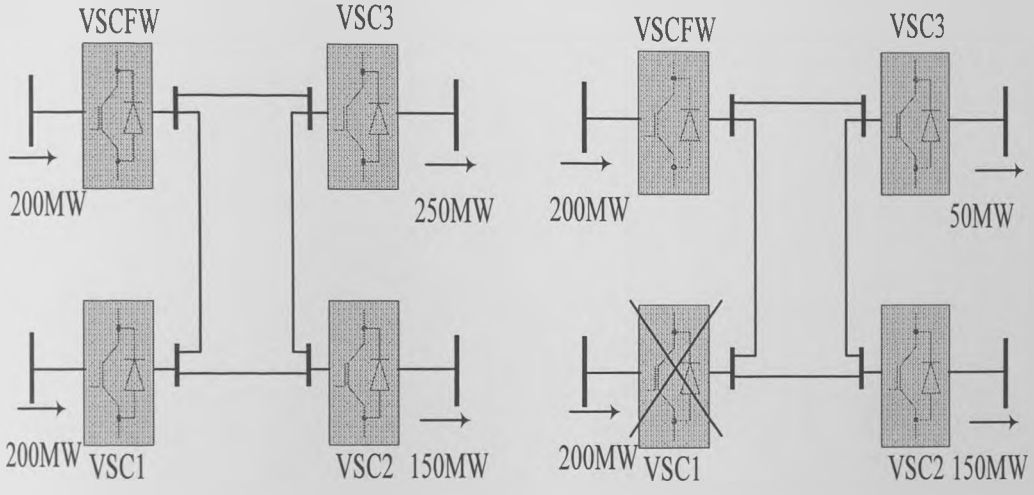


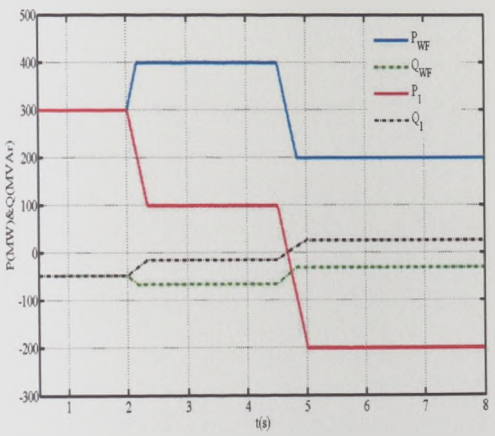
Fig. 4.15: Multi-terminal dc system behavior during loss of one converter.

To demonstrate the viability of using an HVDC network to form a power pool for accommodation of large wind farms with variable output powers and possible power trading in real-time between different regional ac networks, the test system in Fig. 4.12 is started with both wind farm converter VSC_{WF} and ac network 1 converter (VSC_1) injecting 300MW into the power pool (dc grid), and converter VSC_2 importing 200MW from the power pool. At time t=2s, the wind farm output power is gradually increased from 300MW to 400MW, while converter VSC_1 reduces its injected power to the dc grid to 100MW. At the same time, the power imported by converter VSC_2 is gradually increased from 200MW to 300MW. At t=4.5s, the wind farm power output is decreased gradually from 400MW to 200MW and converter VSC_1 is commanded to import 200MW from the dc grid. The imported power by

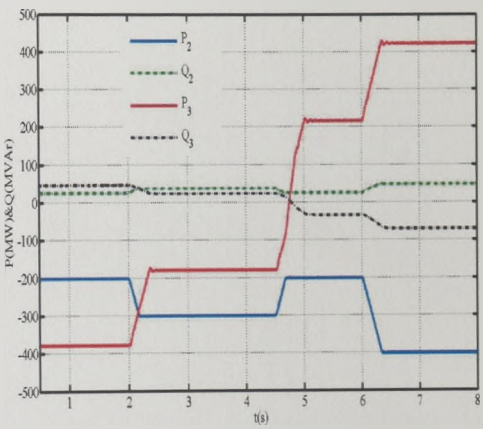
VSC_2 is reduced from 300MW to 200MW. At t=6s, converter VSC_2 is rescheduled to withdraw 400MW from the dc grid.

The results obtained from this case are shown in Fig. 4.16. Figs. 4.16a and 4.16b show the active and reactive power that the converter stations exchange with the wind farm and the three regional ac networks 1, 2 and 3. Figs. 4.16c and 4.16d show the power flow in the dc grid. It can be seen that the converter terminal connected to ac network 3 (VSC_3), which regulates the dc link voltage, acts as slack-bus for the whole system, to maintain an active power balance between the ac and dc sides.

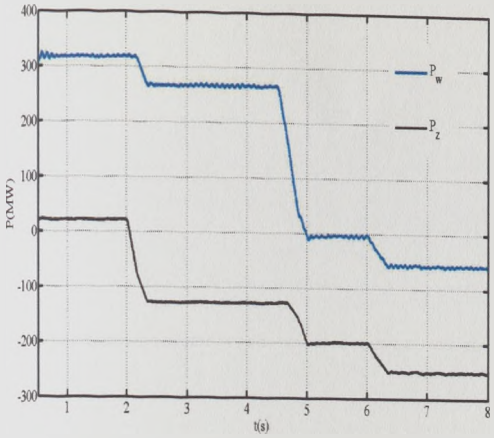
Figs. 4.16a, 4.16b and 4.16e show that during variations of the active power exchange between the converter stations and ac networks, including the wind farm, the converter stations are able to maintain constant voltage magnitudes at the points of common coupling using appropriate reactive power exchange with the ac sides. Fig. 4.16f shows the variation of the converter dc link voltages with respect to converter station VSC_3, which regulates the dc voltage at 300kV as powers exported and imported to/from the power pool vary.



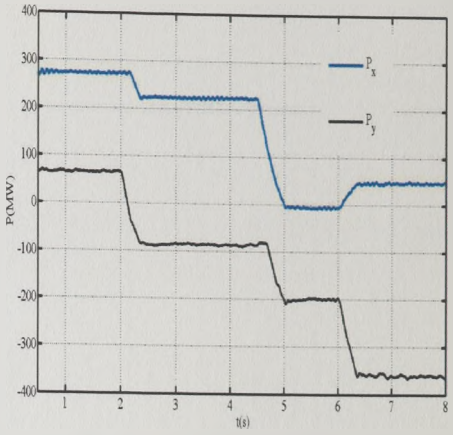
a. Active and reactive power exchange between the wind farm, grid 1 and the dc grid



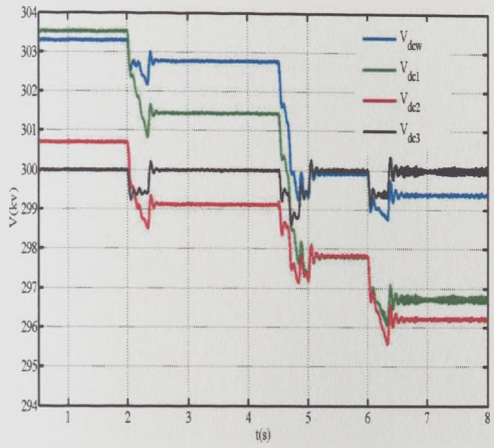
b. Active and reactive power exchange between grids 2 and 3, and the dc grid.



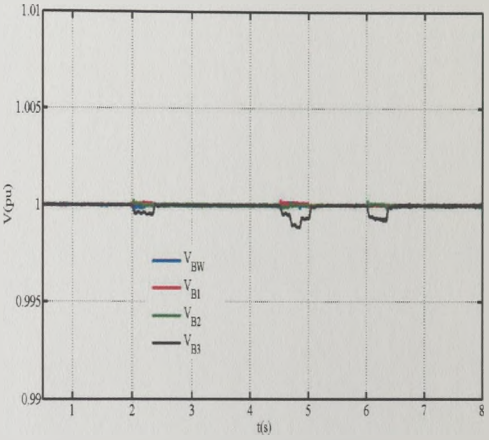
c. Power flow in the dc links between VSC-WF and VSC-1; and VSC-WF and VSC-3.



d. Power flow in the dc links between VSC-1 and VSC_2; and VSC-2 and VSC-3.



e. Voltage magnitude at wind farm bus B_{WF} and points of common coupling B_1 through B_3



f. Voltage magnitude across the dc link of different converter stations

Fig. 4.16: Key results of the multi-terminal dc system power system.

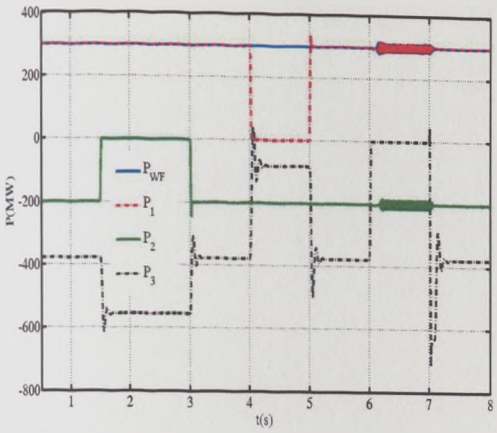
These results illustrate the potential usefulness of HVDC networks in dispatching power to different regional ac networks and to accommodate large amounts of un-scheduled power from wind farms without the need for any storage systems. Any extension of the dc network is achieved by connecting the additional ac regional network or wind farms via VSC converter into dc network.

4-6-4 Multi-terminal dc system performance during loss of a converter station

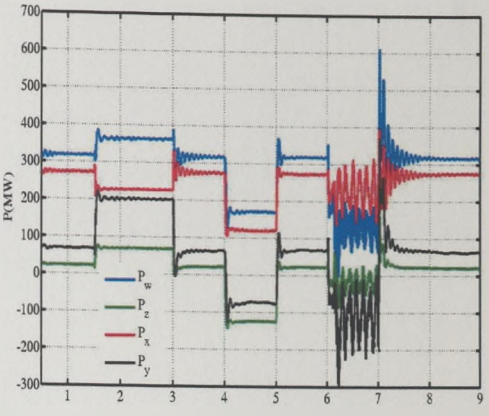
As mentioned previously, the power balancing between the dc networks and the ac grids is achieved by the converter terminal which controls the dc voltage. When this terminal is disconnected from the system the dc voltage is significantly increased and the system is no longer stable. It is very important from the stability and reliability viewpoint to keep the

terminal which controls the dc voltage connected to the system. Such situation can be avoided by assigning more than one converter station to regulate the dc link voltage. The VSC-HVDC network is capable to remain stable when a sudden loss of a converter occurs except the one that control the dc voltage. Any loss of converter stations creates an unbalance in the dc network; the slack-bus converter station controls its output to cope with the new operating conditions. The slack-bus converter must have enough reserve generation to overcome any mismatch in the dc network.

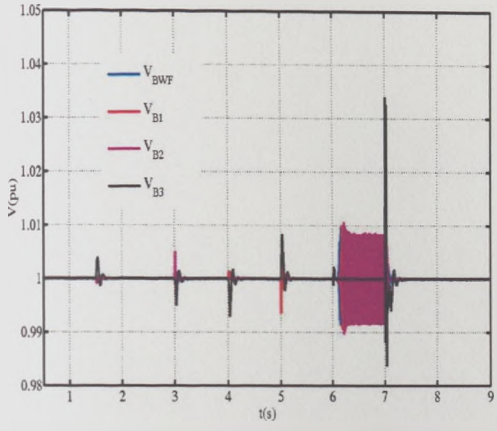
To demonstrate the effectiveness of the HVDC network in improving the transient stability of the overall system during a major fault in one of the ac sides, the test system in Fig. 4.12 is subjected to loss of grid at converter station VSC_1, VSC_2 and VSC_3 by opening the ac circuit breakers connecting VSC_1, VSC_2 and VSC_3 to the dc network at time t=1.5s, t=4s, and t=6s and reclosed at t=3s, t=5s, and t=7s. During this period, the wind farm injects 300MW into the dc grid, network 1 injects 300MW into the dc grid and ac network 2 imports 200MW from the dc grid. It can be seen that the loss of regional ac networks 1 and 2 have no significant effect on the overall system transient stability (see Fig. 4.17a). This effect is reflected as an active power mismatch and handled mainly by the converter terminal that regulates the dc link voltage and operates as slack bus (Fig. 4.17a). A similar situation will exist with the loss of a wind farm or any converter terminal that controls the active power flow. The system loses stability when terminal VSC_3 is suddenly disconnected as shown in Fig. 4.17a. As expected, the dc voltage is significantly increased and the power flow in the dc network cables is affected (Fig. 4.17b). Based on these results, it can be concluded that such HVDC network may be viable for the proposed European SuperGrid, as the ac fault in any of the regional ac networks may not propagate into other regions. However, the system in Fig. 4.12 with the present converters' control objectives is vulnerable to catastrophic overall system collapse when the converter station that controls the dc link voltage is lost. In this case, the active power control flexibility of the system can be maintained with the incorporation of an active power-dc voltage droop within the dc voltage controller of each converter station.



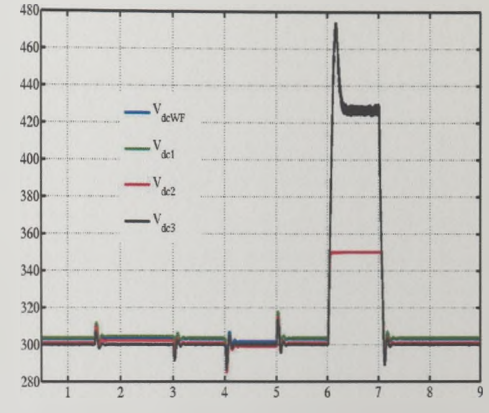
a. Active and reactive power exchange between the wind farm, grid 1 and the dc grid



b. Active and reactive power exchange between grids 2 and 3, and the dc grid



c. Power flow in the dc grid (power pool)



d. dc voltage across the different converter stations

Fig. 4.17: Key results for the multi-terminal dc system behavior during loss of converter stations.

4-7 Summary

In this chapter the multi-terminal dc system operation was investigated. Two possible operation scenarios of MTDC were discussed in detail. First, MTDC operation when the power flow has one direction and the converter could not reverse the power flow. In this case the converter terminals have one mode (rectifier or inverter). This application is suitable for wind farm integration and to supply power to remote isolated areas. The control flexibility of the system allows the converters at the receiving end to share the transmitted power. The power-voltage characteristics of the receiving-end converter could change continuously to achieve this purpose. System reliability is increased especially during loss of receiving-end terminal or dc link cable. The second application is the use of the MTDC to create a regional dc network with huge reserve generation and storage capacity. This scenario facilitates the

connection of the large-scale renewable resources spread in a wide area without the need for load leveling in the system.

The possibility of renewable power variation is reduced because of correlation of different weather conditions. System reliability is high; no power fault could propagate from one ac region to another regions. Loss of any converter terminal is reflected as a power mismatch in the system which is handled by the slack-bus converter. The shortness of the system comes from the vulnerability of the MTDC to lose the slack-bus terminal (the one which controls the dc voltage). The main problem of MTDC systems, which has limited its application during the last decade, is the isolation of a dc fault at the dc link. No reliable dc breakers are in application now although there are some attempts to introduce different techniques in order to protect the dc link cable.

References

[1] W. F. Long, *et al.*, "Application aspects of multiterminal DC power transmission," *Power Delivery, IEEE Transactions on,* vol. 5, pp. 2084-2098, 1990.

[2] V. K. S. Chan-Ki Kim, Gil-Soo Jang,Seong-Joo Lim, Seok-Jin Lee *HVDC Transmission: Power Conversion Application in Power System*: John Wiley & Sons (Asia), Publication, 2009, Singapore.

[3] G. Morin, *et al.*, "Modeling of the Hydro-Quebec-New England HVDC system and digital controls with EMTP," *Power Delivery, IEEE Transactions on,* vol. 8, pp. 559-566, 1993.

[4] G. P. Adam, *et al.*, "Multi-terminal DC transmission system based on modular multilevel converter," in *Universities Power Engineering Conference (UPEC), 2009 Proceedings of the 44th International*, pp. 1-5.

[5] L. Xu, *et al.*, "Multi-terminal DC transmission systems for connecting large offshore wind farms," in *Power and Energy Society General Meeting - Conversion and Delivery of Electrical Energy in the 21st Century, 2008 IEEE*, 2008, pp. 1-7.

[6] Z. Jiebei and C. Booth, "Future multi-terminal HVDC transmission systems using Voltage source converters," in *Universities Power Engineering Conference (UPEC), 2010 45th International*, 2010, pp. 1-6.

[7] K. R. Padiyar, *HVDC power transmission systems: technology and system interactions*. New Delhi: New Age International (P) Limited, Publishers, 2005.

[8] J. Hongbo and A. Ekstrom, "Multiterminal HVDC systems in urban areas of large cities," *Power Delivery, IEEE Transactions on,* vol. 13, pp. 1278-1284, 1998.

[9] T. M. Haileselassie, *et al.*, "Multi-Terminal VSC-HVDC System for Integration of Offshore Wind Farms and Green Electrification of Platforms in the North Sea," *Nordic Workshop on Power and Industrial Electronics, June 2008.*

[10] G. P. Adam, *et al.*, "Multi-terminal DC transmission system based on modular multilevel converter," in *Universities Power Engineering Conference (UPEC), 2009 Proceedings of the 44th International*, 2009, pp. 1-5.

[11] Z. Shu, *et al.*, "Control of multi-terminal VSC-HVDC transmission system for offshore wind power generation," in *Universities Power Engineering Conference (UPEC), 2009 Proceedings of the 44th International*, 2009, pp. 1-5.

[12] L. Jun, *et al.*, "Control of multi-terminal VSC-HVDC transmission for offshore wind power," in *Power Electronics and Applications, 2009. EPE '09. 13th European Conference on*, 2009, pp. 1-10.

[13] D. Povh and D.Retzmann, "Large interconnncted system for econmical and secure power supply," *www.ptd.siemens.de/DEMSEE08_Art.pdf.*

[14] W. Breuer, *et al.*, "Application of HVDC for Large Power System Interconnections," *article avialable at http://www.ptd.siemens.de/B4-106.pdf,* 2004.

[15] P. Bresesti, *et al.*, "HVDC Connection of Offshore Wind Farms to the Transmission System," *Energy Conversion, IEEE Transactions on,* vol. 22, pp. 37-43, 2007.

[16] N. Flourentzou, *et al.*, "VSC-Based HVDC Power Transmission Systems: An Overview," *IEEE Trans on Power Electronics,,* vol. 24, pp. 592-602, 2009.

[17] D. V. Hertem and M. Ghandhari, "Multi-terminal VSC HVDC for the European supergrid: Obstacles " *Renewable and Sustainable Energy Reviews,* vol. Volume 14, pp. 3156–3163, Dec 2010.

[18] A. Yazdani and R. Iravani, *Voltage-Sourced Converters in Power Systems: Modeling, Control, and Applications*. Hoboken, New Jersey: John Wiley & Sons, Inc, 2010.

[19] Y. Liu, *et al.*, "Several Power Transmission Backbone Schemes," *Proceedings of the 14th International Middle East Power Systems Conference (MEPCON'10), Cairo University, Egypt, December 19-21, 2010, Paper ID 182.*

[20] S. Gordon, "Supergrid to the rescue," *Power Engineer,* vol. 20, pp. 30-33, 2006.

[21] J. Blau, "Europe plans a North Sea grid," *Spectrum, IEEE,* vol. 47, pp. 12-13, 2010.

[22] DESERTEC_Foundation, "Clean power from deserts – the Desteric concept for energy, water and climate security.," *Available online at: http://www.desertec.org/fileadmin/downloads/DESERTEC-WhiteBook_en_small.pdf.*

[23] J. Beerten, *et al.*, "A sequential AC/DC power flow algorithm for networks containing Multi-terminal VSC HVDC systems," in *Power and Energy Society General Meeting, 2010 IEEE*, 2010, pp. 1-7.

[24] S. Cole, *et al.*, "Generalized Dynamic VSC MTDC Model for Power System Stability Studies," *Power Systems, IEEE Transactions on,* vol. 25, pp. 1655-1662, 2010.

[25] E. B. Mesut and R. M. Nikhil, "Overcurrent Protection on Voltage-Source-Converter-Based Multiterminal DC Distribution Systems," *Power Delivery, IEEE Transactions on,* vol. 22, pp. 406-412, 2007.

[26] G. P. Adam, *et al.*, "Network fault tolerant voltage-source-converters for high-voltage applications," in *AC and DC Power Transmission, 2010. ACDC. 9th IET International Conference on*, 2010, pp. 1-5.

[27] L. Livermore, *et al.*, "MTDC VSC Technology and its applications for wind power," in *Universities Power Engineering Conference (UPEC), 2010 45th International*, 2010, pp. 1-6.

[28] T. Lianxiang and O. Boon-Teck, "Protection of VSC-multi-terminal HVDC against DC faults," in *Power Electronics Specialists Conference, 2002. pesc 02. 2002 IEEE 33rd Annual*, 2002, pp. 719-724 vol.2.

Chapter Five

High voltage dc transmission system based on voltage source converter (VSC-HVDC) for offshore wind farms integration

5-1 Introduction

Offshore wind farms may be located far away from the shore collection point. As a result the need has increased to develop strong effective methods to transfer the generated offshore wind power to the nearest power network access point and to study the impact of wind power on the power system operation and stability. The integration process of wind farms into power networks faces two challenges: collection of the wind power at the offshore collection point, and transmission of the collected power to the onshore collection point.

The collection system collects the wind power into one particular point. A number of wind turbines is used to convert the kinetic energy in the moving air into mechanical torque and then drive the generator to produce the electrical energy. As currently most wind turbines are operated at a low voltage of 690V, a step-up transformer is required to increase the generator voltage to the transmission voltage level. There are many different layout configurations for offshore wind farms but the popular one is the string cluster configuration, in which a number of wind turbine generators are fed into a distribution feeder with a voltage level enough to carry the total power of the wind turbine generators. Then, all the distribution feeders are connected to an offshore substation transformer in order to increase the voltage to the proper transmission level (see Fig. 5.1) [1-2].

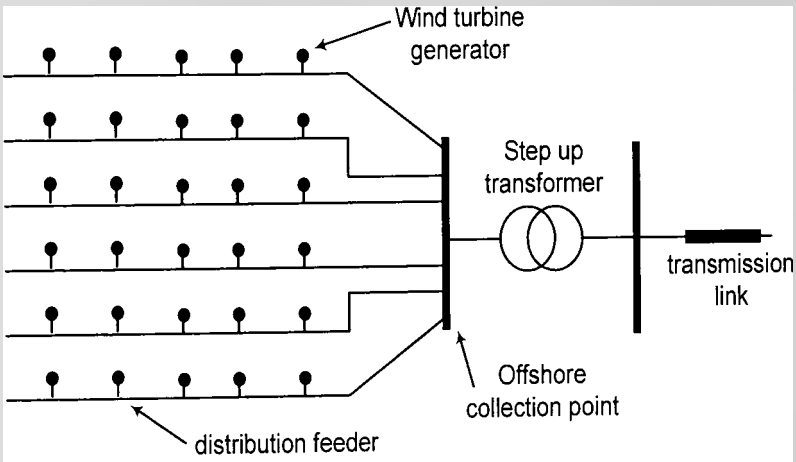


Fig. 5.1: String cluster lay-out configuration.

At present, the two established wind turbine generator technologies are fixed and variable speed. Fixed-speed induction generators wind turbines (FSIGs) are simple, robust, and well proven technology for wind power generation. The FSIG consists of a squirrel-cage induction generator coupled directly to the power system through a connecting transformer. The rotor speed variation of the squirrel-cage induction generator is generally less then 1% of the synchronous speed and changes slightly with power level changes, therefore the FSIGs are normally known as fixed-speed wind turbines [3].

The main disadvantage of fixed-speed wind farms are: the fluctuations in wind speed and turbine mechanical power are directly transferred into electrical power and voltage fluctuations, and produce excessive mechanical and electrical stresses in the drive train and asynchronous machine. Also, FSIGs allow maximum power extraction only at a particular wind speed, and always consume reactive power, and cannot control the reactive power exchange with the grid to maintain the terminal voltage. FSIGs have limited control over their output power, hence they cannot participate in grid frequency stabilization and damping of low-frequency oscillations despite being connected to the grid by their stator [4-5].

Variable-speed wind turbine generators, using doubly-fed induction generators (DFIGs), are asynchronous generators with a wound rotor. The stator is connected to the grid via a coupling transformer and the rotor is connected to the grid through partial scale bi-directional frequency converters. DFIGs are able to control the active and reactive power exchange with the grid, allow variable-speed operation over a wide range, and allow maximum power extraction and inherent reactive power capability at no additional cost. Furthermore, they can absorb any fluctuations in the generated power and voltage coming from the intermittency nature of wind, therefore no flicker is generated, and they can meet most of the current Grid Codes requirements [6-7] .

The transmission of the wind power from the offshore collection point to the onshore collection point is a major challenge from both economical and technical viewpoints. Many factors could influence the choice of the transmission medium for the wind power including: the additional functionality required by the system operator for wind farm integration (Grid Code requirements), wind farm capacity, wind farm type, transmission distance, power losses and environmental considerations.

In general there are three options for offshore wind power transmission [8-9]:

- High-voltage alternating-current transmission system (HVAC).
- High-voltage direct-current transmission system based on line-commutated converter (LCC-HVDC).
- High-voltage direct-current transmission system based on voltage source converter (VSC-HVDC).

5-2 Requirements for wind farm integration

In the past wind farms connected to power networks were small-size capacity and the penetration of wind power was small compared with the total installed generation. There were no special requirements for wind farm integration to the network because their impact on power system network stability was very small and could be neglected; and the wind farms were required to disconnect from the power network under abnormal operating conditions. Nowadays, the situation has changed due to the dramatic increase on installed wind power. An increase in wind power penetration means that wind power plants have considerable impact on system stability, and they must satisfied special requirement before connection to power system. Many countries such as Denmark, Germany, Spain, and UK have issued new connection codes for wind farms connection.

This section reviews the GB Grid Code requirements that any wind farm and dc converters must comply with. The new requirements state that wind farms must provide additional functionality, such as [6, 10-12]:

- Steady-state and dynamic reactive power control and voltage control.
- Active power and frequency control.
- Fault ride-through capabilities.

5-2-1 Voltage and reactive power control

Wind farms are required to be capable to regulate the reactive power at their terminals in order to control the voltage at the point of common coupling (PCC). In the GB Grid Code, the reactive power requirement of the wind farm is defined in Section CC.6.3.2 (see Fig. 5.2) [13]:

1- The wind farm must be able to supply rated MW output at any point between the limits 0.95 lag and 0.95 lead at the PCC with the GB transmission system.

2- With all plants in service, the reactive power limits defined at rated MW at lagging power factor will apply at all active power output levels above 20% of the rated MW output. These reactive power limits are reduced due to the amount of plant in service.

3- With all plants in service, the reactive power limits defined at rated MW at leading power factor will be applied at all active power output levels above 50% of the rated MW output. These reactive power limits will reduce linearly below 50% of active power output unless the requirement to maintain the reactive power limits defined at rated MW at leading power factor down to 20% active power output.

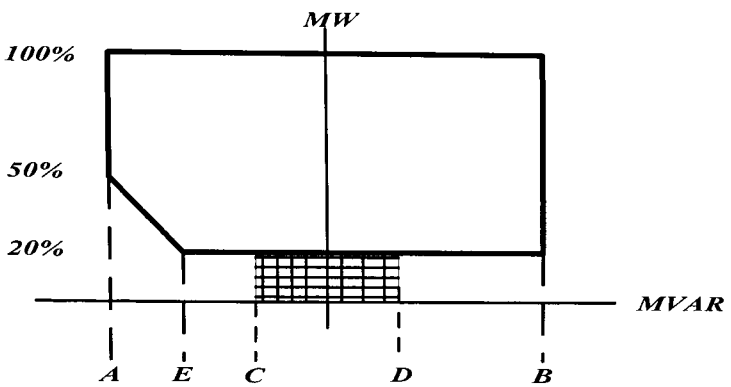


Fig. 5.2: Reactive power requirement for wind farm integration in UK

Point A is equivalent (in MVAr) to: 0.95 leading Power Factor at Rated MW output
Point B is equivalent (in MVAr) to: 0.95 lagging Power Factor at Rated MW output
Point C is equivalent (in MVAr) to: -5% of Rated MW output
Point D is equivalent (in MVAr) to: +5% of Rated MW output
Point E is equivalent (in MVAr) to: -12% of Rated MW output

5-2-2 Fault ride-through capability

If a short circuit occurs somewhere in the ac grid, the fault may extend across the system until the fault is terminated by circuit breakers. Some wind farms may not be able to remain stable and open their circuit breaker. In this case the system needs a higher spinning reserve to prevent the risk of black-out. An essential requirement in the GB Grid Code is that wind farms must remain connected to the system during a transmission system fault. The Fault Ride-Through capability (FRT) can be defined as the ability of a generating unit or power converter to ride through different types of faults. The GB Grid Code FRT capability requirements are given below and summarized in Fig. 5.3 [13]:

- A wind farm must remain transiently stable for a closed-up solid short-circuit with duration of 140ms. In addition, the wind farm has to remain connected to the system for any dip duration on or above the heavy black line in Fig. 5.3.

- The voltage at entry points must be restored to 90% of their pre-fault values within 0.5s as specified in CC.6.3.15.1.
- During the fault period where the voltage is outside the limits specified in CC.6.1.4, the wind farms and dc converters must generate the maximum reactive power possible without exceeding their thermal ratings.
- The terminal voltage of the wind farm should not be less than 15% of the nominal voltage during the fault period.

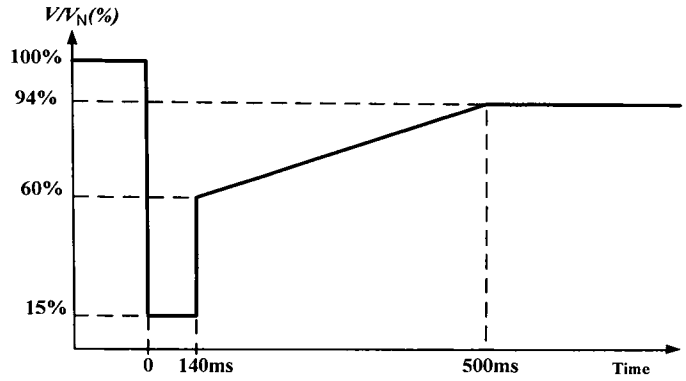


Fig. 5.3: AC Fault Ride-Through capability requirement for wind farm integration in the UK.

5-2-3 Frequency control

As the active power balance in the power network is strongly coupled to the frequency, any mismatch between the generation and demand may cause the system frequency to rise or decrease, depending on the net difference between generation and demand. Primary frequency control installed in each generation plant is used to stabilize the frequency during sudden load changes. The power system operator starts, stops or adjusts the output of generating units in operation in order to support the primary control and re-schedule the generation of power plants.

Fig. 5.4 shows the frequency requirements of wind farms according to the GB Grid Code. Some of the requirements concerning the relationship between the wind farm active power and the AC network frequency are summarized as follows [13]:

- A wind farm must be able to operate continuously with constant active power output for system frequency within 49.5Hz and 50.5 Hz, Grid Code CC.6.3.3 (a).
- The wind farm active power output should not be reduced by more than 5% for system frequency changes within the range 49.5 to 47 Hz.
- The wind farm must be able to operate continuously between 47-52 Hz for period less than 30sec.

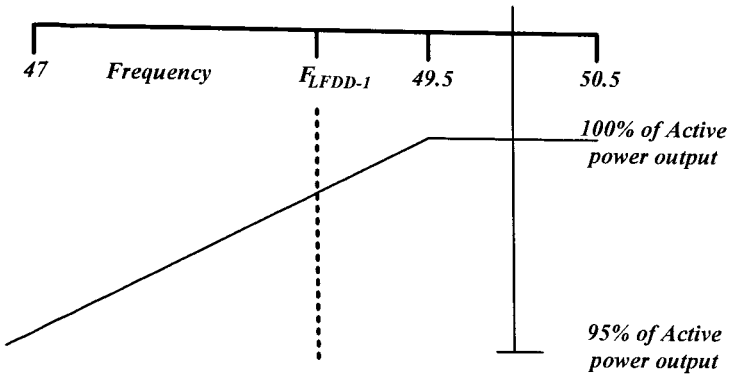


Fig. 5.4: Frequency requirement for wind farm integration in UK.

5-3 Offshore Wind Farms integration options

There are three possible solutions for transmitting the offshore wind power to the shore: The transmission link to the shore can be HVAC, CSC-HVDC or VSC-HVDC.

5-3-1 High-voltage alternating-current transmission (HVAC)

Conventional HVAC transmission systems with submarine or underground cable offer a simple, well-proven and cost-efficient solution for the grid connection of offshore wind farms. They consist of the following main components: An AC collection grid, an offshore substation, one or several three-core XLPE-insulated HVAC cables and onshore substation [3, 9]. Depending on the transmission distance and transmitted power, the offshore/onshore substation may be equipped with reactive power compensation devices to provide the required reactive power. The cable length and carrying capability is limited due to many factors such as power losses, transmission voltage level and complexity of reactive power compensation schemes. Transmission levels in the range 132-170kV for distances up to 30km with reactive power compensation at both ends could increase the maximum transmitted power rating to 300-400MW [3].

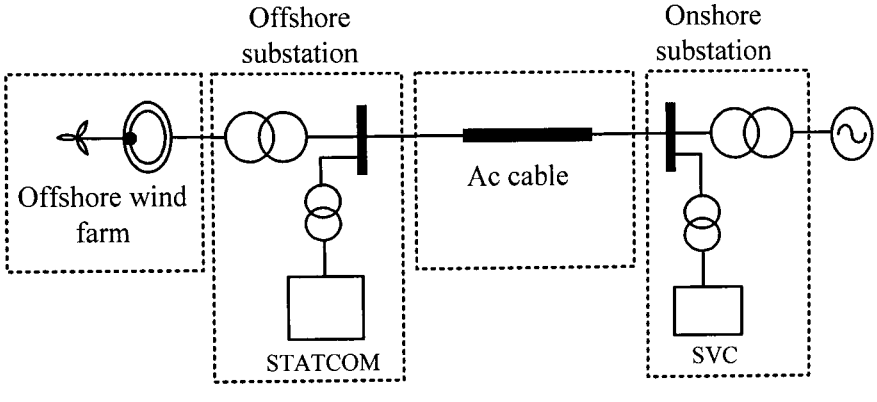


Fig. 5.5: Basic configuration for HVAC system used for wind farm connection.

The main disadvantages of using ac cable as transmission medium are [8, 14]:

- The ac cable produces a large amount of reactive power due to its high stray capacitance and this reduces the active current-carrying capability of the cable and increases the power losses. For long transmission distance reactive power compensation devices are required at both ends of the cable to provide voltage control.
- Because of the high capacitance of the cable, resonances may occur between the onshore and offshore grids that lead to distortion in the shape of the voltage.
- In a synchronous operation between the wind farm and the grid, any faults occurring on the grid will directly affect the wind farm and vice versa, increasing the risk of blackout.
- The technical capability for network support is limited. The voltage support is achieved with extra additional cost using reactive power compensation devices, while frequency regulation is possible only with doubly-fed induction generators (DFIG).

Table 5.1 summarizes some of the existing offshore wind farms connected via HVAC in operation in Europe, the Horns Rev offshore wind farm is the first large-scale wind farm commissioned in the world, while North Hoyle is the first one to be installed in UK. Nowadays, the Thanet offshore wind farm is the largest wind farm ever with 300MW generation capacity.

Table 5.1: Examples of current offshore wind farms connected via HVAC in Europe.

Project	Rating (MW)	ac voltage (KV)	Distance (km)	Commissioning year
Horns Rev (Denmark)	(2x80)=160	150	15	2002
Nysted (Denmark)	(2.3x72)=166	132	10	2003
North Hoyle (UK)	(2x30)=60	33	12	2003
Arklow Bank (Ireland)	(3.6x7)=25	35	16.5	2004
Kentish Flats (UK)	(3x30)=90	33	8.5	2005
Egmond aan Zee (Netherland)	(3x36)=108	34	10-to-18	2007
Lillground (Sweden)	(2.3x48)=110	145	7	2008
Alpha Ventus (Germany)	(5x12)=60	110	45	2009
Thanet (UK)	(3x100)=300	132	11.3	2010

5-3-2 CSC-HVDC transmission system

The CSC-HVDC system for wind farm connection consists of an AC collection grid, offshore substation with 12-pulse converter and additional start-up generator or STATCOM, ac harmonic filter, DC cable, onshore substation with 12-pulse converter and ac harmonic filter. Fig. 5.6 shows the single-line diagram for CSC-HVDC system for wind farm integration.

The main limitations of using CSC-HVDC system for wind farms connection are:

- Special arrangement is needed at the offshore wind farm side to keep strong AC system in order to enable the operation of the line-commutated converters even during periods with little wind. Start-up generator is used to power up the offshore AC grid prior to a possible start-up level. A Hybrid HVDC system combining a CSC-HVDC system with a static compensator (STATCOM) is another solution; the STATCOM provides the commutation voltage to the HVDC converter and the reactive power compensation to the network [15]. It also provides limited active power support to the offshore side during transient conditions such as active power fluctuations from the wind farm.
- CSC-HVDC systems are not capable to provide independent control of the active and reactive powers. Reactive power compensation is needed at both offshore and onshore converter station and this increases the size of the converter station.
- CSC-HVDC systems produce large amounts of harmonics, hence ac harmonic filters are required at converter stations.
- Only suitable for connection of ac networks with a high short-circuit ratio

The technical advantages of classical CSC-HVDC with STATCOM compared to other solutions are: they are a well-established technology with high reliability and require little maintenance, comparatively low operation losses, and they have low capital cost for very high power level. However, CSC-HVDC transmission becomes only interesting for bulk transmission capacities above approximately 600MW. There is no commissioned CSC-HVDC system for offshore wind power connection.

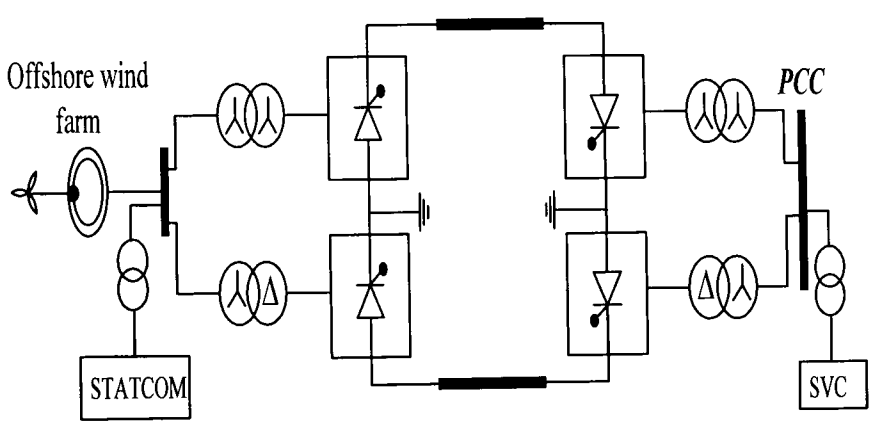


Fig. 5.6: Basic configuration for LCC-HVDC system used for wind farm connection.

5-3-3 VSC-HVDC transmission system for offshore wind farms integration

VSC-HVDC transmission is able to address the shortness of HVAC and CSC-HVDC systems and makes it easier for wind farms to meet the Grid Code requirements due to its new features [16-17]. The VSC-HVDC system for wind farm connection consists of an AC collection grid, offshore substation, DC cable, and onshore substation. Fig. 5.7 shows the single-line diagram of a VSC-HVDC system for wind farm integration. The conversion losses in a VSC converter are considerably higher than in a CSC-HVDC system, the major disadvantage is the vulnerability of DC transmission systems to DC faults.

Table 5.2 summarizes the most recent projects using VSC-HVDC systems for wind farm integration. Gotland project was the first VSC-HVDC system used to transmit the offshore wind power with ±80kV dc link voltage.

Table 5.2: Examples of the VSC- HVDC transmission systems for wind farm integration [18].

Project	Rating (MW)	DC voltage (kv)	Distance (km)	Commissioning year
Gotland (Sweden)	50	±80	2X70 (submarine cable)	1999
Tjaereborg (Denmark)	7.2	±9	2X4.3 (submarine cable)	2000
TROLL A (Norway)	82	±60	67 (cable)	2005
BOWIN1(Germany)	400	±150	2X75 (underground cable)+2X128 (submarine cable)	2009
VALHALL (Norway)	78	150	292 (cable)	2010
DolWin1 (Germany)	800	±320		2013

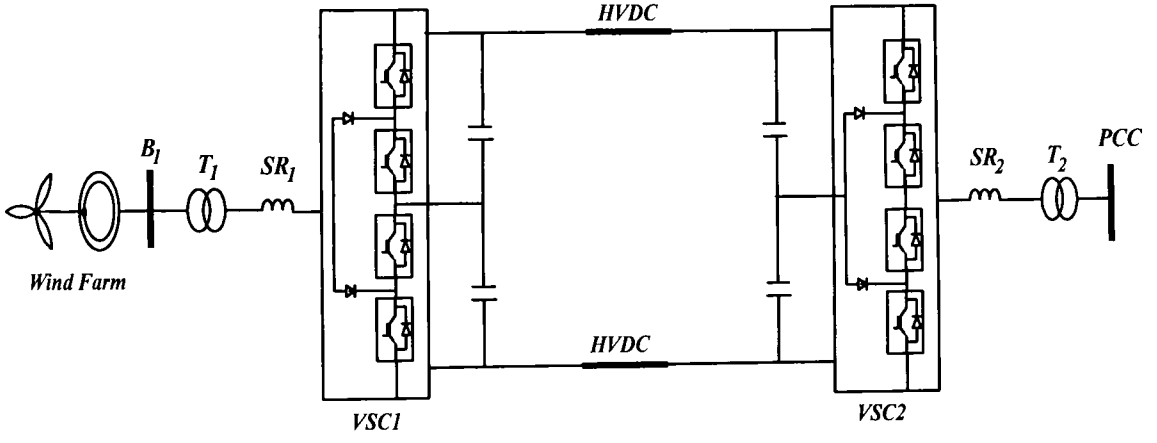


Fig. 5.7: Basic configuration for VSC-HVDC system used for wind farm connection.

5-4 Control system strategies for VSC-HVDC system integrating FSIG wind farms

The control system design of a VSC-HVDC system connecting a fixed-speed wind farm (FSIG) depends on the operation mode of the FSIG wind farms. There are two operation modes for FSIG wind farms:

a) The wind farm delivers all the wind power generated to the network without any control in the generated power.

b) The power delivered by the wind farm is controlled by a reference command.

5-5 VSC-HVDC system integrating FSIG wind farm without power command

If the turbine blades of the FSIG have a fixed position on the hub of the wind turbine, the FSIG wind farm will deliver the generated power without any control in generated power. The FSIG operates at fixed speed without the ability to control the generated power. The FSIG power depends on the wind availability and the turbine characteristics. The VSC converters provide the necessary reactive power at the wind farm level and the PCC with the grid. In order to transmit all the power generated by the wind farm to the power network without assigning a direct power command, the control system of the VSC-HVDC system is chosen as:

- The wind farm-side converter (VSC_1) regulates the reactive power exchange between the VSC converter and the induction generator to maintain the voltage at the wind farm terminal at 1.0. This ensures that each turbine delivers active power and absorbs reactive power according to wind speed variations.
- The grid-side converter (VSC_2) maintains the dc link voltage and regulates the ac voltage at the PCC with the grid.

Fig. 5.8 shows the diagram of the control system at the wind farm and grid-side converters. The wind farm converter requires the i_{dw} and i_{qw} to flow following predetermined reference points. The reference i_{dw}^{*} and i_{qw}^{*}, which are supplied by the outer controllers, are derived from the active (v_{dw}) and reactive (v_{qw}) voltages controllers as shown in equations (5.1), (5.2) and Fig. 5.8a.

$$i_{dw}^{*} = k_{p1}(v_{dw}^{*} - v_{dw}) + k_{i1}\int (v_{dw}^{*} - v_{dw})dt \tag{5-1}$$

$$i_{qw}^{*} = k_{p1}(v_{qw}^{*} - v_{qw}) + k_{i1}\int (v_{qw}^{*} - v_{qw})dt \tag{5-2}$$

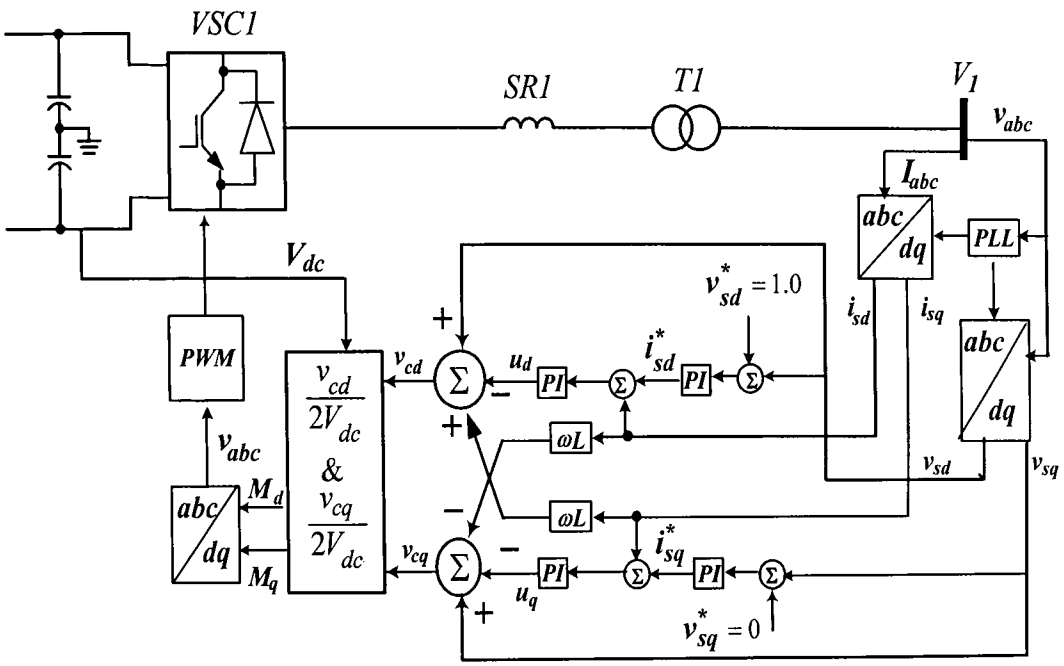
where k_{p1} and k_{i1} are the proportional and integral gains of the active and reactive voltage controllers. The references for the voltage components is chosen as $v_{dw}^{*} = 1.0$ and $v_{qw}^{*} = 0$.

The grid-side converter regulates the dc link voltage and maintains the ac voltage at the PCC with the grid at 1.0 pu. The reference of the d-axis current (i_{dg}^*) and q-axis current (i_{qg}^*) are derived from the dc and ac voltage controllers, respectively (summarized in equations (5.3), (5.4) and Fig. 5.8b)

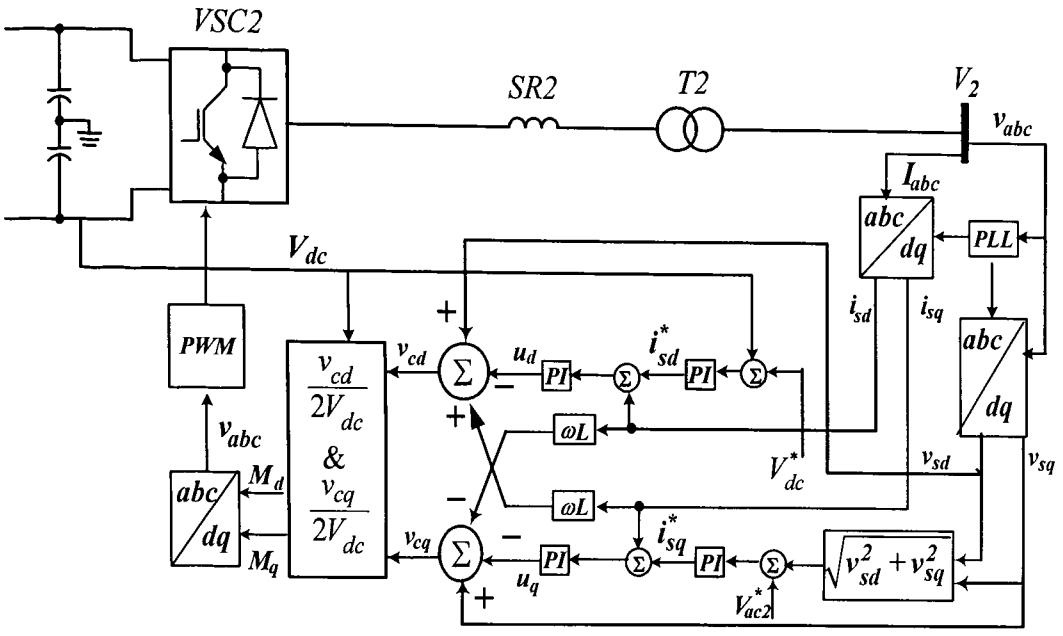
$$i_{dg}^* = k_{p2}(V_{dc}^* - V_{dc}) + k_{i2}\int(V_{dc}^* - V_{dc})dt \tag{5-3}$$

$$i_{qg}^* = k_{p3}(v_g^* - v_g) + k_{i3}\int(v_g^* - v_g)dt \tag{5-4}$$

where k_{p2}, k_{i2}, k_{p3}, k_{i3} are the proportional and integral gains of the dc voltage and the ac voltage controllers, respectively.



(a) Wind farm-side converter control system.



(b) Grid-side converter control system.

Fig. 5.8: Schematic control diagram of a VSC-HVDC connecting an FSIG wind farm.

5-6 Performance evaluation of VSC-HVDC connecting an FSIG wind farm operating without power command

Large integration of wind power may cause problems on the stability of the ac system. The main problems which can generate from large-scale wind integration are: voltage stability, power quality and frequency variations [19-20]. Voltage stability problems occur due to continuous variation in the terminal voltage due to wind power generation variations.

Wind farms power varies according to wind speed, the large power variations can affect the generation-demand balance and lead to frequency variations. In this case, the frequency controllers in conventional power stations must response at a fast rate to adjust the frequency variations. On the other hand, the ability of the wind farm to remain connected to the system during system disturbances is very important because if wind farms are disconnected from the system this will affect the power balance and the frequency will collapse. Power system quality is mainly affected by the wind power fluctuation and the generated harmonics in voltages and currents in the system [21]. The harmonics are generated due to exist of power electronics devices which are used in conversion systems or to control the voltage.

In this section the performance of the FSIG and the VSC-HVDC transmission system and their ability to address the main issues of wind farm integration, as indicated by GB Grid Code, are investigated during wind speed variations and ac system abnormal conditions.

In order to investigate the system performance, a test system of a three-level VSC-HVDC system connecting a fixed-speed offshore wind farm scheme as shown in Fig. 5.9, is used. The FSIG wind farm is modeled with a 600MVA aggregate model (it comprises of 120×5MVA wind turbines connected to a 33kV collection network). A fixed capacitor bank of 20MVAr connected at the wind farm terminals is used as reactive power source. The dc cable length between the offshore wind farms and the shore is 150km. The ac network is represented by a synchronous generator with ratings of 2400MVA, 13.8kV with a 13.8/275kV transformer. Both the synchronous generator and the wind farms fed a static load of 2345+j185. All system parameters are given in Table 5.3. The system may be used to represent a real system, for example the ac network total capacity is 3000 MVA with 2400MVA conventional plant and 600MVA wind power plant which means 20% wind power penetration.

Table 5.3: System parameters (proposed system of using VSC-HVDC for wind power integration)

Induction generator	600MVA , 33kV, f=50, Stator variables [R=0.011, L=0.133], Rotor variables [R=0.022, L=0.122], mutual inductance=2.9, Inertia=3.54, pair of pole=3.0.
ac_1 network	Transformer T_1 (33/132 kV, 300MVA, R_{T1}=0.0005pu, L_{T1}=0.3pu), phase reactance (L_{F1}= 0.25pu based on 500MVA&132kV)
ac_2 network	Transformer T_2 (132/375 kV, 500MVA, R_{T2}=0.0005pu, L_{T2}=0.3pu), phase reactance (L_{F2}= 0.25pu based on 500MVA&132kV), TL data (0.02Ω/km, 100km)
dc side circuit	V_{dc}=300kV, the capacitor C =300μF , cable data (0.02Ω/km, 100km)
Synchronous generator	2400MVA, 13.8kV,50Hz, x_d=1.305, x_q=0.445, x'_d = 0.296, x'_q = 0.243 , xl= 0.18 R_s=0.003,H=6.25

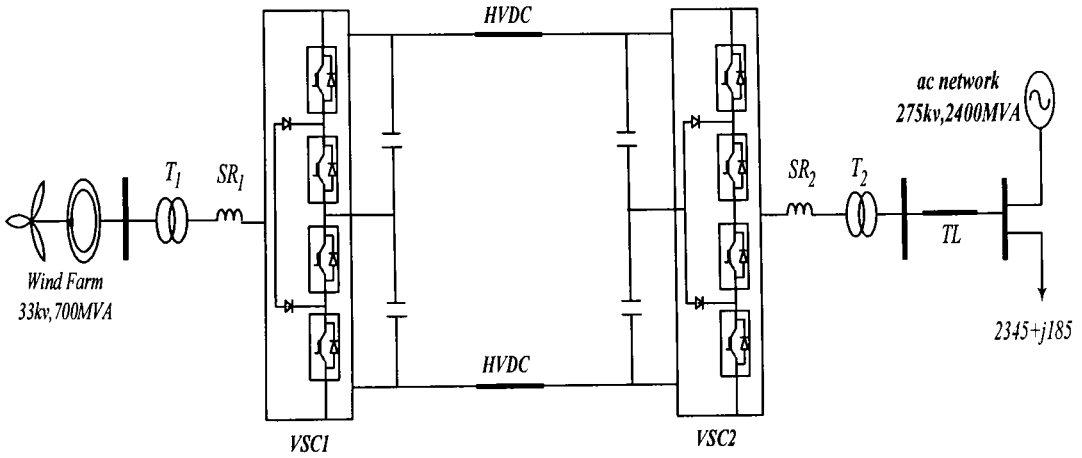


Fig. 5.9: VSC-HVDC connecting offshore wind farms to an ac network.

The function of the VSC-HVDC is to transport offshore wind power to the ac network without causing problems on power system operation. In order to achieve this function, the integration process with VSC-HVDC system must meet all requirements set by the power system operators.

1- The voltage at the PCC with the ac system must keep within the allowed deviation from their nominal value.
2- The FSIG wind farm must remain connected to the system during an ac fault at the network.
3- The total harmonic distortion (THD) in the voltage and current waveforms should be within the specified range.
4- Eliminate the fluctuation in the wind power.

To investigate the performance and the impact of the VSC-HVDC integrating FSIG wind farm on the ac system performance, two scenarios are analyzed:

- ❖ Scenario I: Wind speed variations.
- ❖ Scenario II: Three-phase fault at the ac network side.

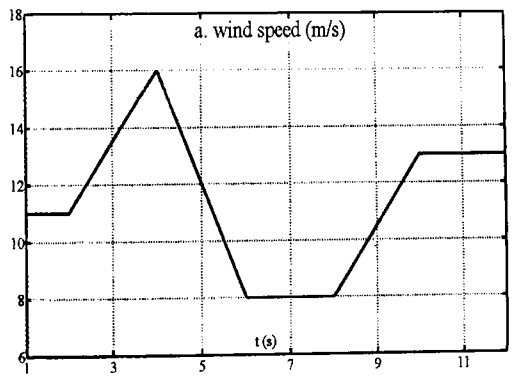
5-6-1 Scenario I: System performance during wind speed variations

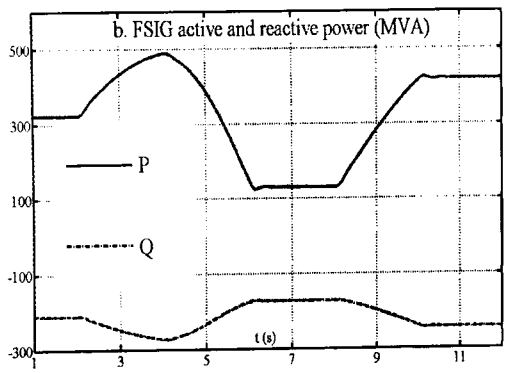
The reactive power required by the FSIGs depends on the amount of the FSIG generated power. In large offshore wind farms the reactive power consumption may cause operation problem unless the wind farms are equipped with effective controllable reactive power devices capable to adjust their output with the FSIG active power, in order to maintain the voltage at the wind farm terminals. When the FSIG is connected via a VSC-HVDC system the VSC converters could be used to provide the reactive power required by the FSIG to keep the voltage magnitude at the desired value. Also at the PCC the grid-side converter provides the same function to keep the voltage magnitude at the PCC.

Fig. 5.10 shows the system behaviour during wind speed variations. The wind speed variation with time is shown in Fig. 5.10a. As the FSIG wind farm delivers full power, the blades have fixed position ($\beta=0°$) at all wind speeds as shown in Fig. 5.10c. The wind power generation and the reactive power consumption increase at high wind speed and decrease at low wind speed (Fig. 5.10b). The turbine rotational speed is approximately constant with very little change (Fig. 5.10d) regardless of the change in power level. The wind farm terminal voltage is kept constant because the wind farm-side VSC converter adjusts its reactive power to keep the voltage at 1.0pu.

The great impact of wind power variation is on the ac network frequency, the frequency of the ac network can be considered a measure of the balance or imbalance between generation and demand in the network. Any mismatch between the generation and demand may cause the system frequency to increase or decrease depending on the net difference between generation and demand. The primary frequency controller acts to maintain the frequency within the nominal value (50Hz) by adjusting the conventional plant power output. The continuous variation of the wind power delivered by the VSC-HVDC transmission system causes mismatches between the generation and demand and leads to frequency fluctuations as shown in Fig. 5.10h. When the synchronous machine senses the frequency variation, the primary control is automatically activated to maintain the frequency by changing the generated power (Fig. 5.10g). The synchronous machine power increases when the wind speed decreases and vice versa. In reality the frequency deviation depends mainly in the net difference between mechanical and electrical power in the machine and the machine inertia according to $\frac{d\omega}{dt} = \frac{\omega_0}{2H}(P_m - P_e)$. The frequency in Fig.5.10h suffers relatively high deviation and recovers with slow response due to the large inertia of the synchronous machine (H=3.51); this may require using tertiary control by stopping or varying the output of generating units.

If there is not enough reserve generation during low wind speed to cover the shortness in wind generation, or if the wind power penetration is so high that the primary frequency control is not able to decrease the power of the synchronous machine within suitable time, black-out of the whole system may occur. As PWM techniques are used, the ac harmonics generated by the VSC converter are relatively small. The ac harmonics filter can be eliminated if a multilevel converter topology is used. The THD in the ac voltage at B_2 is 0.6758% and this complies with the harmonic level limit of 1.5% stated in the IEEE Std 519-1992 [22]. The ac voltage and current waveforms are shown in Fig. 5.10i and Fig. 5.10j.





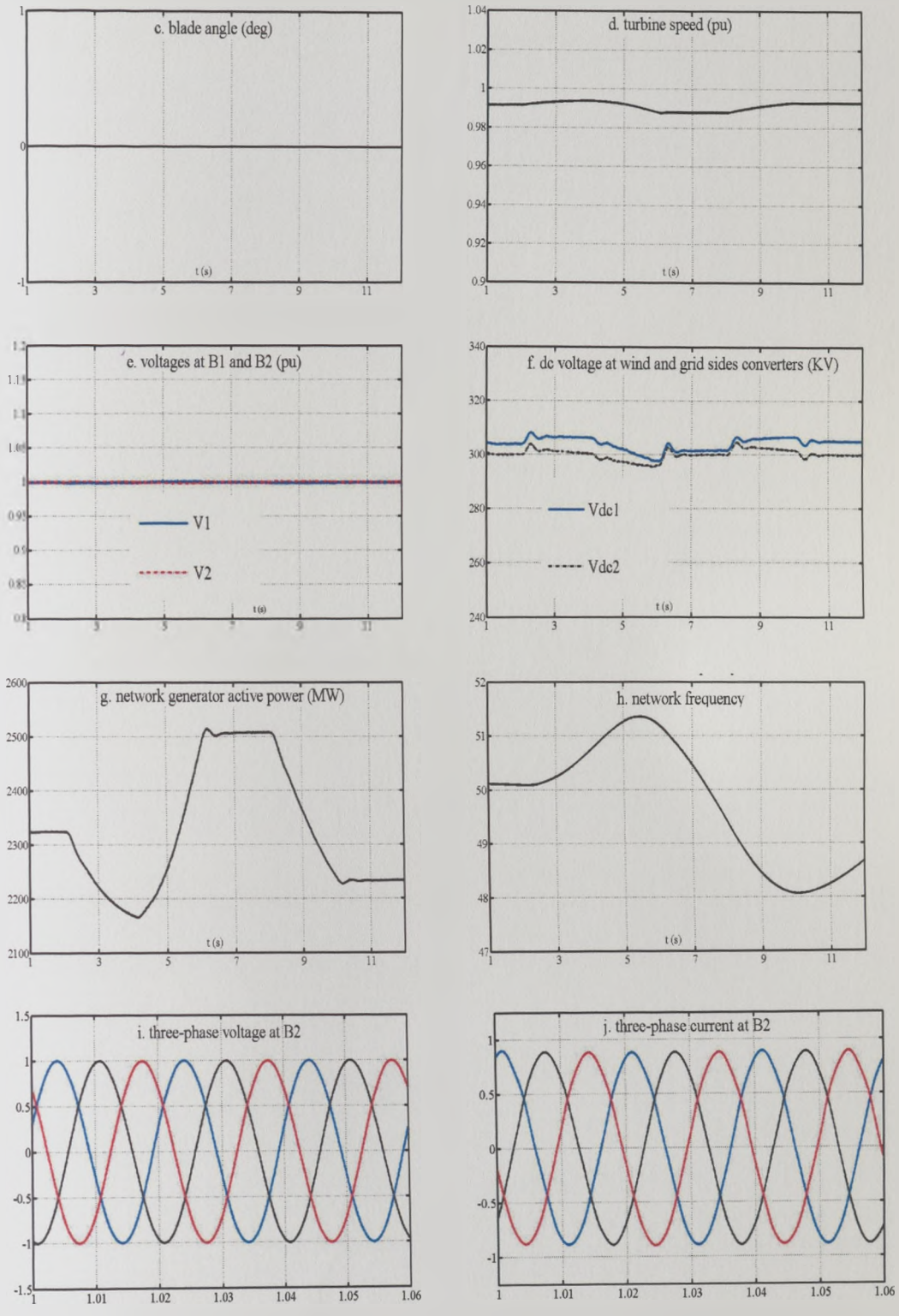


Fig. 5.10: Results of FSIG and VSC-HVDC operated without power command during wind speed variation.

5-6-2 System performance during a solid three-phase fault at the grid side

As stated in the GB Grid Code, each wind farm must be able to remain connected during different ac faults. This requirement is examined by subjecting the test system in Fig. 5.9 to a solid three-phase fault at the PCC (B_2) with fault duration of 5 cycles. The results obtained from this case are shown in Fig. 5.11. This figure shows that the VSC-HVDC system is able to prevent the propagation of the abnormal condition on the ac side to the wind farm (HVDC links act as an effective "firewall" against propagation of cascading outages in one network from passing to another network [23-24]). It is observed that the power and voltage at the wind farm side remains less sensitive to the fault at the grid side (Fig. 5.11a and Fig. 5.11b). The wind farm remains stable and connected to the grid despite that the voltage at the terminals of the grid side converters VSC_2 collapses to 0% of the nominal voltage during the fault period, and recovers to pre-fault nominal voltage after the fault is cleared. The DC link voltage is subjected to transient oscillatory conditions during the fault, the dc capacitor is trying to maintain the dc voltage and this produces the transient in the power and voltage waveform at B_2 after the fault is terminated.

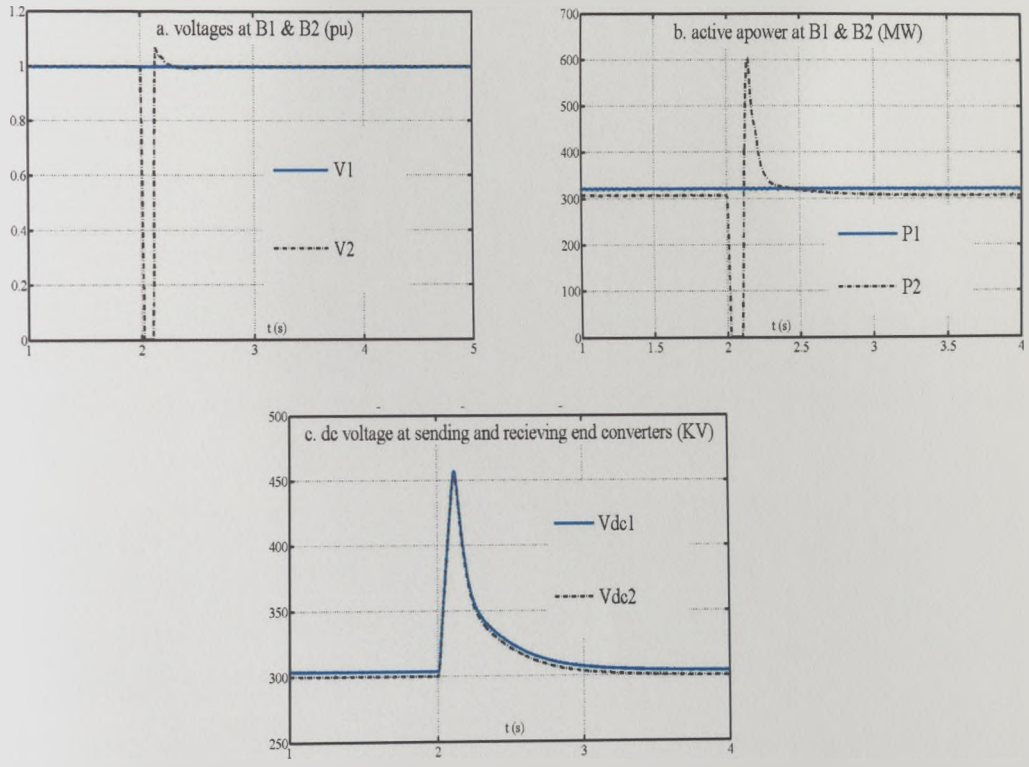


Fig. 5.11: Key simulation results of FSIG and VSC-HVDC system operated without power command during three-phase fault at ac side (at B_2).

5-7 VSC-HVDC system integrating FSIG wind farm with power command

As mentioned in the previous section the wind farms power variation could cause frequency problems. In order to restore the nominal frequency the rotational energy stored in large synchronous machines is used to keep the power balance between generation and demand. The FSIG and VSC-HVDC system can be used to contribute in the frequency regulation in the ac grid, if the FSIG is operated with an assigned power command.

In this case the FSIG is operated under the rated limit, then the FSIG could adjust the blade position in order to keep the generated power within the desired value. The VSC-HVDC system decouples the FSIG wind farm from the ac system; therefore the rotor turbine could rotate freely with the wind speed variation.

The faster response of a voltage source converter compared to conventional synchronous machines with relative large mechanical inertia, can be used to allow the FSIG to provide short-term frequency stabilization. The dynamic response of the dc system during a load change is described by [25-26]:

$$2H_c \frac{d\Delta\omega}{dt} = \Delta P_{dc} - \Delta P_L \tag{5-5}$$

Where $\Delta\omega$ is the frequency deviation, ΔP_{dc} is the change on the dc transmitted power, ΔP_L is the load change, and H_c is the effective dc inertia constant, defined as:

$$H_c = \frac{\text{Total ac system inertia}}{\text{MW rating of the dc system}} \tag{5-6}$$

Wind turbines have a limited capability of participating in primary frequency control in the same way as conventional generation units. For instance, if the demand changes and system frequency increases/decreases, the wind farms can adjust their output by changing the blade position. The ability of wind farms to provide frequency control is in expanse of maximum power tracking), the wind farms at normal conditions operates under the rated limit (in this case the wind farm can not converter all available wind power into electrical power). In general, there are some strategies to limit the wind farm power output [3, 10]:

- *Absolute power constraint*: This control approach limits the total power output of the wind farm to a predefined set point.
- *Balance control*: The balance control approach allows a reduction in the power production of the overall wind farm at a predefined rate and later an increase in the overall power output, also at a predefined ramp rate.

- *Delta control*: This reduces the amount of total power production of the wind farm by a predefined set point (e.g. 50 MW).
- *Power rate limitation control*: This approach limits the increase in power production to a predefined set point (e.g. maximum increase in power production 2MW per minute).

5-7-1 Control system design of FSIG wind farm and VSC-HVDC system

The power extracted from the wind turbine can be controlled by adjusting the pitch angle (β). A PI controller is used to adjust the pitch angle by comparing the reference rotor speed ω^* and the measured rotor speed (ω) as shown in Fig. 5.12 and equation (5.16). The blade angle will not change immediately, practically, the rate-of-change in pitch angle is in the range (3-10) degree/s depending on the wind turbine design.

$$\beta = k_p(\omega^*_{Turb} - \omega_{Turb}) + k_i\int(\omega^*_{Turb} - \omega_{Turb})dt \tag{5-7}$$

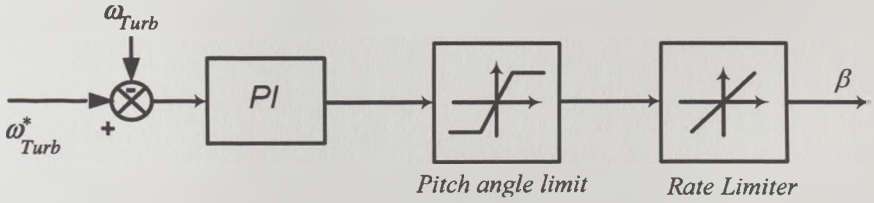


Fig. 5.12: Control scheme of pitched-regulated wind turbine.

According to the wind turbine characteristics shown in Fig. 5.13, the extracted wind power is changed significantly with the turbine blade position. When the FSIG generator senses any change in system frequency, the induction generator speed will change resulting in activating the pitch angle controller and therefore the generated power will change to participate in stabilizing the frequency.The maximum power extraction is achieved when β=0°.

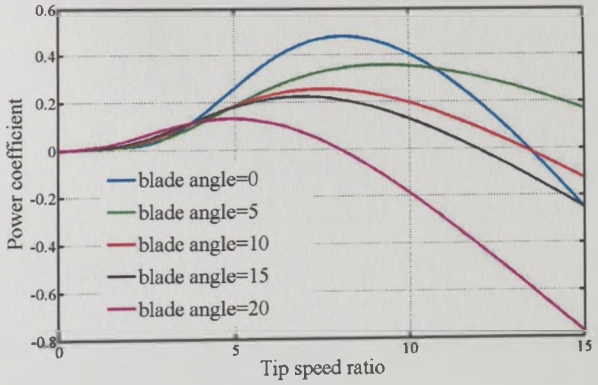


Fig. 5.13: c_p-λ characteristics for wind turbine β=0.

The control system of the VSC-HVDC is such that the wind farm-side VSC converter controls the power and regulates the voltage of the wind farm. While the grid-side VSC converter maintains the dc voltage and regulates the ac voltage at the PCC with the ac network (as in the FSIG operated without power command).

According to equation (5.8) and Fig. 5.14, the reference current components i_{dw}^{*} and i_{qw}^{*} supplied by the outer controller are derived from the active power controller and the AC voltage controller, respectively.

$$i_{dw}^{*} = \frac{P^{*}}{v_{wd}} \tag{5-8a}$$

$$i_{qw}^{*} = k_{p1}(v_{w}^{*} - v_{w}) + k_{i1}\int (v_{w}^{*} - v_{w})dt \tag{5-8b}$$

where k_{p1} and k_{i1} are the proportional and integral gains of the ac voltage controller.

The active power controller of the wind farm-side converters is equipped with a supplementary frequency controller to provide the frequency regulation to the grid if any change happens in the generation-demand balance. The frequency controllers are based on the active power-frequency characteristic as in conventional synchronous generators, which can be represented by a linear equation as $f - f_0 = K(P - P_0)$ [27]. If any change occurs in the ac system frequency, the frequency controller will adjust the active power generated by the FSIG to regulate the system frequency. The correction signal generated by the frequency controller can be expressed as:

$$i_{corc}^{*} = k_{p5}(f^{*} - f) + k_{i5}\int (f^{*} - f)dt \tag{5-9}$$

where k_{pf} and k_{if} are the proportional and integral gains of the frequency controller. The complete control system block diagram of the wind farm-side converter is shown in Fig. 5.14.

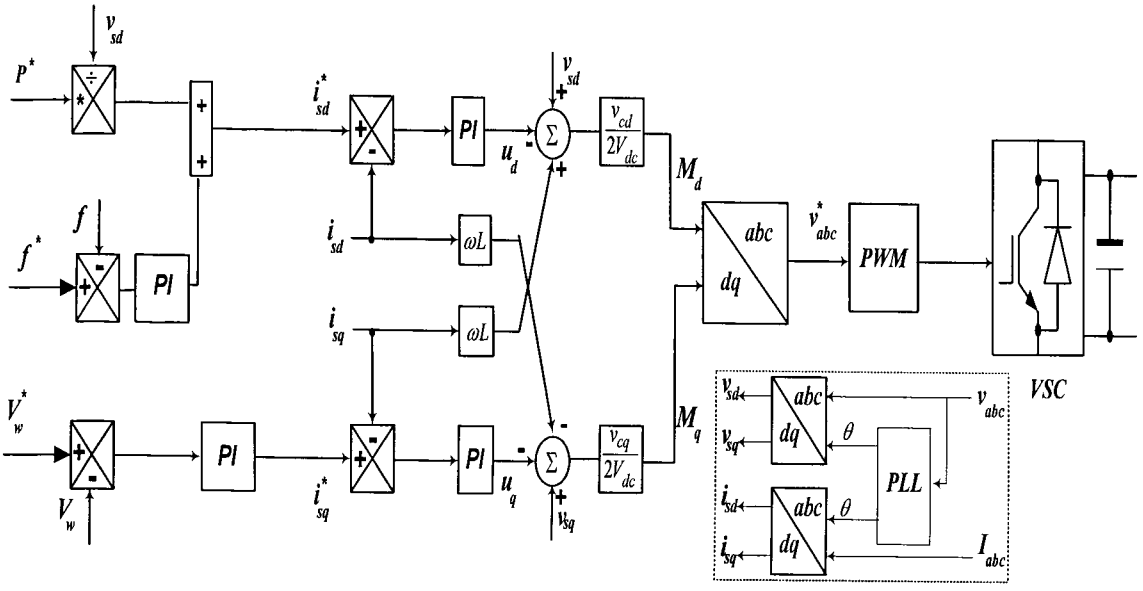


Fig. 5.14: Wind farm-side converter control system.

The operation of VSC-HVDC system connecting wind farms with assigned power command is investigated with the same parameters provided in Table. 5.3, but the induction generator rating is increased to 750MW. Fig. 5.15 shows the system behavior when the wind speed varies as indicated in Fig. 5.15a. At the normal conditions, when the wind farm operates with average wind speed, which is taken as 11m/s, the wind farm-side converter power command is 350MW which is under the rated limit of the FSIG wind farm; the blade angle position is at 4°. When the wind speed suddenly increases at t=2s, the wind farm increases the blade angle in order to keep the generated power at the desired level. Then, at t=4s, when the wind speed is decreased, the FSIG wind farms response is to decrease the blade angle in order to keep the generated power at the desired level (see Fig. 5.15c).

In all cases, the turbine rotor speed which is operated independently from the ac-side synchronous speed is varied to maintain the generated power at 350MW as shown in Fig. 5.15d. The FSIG wind farm now is operated with variable speed and this adds valuable control functionality.

The main disadvantage of this approach is the availability of the wind at the wind turbine level because at low wind speed the wind farm adjusts the blade angle to values lower than the pre-position angle, and the maximum extraction occurs when $\beta=0°$, so it is not possible to increase the generated power when the blade angle is at this position. This approach is valuable to power system operators since the wind farm does not have a negative impact on system stability but this in expanse of maximum power tracking at wind farms level. Moreover, it could provide frequency stabilization as shown in Fig. 5.15f.

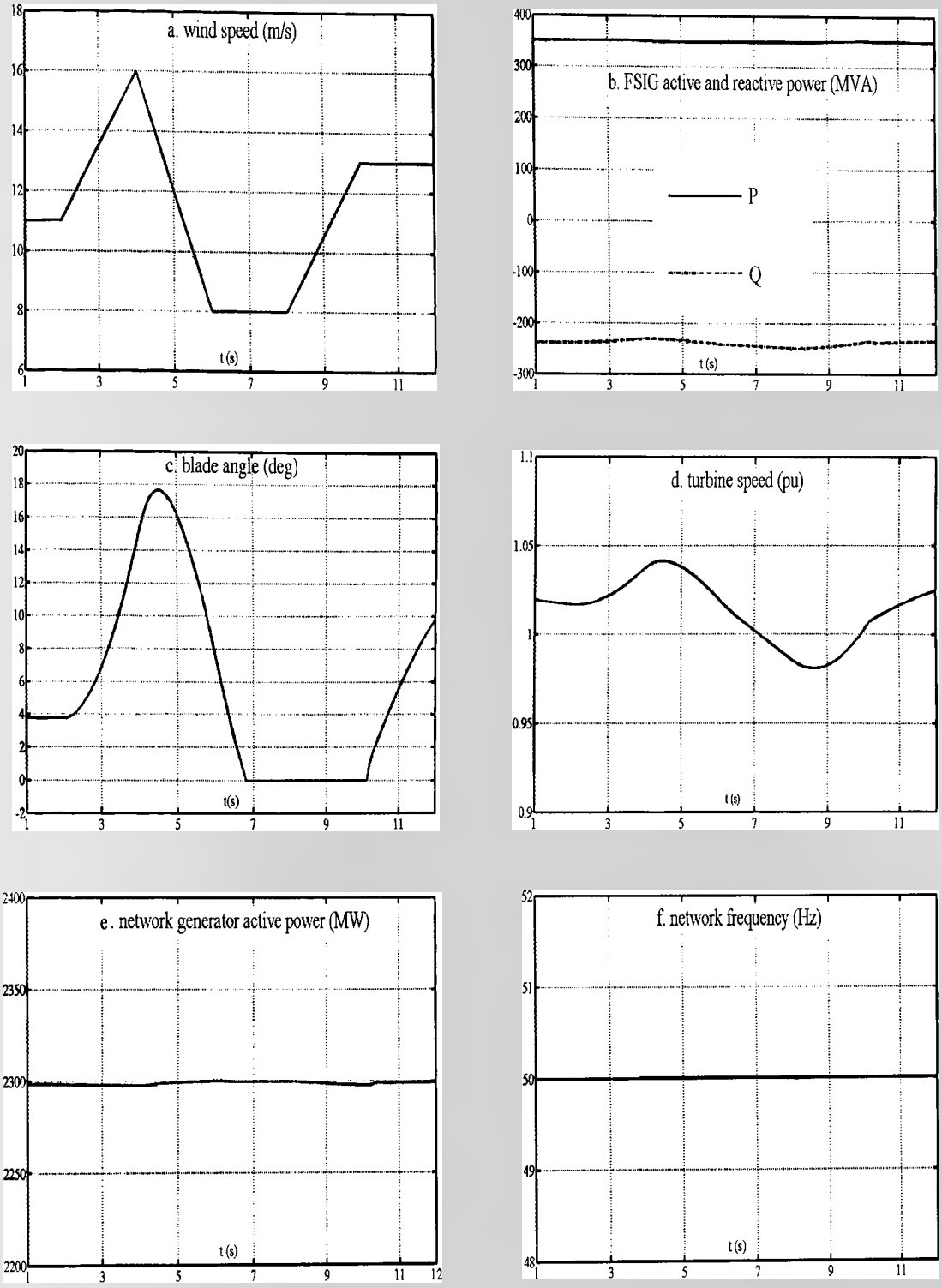


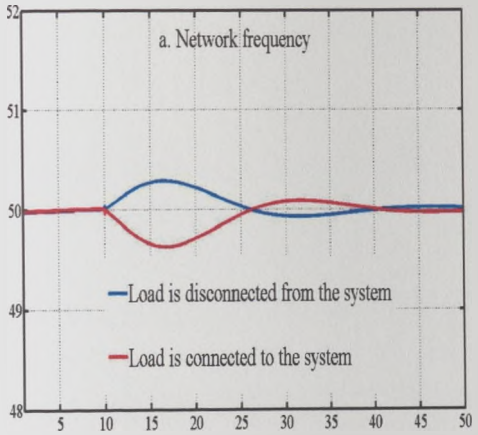
Fig. 5.15: Key simulation results of FSIG and VSC-HVDC system operated with power-command during wind speed variation.

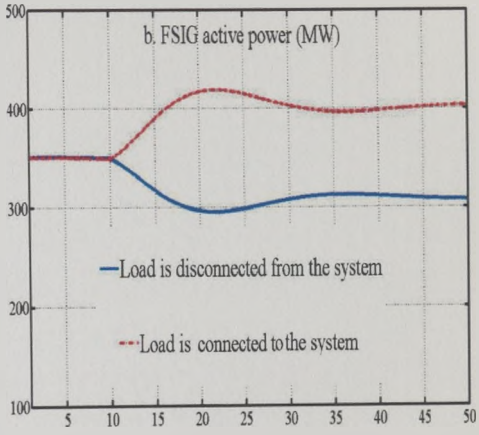
5-7-2 FSIG and VSC-HVDC response during power demand change

Electric power systems include power plants, consumers of electric energy and transmission and distribution networks connecting the production and demand sites. These interconnected systems experience a continuous change in demand and the challenge is to maintain at all times a balance between generation and demand of electric energy. To demonstrate the capability of FSIG wind farms to provide the short-term frequency stabilization to the ac network during a load change, the system in Fig. 5.16 is subjected to over-frequency and under-frequency events respectively initiated by the loss or addition of (70+j40) MVA at time t=10s. Fig. 5.16a shows that the grid frequency is affected by the power imbalance and it slightly increases (over-frequency case), or decreases (under-frequency case); and then it stabilizes at the nominal frequency of 50 Hz.

When the load changes, the wind farms adjust the blade angle to increase or decrease the turbine rotational speed in order to adjust the generated power to match the new demand. The FSIG increases the generated power when additional load is connected to the system to share it with the synchronous generation in order to cover the additional load, and stabilize the system frequency. Converters VSC_1 and VSC_2 adjust their reactive power exchange with the wind farms generator and the ac grid respectively to maintain the reactive power balance in order to maintain the voltage at B_1 and B_2 at 1.0pu (nominal voltage) (Fig. 5.16f). Due to the fast response of the VSC-HVDC system, the contribution of the FSIG wind farm to stabilize the system frequency is more than that provided by the conventional generators.

The maximum generated power occurs when $\beta=0$, at that point the wind farms could not participate in the frequency regulation.





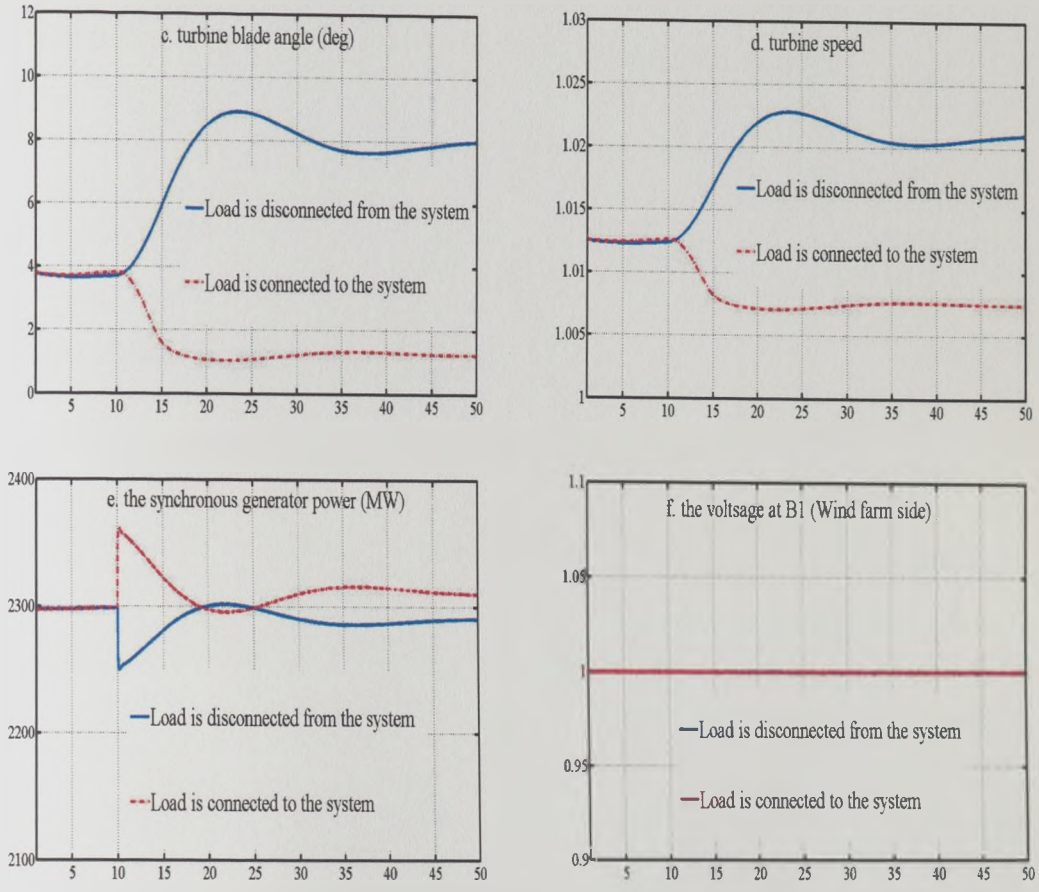


Fig. 5.16: FSIG and VSC-HVDC system operated with power-command response during load demand change at the ac system network

5-7-3 System performance during solid three-phase fault at the grid side

The FSIG connected to the ac network via a VSC-HVDC system operated with a power command manages to remain connected to the system after a three-phase fault on the ac side occurs at bus B_2 at t=3s, with duration of 140ms (7 cycles for 50Hz). Fig. 5.17a indicates that the FSIG wind farm is not affected by the fault in the ac side network as the offshore wind farm terminal voltage maintains a constant profile.

Two scenarios are investigated to study the effect of the frequency controller implemented in the wind farm-side converter during the fault. In the first scenario the FSIG wind farm is operated without frequency controller, whilst in the second scenario the FSIG wind farm is operated with frequency controller.

The system recovery after the fault clearance is much better with the second scenario as shown in Fig. 5.17c. During the fault, the system frequency increases and recovers to the

nominal value once the fault is terminated. In the second scenario, when the system frequency increases, the FSIG wind farm response is to reduce the generated power to help in frequency stabilization. This leads to a fast recovery with less overshoot compared to the system without frequency controller at the wind farm side (Fig. 5.17b and c). The voltage at bus B_2 collapses during the fault period, and the delivered power is cut off from the system until the ac breaker clears the fault.

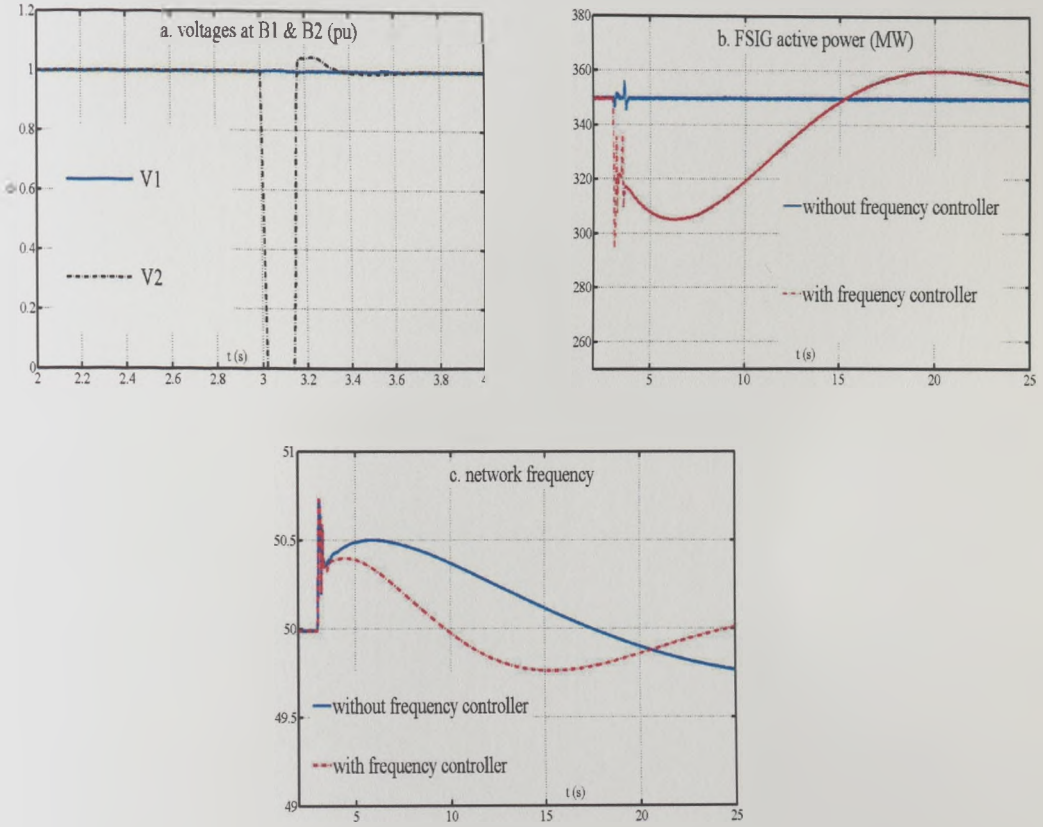


Fig. 5.17: Key simulation results of FSIG and VSC-HVDC system operating with power command during three-phase fault at the ac side (at B_2)

5-8 Features of FSIG and VSC-HVDC system

Based on the previous discussion, the features of the VSC-HVDC connecting FSIG wind farms operated without/with power command is summarized in Table 5.4. Both approaches are compliant with all requirements set by the GB Grid Code. Conflict of interest arises between the wind farms owners and transmission system operator (TSO) regarding the proposed control strategies. The wind farms owners prefer the approach without power command to extract maximum power and improve their investments, while the transmission

system operator prefers the approach with the power command, because additional controllability is obtained and the wind farm participates in frequency regulation.

Table 5.4: Comparison of the FSIG wind farm integration via VSC-HVDC system.

Feature	Without power command	With power command
Provide voltage and reactive power control	YES	YES
FSIG remains connected at ac fault at the ac gird	YES	YES
Provides frequency control	NO	YES
Comply with THD specified range	YES	YES
Variable-speed operation	NO	YES
Eliminates the fluctuation in the wind power	YES	YES
Maximum power tracking	YES	NO

5-9 Multi-terminal VSC-HVDC System for FSIG wind Farm Integration

In a multi-terminal VSC-HVDC system used for offshore FSIG wind farm integration, the dc converters connected to the wind farms always operate as rectifiers and the dc converters connected to the ac grid operate as inverters. The multi-terminal VSC-HVDC control system is designed depending on the wind farms operation mode as described in sections 5.5 and 5.7.

The potential benefit of using a VSC-MTDC system for wind farms integration is the control flexibility, power sharing between grid-side converters and the improvement in the transmission system reliability during the sudden loss of a grid converter or one of the dc cables.

The four multi-terminal system shown in Fig. 5.18 is used to transmit the power from the offshore FSIG wind farm to the ac network with the parameters shown in the figure. The VSC-HVDC system is operated with a power-command of 350MW for each unit. The dc link circuit is composed of DC links connecting VSC_1-VSC_3 and VSC_2-VSC_4 with auxiliaries' links connecting VSC_1-VSC_2 and VSC_3-VSC_4. A 2400MVA, 13.8 kV synchronous generators with AVR and governor-turbine control systems represents the ac network. Both the ac system and the wind farms supply a static load of 2345+j135MVA.

The power sharing between the grid-side converters is achieved using droop control equipped in addition to the dc voltage controller in VSC_2 converter. Fig. 5.19 shows the power management if the droop controller is activated. The multi-terminal system is operated normally without droop controller until t=2s, the power is divided equally between VSC_1 and VSC_2 and no power flows in the auxiliaries cables, the droop control is activated at t=2s to allow transmission of 120MW from VSC_2 to VSC_1 between t=2s and t=4s. At t=4s the droop

controller is inactivated and the power share is returned to be half-half, but at t= 6s the new command is to transmit 150MW from VSC_1 to VSC_2. The dc voltage at VSC_1 remains constant while the dc voltage of VSC_2 is changed due to the power share command.

To demonstrate the improvement of transmission reliability, two cases are investigated. The first case is the disconnection of VSC_1 at t=2s and reconnection at t=4s. The second case is the disconnection of DC $link_1$ at t=2s and reconnection at t=4s. In both cases, the wind farms generation was delivered with alternative route through the auxiliary cable to the healthy and unaffected DC cable or VSC converter, until the dc cable or the VSC converter is reconnected again. In Fig. 5.20 all wind power, during the sudden loss of the converter or dc cable was delivered to the grid through VSC_2 converter.

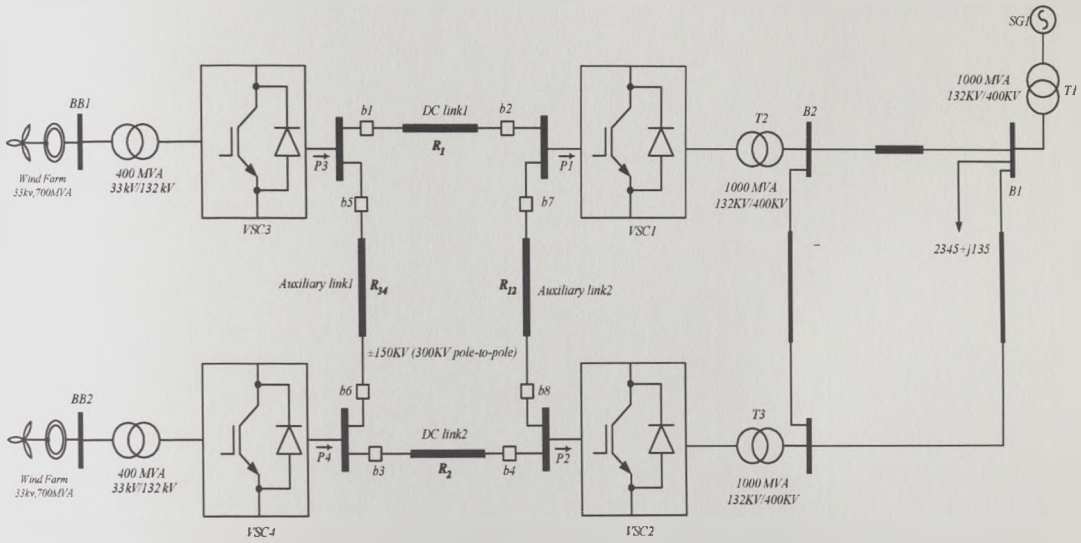


Fig. 5.18: Four multi-terminal VSC-HVDC system connecting FSIG wind farms.

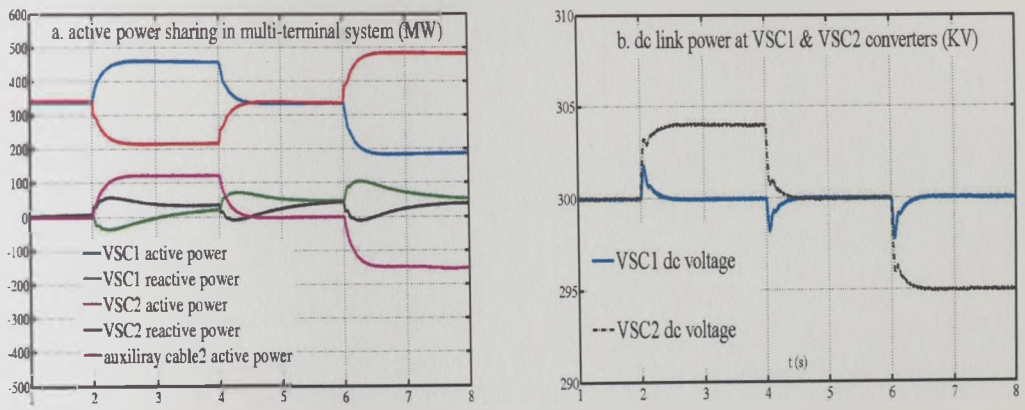


Fig. 5.19: Grid-side converters active power sharing (between VSC_1 and VSC_2).

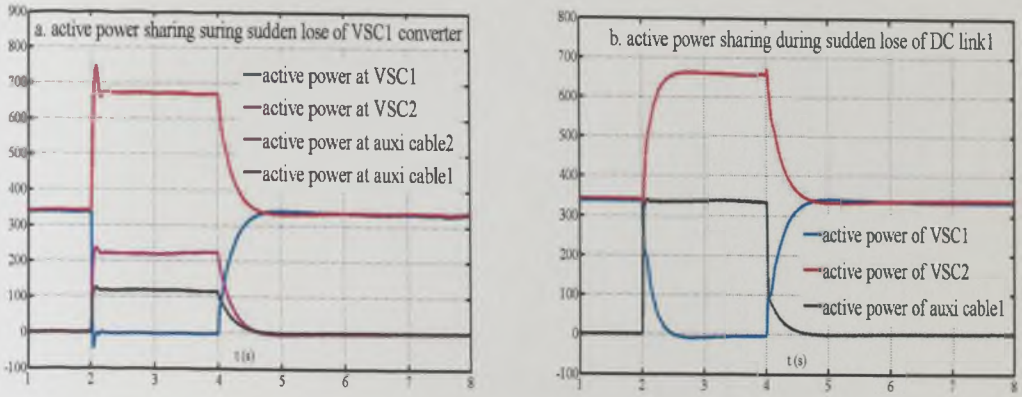


Fig. 5.20: Multi-terminal VSC-HVDC system behavior during sudden loss of VSC_1 and dc $link_1$.

5-10 VSC-HVDC system for integration of other wind farm technologies

The VSC-HVDC system decouples the offshore wind farm from the ac onshore power system. This condition makes it possible to use different generators technologies at the offshore wind farm. The basic concern of the different generators technologies is to find the optimal economic of the overall system including the wind turbine in the VSC-HVDC transmission system [3]. In terms of the generators for wind-power application, there are different concepts in use nowadays. In general the wind farms are classified into:

1- Fixed speed wind farms, which employ asynchronous induction generator (FSIGs).

2- Variable-speed wind farms, which use doubly fed induction generators (DFIGs).

3- Direct-drive wind farms, which use synchronous generators (SG) or permanent magnetic synchronous generators (PMSGs).

The DFIG consists of a wound rotor induction generator with the stator winding connected directly to the ac network, while the rotor windings are connected via back-to-back partial scale power electronic converters. The power electronic converter decouples the mechanical and electrical frequencies and makes it possible for variable speed operation; therefore the DFIG could adjust the rotor speed in order to maximize the wind power extraction over a wide range of wind speeds. Furthermore, they can absorb any fluctuations and eliminate the flickers in the generated power and voltage due to the varying wind. The size of the power converter determines the variable speed range.

The grid-side converter of the DFIG is used to maintain the dc link voltage and control the reactive power exchange with the ac gird. The rotor converter of the DFIG controls the active and reactive power of the wind farm by regulating the rotor speed to extract maximum wind power [28-29].

A VSC-HVDC system can be used to integrate a DFIG wind farm when the transmitted power and transmission distance are reasonable. There is no redundancy between the power electronic converter in the DFIG circuit and the sending end converter of the VSC-HVDC. The DFIG converter is used for ensuring maximum power extraction and VSC-HVDC converter is used for power accommodation [30]. Similar to the VSC-HVDC system used to connect the FSIG wind farm, the control strategy depends on the operation mode of the system. If the VSC-HVDC system is used to transport the wind power with the power command then, the sending-end converter is responsible for accommodating wind power with a predetermined power command in addition to maintaining the ac voltage in the wind farm grid. While the receiving-end converter is used to control the dc link voltage and the ac voltage at the PCC with the ac onshore network [29, 31]. In this approach the VSC-HVDC system could be used to provide frequency control by installing a frequency controller in the sending-side converter. The alternative operation mode is to use the VSC-HVDC system to transport the wind power without a power command. In this case the sending-converter is used to maintain the ac voltage at the wind farm grid [32]. Fig. 5.21 shows the single-line diagram of the VSC-HVDC system connecting a DIFG wind farm.

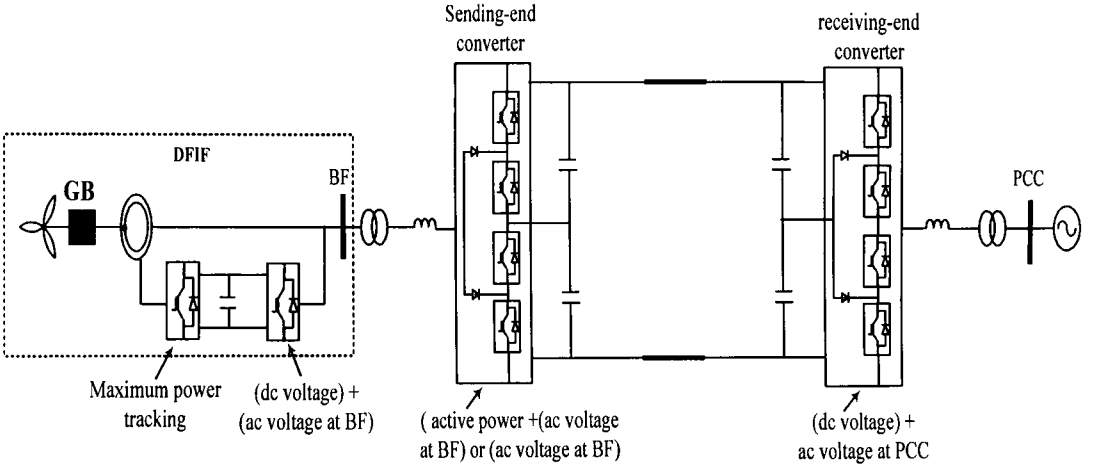


Fig. 5.21: VSC-HVDC system for DFIG wind farm integration

The multi-pole synchronous generator (SG) is one of the possible options for the wind farm integration. The main advantage of the synchronous generator is that it could be connected to a diode rectifier [33-34]. When the diode rectifier is connected to the SG, the SG operates at unity power factor with zero reactive power exchange with the diode rectifier. A dc/dc step-up converter raises the dc voltage of the diode rectifier because the synchronous generator is not capable of generating high voltage at low speed. Since the diode rectifier is uncontrollable, the control of wind farm is achieved through the dc/dc step-up converter or

the excitation system. The dc/dc step-up converter divides the dc link voltage into two levels, the input dc voltage from the rectifier diode and the output dc voltage at the VSC converter. By adjusting the duty cycle of the dc/dc step-up converter the shaft speed can be controlled to extract maximum wind power according to the wind speed change. The VSC converter at the receiving-end maintains the dc link voltage and the ac voltage at the PCC in the onshore ac grid. Two control strategies could be used for the wind farm integration as described in [33]:

1- The power control of the wind turbine is made through the excitation system while the dc/dc step-up converter regulates the generator voltage.

2- The excitation system regulates the generator voltage, while the dc/dc step-up converter ensures the maximum power extraction by regulating the rotor speed.

The low cost of the rectifier and the low conversion losses make the synchronous generator probably the most economic option today [34]. Fig. 5.22 shows the single-line diagram of the VSC-HVDC system connecting a SG-based wind farm.

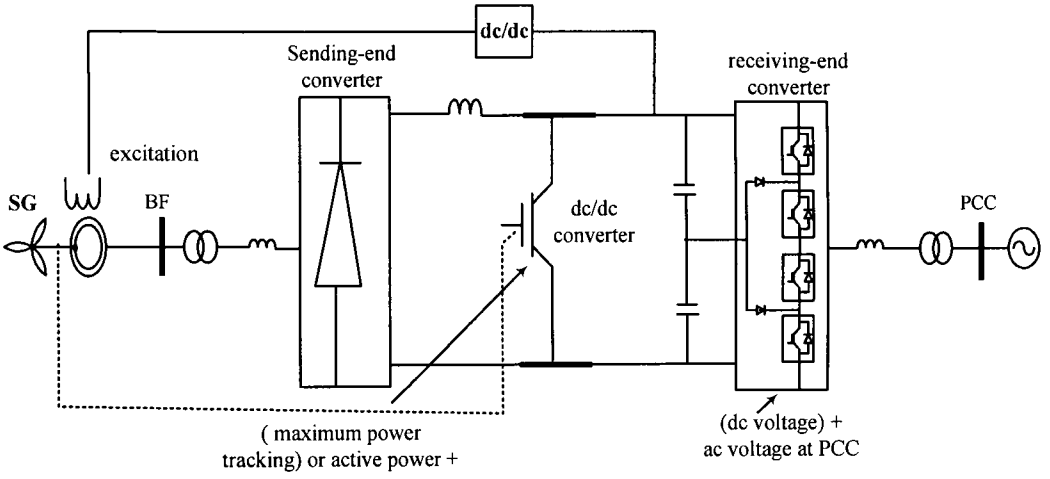


Fig. 5.22: VSC-HVDC system for SG-based wind farm integration

Permanent magnets synchronous generator represents another alternative instead of the synchronous generator for direct-drive wind turbines. PMSG is simpler than the synchronous generator because no excitation system is needed. In addition, it is more competitive for low wind-speed wind farms because it could have higher pole number than the conventional synchronous generator. Similar to the synchronous generator, the PMSG is connected to diode rectifier, dc/dc converter used in the dc circuit to step-up the rectifier dc voltage [35-36]. The control of the PMSG is achieved through the dc/dc step-up converter as described in [37-38]. In this approach, by changing the duty cycle of the dc/dc step-up converter

maximum power extraction is guaranteed over a wide range of wind speed variation, while the grid-side converter is used to control the dc link voltage and the ac voltage at the PCC in the onshore network. The dc/dc step-up converter is used to control the active power of the wind farm, this strategy is useful if the wind farm is operated with a pre-determined power command. Fig. 5.23 shows the single-line diagram of the VSC-HVDC system connecting a PMSG wind farm.

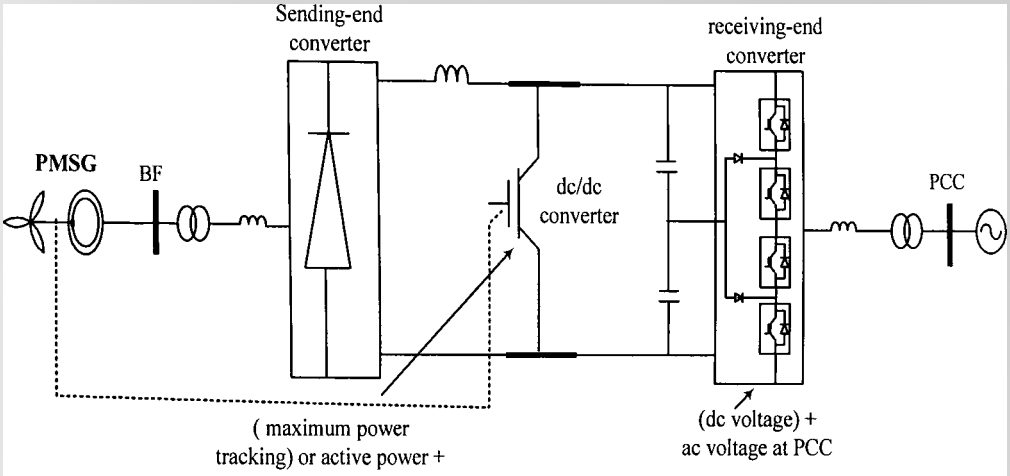


Fig. 5.23: VSC-HVDC system for PMSG wind farm integration.

In all case of VSC-HVDC system with different wind turbine technologies, the receiving-end converter is responsible for maintaining the dc link voltage and the ac voltage at the PCC in the offshore network. Two control strategies could be implemented in the sending-end converter:

1- To control the active power of the transmitted power: in this strategy the wind farm is operated under the rated limit. Therefore the wind farm could reduce or increase the generated power. In this case, the wind farm and the VSC-HVDC system could participate in frequency regulation at the onshore network.

2- To regulate the shaft speed to guarantee maximum power extraction: in this strategy the VSC-HVDC system is used to accommodate the wind power without power command.

In general, Table 5.5 shows a brief compassion of the different wind turbine technologies used with the VSC-HVDC system.

Table 5.5: Compassion of the different wind turbine technologies

	FSIG	DFIG	SG	PMSG
Size and weight	Low specific mass (kg/kW), smaller outer diameter and low number of poles	Low specific mass, smaller outer diameter ,low number of poles & partial power converter is connected at rotor circuit	high specific mass, large outer diameter ,high number of poles & electrical excitation system	high specific mass, large outer diameter and high number of poles
Mechanical drive system	Gearbox is required	Gearbox is required	No gearbox	No gearbox
Reactive power requirement	Supplied by capacitor bank + Sending-end converter	Supplied by converter connected at the rotor circuit	No requirement	No requirement
Sending-end converter	VSC	VSC	diode	diode
receiving-end converter	VSC	VSC	VSC	VSC
Sending-end converter control	the ac voltage at wind farm gird (no power command) or the active power (with power command	the ac voltage at wind farm gird (no power command) or the active power (with power command	maximum power tracking or active power control + regulates the generator voltage	Adjust shaft speed (maximum wind power capture) or the transmitted power (with power command
receiving-end converter control	dc voltage+ the ac voltage at the PCC in the onshore gird	dc voltage+ the ac voltage at the PCC in the onshore gird	dc voltage+ the ac voltage at the PCC in the onshore gird	dc voltage+ the ac voltage at the PCC in the onshore gird
Speed control to maximize wind power capture.	limited	+	++	++
Transmission losses	sending-end VSC losses is high	sending-end VSC losses is high +additional losses in VSC-HVDC system in rotor circuit	diode rectifier loss is low losses in dc/dc converter and excitation losses	diode rectifier loss is low losses in dc/dc converter

5-11 Summary

In this chapter the use of VSC-HVDC transmission system for integration of FSIG wind farms was investigated. The VSC-HVDC system facilitates the connection of the FSIG wind farms in order to meet the requirements set by the GB grid operator. Two control strategies for VSC-HVDC system were investigated. In the first approach the VSC-HVDC accommodates the wind power without a power command. The sending-end converter is used to maintain the ac voltage at the wind farm grid and supply the reactive power required for the wind farm according to wind speed variation. The FSIG plus the VSC-HVDC met all the requirement set

by power system operator; improve the power quality as investigated in this chapter. However with this control approach the FSIG+VSC-HVDC do not provide frequency support.

In the second control approach, the VSC-HVDC system accommodates the wind power with following an assigned power command. The FSIG plus the VSC-HVDC system met the grid code requirements and add additional frequency control functionality. In this case the wind farm is operated below the rated limit. Therefore, the VSC-HVDC system could increase or reduce the accommodated power to help in stabilization of the onshore frequency if any power mismatch occurs. The wind farm owner does not prefer this approach for economical reasons, whereas it is valuable for power system operators from the controllability point of view.

A multi-terminal VSC-HVDC system can be used to integrate the FSIG wind farm in order to improve the transmission system reliability. Alternative routes are available to push the wind power to the onshore network during emergencies such as maintenance, sudden loss of grid side converters or loss of one of the dc links. The initial cost is high in this case, because additional auxiliary cables are required in addition to increases in converters and dc links ratings to be able to withstand the total power during emergencies.

The transient stability of the VSC-HVDC system connecting the FSIG wind farm was investigated during a three-phase fault at the grid side. The VSC-HVDC system can be used with different turbine technologies. The operation of the VSC-HVDC is similar with all technologies with minor differences in the control strategies adopted for each technology. The only concern is to find the optimal economic solution including both the turbine technology and the HVDC system.

References

[1] Y. Jin, *et al.*, "Redundancy analysis of offshore wind farm collection and transmission systems," in *Sustainable Power Generation and Supply, 2009. SUPERGEN '09. International Conference on*, 2009, pp. 1-7.

[2] M. Banzo and A. Ramos, "Stochastic Optimization Model for Electric Power System Planning of Offshore Wind Farms," *Power Systems, IEEE Transactions on,* vol. PP, pp. 1-1, 2010.

[3] T.Ackermann, *Wind Power in Power System*: John Wiley & Sons. Ltd, 2005.

[4] O. Anaya-Lara, *et al.*, "Influence of Windfarms on Power System Dynamic and Transient Stability," *Wind Engineering Vol 30, NO. 2, 2006.*

[5] H. Li and Z. Chen, "Overview of different wind generator systems and their comparisons," *Renewable Power Generation, IET,* vol. 2, pp. 123-138, 2008.

[6] L. Shuhui and T. A. Haskew, "Energy capture, conversion, and control study of DFIG wind turbine under weibull wind distribution," in *Power & Energy Society General Meeting, 2009. PES '09. IEEE*, 2009, pp. 1-9.

[7] S. S. Murthy, *et al.*, "A Comparative Study of Fixed Speed and Variable Speed Wind Energy Conversion Systems Feeding the Grid," in *Power Electronics and Drive Systems, 2007. PEDS '07. 7th International Conference on*, 2007, pp. 736-743.

[8] P. Bresesti, *et al.*, "HVDC Connection of Offshore Wind Farms to the Transmission System," *Energy Conversion, IEEE Transactions on*, vol. 22, pp. 37-43, 2007.

[9] L. Xu, *et al.*, "Power Electronics Options for Large Wind Farm Integration: VSC-Based HVDC Transmission," in *Power Systems Conference and Exposition, 2006. PSCE '06. 2006 IEEE PES*, 2006, pp. 760-767.

[10] I. M. d. Alegri, *et al.*, "Connection requirements for wind farms: A survey on technical requirements and regulation," *Renewable and Sustainable Energy Reviews Volume 11, Issue 8, October 2007, Pages 1858-1872.*

[11] A. Johnson and N. Tleis, "The development of grid code requirements for new and renewable forms of generation in Great Britain," *Wind Engineering 29 (3) (2005), pp. 201–215.*

[12] S. Chondrogiannis, *et al.*, "Modelling and GB Grid Code Compliance Studies of Offshore Wind Farms with Doubly-Fed Induction Generators," in *Power Electronics, Machines and Drives, 2006. The 3rd IET International Conference on*, 2006, pp. 22-26.

[13] *The Grid Code, Issue 3, Revision 12,* vol. National Grid Electricity Transmission plc, available at, http://www.nationalgrid.com/uk/Electricity/Codes/gridcode/gridcodedocs/.

[14] O. A. Giddani, *et al.*, "Grid integration of a large offshore wind farm using VSC-HVDC in parallel with an AC submarine cable," in *Universities Power Engineering Conference (UPEC), 2009 Proceedings of the 44th International*, 2009, pp. 1-5.

[15] S. V. Bozhko, *et al.*, "Control of Offshore DFIG-Based Wind Farm Grid With Line-Commutated HVDC Connection," *Energy Conversion, IEEE Transactions on*, vol. 22, pp. 71-78, 2007.

[16] N. Flourentzou, *et al.*, "VSC-Based HVDC Power Transmission Systems: An Overview," *IEEE Trans on Power Electronics,*, vol. 24, pp. 592-602, 2009.

[17] H. Livani, *et al.*, "Improvement of voltage quality in connection of wind farms to transmission network using VSC-HVDC," in *Power Quality and Supply Reliability Conference, 2008. PQ 2008*, 2008, pp. 137-142.

[18] article, "Grid connection of offshore wind farms - BorWin1," *avialable at http://www05.abb.com/global/scot/scot221.nsf/veritydisplay/f57c59bbade4cebbc12577dd002e06f6/$file/pow-0050%20borwin%20rev10%20lr.pdf.*

[19] D. Z. Yang, *et al.*, "Wind power impact on system operations and planning," in *Power and Energy Society General Meeting, 2010 IEEE*, 2010, pp. 1-5.

[20] M. Ma, *et al.*, "Research on the impact of large-scale integrated wind farms on the security and stability of regional power system," in *Power System Technology (POWERCON), 2010 International Conference on*, 2010, pp. 1-6.

[21] E. Vilchez and J. Stenzel, "Wind energy integration into 110 kV system - impact on power quality of MV and LV networks," in *Transmission and Distribution Conference and Exposition: Latin America, 2008 IEEE/PES*, 2008, pp. 1-6.

[22] "IEEE Recommended Practice for Determination of Power Losses in High-Voltage Direct-Current (HVDC) Converter Stations," *IEEE Std 1158-1991,* p. 1, 1992.

[23] M. P. Bahrman and B. K. Johnson, "The ABCs of HVDC transmission technologies," *Power and Energy Magazine, IEEE,* vol. 5, pp. 32-44, 2007.

[24] L. Carlsson, "HVDC a firewall agianst disturbances in high voltage grids," *ABB Review 3/2005, the article avialable in ABB website.*

[25] D. Cuiqing, *et al.*, "A New Control Strategy of a VSC-HVDC System for High-Quality Supply of Industrial Plants," *Power Delivery, IEEE Transactions on,* vol. 22, pp. 2386-2394, 2007.

[26] *Review of HVDC Link Technology Issues, Electricity Network Investment (ENI), March 2009.*

[27] P. Kundur, *Power System Stability and Control*: Electric Power Research Institute, Power System Engineering Series, 1994.

[28] A. D. Hansen;, *et al.*, "overall control strategy of variable speed doubly-fed induction generator wind turbine," *NORDIC Wind Power Conference, March 2004, Chalmers University of Technology.*

[29] C. Feltes and I. Erlich, "Variable Frequency Operation of DFIG based Wind Farms connected to the Grid through VSC-HVDC Link," in *Power Engineering Society General Meeting, 2007. IEEE*, 2007, pp. 1-7.

[30] X. Dawei, *et al.*, "Coordinated control of an HVDC link and doubly fed induction generators in a large offshore wind farm," *Power Delivery, IEEE Transactions on*, vol. 21, pp. 463-471, 2006.

[31] D. C. Kong and X. P. Zhang, "Modelling and control of offshore wind farm with VSC-HVDC transmission system," in *AC and DC Power Transmission, 2010. ACDC. 9th IET International Conference on*, 2010, pp. 1-6.

[32] L. Xu, *et al.*, "Multi-terminal DC transmission systems for connecting large offshore wind farms," in *Power and Energy Society General Meeting - Conversion and Delivery of Electrical Energy in the 21st Century, 2008 IEEE*, 2008, pp. 1-7.

[33] I. D. Margaris and N. D. Hatziargyriou, "Direct drive synchronous generator wind turbine models for power system studies," in *Power Generation, Transmission, Distribution and Energy Conversion (MedPower 2010), 7th Mediterranean Conference and Exhibition on*, 2010, pp. 1-7.

[34] J. M. Carrasco, *et al.*, "Power-Electronic Systems for the Grid Integration of Renewable Energy Sources: A Survey," *Industrial Electronics, IEEE Transactions on*, vol. 53, pp. 1002-1016, 2006.

[35] R. Bharanikumar, *et al.*, "Novel Maximum Power Point Tracking Controller for Wind Turbine Driven Permanent Magnet Generator," in *Power System Technology and IEEE Power India Conference, 2008. POWERCON 2008. Joint International Conference on*, 2008, pp. 1-6.

[36] M. G. Molina, *et al.*, "Advanced power conditioning system for grid integration of direct-driven PMSG wind turbines," in *Energy Conversion Congress and Exposition (ECCE), 2010 IEEE*, 2010, pp. 3366-3373.

[37] C. Yiguang, *et al.*, "A control strategy of direct driven permanent magnet synchronous generator for maximum power point tracking in wind turbine application," in *International Conference onElectrical Machines and Systems. ICEMS 2008.* , 2008, pp. 3921-3926.

[38] D. Fujin and C. Zhe, "Power control of permanent magnet generator based variable speed wind turbines," in *Electrical Machines and Systems, 2009. ICEMS 2009. International Conference on*, 2009, pp. 1-6.

Chapter Six

Small-signal stability of multi-terminal VSC-HVDC connecting wind farms

6-1 Introduction

Offshore wind power utilization has dramatically increased in the last decade. This increase creates new challenges on how to integrate offshore wind farms into ac power systems without causing operational and stability problems. Multi-terminal VSC-HVDC systems present one of the possible solutions for offshore power integration as discussed in Chapter 4.

Due to the continuous growth of HVDC transmission systems, several HVDC systems may be connected to the ac power network buses resulting in a complex ac/dc interconnected system. The transient and dynamic behavior of the ac/dc interconnected system depends on the characteristics of the ac/dc interconnected system and its controllers.
The major factors influencing the stability of the ac/dc interconnected system are [1-2]:

- The ac system: synchronous machines exhibit low-frequency oscillations due to the slow response of AVR and turbine-governor controllers (power system stabilizers - PSSs - may be used to damp these oscillations). Other factors which affect the ac system stability include reactive power compensation equipment and active filters for harmonics mitigation.

- The dc system: acts as an active power source and introduces harmonics in the system.

- The dc converters: VSC converters with high-switching frequencies are a source of harmonics; these may cause operational problems in the system unless unwanted harmonics are eliminated. Also the VSC controllers exhibit high-frequency oscillations. The VSC converter provides the reactive power during a fault within a short duration period until the synchronous machines adjust their controllers to ride through the disturbance [3].

From the stability viewpoint, the HVDC system connected to the ac system network does not have a negative effect on the dc/ac interconnected system stability. The overall system must remain stable during normal operating conditions and return to its steady state after system disturbances.

In order to study the stability of the interconnected system, two distinct stability concerns exist in power system analysis [4-5]:

- Transient stability, which is concerned with the ability of synchronous machines to remain in synchronism following a large perturbation, such as that caused by a three-phase fault with automatic reconnection following fault clearance.
- Small-signal stability, which is concerned with the ability of power systems to maintain synchronism following small disturbances.

The small-signal stability of multi-terminal VSC-HVDC systems connecting wind farms) is assessed in this Chapter using Eigenvalue Analysis. In small-signal stability analysis the disturbance is considered sufficiently small to permit the linearization of the equations representing the system and to express them in state-space representation [6].

The eigenvalues of the lineralized system model are calculated to evaluate the small-signal stability of the system. The eigenvalues provide the necessary information about the system stability: if all eigenvalues have negative real parts then the system will remain stable after small disturbances, otherwise it will not [7]. Complex conjugate eigenvalues correspond to oscillatory modes, the time constant of the amplitude decay is the reciprocal of the real part of the eigenvalues, and their imaginary parts represent the oscillations frequencies.

The way in which system operating conditions, system parameters and controllers gains influence the dynamic performance of the interconnected system can be demonstrated by observing their influence on the loci of the dominant eigenvalues (the eigenvalues with the most significant influence on network dynamic performance). The participation factor matrix formed from the left and right eigenvalues matrix gives the required information about the relationship between the eigenvalues and the state modes.

The dynamic performance of the interconnected system is described using first-order nonlinear differential equations expressed as [8-9]:

$$\frac{d\Delta x}{dt} = A\Delta x + B\Delta u \tag{6-1}$$

where

Δx is the state vector

Δu is the input vector

A is the state matrix

B is the input

6-2 State-space model of multi-terminal VSC-HVDC connecting wind farms

In order to derive the state-space model of the multi-terminal VSC-system shown in Fig. 6.1, the system is divided into small subsystems. The nonlinear behaviour of each subsystem is linearized at a particular steady-state operating point. It is assumed that the power system is balanced among the three phases, therefore, only the positive-sequence relationships are considered. The system in Fig. 6.1 is composed of the following subsystems:

- The offshore system: consists of the FSIG model ($FSIG_1$ and $FSIG_2$) and the wind-side VSC converters (VSC_3 and VSC_4).
- The dc circuit system: consists of the dc links cables (dc $link_1$, dc $link_2$, auxiliary $link_1$ and auxiliary $link_2$).
- The onshore system: consists of the synchronous generator (SG), the grid-side VSC converters (VSC_1 and VSC_2), and the onshore network (TL_1, TL_2 and TL_3).

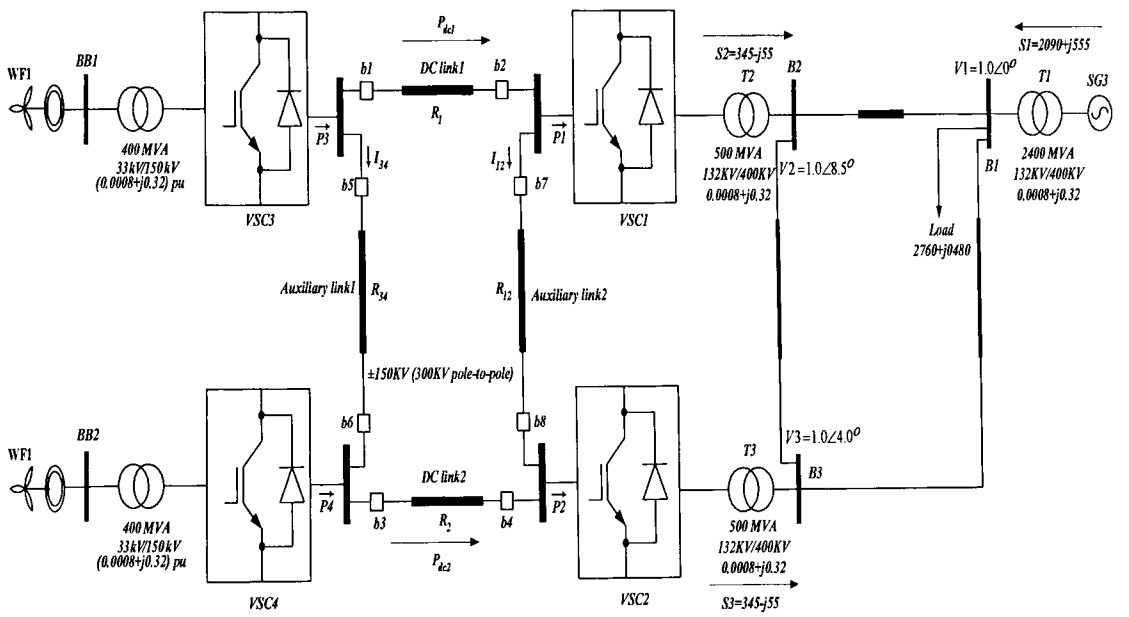


Fig. 6.1: Multi-terminal VSC-HVDC for offshore wind farm integration.

In the following section, the state-space model representation of the individual subsystems is derived.

6-3 Grid-side VSC Converter Model

The dynamic equations representing the VSC converter operating as inverter in the *dq*-frame are [10-11]:

$$L_c \frac{di_{sdi}}{dt} = -R_c i_{sdi} + \omega L_c i_{sqi} + v_{cdi} - v_{sdi} \tag{6-2a}$$

$$L_c \frac{di_{sqi}}{dt} = -R_c i_{sqi} - \omega L_c i_{sdi} + v_{cqi} - v_{sqi} \tag{6-2b}$$

If the VSC converter is assumed lossless, the dc-side dynamics can be related to the ac side by [11]:

$$\frac{dV_{dc1}}{dt} = -\frac{\left[v_{cdi} i_{sdi} + v_{cqi} i_{sqi}\right]}{C V_{dc1}} + \frac{I_{dc}}{C} \tag{6-2c}$$

In equation (6.2) R_c and L_c are the total resistance and inductance between the VSC and the PCC; v_{ci}, v_{si} are the voltages at the VSC terminals and PCC, respectively. While V_{dc1} is the dc voltage at the inverter side and C is the dc capacitor.

After linearization of equations (6.2), the state-space model of the grid-side VSC converter is:

$$\frac{d\Delta i_{sdi}}{dt} = -\frac{R_c}{L_c}\Delta i_{sdi} + \frac{\omega L_c \Delta i_{sqi}}{L_c} + \frac{\Delta v_{cdi}}{L_c} - \frac{\Delta v_{sdi}}{L_c} \tag{6-3a}$$

$$\frac{d\Delta i_{sqi}}{dt} = -\frac{R_c}{L_c}\Delta i_{sqi} - \frac{\omega L_c \Delta i_{sdi}}{L_c} + \frac{\Delta v_{cqi}}{L_c} - \frac{\Delta v_{sqi}}{L_c} \tag{6-3b}$$

$$\frac{d\Delta V_{dc1}}{dt} = -\frac{v_{cdi}}{C V_{dc1}}\Delta i_{sdi} - \frac{v_{cqi}}{C V_{dc1}}\Delta i_{sqi} + \frac{(v_{cdi} i_{sdi} + v_{cqi} i_{sqi})}{C V_{dc1}^2}\Delta V_{dc1} - \frac{i_{sdi}}{C V_{dc1}}\Delta v_{cdi} - \frac{i_{sqi}}{C V_{dc1}}\Delta v_{cqi} + \frac{\Delta I_{dc}}{C} \tag{6-3c}$$

In the test system of Fig. 6.1, converters VSC_3 and VSC_4 regulate the active power and the ac voltage at the wind farm network, while converters VSC_1 and VSC_2 regulate the dc link voltage and ac voltage at the PCCs (buses B_3 and B_4), using conventional control as shown in Fig. 6.2. The grid-side converters' control system is included in the state-space model as follows.

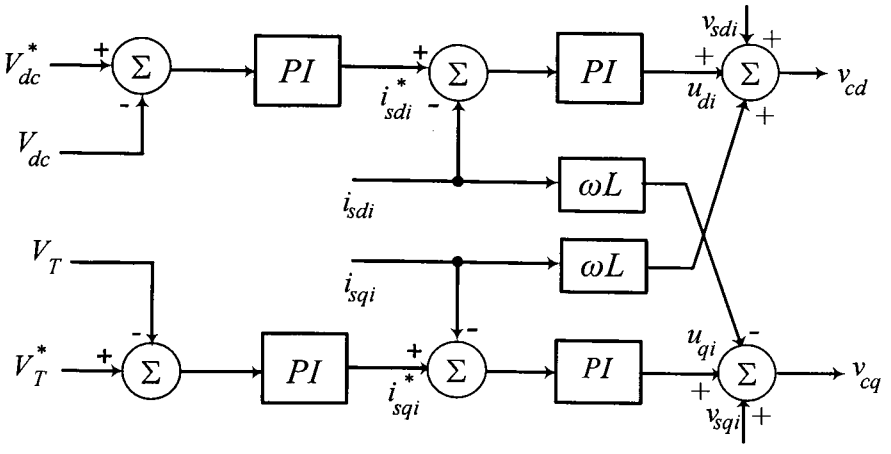


Fig. 6.2: Control system of the grid-side converters.

The reference currents obtained from the dc voltage and ac voltage controllers are:

$$\begin{aligned} i_{sdi}^* &= k_{pdc}(V_{dc1}^* - V_{dc1}) + k_{idc}\int(V_{dc1}^* - V_{dc1})dt \\ &= k_{pdc}(V_{dc1}^* - V_{dc1}) + z_{3i} \end{aligned} \tag{6-4a}$$

$$\begin{aligned} i_{sqi}^* &= k_{pac}(V_{T1}^* - V_{T1}) + k_{iac}\int(V_{T1}^* - V_{T1})dt \\ &= k_{pac}(V_{T1}^* - V_{T1}) + z_{4i} \end{aligned} \tag{6-4b}$$

Where k_{pdc}, k_{idc} k_{pac} and k_{iac} are the dc voltage and ac voltage controllers gains respectively. z_{3i} and z_{4i} are the integral parts of the dc voltage and ac voltage controllers.

The voltages at buses B_1-B_3 and their state-space representation are defined as:

$$V_T = \sqrt{v_{sd}^2 + v_{sq}^2} \tag{6-5}$$

$$\Delta V_{T1} = \frac{v_{sdi}}{V_{T1}}\Delta v_{sdi} + \frac{v_{sqi}}{V_{T1}}\Delta v_{sqi} \tag{6-6}$$

The state-space model for the reference currents then are:

$$\Delta i_{sdi}^* = -k_{pdc}\Delta V_{dc1} + \Delta z_{3i} + k_{pdc}V_{dc1}^* \tag{6-7a}$$

$$\Delta i_{sqi}^* = -k_{pac}\frac{v_{sdi}}{V_{T1}}\Delta v_{sdi} - k_{pac}\frac{v_{sq}}{V_{T1}}\Delta v_{sqi} + \Delta z_{4i} + k_{pac}V_{T1}^* \tag{6-7b}$$

From Fig. 6.2, the VSC converter voltage components (v_{cd} & v_{cq}) are:

$$v_{cdi} = k_{pi}(i^*_{sdi} - i_{sdi}) + k_{ii}\int(i^*_{sdi} - i_{sdi})dt + \omega L_c i_{sqi} + v_{sdi}$$
$$= k_{pi}(i^*_{sdi} - i_{sdi}) + z_{1i} + \omega L_c i_{sqi} + v_{sdi} \quad (6\text{-}8a)$$

$$v_{cqi} = k_{pi}(i^*_{sqi} - i_{sqi}) + k_{ii}\int(i^*_{sqi} - i_{sqi})dt - \omega L_c i_{sdi} + v_{sqi}$$
$$= k_{pi}(i^*_{sqi} - i_{sqi}) + z_{2i} - \omega L_c i_{sdi} + v_{sqi} \quad (6\text{-}8b)$$

Where i_{sdi}, i_{sqi}, are the active and reactive components of the current, k_{pi} and k_{ii} are the proportional and integral gains of the current controller, while z_{1i} and z_{2i} are the integral part of the current controllers.

Now, equations (6.3) after substitution for v_{cd} and v_{cq} from equation (6.8) are:

$$\frac{d\Delta i_{sdi}}{dt} = \frac{-(R_c + k_{pi})}{L_c}\Delta i_{sdi} + \frac{2\omega L_c}{L_c}\Delta i_{sqi} - \frac{k_{pi}k_{pdc}}{L_c}\Delta V_{dc1} + \frac{1}{L_c}\Delta z_{1i} + \frac{k_{pi}}{L_c}\Delta z_{3i} + \frac{k_{pi}k_{pdc}}{L_c}\Delta V^*_{dc1} \quad (6\text{-}9a)$$

$$\frac{d\Delta i_{sqi}}{dt} = \frac{-(R_c + k_{pi})}{L_c}\Delta i_{sqi} - \frac{2\omega L_c}{L_c}\Delta i_{sdi} + \frac{1}{L_c}\Delta z_{2i} - \frac{k_{pi}k_{pdc}v_{sdi}}{L_c V_{T1}}\Delta v_{sdi} - \frac{k_{pi}k_{pdc}v_{sqi}}{L_c V_{T1}}\Delta v_{sqi}$$
$$+ \frac{k_{pi}}{L_c}\Delta z_{4i} + \frac{k_{pi}k_{pdc}}{L_c}\Delta V^*_{T1} \quad (6\text{-}9b)$$

$$\frac{d\Delta V_{dc1}}{dt} = \frac{(-v_{cdi} + k_{pi}i_{sdi} + \omega L_c i_{sqi})}{CV_{dc1}}\Delta i_{sdi} + \frac{(-v_{cqi} + k_{pi}i_{sqi} - \omega L_c i_{sdi})}{CV_{dc1}}\Delta i_{sqi}$$
$$+ \frac{(v_{cdi}i_{sdi} + v_{cqi}i_{sqi} + k_{pdc}k_{pi}i_{sdi})}{CV^2_{dc1}}\Delta V_{dc1} - \frac{i_{sdi}}{CV_{dc1}}\Delta z_{1i} - \frac{i_{sqi}}{CV_{dc1}}\Delta z_{2i} - \frac{i_{sdi}k_{pi}}{CV_{dc1}}\Delta z_{3i} - \frac{i_{sqi}k_{pi}}{CV_{dc1}}\Delta z_{4i} \quad (6\text{-}9c)$$
$$- \frac{(i_{sdi}V_{T1} - k_{pi}k_{pac}i_{sqi}v_{sdi})}{CV_{dc1}V_{T1}}\Delta v_{sdi} - \frac{(i_{sdi}V_{T1} - k_{pi}k_{pac}i_{sqi}v_{sqi})}{CV_{dc1}V_{T1}}\Delta v_{sqi} + \frac{\Delta I_{dc}}{C} - \frac{i_{sdi}k_{pi}k_{pdc}}{CV_{dc1}}\Delta V^*_{dc1}$$
$$- \frac{i_{sqi}k_{pi}k_{pdc}}{CV_{dc1}}\Delta V^*_{T1}$$

The state-space representation of the integral parts of the dc voltage, ac voltage and current controllers are:

$$\frac{d\Delta z_{1i}}{dt} = -k_{ii}\Delta i_{sdi} - k_{ii}k_{pdc}\Delta V_{dc1} + k_{ii}\Delta z_{3i} + k_{ii}k_{pdc}V^*_{dc1} \quad (6\text{-}10a)$$

$$\frac{d\Delta z_{2i}}{dt} = -k_{ii}\Delta i_{sqi} - k_{ii}k_{pac}\frac{v_{sdi}}{V_{T1}}\Delta v_{sdi} - k_{ii}k_{pac}\frac{v_{sqi}}{V_{T1}}\Delta v_{sqi} + k_{ii}\Delta z_{4i} + k_{ii}k_{pac}\Delta V^*_{T1} \quad (6\text{-}10b)$$

$$\frac{d\Delta z_{3i}}{dt} = -k_{idc}\Delta V_{dc1} + k_{idc}\Delta V^*_{dc1} \quad (6\text{-}10c)$$

$$\frac{d\Delta z_{4i}}{dt} = \frac{-k_{iac}v_{sdi}}{V_{T1}}\Delta v_{sdi} - \frac{k_{iac}v_{sqi}}{V_{T1}}\Delta v_{sqi} + k_{iac}\Delta V^*_{T1} \quad (6\text{-}10d)$$

The complete state-space model for the grid-side VSC converter and associated controllers is:

$$\frac{d}{dt}\begin{bmatrix}\Delta i_{sdi}\\ \Delta i_{sqi}\\ \Delta V_{dc1}\\ \Delta z_{1i}\\ \Delta z_{2i}\\ \Delta z_{3i}\\ \Delta z_{4i}\end{bmatrix}=\begin{bmatrix}\frac{-(R_c+k_{pi})}{L_c} & \frac{2\omega L_c}{L_c} & \frac{-k_{pi}k_{pdc}}{L_c} & \frac{1}{L_c} & 0 & \frac{k_{pi}}{L_c} & 0\\ \frac{-2\omega L_c}{L_c} & \frac{-(R_c+k_{pi})}{L_c} & 0 & 0 & \frac{1}{L_c} & 0 & \frac{k_{pi}}{L_c}\\ \frac{(-v_{cdi}+k_{pi}i_{sdi}+\omega L_c i_{sqi})}{CV_{dc1}} & \frac{(-v_{cqi}+k_{pi}i_{sqi}-\omega L_c i_{sdi})}{CV_{dc1}} & \frac{(v_{cdi}i_{sdi}+v_{cqi}i_{sqi}+k_{pdc}k_{pi}i_{sdi})}{CV_{dc1}^2} & \frac{-i_{sdi}}{CV_{dc1}} & \frac{-i_{sqi}}{CV_{dc1}} & \frac{-i_{sdi}k_{pi}}{CV_{dc1}} & \frac{-i_{sqi}k_{pi}}{CV_{dc1}}\\ -k_{ii} & 0 & -k_{ii} & 0 & 0 & -k_{ii} & 0\\ 0 & -k_{ii} & 0 & 0 & 0 & 0 & -k_{ii}\\ 0 & 0 & -k_{ii} & 0 & 0 & 0 & 0\\ 0 & 0 & 0 & 0 & 0 & 0 & 0\end{bmatrix}\begin{bmatrix}\Delta i_{sdi}\\ \Delta i_{sqi}\\ \Delta V_{dc1}\\ \Delta z_{1i}\\ \Delta z_{2i}\\ \Delta z_{3i}\\ \Delta z_{4i}\end{bmatrix}$$
$$+\begin{bmatrix}0 & 0 & 0\\ \frac{-k_{pi}k_{pdc}v_{sdi}}{L_cV_{T1}} & \frac{-k_{pi}k_{pdc}v_{sqi}}{L_cV_{T1}} & 0\\ \frac{(i_{sdi}V_{T1}-k_{pi}k_{pac}i_{sqi}v_{sdi})}{CV_{dc1}V_{T1}} & \frac{-(i_{sdi}V_{T2}-k_{pi}k_{pac}i_{sqi}v_{sqi})}{CV_{dc1}V_{T1}} & \frac{1}{C}\\ 0 & 0 & 0\\ -k_{ii}k_{pac}\frac{v_{sdi}}{V_{T1}} & -k_{ii}k_{pac}\frac{v_{sqi}}{V_{T1}} & 0\\ 0 & 0 & 0\\ \frac{-k_{iac}v_{sdi}}{V_{T1}} & \frac{-k_{iac}v_{sqi}}{V_{T1}} & 0\end{bmatrix}\begin{bmatrix}\Delta v_{sdi}\\ \Delta v_{sdi}\\ \Delta I_{dc}\end{bmatrix}+\begin{bmatrix}\frac{k_{pi}k_{pdc}}{L_c} & 0\\ 0 & \frac{k_{pi}k_{pdc}}{L_c}\\ \frac{-i_{sdi}k_{pi}k_{pdc}}{CV_{dc1}} & \frac{-i_{sqi}k_{pi}k_{pdc}}{CV_{dc1}}\\ k_{ii}k_{pdc} & 0\\ 0 & k_{ii}k_{pdc}\\ k_{idc} & 0\\ 0 & k_{idc}\end{bmatrix}\begin{bmatrix}\Delta V_{dc1}^*\\ \Delta V_{T1}^*\end{bmatrix} \qquad (6\text{-}11)$$

6-4 Synchronous Generator, AVR, and governor-turbine models

The synchronous generator in the onshore grid is modeled with a seventh-order model in the synchronous reference frame with AVR and turbine-governor controls. The state-space model of the synchronous generator is as follow [8, 12]:

$$\begin{bmatrix}L_d & M_F & M_D & 0 & 0 & 0 & 0\\ M_F & L_F & M_R & 0 & 0 & 0 & 0\\ M_D & M_R & M_D & 0 & 0 & 0 & 0\\ 0 & 0 & 0 & L_q & M_Q & 0 & 0\\ 0 & 0 & 0 & M_Q & L_Q & 0 & 0\\ 0 & 0 & 0 & 0 & 0 & 2H\omega_o & 0\\ 0 & 0 & 0 & 0 & 0 & 0 & 1\end{bmatrix}\begin{bmatrix}\Delta i_d\\ \Delta i_F\\ \Delta i_D\\ \Delta i_q\\ \Delta i_Q\\ \Delta\omega\\ \Delta\delta\end{bmatrix}\frac{d}{dt}=-\begin{bmatrix}r_a & 0 & 0 & \omega_o L_q & \omega_o M_Q & \lambda_{qo} & -\cos\delta_o\\ 0 & r_F & 0 & 0 & 0 & 0 & 0\\ 0 & 0 & r_D & 0 & 0 & 0 & 0\\ -\omega_o L_d & -\omega_o L_d M_F & -\omega_o L_d M_D & r_a & 0 & \lambda_{do} & -\sin\delta_o\\ 0 & 0 & 0 & 0 & r_Q & 0 & 0\\ \lambda_{qo}-L_d i_{qo} & -M_F i_{qo} & -M_D i_{qo} & -\lambda_{do}+L_q i_{do} & -M_Q i_{do} & D & 0\\ 0 & 0 & 0 & 0 & 0 & -1 & 0\end{bmatrix}\begin{bmatrix}\Delta i_d\\ \Delta i_F\\ \Delta i_D\\ \Delta i_q\\ \Delta i_Q\\ \Delta\omega\\ \Delta\delta\end{bmatrix}-\begin{bmatrix}\Delta v_d\\ -\Delta v_F\\ 0\\ \Delta v_q\\ 0\\ \Delta T_m\\ 0\end{bmatrix} \qquad (6\text{-}12)$$

The excitation system used with the synchronous generator is static excitation (shown in Fig. 6.3) with the following parameters: K_A=250, T_A=0.01s, K_F=10, T_F=1s. The state-space representation of the excitation system is:

$$\frac{d}{dt}\begin{bmatrix}\Delta V_F\\ \Delta V_A\end{bmatrix}=\begin{bmatrix}\frac{-1}{T_A} & \frac{K_A}{T_A}\\ \frac{-K_F}{T_AT_F} & \frac{-(K_AK_F+T_A)}{T_AT_F}\end{bmatrix}\begin{bmatrix}\Delta V_F\\ \Delta V_A\end{bmatrix}+\begin{bmatrix}\frac{K_A}{T_A} & \frac{K_A}{T_A}\\ \frac{K_AK_F}{T_AT_F} & \frac{-K_AK_F}{T_AT_F}\end{bmatrix}\begin{bmatrix}\Delta V_{REF}\\ \Delta V_T\end{bmatrix} \quad (6\text{-}13)$$

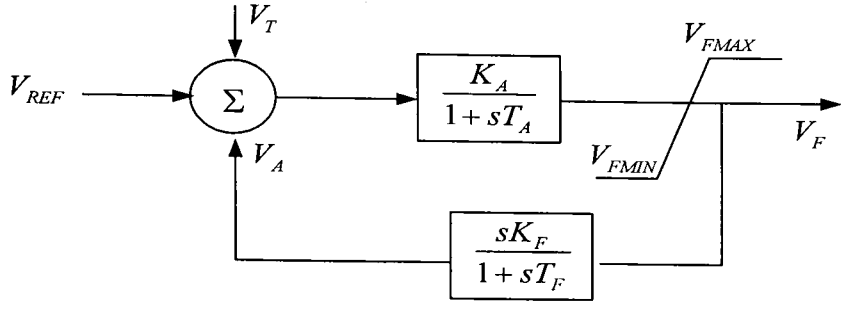


Fig. 6.3: Excitation system block diagram.

The block diagram of the turbine-governor system used with the synchronous generator is shown in Fig. 6.4. The turbine-governor model parameters are: T_{SR}=250, T_{SM}=0.01s, T_{CH}=10, K_G=1s. The state-space representation is given in equation (6.14).

$$\frac{d}{dt}\begin{bmatrix}\Delta Y_2\\ \Delta Y_3\\ \Delta P_m\end{bmatrix}=\begin{bmatrix}\frac{-1}{T_{SR}} & 0 & 0\\ \frac{1}{T_{SM}} & \frac{-1}{T_{SM}} & 0\\ 0 & \frac{1}{T_{CH}} & \frac{-1}{T_{CH}}\end{bmatrix}\begin{bmatrix}\Delta Y_2\\ \Delta Y_3\\ \Delta P_m\end{bmatrix}+\begin{bmatrix}\frac{1}{T_{SR}} & \frac{-K_G}{T_{SR}}\\ 0 & 0\\ 0 & 0\end{bmatrix}\begin{bmatrix}\Delta SR\\ \Delta\omega\end{bmatrix} \quad (6\text{-}14)$$

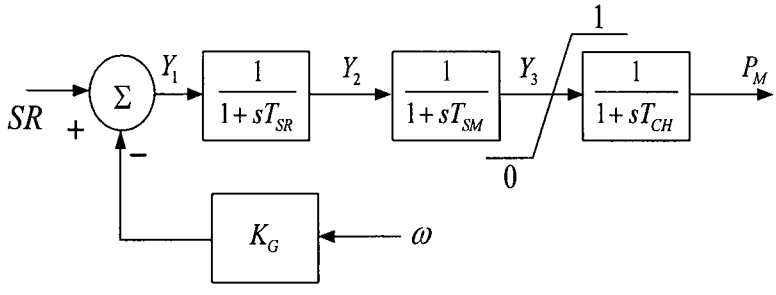


Fig. 6.4: Steam turbine-governor system block diagram.

6-5 Onshore network model

The impedance matrix is used to model the onshore power network in the *dq* reference frame [12]. The current and voltage components in each bus are referred to a common reference frame using the concept of the common reference frame [12-13]. The relationship between the voltage and current components at the nodes where the synchronous generator and voltage source converters are connected is:

$$[V]=[Z][I] \tag{6-15}$$

where [Z] is the impedance matrix. Since the voltage/current relationship is:

$$V_d + jV_q = (R + jX)(I_d + jI_q) \tag{6-16}$$

Then the state-space representation of the onshore network is derived as follow:

$$\begin{bmatrix} \Delta v_{sd1} \\ \Delta v_{sq1} \\ \Delta v_{sd2} \\ \Delta v_{sq2} \\ \Delta v_{sd3} \\ \Delta v_{sq3} \end{bmatrix} = \begin{bmatrix} R_{11} & -X_{11} & R_{12} & -X_{12} & R_{13} & -X_{13} \\ X_{11} & R_{11} & X_{12} & R_{12} & X_{13} & R_{13} \\ R_{21} & -X_{21} & R_{22} & -X_{22} & R_{23} & -X_{23} \\ X_{21} & R_{21} & X_{22} & R_{22} & X_{23} & R_{23} \\ R_{31} & -X_{31} & R_{32} & -X_{32} & R_{33} & -X_{33} \\ X_{31} & R_{31} & X_{32} & R_{32} & X_{33} & R_{33} \end{bmatrix} \begin{bmatrix} \Delta v_{sd1} \\ \Delta v_{sq1} \\ \Delta v_{sd2} \\ \Delta v_{sq2} \\ \Delta v_{sd3} \\ \Delta v_{sq3} \end{bmatrix} \tag{6-17}$$

where Δi_s and Δv_s are the current and the voltage at B_1, B_2, and B_3. While R and X are the impedance matrix components.

6-6 DC link circuit model

The single-line diagram of the dc link circuit is shown in Fig. 6.5. The stray capacitors of the dc cables are added to the reservoir capacitors of the VSC converter stations. The dc link dynamic equation is [14]:

$$\frac{dI_{dc31}}{dt} = -\frac{R_{dc}}{L_{dc}} I_{dc31} + \frac{1}{L_{dc}} V_{dc3} - \frac{1}{L_{dc}} V_{dc1} \tag{6-18}$$

Where I_{dc} is the dc link current, V_{dc3} is the dc voltage at the rectifier/inverter side, R_{dc} is the dc cable resistance, and L_{dc} is the dc cable inductance.

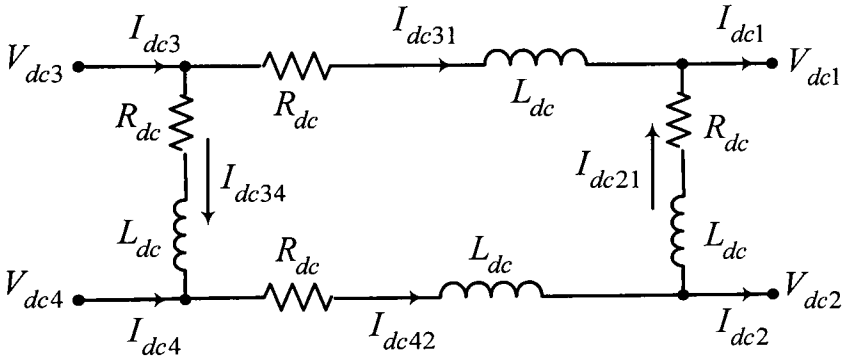


Fig. 6.5: Single-line diagram of the dc link circuit.

Based on equation (6.18) the state-space model of the dc link currents flowing in the dc link circuit is derived as follow:

$$\frac{d\Delta I_{dc31}}{dt} = -\frac{R_{dc}}{L_{dc}}\Delta I_{dc31} + \frac{1}{L_{dc}}\Delta V_{dc3} - \frac{1}{L_{dc}}\Delta V_{dc1} \tag{6-19a}$$

$$\frac{d\Delta I_{dc42}}{dt} = -\frac{R_{dc}}{L_{dc}}\Delta I_{dc42} + \frac{1}{L_{dc}}\Delta V_{dc4} - \frac{1}{L_{dc}}\Delta V_{dc2} \tag{6-19b}$$

$$\frac{d\Delta I_{dc34}}{dt} = -\frac{R_{dc}}{L_{dc}}\Delta I_{dc34} + \frac{1}{L_{dc}}\Delta V_{dc3} - \frac{1}{L_{dc}}\Delta V_{dc4} \tag{6-19c}$$

$$\frac{d\Delta I_{dc21}}{dt} = -\frac{R_{dc}}{L_{dc}}\Delta I_{dc21} + \frac{1}{L_{dc}}\Delta V_{dc2} - \frac{1}{L_{dc}}\Delta V_{dc1} \tag{6-19d}$$

The state-space model of the equivalent dc currents of the VSC converters (I_{dc1} to I_{dc4}), which combines the dc and the ac circuit, is derived as follow:

$$\begin{aligned}\Delta I_{dc1} &= \Delta I_{dc31} + \Delta I_{dc21} \\ &= -\frac{L_{dc}d\Delta I_{dc31}}{R_{dc}dt} - \frac{L_{dc}d\Delta I_{dc21}}{R_{dc}dt} - \frac{2}{R_{dc}}\Delta V_{dc1} + \frac{1}{R_{dc}}\Delta V_{dc2} + \frac{1}{R_{dc}}\Delta V_{dc3}\end{aligned} \tag{6-20a}$$

$$\begin{aligned}\Delta I_{dc2} &= \Delta I_{dc42} - \Delta I_{dc21} \\ &= \frac{L_{dc}d\Delta I_{dc21}}{R_{dc}dt} - \frac{L_{dc}d\Delta I_{dc42}}{R_{dc}dt} + \frac{1}{R_{dc}}\Delta V_{dc4} - \frac{2}{R_{dc}}\Delta V_{dc2} + \frac{1}{R_{dc}}\Delta V_{dc1}\end{aligned} \tag{6-20b}$$

$$\begin{aligned}\Delta I_{dc3} &= \Delta I_{dc31} + \Delta I_{dc34} \\ &= -\frac{L_{dc}d\Delta I_{dc31}}{R_{dc}dt} - \frac{L_{dc}d\Delta I_{dc34}}{R_{dc}dt} + \frac{2}{R_{dc}}\Delta V_{dc3} - \frac{1}{R_{dc}}\Delta V_{dc1} - \frac{1}{R_{dc}}\Delta V_{dc4}\end{aligned} \tag{6-20c}$$

$$\begin{aligned}\Delta I_{dc4} &= \Delta I_{dc42} - \Delta I_{dc34} \\ &= -\frac{L_{dc}d\Delta I_{dc42}}{R_{dc}dt} + \frac{L_{dc}d\Delta I_{dc34}}{R_{dc}dt} + \frac{2}{R_{dc}}\Delta V_{dc4} - \frac{1}{R_{dc}}\Delta V_{dc2} - \frac{1}{R_{dc}}\Delta V_{dc3}\end{aligned} \tag{6.20d}$$

6-7 Wind farm-side VSC Converter Model

Similarly, the state-space model of the wind farm-side VSC for small-signal stability analysis is as follows:

$$\frac{d\Delta i_{sdr}}{dt} = -\frac{R_c}{L_c}\Delta i_{sdr} + \frac{\omega L_c \Delta i_{sqr}}{L_c} + \frac{\Delta v_{sdr}}{L_c} - \frac{\Delta v_{cdr}}{L_c} \tag{6.21a}$$

$$\frac{d\Delta i_{sqr}}{dt} = -\frac{R_c}{L_c}\Delta i_{sqr} - \frac{\omega L_c \Delta i_{sdr}}{L_c} + \frac{\Delta v_{sqr}}{L_c} - \frac{\Delta v_{cqr}}{L_c} \tag{6-21b}$$

$$\frac{d\Delta V_{dc3}}{dt} = \frac{v_{cdr}}{CV_{dc3}}\Delta i_{sdr} + \frac{v_{cqr}}{CV_{dc3}}\Delta i_{sqr} - \frac{\left[v_{cdr} i_{sdr} + v_{cqr} i_{sqr}\right]}{CV_{dc3}^2}\Delta V_{dc3} + \frac{i_{sdr}}{CV_{dc3}}\Delta v_{cdr} + \frac{i_{sqr}}{CV_{dc3}}\Delta v_{cqr} - \frac{\Delta I_{dc}}{C} \tag{6-21c}$$

The wind farm-side converters' control system is chosen such that they control the active power and regulate the ac voltage at the wind farms terminals (B_3 and B_4). The control system block diagram of the wind farm-side converters is shown in Fig. 6.6.

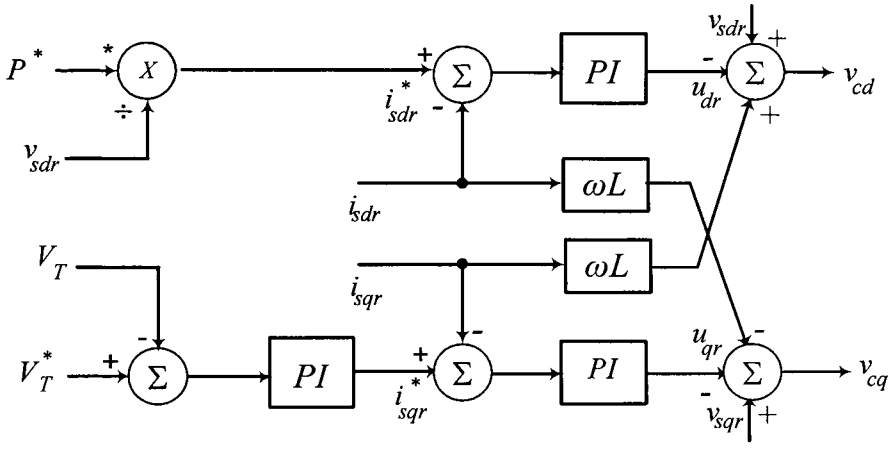


Fig. 6.6: Control system of the wind farm-side converters.

The reference currents obtained from the active power and ac voltage controllers from Fig. 6.6 are:

$$i_{sdr}^{*} = \frac{P^{*}}{v_{sdr}} \tag{6-22a}$$

$$\begin{aligned} i_{sqr}^{*} &= k_{pac}(V_{T3}^{*} - V_{T3}) + k_{iac}\int (V_{T3}^{*} - V_{T3})dt \\ &= k_{pac}(V_{T3}^{*} - V_{T3}) + z_{4r} \end{aligned} \tag{6-22b}$$

where k_{pac} and k_{iac} are the ac voltage controllers' gains and z_{4r} is the integral part of the ac voltage controllers.

The state-space equations for the reference currents then are:

$$\Delta i_{sdr}^{*} = \frac{-P^{*}}{v_{sdr}^{2}}\Delta v_{sdr} + \frac{1}{v_{sdr}}\Delta P^{*} \tag{6-23a}$$

$$\Delta i_{sqr}^{*} = -k_{pac}\frac{v_{sdr}}{V_{T3}}\Delta v_{sdr} - k_{pac}\frac{v_{sqr}}{V_{T3}}\Delta v_{sqr} + \Delta z_{4r} + k_{pac}V_{T3}^{*} \tag{6-23b}$$

The complete state-space representation of the wind farm-side VSC converters is:

$$\frac{d\Delta i_{sdr}}{dt} = -\frac{\left(R_C + k_{pi}\right)}{L_c}\Delta i_{sdr} + \frac{\Delta z_{1r}}{L_c} + \frac{k_{pi}P^{*}}{L_c v_{sdr}^{2}}\Delta v_{sdr} - \frac{k_{pi}}{L_c v_{sdr}}\Delta P^{*} \tag{6-24a}$$

$$\frac{d\Delta i_{sqr}}{dt} = \frac{-\left(R_c + k_{pi}\right)}{L_c}\Delta i_{sqr} + \frac{\Delta z_{2r}}{L_c} + \frac{k_{pi}}{L_c}\Delta z_{4r} - \frac{k_{pi}k_{pac}v_{sdr}}{L_c V_{T3}}\Delta v_{sdr} - \frac{k_{pi}k_{pac}v_{sqr}}{L_c V_{T3}}\Delta v_{sqr} + \frac{k_{pi}k_{pac}}{L_c}V_{T2}^{*} \tag{6-24b}$$

$$\begin{aligned}\frac{d\Delta V_{dc3}}{dt} &= \frac{\left(v_{cdr} - \omega L_c i_{sqr} + k_{pi}i_{sdr}\right)}{CV_{dc3}}\Delta i_{sdr} + \frac{\left(v_{cqr} + \omega L_C i_{sdr} + k_{pi}i_{sqr}\right)}{CV_{dc3}}\Delta i_{sqr} \\ &- \frac{\left(v_{cdr}i_{sdr} + v_{cqr}i_{sqr}\right)}{CV_{dc3}^{2}}\Delta V_{dc3} - \frac{\Delta I_{dc}}{C} - \frac{i_{sdr}}{CV_{dc3}}\Delta z_{1r} - \frac{i_{sqr}}{CV_{dc3}}\Delta z_{2r} - \frac{k_{pi}i_{sqr}}{CV_{dc3}}\Delta z_{4r} \\ &\frac{k_{pi}i_{sdr}P^{*}}{CV_{dc3}v_{sdr}^{2}}\Delta v_{sdr} + \frac{i_{sdr}}{CV_{dc3}}\Delta v_{sdr} + \frac{k_{pi}k_{pac}i_{sqr}v_{sdr}}{CV_{dc3}V_{T3}}\Delta v_{sdr} + \frac{i_{sqr}}{CV_{dc3}}\Delta v_{sqr} \\ &+ \frac{k_{pi}k_{pac}i_{sqr}v_{sqr}}{CV_{dc3}V_{T3}}\Delta v_{sdr} - \frac{k_{pi}k_{pac}i_{sqr}}{CV_{dc3}}V_{T3}^{*} - \frac{k_{pi}i_{sdr}}{CV_{dc3}v_{sdr}}\Delta P^{*}\end{aligned} \tag{6-24c}$$

And the state-space representation of the integral parts of the ac voltage and current controllers are:

$$\frac{d\Delta z_{1r}}{dt} = -k_{pi}\Delta i_{sdr} + \frac{k_{pi}P^{*}}{\Delta v_{sdr}^{2}}\Delta v_{sdr} - \frac{k_{pi}}{v_{sdr}}\Delta P^{*} \tag{6-25a}$$

$$\frac{d\Delta z_{2r}}{dt} = -k_{ii}\Delta i_{sqr} - k_{ii}k_{pac}\frac{v_{sdr}}{V_{T3}}\Delta v_{sdr} - k_{ii}k_{pac}\frac{v_{sqr}}{V_{T3}}\Delta v_{sqr} + k_{ii}\Delta z_{4r} + k_{ii}k_{pac}\Delta V_{T3}^{*} \tag{6-25b}$$

$$\frac{d\Delta z_{4r}}{dt} = \frac{-k_{iac}v_{sdr}}{V_{T3}}\Delta v_{sdr} - \frac{k_{iac}v_{sqr}}{V_{T3}}\Delta v_{sqr} + k_{iac}\Delta V_{T3}^{*} \tag{6-25c}$$

The complete state-space model of the wind farm-side VSC converters and associated control system is:

$$\frac{d}{dt}\begin{bmatrix}\Delta i_{sd}\\ \Delta i_{sq}\\ \Delta V_{dc}\\ \Delta z_{1r}\\ \Delta z_{2r}\\ \Delta z_{4r}\end{bmatrix}=\begin{bmatrix}\frac{-(R_c+k_{pi})}{L_c} & 0 & 0 & \frac{1}{L_c} & 0 & 0\\ 0 & \frac{-(R_c+k_{pi})}{L_c} & 0 & 0 & \frac{1}{L_c} & \frac{k_{pi}}{L_c}\\ \frac{(v_{cd}-\omega L_c i_{sq}+k_{pi}i_{sd})}{CV_{dc}} & \frac{(v_{cq}+\omega L_c i_{sd}+k_{pi}i_{sq})}{CV_{dc}} & -\frac{(v_{cd}i_{sd}+v_{cq}i_{sq})}{CV_{dc}^2} & \frac{i_{sd}}{CV_{dc}} & \frac{i_{sq}}{CV_{dc}} & \frac{k_{pi}i_{sq}}{CV_{dc}}\\ -k_{pi} & 0 & 0 & 1 & 0 & 0\\ 0 & -k_{pi} & 0 & 0 & 0 & 0\\ 0 & 0 & 0 & 0 & 0 & 0\end{bmatrix}\begin{bmatrix}\Delta i_{sd}\\ \Delta i_{sq}\\ \Delta V_{dc}\\ \Delta z_{1r}\\ \Delta z_{2r}\\ \Delta z_{4r}\end{bmatrix}$$

$$+\begin{bmatrix}\frac{k_{pi}P^*}{L_c v_{sd}^2} & 0 & 0\\ \frac{-k_{pi}k_{poc}v_{sdr}}{L_c V_{T3}} & \frac{-k_{pi}k_{poc}v_{sqr}}{L_c V_{T3}} & 0\\ \left(\frac{k_{pi}i_{sd}P^*}{CV_{dc}v_{sd}^2}+\frac{i_{sd}}{CV_{dc}}+\frac{k_{pi}k_{poc}i_{sq}v_{sd}}{CV_{dc}V_T}\right) & \left(\frac{i_{sq}}{CV_{dc}}+\frac{k_{pi}k_{poc}i_{sq}v_{sq}}{CV_{dc}V_T}\right) & \frac{-1}{C}\\ \frac{k_{pi}P^*}{v_{sd}^2} & 0 & 0\\ \frac{-k_{ii}k_{poc}v_{sdr}}{V_{T3}} & \frac{-k_{ii}k_{poc}v_{sqr}}{V_{T3}} & 0\\ \frac{-k_{iac}v_{sdr}}{V_{T3}} & \frac{-k_{iac}v_{sqr}}{V_{T3}} & 0\end{bmatrix}\begin{bmatrix}\Delta v_{sdr}\\ \Delta v_{sqr}\\ \Delta I_{dc}\end{bmatrix}+\begin{bmatrix}-\frac{k_{pi}}{L_c v_{sdr}} & 0\\ 0 & \frac{k_{pi}k_{poc}}{L_c}\\ \frac{k_{pi}i_{sdr}}{CV_{dc}v_{sdr}} & \frac{-k_{pi}k_{poc}i_{sqr}}{CV_{dc}}\\ \frac{-k_{pi}}{v_{sdr}} & 0\\ 0 & k_{ii}k_{poc}\\ 0 & k_{iac}\end{bmatrix}\begin{bmatrix}\Delta P^*\\ \Delta V_{T3}^*\end{bmatrix} \quad (6\text{-}26)$$

6-8 Wind farm state-space model

A fifth-order model is used to describe the stator and rotor circuits of the FSIG generator [15-16].

$$v_{dsf}=-R_{sf}i_{dsf}-\omega_s\psi_{qsf}+\frac{d\psi_{dsf}}{dt} \quad (6\text{-}27a)$$

$$v_{qsf}=-R_s i_{qsf}+\omega_s\psi_{dsf}+\frac{d\psi_{qsf}}{dt} \quad (6\text{-}27b)$$

$$0=-R_{rf}i_{drf}-s\omega_s\psi_{qrf}+\frac{d\psi_{drf}}{dt} \quad (6\text{-}27c)$$

$$0=-R_{rf}i_{qrf}+s\omega_s\psi_{drf}+\frac{d\psi_{qrf}}{dt} \quad (6\text{-}27d)$$

$$\frac{d\omega_{mf}}{dt}=\frac{1}{2H_{mf}}(T_{mf}-T_{ef}) \quad (6\text{-}27e)$$

where v is the voltage, R is the resistance, i the current, ω_s is the stator frequency, S is the machine slip, and ψ is the flux linkage. The subscripts d and q indicate the direct and quadrature axis frame respectively, and subscripts r and s stand for rotor and stator quantities. T_{mf} is the mechanical power while the electrical power is defined as:

$$T_{ef} = \psi_{qrf} i_{drf} - \psi_{drf} i_{qrf} \tag{6-28}$$

The flux linkage is calculated using the following equation:

$$\psi_{dsf} = -(L_{sf} + L_{mf}) i_{dsf} - L_{mf} i_{drf} \tag{6-29a}$$

$$\psi_{qsf} = -(L_{sf} + L_{mf}) i_{qsf} - L_{mf} i_{qrf} \tag{6-29b}$$

$$\psi_{drf} = -(L_{rf} + L_{mf}) i_{drf} - L_{mf} i_{dsf} \tag{6-29c}$$

$$\psi_{qrf} = -(L_{rf} + L_{mf}) i_{qrf} - L_{mf} i_{qsf} \tag{6-29d}$$

Based on equations (6.26) to (6.28) the state-space model of the FSIG generator is:

$$L_{smf} \frac{d\Delta i_{dsf}}{dt} + L_{mf} \frac{d\Delta i_{drf}}{dt} = -R_{sf} \Delta i_{dsf} + \omega_s L_{smf} \Delta i_{qsf} + \omega_s L_{mf} \Delta i_{qrf} - \Delta v_{dsf} \tag{6-30a}$$

$$L_{smf} \frac{d\Delta i_{qsf}}{dt} + L_{mf} \frac{d\Delta i_{qrf}}{dt} = -R_{sf} \Delta i_{qsf} - \omega_s L_{smf} \Delta i_{dsf} - \omega_s L_{mf} \Delta i_{drf} - \Delta v_{qsf} \tag{6-30b}$$

$$\begin{aligned} L_{rmf} \frac{d\Delta i_{drf}}{dt} + L_{mf} \frac{d\Delta i_{dsf}}{dt} = &-R_{rf} \Delta i_{drf} + \left(\omega_s - \omega_{rf}\right) L_{rmf} \Delta i_{qrf} + \left(\omega_s - \omega_{rf}\right) L_{mf} \Delta i_{qsf} \\ &- L_{mf} i_{qsf} \Delta \omega_{rf} - L_{rmf} i_{qrf} \Delta \omega_r \end{aligned} \tag{6-30c}$$

$$\begin{aligned} L_{rmf} \frac{d\Delta i_{qrf}}{dt} + L_{mf} \frac{d\Delta i_{qsf}}{dt} = &-R_{rf} \Delta i_{qrf} - \left(\omega_s - \omega_{rf}\right) L_{rmf} \Delta i_{drf} - \left(\omega_s - \omega_{rf}\right) L_{mf} \Delta i_{dsf} \\ &+ L_{rmf} i_{drf} \Delta \omega_{rf} + L_{mf} i_{dsf} \Delta \omega_r \end{aligned} \tag{6-30d}$$

$$\frac{d\omega_{mf}}{dt} = \frac{1}{2H_{mf}} (T_{mf} - L_{mf} i_{dsf} \Delta i_{qrf} + L_{mf} i_{qsf} \Delta i_{drf} + L_{mf} i_{drf} \Delta i_{qsf} - L_{mf} i_{qrf} \Delta i_{dsf}) \tag{6-30e}$$

The state-space model for the three-phase capacitor bank connected with the FSIG generators is [17]:

$$\frac{d\Delta v_{dsf}}{dt} = \frac{1}{C_{ba}} \left(\Delta i_{dsf} - \Delta i_{sdsr}\right) + \Delta v_{sqf} \tag{6-31a}$$

$$\frac{d\Delta v_{qsf}}{dt} = \frac{1}{C_{ba}} \left(\Delta i_{qsf} - \Delta i_{sqr}\right) - \Delta v_{sdf} \tag{6-31b}$$

The complete state-space model of the FSIG and the capacitor banks is:

$$\begin{bmatrix} L_{rmf} & 0 & L_{mf} & 0 & 0 & 0 & 0 \\ 0 & L_{rmf} & 0 & L_{mf} & 0 & 0 & 0 \\ L_{mf} & 0 & L_{rmf} & 0 & 0 & 0 & 0 \\ 0 & L_{mf} & 0 & L_{rmf} & 0 & 0 & 0 \\ 0 & 0 & 0 & 0 & 2H_{mf} & 0 & 0 \\ 0 & 0 & 0 & 0 & 0 & 1 & 0 \\ 0 & 0 & 0 & 0 & 0 & 0 & 1 \end{bmatrix} \frac{d}{dt} \begin{bmatrix} \Delta i_{dsf} \\ \Delta i_{qsf} \\ \Delta i_{drf} \\ \Delta i_{qrf} \\ \Delta \omega_{mf} \\ \Delta v_{dsf} \\ \Delta v_{qsf} \end{bmatrix} = \tag{6-32}$$

$$\begin{bmatrix} -R_{sf} & \omega_s L_{smf} & 0 & \omega_s L_{mf} & 0 & -1 & 0 \\ -\omega_s L_{smf} & -R_{sf} & -\omega_s L_{mf} & 0 & 0 & 0 & -1 \\ 0 & (\omega_s - \omega_{rf}) L_{mf} & -R_{rf} & (\omega_s - \omega_{rf}) L_{rmf} & -L_{mf} i_{qsf} - L_{rmf} i_{qrf} & 0 & 0 \\ (\omega_s - \omega_{rf}) L_{mf} & 0 & -(\omega_s - \omega_{rf}) L_{rmf} & -R_{rf} & -L_{mf} i_{drf} + L_{mf} i_{dsf} L_{rmf} & 0 & 0 \\ -L_{mf} i_{qrf} & L_{mf} i_{drf} & L_{mf} i_{qsf} & -L_{mf} i_{dsf} & 0 & 0 & 0 \\ \frac{1}{C_{ba}} & 0 & 0 & 0 & 0 & 0 & 1 \\ 0 & \frac{1}{C_{ba}} & 0 & 0 & 0 & -1 & 0 \end{bmatrix} \begin{bmatrix} \Delta i_{dsf} \\ \Delta i_{qsf} \\ \Delta i_{drf} \\ \Delta i_{qrf} \\ \Delta \omega_{mf} \\ \Delta v_{dsf} \\ \Delta v_{qsf} \end{bmatrix} - \begin{bmatrix} 0 \\ 0 \\ 0 \\ 0 \\ -\Delta T_{mf} \\ \Delta i_{sdr} \\ \Delta i_{sqr} \end{bmatrix}$$

6-9 The complete state-space model of interconnected ac/dc system

The complete state-space model of the system shown in Fig. 6.1 for small-signal stability analysis is obtained by combining the individual state-space models of grid-side converters, synchronous machine and associated controllers, onshore ac network, dc link circuit, wind farm-side converters and FSIG generator. In this chapter, the wind speed is assumed constant hence wind farms aerodynamic system is neglected and the mechanical system is represented by an equivalent mechanical torque T_m. Power balance equations are used to link the converters models into dc network. The dc currents and voltages of the onshore network (in Eq. 6.17) are used to link the grid-side converters into the ac network. The wind farms are linked to the wind farm-side converters using current injection theory. The block diagram in Fig. 6.7 explains how individual subsystems are linked together to obtain the complete linearized model for small-signal stability analysis. The complete state matrix has a dimension of 56×56.

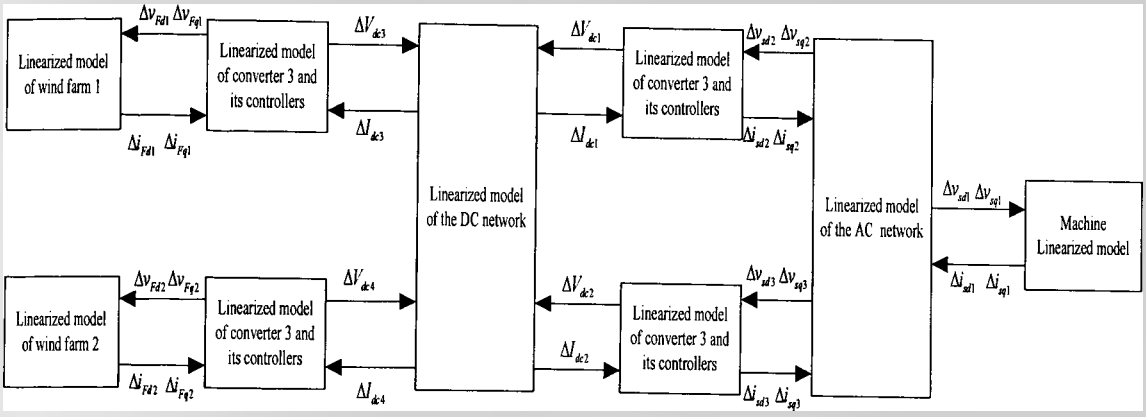


Fig. 6.7: Methodology used to obtain the complete state-space model of the test system.

6-10 The initial values of the interconnected ac/dc system

Before investigating the dynamic stability of the studied system, the initial steady-state condition of the system must be known (before applying a disturbance). All the differential equations disappear when the system is in steady-state operation. A well-known phasor diagram of synchronous machine given in [8] is used to obtain the initial conditions of the synchronous generator, while the steady state model for VSC given in section 3-4 is used to obtained the initial values of the converters. The initial values of the FSIG are obtained by solving the 5th order model (in this case the differential parts are neglected). In all cases for calculating the initial conditions, the power output, power factor and the voltages are given for each individual subsystem. Taking all this in consideration, the initial conditions of the ac/dc interconnected system are given in Table 6.1.

Table 6.1: Initial operating conditions of the interconnected system.

	FSIG		VSC_1	VSC_2	VSC_3	VSC_4		SG
V	1.0	V	1.0	1.0	1.0	1.0	V	1.0
P	0.35	P	0.35	0.35	0.34	0.34	P	2.4
v_{dsf}	1.0	v_{cd}	-0.3966	-0.3966	-0.1739	-0.1739	v_d	-0.7525
v_{qsf}	0.0	v_{cq}	0.9179	0.9179	0.9847	0.9847	v_q	0.658
i_{dsf}	0.846	I_d	0.0358	0.0358	0.0147	0.0147	I_d	-2.32
i_{qsf}	0.302	I_q	0.3960	0.3960	0.3478	0.3478	I_q	0.9869
i_{drf}	0.885	δ	23.38	23.38	10.02	10.02	E	2.51
i_{qrf}	0.029						δ	67.03
							λ_d	0.6594
							λ_q	0.7546

6-11 Small-signal stability analysis of the dc/ac interconnected system

The small-signal stability of a multi-terminal dc system connected to an ac network is assessed using eigenvalue Analysis technique. The eigenvalues of the state matrix are calculated to study the system dynamic stability after a small disturbance, and to explore the influence of dominant modes on system damping and stability limits. The power flow results of the interconnected system are also indicated in Fig. 6.1.

The calculated eigenvalues are presented in Table 6.2. It can be seen from Table 6.2 that all eigenvalues have negative real parts indicating a stable operating condition after a small perturbation is applied. The eigenvalues that dominate the transient response of the system are the pair $\lambda_{43,44}$ and λ_{47}. The participation factor matrix (given in Appendix E) indicates that machine states (I_F, δ and ω) have a dominant effect on the complex pairs $\lambda_{43,\ 44}$ (with time constant of 2.12s and frequency of 1.64 Hz). While the VSC converters states (i_{cd}, i_{cq}, v_{cd}, v_{cq}, $i_{d\text{-}ref}$ and $i_{q\text{-}ref}$) have a dominant effect on the eigenvalues associated with the high-frequency oscillations. Therefore any attempt to improve the network damping must take these states into account. For example, a power system stabilizer (PSS) can be used to improve the damping of the oscillations associated with λ_{43} and λ_{44}, while proper tuning of VSC converter controllers will damp the high-frequency oscillations.

In Table 6.2 the complex pairs $\lambda_{1,2}$ and $\lambda_{2,4}$ (corresponding to fast switching of the converters, with frequencies of 3169 Hz and time constant 0.00315 sec), are damped out at a much faster rate. These modes are often caused by super-synchronous oscillations due to interaction between adjacent converters, as reported in [18].

Table 6.2: Eigenvalues for the test system (eigenvalues are multiplied by system frequency 50Hz)

λ	VSC_1 & VSC_2 (k_{pi}=1,k_{ii}=40,k_{pdc}=10, K_{idc}= 400 k_{pac}=0.01,k_{iac}=500), VSC_3 & VSC_4 (K_{pi}=1.5, k_{ii}= 500, k_{pac}=0.01,k_{iac}=500)	Oscillations frequency (Hz)	Damping time (sec)
λ_1&λ_2	-50.54 ± 3169i	3169	0.00315
λ_3 & λ_4	-50.54 ± 3169i	3169	0.00315
λ_5 & λ_6	-177.31 ± 2121i	2121	0.00089
λ_7 & λ_8	-424.22 ±1523i	1523	0.00037
λ_9 & λ_{10}	-11.97± 1564i	1564	0.0133
λ_{11}&λ_{12}	-221.11 ± 2083i	2083	0.00072
λ_{13} & λ_{14}	-12.89 ± 2640i	2640	0.0123
λ_{15} & λ_{16}	-46.42 ± 2264i	2264	0.00343
λ_{17} & λ_{18}	-50.22 ± 1697.4i	1697	0.00317

λ_{19} & λ_{20}	-75.05 ± 1579i	1579	0.00212
λ_{21} & λ_{22}	-75.05 ± 1579i	1579	0.00212
λ_{23} & λ_{24}	-0.240 ± 53.42i	53.42	0.66348
λ_{25} & λ_{26}	-63.21 ± 54.06i	54.06	2.52
λ_{27} & λ_{28}	-63.21 ± 54.06i	54.06	2.52
λ_{29} & λ_{30}	-01.89 ± 35.79i	35.79	0.0842
λ_{31} & λ_{32}	-11.54 ± 51.33i	51.33	0.0137
λ_{33} & λ_{34}	-11.54 ± 51.33i	51.33	0.0137
λ_{35} & λ_{36}	-0.785 ± 50.13i	50.13	0.202
λ_{37} & λ_{38}	-0.785 ± 50.13i	50.13	0.202
λ_{39} & λ_{40}	-01.39 ± 35.29i	35.29	0.114
λ_{41} & λ_{42}	-01.03 ± 34.30i	34.30	0.155
λ_{43} & λ_{44}	-0.0718 ± 1.64i	1.64	2.217
λ_{45}	-50.12		
λ_{46}	-16.21		
λ_{47}	-0.0125		
λ_{48}	-0.131		
λ_{49}	-02.93		
λ_{50}	-02.05		
λ_{51}	-0.498		
λ_{52}	-0.497		
λ_{53}	-0.498		
λ_{54}	-37.45		
λ_{55}	-5000		
λ_{56}	-1000		

6-12 Impact of grid-side VSC current controllers on system stability

The effect of the current controller gains of the grid-side converters on the system transient and small-signal stability is investigated in this section. This allows identifying suitable tuning for the VSC converter controllers that will ensure network stability. Time-domain simulations were also carried out to validate the effectiveness of the gains calculated through the small-signal stability analysis. The proportional and integral gains (k_{pi} and k_{ii}) of the current controllers of the grid-side converters are assumed to be equal.

Based on small-signal analysis it has been found that the integral gains of the current controllers have a wide range of operational parameters where the system remains stable. The integral gain lays in the range $100 \leq k_{ii} \leq 1000$.

Table 6.3a shows some of the eigenvalues for different values of the integral gain of the current controllers. From the small-signal stability analysis viewpoint, the optimal integral gain is the one that generates the lowest frequencies of oscillation and shortest damping times; and from the transient stability (time-domain simulations) viewpoint, the optimal integral gain is that which provides a shorter transient response and lower overshoot after system abnormal conditions. The variation of k_{ii} has effect on the frequencies of oscillation and the damping of the oscillations after system disturbances, that is, on both the magnitude of the oscillations and the time required to damps these oscillations. From Table 6.3a the best responses are obtained with k_{ii}=400, for example, the pair $\lambda_{1,2}$ has a oscillation frequency of 20049Hz with damping time of 0.00318s if k_{ii}=400, compared to 27454 Hz with damping time of 0.00318s if k_{ii}=750, and 31701Hz with damping time of 0.00318s if k_{ii}=1000. While the system is instable for any value of k_{ii} less than 100. The validation of the results obtained from the small-signal stability analysis is carried on using time-domain simulations as shown in Fig. 6.8a. The test system is subjected to a sudden line-to-ground fault with high fault resistance at t=1.5s with 0.05s duration; therefore, the disturbance is considerably small. The effect of changing the k_{ii} is carried out with the grid-side converters control parameters equal to k_{pi}=1, k_{pdc}=10, K_{idc}=400, k_{pac}=0.01, k_{iac}=500.

The effect of the proportional gain of the current controllers on system stability is investigated with (k_{pi} = 0.1, 0.5, 1, 6, 10). Similarly, the variation of k_{pi} of the current controllers affects the oscillation frequencies and the damping time. Based on the small-signal stability analysis, the operational range of k_{pi}, which ensures a stable system lays in the range 0.6-55. From Table 6.3b, the best responses are obtained with k_{ii}=*10*, the pair $\lambda_{11,12}$ has an oscillation frequency of 1327Hz with damping time of 0.00032s if k_{ii}=10, compared to 1394Hz with damping time of 0.00066s if k_{ii}=6 and 1407Hz with damping time of 0.012s if k_{ii}=1, while the system is unstable for any value less than 0.6.

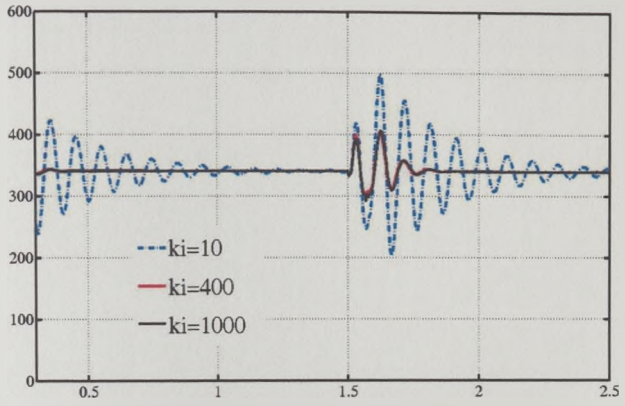
Fig. 6.8b shows the system behaviour after a small disturbance with different proportional gains of the current controller. The effect of changing the k_{pi} is carried out with the grid-side converters control parameters equal to (k_{ii}=400, k_{pdc}=10, K_{idc}=400, k_{pac}=0.01, k_{iac}=500).

Table 6.3a: Effect of changing k_{ii} of the grid-side VSC current controllers (eigenvalues are multiplied by system frequency 50Hz).

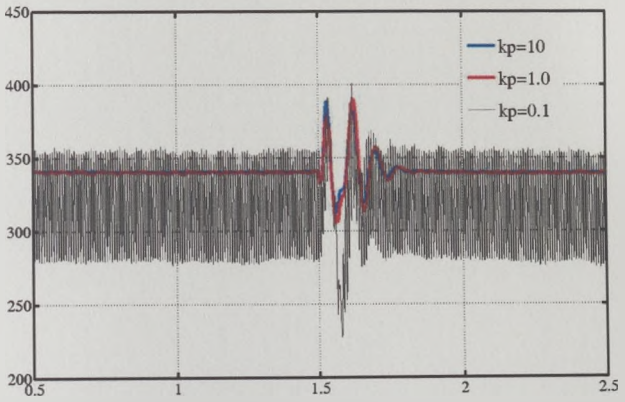
λ	k_{ii}=10	k_{ii}=50	k_{ii}=400	k_{ii}=750	k_{ii}=1000
λ_1&λ_2	-50.06 ± 3169i	-50.01 ± 20049i	-50.01 ± 20049i	-50.01 ± 27454i	-50.01 ± 31701i
λ_{15}&λ_{16}	+46.63 ± 270i	+6.66 ± 477i	-224 ± 212i	-224 ± 212i	-224 ± 212i

Table 6.3b: Effect of changing k_{pi} of the grid-side VSC current controllers (eigenvalues are multiplied by system frequency 50Hz)

λ	k_{pi}=0.1	k_{pi}=0.5	k_{pi}=1	k_{pi}=6	k_{pi}=10
λ_1&λ_2	-50.03 ± 2.0049i	-250±20049i	-50.03 ± 2.0049i	-50.03 ± 2.0049i	-50.03 ± 2.0049i
λ_{11}&λ_{12}	+5.39 ± 1414i	+13.93 ± 1406i	-12.62 ± 1407i	-23.96 ± 1394i	-489 ± 1327i
λ_{23} & λ_{24}	-10.47 ± 95.91i	-9.81 ± 92.78i	-10.35 ± 95.34i	-9.81 ± 92.78i	-9.20 ± 89.53i



(a) Effect of the integral gain.



(b) Effect of the proportional gain.

Fig. 6.8: Effect of the grid-side VSC current controllers on system stability

6-13 Impact of grid-side VSC converter ac voltage controllers on system stability

The effect of the ac voltage controller of the grid-side converters is investigated with different values of the proportional and integral gains. This section attempts to find the range of the integral and proportional gains for the grid-side VSC ac voltage controllers that ensure

a stable system. The small-signal stability analysis indicates that for stable operation the integral gain k_{iac} should lay in the range $50 \leq k_{ii} \leq 1800$. The oscillation frequencies and their damping time after system disturbances vary with the integral gain of the ac voltage controllers. Based on the small-signal stability analysis the best damping response is obtained when k_{iac}=50. As shown in Table 6.4a, the pair $\lambda_{13,14}$ has a oscillation frequency of 1426Hz and damping time of 0.0032sec if k_{iac}=50, compared to 1424Hz and 0.0035sec damping time if k_{iac}=100, 1414Hz and damping time of 0.004sec if k_{iac}=500, while the system is unstable for k_{iac}=2000 and k_{iac}=3000. Time-domain simulations validate the results obtained from the small-signal stability analysis as shown in Fig. 6.9a, where the responses' transient overshoot and recovery time is better with k_{iac}=50.

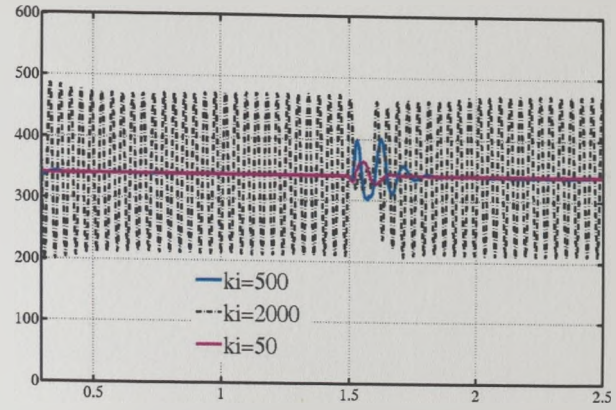
Similarly, the proportional gain of the ac voltage controller influences the transient oscillation and the associated damping time. Based on the small-signal stability analysis, the k_{pac} has a wide range of operational values that ensures a stable system as shown in Table 6.4b. The gain k_{pac} may have any value in the range 0.001-10, but in this case the best response is obtained with k_{pac} =10. It is noticeable that the pair $\lambda_{11,12}$ has an oscillation frequency of 1407Hz and 0.0126sec damping time if k_{pac}=0.001, 1405Hz and 0.0114sec damping time if k_{pac}=1, 1395Hz and 0.008sec damping time if k_{pac}=5, compared to 1383Hz and 0.006sec for k_{pac}=10. The time-domain simulation validates the results obtained from the small-signal stability analysis as shown in Fig. 6.9b.

Table 6.4a: Effect of changing k_{iac} of the grid-side VSC ac voltage controllers (eigenvalues are multiplied by system frequency 50Hz)

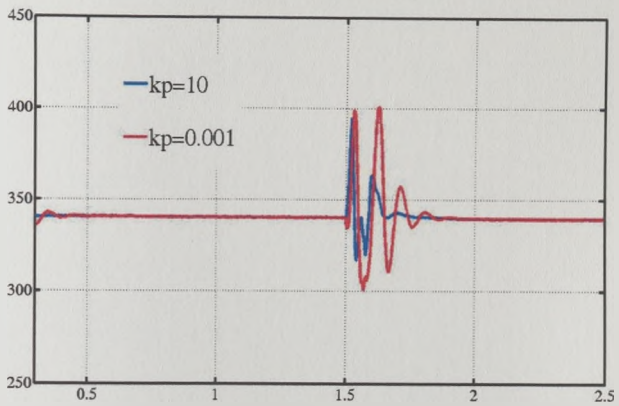
λ	k_{iac}=50	k_{iac}=100	k_{iac}=500	k_{iac}=2000	k_{iac}=3000
λ_1&λ_2	-50.01 ± 20049i	-50.01 ± 20049i	-50.01 ± 20049i	-50.01 ± 20049i	-50.01 ± 20049i
λ_{13}&λ_{14}	-49.75 ± 1426i	-45.82 ± 1424i	-39.60 ± 1414i	+141.2 ± 1368i	+248.9+ 1381i

Table 6.4b: Effect of changing k_{pac} of the grid-side VSC ac voltage controllers (eigenvalues are multiplied by system frequency 50Hz)

λ	k_{pac}=0.001	k_{pac}=1	k_{pac}=5	K_{pac}=10
λ_1&λ_2	-50.03 ± 20049i	-50.03 ± 20049i	-50.03 ± 20049i	-50.03 ± 20049i
λ_{11}&λ_{12}	-12.61 ± 1407i	-13.92 ± 1405i	-19.26 ± 1395i	26.16 ± 1383i



(a) Effect of the proportional gain.



(b) Effect of the integral gain.

Fig. 6.9: Effect of the grid-side VSC ac voltage control parameters on system stability.

6-14 Impact of the grid-side VSC dc voltage controllers on system stability

The integral gain of the dc controllers (k_{idc}) has a wide range of operational values which ensure a stable system. Any value between ($40 \leq k_{ii} \leq 1000$) can be used to set the integral gain of the dc voltage controller. Table 6.5a shows the frequency of the oscillations and the corresponding damping time of some eigenvalues for different values of k_{idc} (k_{idc} = 40, 100, 400, 600, and 800). It can be seen from Table 6.5a that the best damping response is associated with the integral gain with lower high frequency and faster damping time. If k_{idc}=40, the disturbance has lower oscillation frequencies and faster damping time compared to the other gains (frequencies of 6480 Hz and time constant 0.00318 sec for the pair $\lambda_{1,2}$ and frequencies of 1407 Hz and time constant 0.0125 sec for the pair $\lambda_{9,10}$). The time-domain simulation validates the choice of $k_{idc}=40$. The simulation is carried out with the grid-side converters parameters equal to (k_{ii}=400, k_{pi}=1, k_{pdc}=10, k_{pac}=0.01, k_{iac}=500). Based on Fig.

6.10a, k_{idc}=40 provides the best transient response after a system disturbance with fast recovery time.

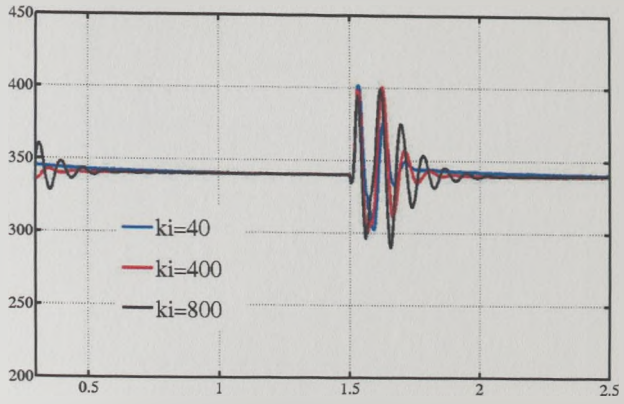
Table 6.5b shows the effect of the different values of proportional gain of the dc voltage controller (k_{pdc}) on the damping of oscillations after a disturbance. When a large k_{pdc} is used the damping time decreases, for example when k_{pdc}=50 the damping time for the oscillations associated with the pair $\lambda_{11,12}$ is 0.004sec, while the damping time for the same pair is 0.007sec for k_{pdc}=40, 0.0083sec for k_{pdc}=30, 0.01sec for k_{pdc}=20, and 0.0125sec for k_{pdc}=10. The time-domain simulation validates the results obtained from the small-signal stability analysis as shown in Fig. 6.10b. The best recovery response after the disturbance is obtained when k_{pdc}=50. The time-domain simulation is carried out with the grid-side converters parameters equal to (k_{ii}=400, k_{pi}=1, k_{idc} = 400, k_{pac}=0.01, k_{iac}=500).

Table 6.5a: Effect of changing k_{idc} of the grid-side VSC dc voltage controller (eigenvalues are multiplied by system frequency 50Hz)

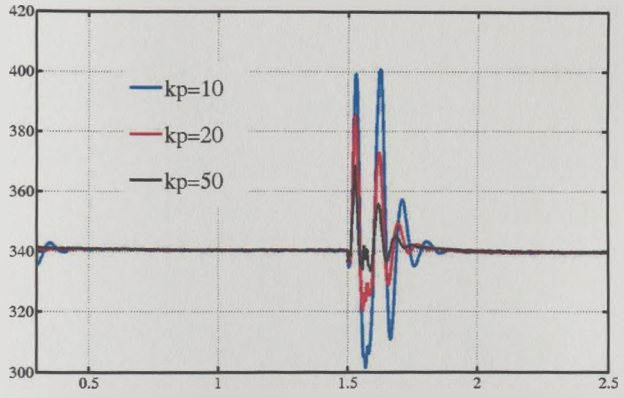
λ	k_{idc}=40	k_{idc}=100	k_{idc}=400	k_{idc}=600	k_{idc}=800
λ_1&λ_2	-50.04 ± 6480i	-50.04 ± 10099i	-50.01 ± 20049i	-50.04 ± 24535i	-50.01 ± 28319i
λ_9&λ_{10}	-12.7 ± 1407i	-6.36 ± 1567i	-6.36 ± 1567i	-6.36 ± 1567i	-6.36 ± 1567i

Table 6.5b: Effect of changing k_{pdc} of the grid-side VSC dc voltage controller (eigenvalues are multiplied by system frequency 50Hz)

λ	k_{pdc}=10	k_{pdc}=20	k_{pdc}=30	k_{pdc}=40	k_{pdc}=50
λ_1&λ_2	-50.03 ± 2.0049i	-50.03 ± 2.0049i	-50.03 ± 2.0049i	-50.03 ± 2.0049i	-50.03 ± 2.0049i
λ_{11} & λ_{12}	-12.67 ± 1407i	-15.80 ± 1409i	-19.05 + 1411i	-22.45 + 0.1412.8i	-39.6 ± 1414i
λ_{13} & λ_{14}	-25.98 ± 1414i	-39.60 ± 1414i	-39.6 ± 1414i	-39.6 ± 1414i	-39.6 ± 1414i



a) Effect of the proportional gain.



(b) Effect of the integral gain.

Fig. 6.10: Effect of the grid-side VSC dc voltage controller on system stability.

6-15 The effect of synchronous machine loading on system stability

As the interconnected ac/dc system load flow changes during the day (morning-day-night), and during the year (summer-winter), the stability of the interconnected system is investigated during peak, rated, and light load conditions by considering different ratings of the synchronous machine. Three different scenarios for the machine loading are considered (full-rating, half-rating and over-rating based on 2400MVA the rated of the machine). The eigenvalues obtained for these scenarios are given in Table 6.6. It can be seen that the loading increases the effect on the dominant eigenvalues ($\lambda_{43,44}$, λ_{48} and λ_{48}), while the high-frequency eigenvalues remain unaffected. The oscillation frequency of the pair $\lambda_{43,44}$ increases, and the corresponding damping time decreases when the machine rating increases. The effect of the machine loading on the real part of the eigenvalues is noticeable on the pair $\lambda_{47,48}$. It can be

seen that λ_{48} move towards the imaginary axis when the machine loading increases while that λ_{47} move towards the imaginary axis when the machine loading decreases as shown in Table 6.6, indicating a reduction in damping and an increase in the oscillation frequency (that is, a reduction in the small-signal stability margins). The system may lose its stability if the machine rating is further increased or decreased.

Table 6.6: Eigenvalues for different loading scenarios (based on 2400MVA machine rating).

Eigenvalues	$P_1=0.5*P_{rating}$	$P_1=0.75*P_{rating}$	$P_1=P_{rating}$	$P_1=1.25*P_{rating}$	$P_1=1.5*P_{rating}$
λ_1 & λ_2	-50.03 ± 20049i	-50.03 ± 20049i	50.03 ± 20049i	-50.03 ± 20049i	-50.03 ± 20049i
λ_5 & λ_6	-172.76 ± 2119i	-172.76 ± 2119i	-172.7 ± 2119i	-172.76 ± 2119i	-172.76 ± 2119i
λ_{43} & λ_{44}	-0.087 ± 1.72i	-0.076 ± 1.64i	-0.066 ± 1.58i	-0.058 ± 1.55i	-0.049 ± 1.54i
λ_{47}	-0.0109	-0.0113	-0.0121	-0.0139	-0.019
λ_{48}	-0.178	-0.156	-0.131	-0.096	-0.058

6-16 Summary

In this chapter the small-signal stability of a multi-terminal VSC-HVDC transmission system connecting FSIG wind farms was investigated. The eigenvalue Analysis technique was used to study the system behavior after small perturbations. The state-space model of the interconnected ac/dc system was derived by dividing the system into small subsystems and then the complete model was obtained by combining the individual subsystems together using the mathematical relation between them (power balance equation to link the converters and the dc link system, current injection theory to link the FSIG to grid-side converter, and the impedance matrix to link the synchronous machine into grid-side converters). The small-signal stability analysis is well known in the literature for networks with only conventional synchronous generation, therefore the model in this chapter was developed to investigate the small-signal stability of modern power systems that will include a large number of power electronic converters such as VSC-HVDC. Under these conditions, when conducting small-signal stability analysis, attention must be paid to super-synchronous frequencies due to the high switching control systems of the converters and their effect on system stability. The impact of the grid-side VSC controllers was carried out using small-signal stability analysis considering the oscillations frequencies and the time required to damp out these oscillations. Time-domain simulations with the controller parameters under investigation was carried out to validate the results obtained from the small-signal stability analysis. Finally the effect of the machine rating was studied to ensure stable operation if the system load flows change.

References

[1] V. K.Sood, *HVDC and FACTS Controllers Application of Static Converter in Power System*: Kluwar Academic Publisher, 2004.

[2] L. X. Bui, *et al.*, "Dynamic interactions between HVDC systems connected to AC buses in close proximity," *Power Delivery, IEEE Transactions on,* vol. 6, pp. 223-230, 1991.

[3] M. A. Choudhry, *et al.*, "Stability Analysis of a Modulated AC/DC System Using the Eigenvalue Sensitivity Approach," *Power Systems, IEEE Transactions on,* vol. 1, pp. 128-136, 1986.

[4] O. Anaya-Lara, *et al.*, "Influence of Windfarms on Power System Dynamic and Transient Stability," *Wind Engineering Vol 30, NO. 2, 2006.*

[5] J. P. Therattil and P. C. Panda, "Dynamic stability enhancement of a multi-area multi-terminal DC-AC system with self-tuning Static Var Compensator," in *Power Electronics, Drives and Energy Systems (PEDES) & 2010 Power India, 2010 Joint International Conference on*, 2010, pp. 1-6.

[6] C. Karawita and U. D. Annakkage, "Multi-Infeed HVDC Interaction Studies Using Small-Signal Stability Assessment," *Power Delivery, IEEE Transactions on,* vol. 24, pp. 910-918, 2009.

[7] L. Rouco, "Eigenvalue-based methods for analysis and control of power system oscillations," in *Power System Dynamics Stabilisation (Digest No. 1998/196 and 1998/278), IEE Colloquium on*, 1998, pp. 3/1-3/6.

[8] P.Anderson and A. Fouad, *Power System Control and Stability,* : John Wiley & Sons Publication, 2007.

[9] C. Karawita and U. D. Annakkage, "A Hybrid Network Model for Small Signal Stability Analysis of Power Systems," *Power Systems, IEEE Transactions on,* vol. 25, pp. 443-451, 2010.

[10] A. Yazdani and R. Iravani, "Dynamic model and control of the NPC-based back-to-back HVDC system," *Power Delivery, IEEE Transactions on,* vol. 21, pp. 414-424, 2006.

[11] L. Xu, *et al.*, "VSC transmission operating under unbalanced AC conditions - analysis and control design," *Power Delivery, IEEE Transactions on,* vol. 20, pp. 427-434, 2005.

[12] M. A. A. Alyan, *et al.*, "Assessment of steady state stability of a multi-machine power system with and without a superconducting machine," *Power Systems, IEEE Transactions on,* vol. 5, pp. 730-736, 1990.

[13] P. Kundur, *Power System Stability and Control*: Electric Power Research Institute, Power System Engineering Series, 1994.

[14] S. Poullain, *et al.*, "Modelling of the dynamic characteristics of the DC line for VSC transmission scheme," in *AC-DC Power Transmission, 2001. Seventh International Conference on (Conf. Publ. No. 485)*, 2001, pp. 305-310.

[15] S. Tohidi, *et al.*, "Influence of model simplifications and parameters on dynamic performance of grid connected fixed speed wind turbines," in *Electrical Machines (ICEM), 2010 XIX International Conference on*, 2010, pp. 1-7.

[16] H. A. Pulgar-Painemal and P. W. Sauer, "Dynamic modeling of wind power generation," in *North American Power Symposium (NAPS), 2009*, 2009, pp. 1-6.

[17] A. Radunskaya, *et al.*, "A Dynamic Analysis of the Stability of a Network of Induction Generators," *Power Systems, IEEE Transactions on,* vol. 23, pp. 657-663, 2008.

[18] "IEEE Guide for Planning DC Links Terminating at AC Locations Having Low Short-Circuit Capacities," *IEEE Std 1204-1997,* p. i, 1997.

Chapter Seven

Network Reinforcement of the 400kV Scottish-English Interconnectors using VSC-HVDC Transmission

7-1 Introduction

The UK government targets to meet its obligation in reducing the CO_2 emissions, and to increase the share of renewable power in total generation mixture to 20% by 2020, requires the installation of new large generation units based on renewable sources. The majority of this power is expected to come from wind farms in northern and eastern parts of UK, and Scotland is set to play a major role to meet this demand. Many of the sites being considered for developing offshore/onshore wind farms in Scotland are located in remote areas and often at considerable distance from the existing transmission system. The installation of large-scale wind farms requires significant extension of the existing network in order to accept the additional generation plants and to increase the transmission capacity. The GB electricity network is a large interconnected network covering Scotland, England and Wales. Three power system operators share the control and operation of the GB electricity network: National Grid Electricity Transmission (NGET), Scottish Hydro Electric Transmission Ltd (SHETL) and Scottish Power Transmission (SPT).

In the literature, there are many studies considering the reinforcement of the GB network to handle the large-scale installed wind power. The proposed studies agree on building new transmission lines, and upgrade some of the existing transmission lines and substations. The major reinforcement projects in the SHETL and SPT networks (Scotland network) to transfer the wind power to the load centres in England according to [1-2] are (see Fig. 7.1):

- Build new 220km, 400kV Beauly-Denny transmission line in north Scotland in SHETL licensed area: This transmission line is required to transmit the wind farms power installed in the north of Scotland from SHETL licensed area to the SPT licensed area.
- Maximize the existing transmission system in the SHETL licensed area by reconductoring and re-insulation of existing tower routes, extensions to existing substations or by installation of flexible ac transmission devices (FACTS). This upgrade is planned to be in the Dounreay–Beauly–Kintore and Caithness and Moray transmission lines.



Fig. 7.1: Reinforcement projects in Scotland network to transmit the large-scale wind power to England [3].

- ❖ Sloy Area Reinforcement: This development is required to accommodate 250MW of wind power in Argyle (west of Scotland) using new 275kV line connection to the main network.
- ❖ Upgrade Scotland-England Interconnector in SPT licensed area: This requires the upgrading of the western and eastern interconnectors from a dual 400kV circuit to a double circuit. In addition to reconductoring and re-insulation of existing tower routes and existing substations, installation of reactive power compensation devices is required.
- ❖ Build of western sub-sea HVDC system between Hunterston and Deeside and eastern sub-sea HVDC system between Peterhead and Hawthorne Pit. These new HVDC systems are proposed to transmit 3.6GW from Scotland to England.

7-2 Scotland-England interconnectors

For the purpose of illustrating system performance and transmission reinforcement, it is useful to divide the network into zones and to consider power transfers across certain critical boundaries. The GB electricity network is divided into 17 boundaries and zones (6 for Scotland and 11 for England and Wales) [3]. The power transfer from Scotland to England is achieved via two interconnectors based on HVAC transmission located in the SPT and NGET licensed areas (Z_6 and Z_7). These interconnectors are labeled as western and eastern interconnectors in Fig. 7.1.

The main focus of this Chapter is to enhance and reinforce the interconnector links between Scotland and England, and to maximize their transfer capacity without creating operational problems concerning voltage stability. The future installed wind farms in Scotland necessitate the reinforcement of the existing interconnector links to be able to transfer the large power from Scotland down south to England and Wales. Since, the GB network is a complex interconnected network composed of many generation plants and thousands of transmission and distribution lines, a generic model including the Scotland network, the interconnectors, and England network has been built to investigate the possible options for the reinforcement of the interconnectors.

Fig. 7.2 shows the generic model of the Scotland-England network. The Scotland network is simplified by considering just the generation plants and the 400kV substations in Z_6 while the power transmission from Z_5 to Z_6 is represented by equivalent power generation plant. The England network is represented with two aggregate power plants and static loads. The main generation plants and the 400kV substations used to represent the Scotland-England network in Fig. 7.2 are:

1- The generation plant in COCKENZE: this plant comprises 4x276 MW generation units injecting 1104 MW into COCK4 substation. A 66km, 400kV double circuit transmission line is used to transmit the power from COCK4 substation to ECCL4 substation.

2- The generation plant in TORNESS: this plant comprises 2X607 MW generation units injecting 1214MW into TORN4 substation. TORN4 substation is connected to STRAV4 substation via a 85km, 400kV dual transmission line, and to ECCL4 substation through a 35km, 400kV double transmission line.

3- The substation in KILS4: this substation receives the power from HUER4 substation in Z_5 and transmits it to STRAV4 substation using 35km, 400kV dual transmission line.

4- The generation plant in STRAV: this station represents the sum of the power received from Z5. Substation STRAV4 is connected to substation TORN4 through a 85km, 400kV line, to KILS4 via a 35km, 400kV dual line and to the ELVA4 substation via a 62km, 400kV line.

5- A 500MW generation unit represents the CLDYE generation plant (300MW) and future EAALSHAUGH generation plant (200MW). These units inject the power into ELVA4 substation; ELVA4 is connected to HOFF4 substation through a 62km, 400kV line. Substation ELVA4 may be considered as the start-end of the western interconnector.

6- Substation HOFF4: this substation receives the power from ELVA4 and delivers it to HAKB4 substation in the England network through a 65km, 400kV line.

7- Substation ECCL4: This substation receives the power from COCK4 substation and TORN4 substation, and delivers it into STWBA4 substation in England. ECCL4 is the start-end of the Eastern interconnector transmission line.

8- The England network is represented with two aggregate power plants (12GW and 3GW generation units), and static loads (with sum 15200+400MVA) as shown in Fig. 7.2. A 90km, 400kV transmission line is used to connect STWBA4 and HAKB4.

The transmission line parameters used in the generic model are obtained from the Seven Year Statement [3] issued by GB National Grid. The increases of interconnectors' capacities during the next seven years are presented in Table 7.1, which shows the transmission power in the boundaries between Scotland and England from 2011 to 2018.

Table 7.1: Amount of the transmitted power from Scotland to England in MW [3](2011-to-2018).

year	Western line	Eastern line
2011/2012	1266	1634
2012/2013	1372	1616
2013/2014	1421	1612
2014/2015	2033	1930
2016/2017	1404	1570
2017/2018	1700	1740

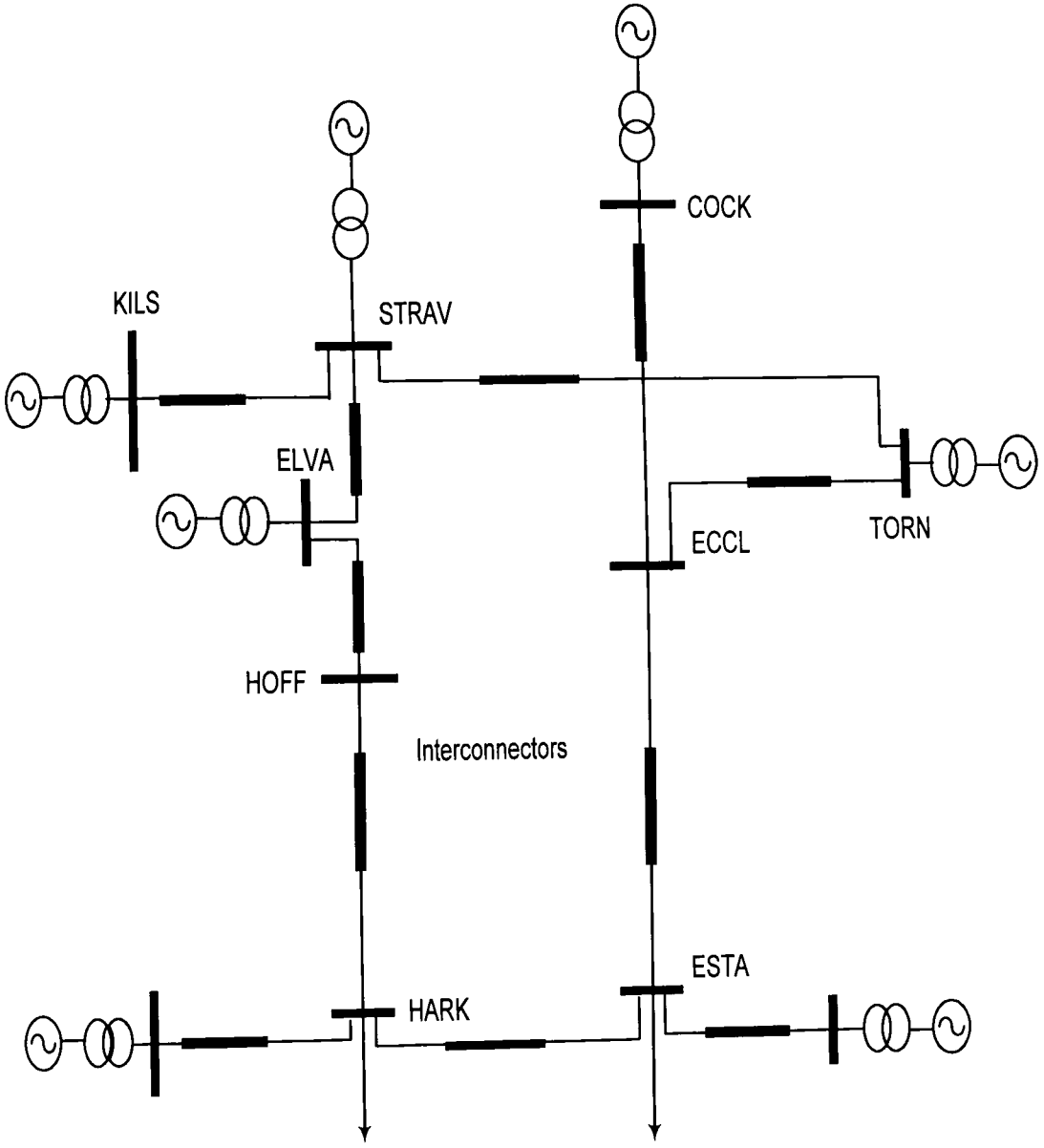


Fig. 7.2: Generic model of Scotland network, the interconnectors and England network.

There are three possible scenarios to enhance and reinforce the Scottish-English 400kV interconnectors in order to maximize their transfer capacity [4-5].

- The first scenario is to upgrade the interconnectors from a dual to a double circuit transmission line, reconductoring and re-insulation of existing tower routes, build new substations or to extend existing ones, and installation of flexible ac transmission systems (FACTS) devices to provide reactive power compensation, improve power flows controllability and to reduce power transmission losses. This scenario prefers to invest in reinforcement devices rather than to build new lines and to overcome the difficulties of new right-of-ways and to address public opinion concerning health issues, wildlife protection.
- The second scenario is to convert the existing high-voltage ac lines to high-voltage dc lines using VSC-HVDC transmission. The main features of this solution are increased transmission capacity, full control over power flows, inherent reactive power capability in each converter station and small footprint. VSC-HVDC transmission requires less space and has less environmental effect compared to an HVAC system.
- The third scenario is to use the VSC-HVDC link in parallel with the existing high-voltage ac transmission lines. In this case the VSC converter may be used to provide the reactive power compensation at the point of the common coupling.

7-3 Using FACTS devices for reinforcement of the interconnectors

Flexible ac transmission systems (FACTS) are power electronic devices used to control voltage and power flows in electrical transmission and distribution systems. FACTS devices could address the new challenges resulting from the increase of power transmission to the England network. The capacity of the interconnectors could be increased with minimal infrastructure investment, environmental impact, and implementation time compared to traditional transmission solutions by improving the utilization of the existing power system through the application of advanced control technologies. The main contributions of FACTS devices in power networks are [6-7]:

- ❖ Increase transmission line controllability (voltage, active and reactive power control)
- ❖ Increase the loading capability of lines
- ❖ Provide reactive power compensation
- ❖ Improve power quality and power oscillation damping

In general, FACTS technology are classified into line-commutated thyristor-based devices and self-commutated IGBT/IGCT devices [8].

Line-Commutated FACTS: Line-commutated FACTS may be regarded as a means of inserting variable impedance either in shunt (static VAR compensators, SVC) or in series (thyristor-controlled series compensation TSSC/TCSC). The use of thyristor technology readily achieves high-power handling capability with low losses and robust overload capability, but they have relatively long response times corresponding to the limits of the line frequency switching, and the inherent time constant of the controlled reactive power component.

Self-Commutating FACTS Devices: Self-commutating FACTS act as controlled sources, which are capable of injecting voltage or current at the point of common coupling. This provides better decoupling between the compensation function and network conditions. These FACTS devices are switched ON/OFF with a high switching frequency, eliminating the low-order harmonics associated with line-commutated systems. Self-commutating devices may be connected in parallel (STATCOM), series (dynamic voltage restorers, DVR, static synchronous series compensator SSSC), or in series/parallel connection (unified power flow controller, UPFC). These systems are generally based around pulse-width modulated (PWM) voltage source converter (VSC) technology, similar to that employed in VSC-HVDC systems. VSC-based FACTS devices achieve faster response times, improved transient response, and reduced size relative to thyristor-based systems. Table 7.2 provides a comprehensive summary of FACTS devices applications in power systems.

Table 7.2: Summary of flexible ac transmission system (FACTS) devices (based on [6-7, 9]).

Functionalities	Series devices				Shunt devices		Series/shunt devices
	TCSC	TSSC	SSSC	DVR	SVC	STATCOM	UPFC
components	Fixed capacitor + thyristor	Fixed and switched capacitor + thyristor	IGBT based VSC converter	IGBT based VSC converter	Thyristor, capacitor and reactor	IGBT based VSC converter	IGBT based VSC converter
VAr compensation	Yes but discrete	Yes but discrete	Yes, continuous	Yes, continuous	Yes but discrete	Yes, continuous	Yes, continuous
Voltage control	Yes	Yes	Yes	Yes	Yes	Yes	Yes
SSR damping	good	good	excellent	possible	limited	limited	
oscillation damping	Very good	Very good	Very good	possible if configured	limited	limited	Very good
Active power control capability	yes	yes	yes	yes	no	no	yes
Unbalanced Minimization	no	no	no	yes	Yes	no	yes
Voltage quality improvement	limited	limited	limited	limited	yes	yes	yes

7-4 VSC converter reactive power capability to provide voltage provision

Figure 7.3 shows the single-line diagram of a VSC converter and the vector diagrams for the VSC leading and lagging modes of operation. The reactive power exchange with the point of common coupling is regulated by controlling the converter voltage as described in equation (7-1) [10-11]:

$$Q_{SC} = V_T \times \frac{V_T - V_{SC}\cos(\delta_T - \delta_{SC})}{X_{SC}} \tag{7-1}$$

By controlling the converter voltage (V_{SC}), the VSC converter acts exactly like a STATCOM but with active power flow. As illustrated in Fig. 7.3, the voltage may lead or lag the current to regulate the voltage at the PCC (V_T) at the desired nominal value. This feature can be used in VSC-HVDC systems to provide ac voltage control (in addition to active power and dc voltage control) to the ac systems at the ends of the line [12]. The reactive power capability of the VSC converter provides greater flexibility for the ac system, such as reducing transmission losses, stabilizing a particular bus voltage, and operating at unity power factor to minimize the transmission current. The reactive power requirements to maintain the voltage at the PCCs at the ends of the VSC-HVDC system differ according to the ac systems strength.

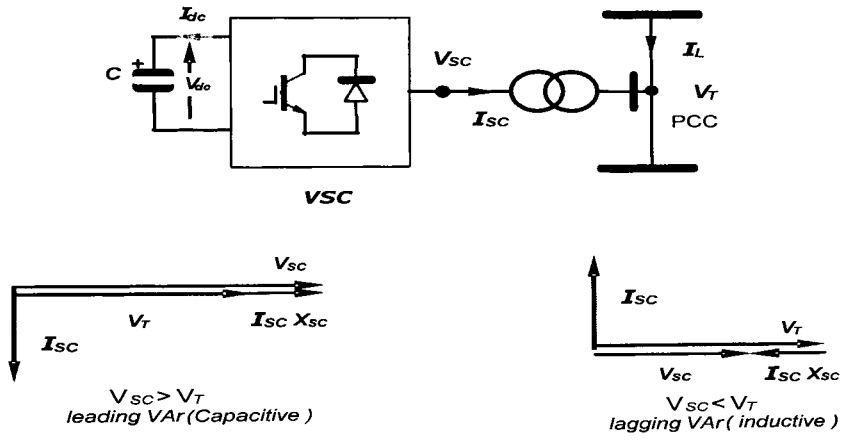


Fig. 7.3: Single-line diagram of VSC converter and vector diagrams for leading and lagging modes of operation.

Hence, VSC-HVDC transmission can be used to enhance the ac systems performance and power transmission capability by regulating the reactive power at the PCCs. This can be achieved either by connecting the ac systems directly via the VSC-HVDC system, in this case the VSC converters provide the voltage regulation at the PCCs. The other option is to connect the VSC-HVDC in parallel with the HVAC system, in this case the VSC-HVDC system is used to regulate the voltage at both ends of the HVAC to increase the HVAC capacity, and to reduce transmission losses.

7-5 Reinforcement of Scotland-England interconnectors using VSC-HVDC transmission

The capacity and controllability of the interconnectors could be increased by converting the existing HVAC lines into VSC-HVDC lines, resulting in the decoupled operation between the Scotland and England networks. The VSC-HVDC system may be installed as point-to-point or in a back-to-back configuration. Moreover, the VSC-HVDC system is required to operate in parallel in order to accommodate the large power delivered by the HVAC lines. The decoupling of the Scotland and England networks is achieved by replacing the eastern interconnector between ECCL4 and STWBA4 with an 8km, 2150MW point-to-point VSC-HVDC system and part of the western interconnectors, between HOFF and HARK substations, with a 65km, 2400MW point-to-point VSC-HVDC system as shown in Fig. 7.4.

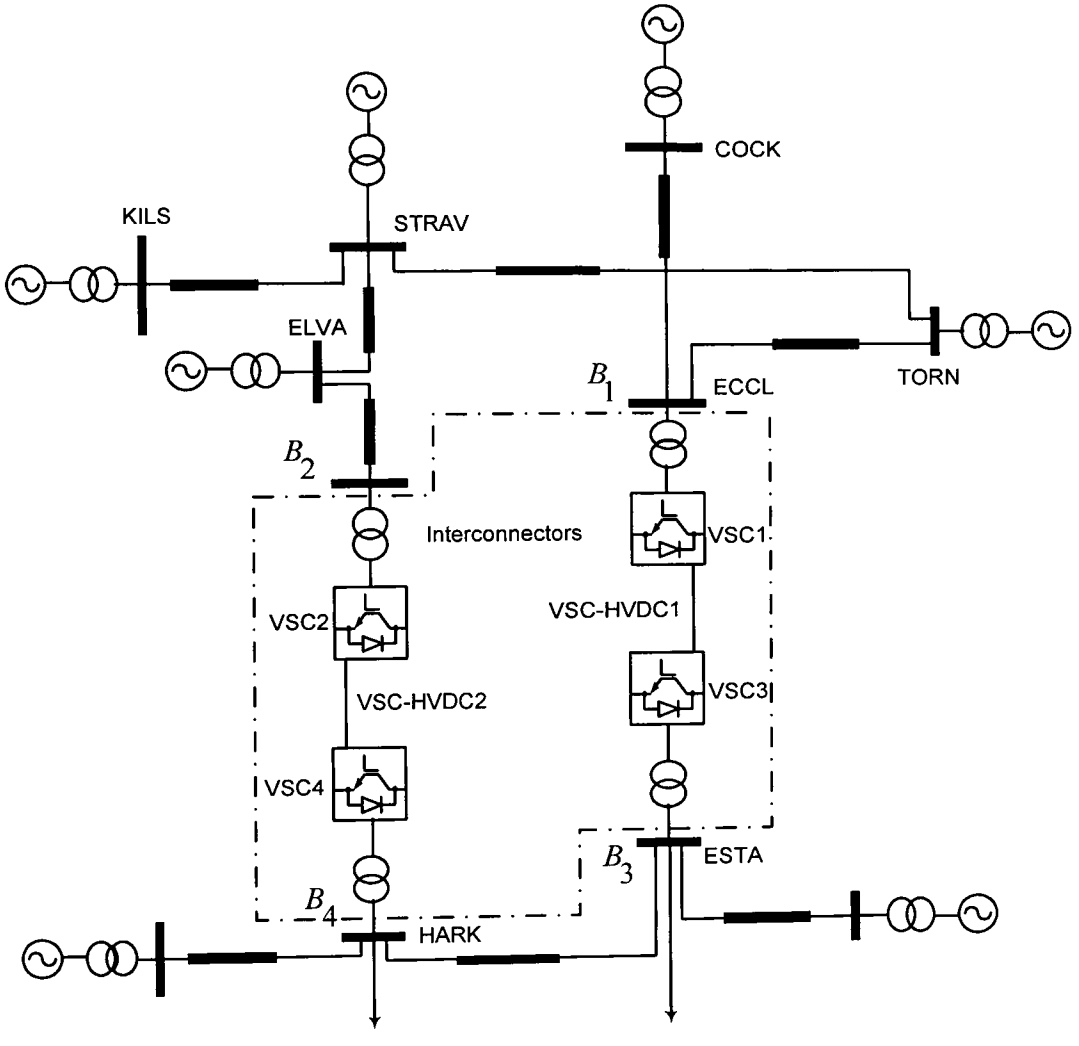


Fig. 7.4: Using VSC-HVDC systems to interconnect Scotland and England networks.

The potential benefits of transmitting the power through VSC-HVDC systems (decoupled operation) are summarized as follow [4, 13]:

- ❖ Large power can be accommodated without affecting the voltages at the interconnectors, because the VSC converters provide the reactive power support at the PCCs.
- ❖ The VSC converters in Scotland can be utilized to provide additional functionality such as voltage control and frequency regulation to the Scotland network. The England network is strong with huge reserve generation to cope with the variations in transmitted power from Scotland.
- ❖ The decoupled operation prevents the propagation of abnormal conditions from the English network to the Scottish network.

7-5-1 Frequency regulation at the Scottish network in decoupled operation

In power systems the active power balance is strongly coupled to the frequency. Any mismatch between generation and demand causes the system frequency to rise or decrease, depending on the net difference between generation and demand. Frequency stability is a serious issue for power system operators in networks highly populated with wind power plants. The installation of wind power plants in Scotland may cause active power mismatch and frequency instability in the Scottish network due to the nature of the wind power, uncertainty of the wind and variation in wind speed [14]. This requires robust, high response technology to stabilize the network frequency in the event of wind generation increase or decrease. Also, the active power balance is affected by the connection/disconnection of generation units or large loads and this affects the network and causes the remaining units turbines to over-speed or under-speed in order to restore the network frequency.

The GB Grid Code specifies that all generation units must operate continuously with constant active power output in the frequency range of 49.5-50.5Hz, and the frequency could rise to 52Hz or fall to 47Hz in exceptional circumstances for period less than 30s [3, 15]. The generation equipments are designed to operate in this ranges and the protection system of the generators trips if the frequency is out of the specified range.

In conventional networks, frequency stabilization is achieved through adjustment of the mechanical power of the generators using turbine-governor control. The turbine-governor control has relatively long response time due to the high inertia of the generators. The frequency regulation ancillary service in generation plants is composed of three functions [16] as shown in Fig. 7.5:

- ❖ Primary frequency control: limits the frequency variation caused by a sudden power unbalance in the grid by adjusting the governor speed of each generating unit within 15-30s.
- ❖ Secondary frequency control: allows restoring frequency and interchange power to their scheduled values. This is done using units under control of an automatic central regulator within 15-30 minutes.
- ❖ Tertiary control: consists in starting, stopping or varying the output of generating units in operation, in order to support the secondary control.

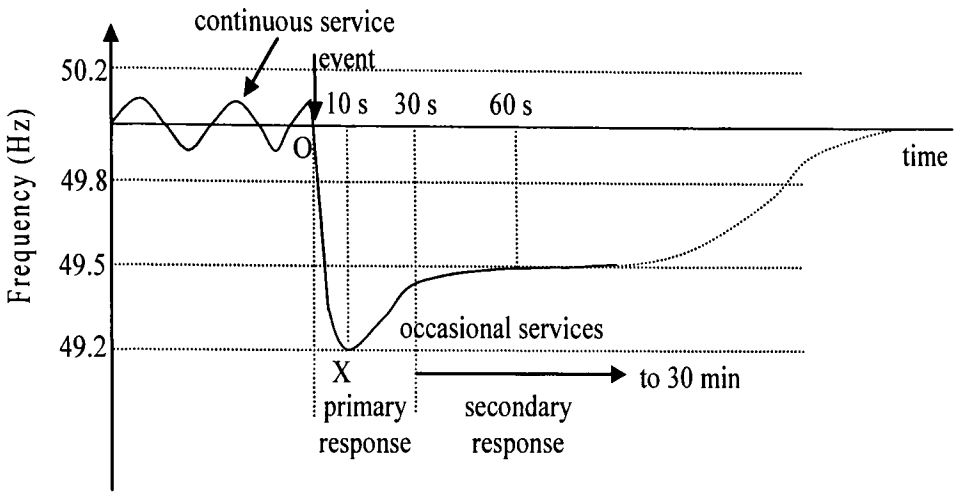


Fig. 7.5: Typical frequency response under the event of loss of generation.

The capability of the VSC-HVDC system to control the power flow could be utilized to provide frequency support together with conventional generation units in the Scottish network during emergencies (wind power variation, disconnection of generation area, and add/remove of major load). The advantage of using VSC converters for frequency stabilization is to increase the dynamic response of the Scottish network during power imbalance events. A combined active power and frequency controller equipped in the VSC converter is used to regulate the system frequency; the controller is activated in response to moderate changes in the generator rotor speed or busbar frequency in the Scotland network [17]. Therefore the VSC converter responds by adjusting the power transmitted to the England network in the right amount to stabilize the frequency.

The VSC_1 and VSC_2 in the Scotland side (in Fig. 7.4) sense the Scottish network frequency and compare it with the nominal frequency (50Hz). Any difference between the nominal and the sensed frequency activates the frequency controller to generate a correction signal in order to stabilize the system frequency. The correction signal (ΔP) is added to the active

power reference set-point (P^*_{old}) to obtain a new power reference set-point P^*_{new} that incorporates the effect of any active power mismatch. The maximum value for the correction factor is set such that the VSC converter stations in Scotland can increase or decrease their output power at any time by ±25% of the converter rating without exceeding its current limit. The frequency controller correction signal to modify the active power reference set-point is derived as follow:

$$\Delta P = k_{pf}(f - f^*) + k_{if}\int(f - f^*)dt \tag{7-2}$$

where, k_{pf} and k_{if} are the proportional and integral gains of the frequency controller. If the Scottish network frequency is lower than the nominal, that means that the demand is more than the generation, the frequency controller generates a negative correction signal to reduce the power transmitted to the England network. If the Scottish network frequency is higher than the nominal, that means that the demand is less than the generation, then the frequency controller generates a positive correction signal to increase the power transmitted to the England network.

In addition, the VSC converters at both sides are used to provide voltage control at the points of common coupling (B_1-to-B_4) by manipulating their reactive power exchange with the ac network using an ac voltage controller as described in Chapter 3.

7-5-2 Simulation results to demonstrate the ability of VSC-HVDC transmission to provide frequency regulation in the Scottish network

The capability of VSC-HVDC transmission to support the frequency control in the Scotland network and to regulate the voltages at the PCCs is investigated in this Section. The system behavior during under-frequency cases resulting from decrease in wind farm generation, disconnection of generation unit, or addition of major load is studied with the sudden addition of (500+j150) MVA load at time t=5s in the Scotland network. Fig. 7.6 shows the key waveforms obtained from simulations, which demonstrate the ability of VSC-HVDC transmission to improve the frequency stability in the Scotland network and to regulate the voltage at the HVDC systems interconnector ends. To explain the advantages of using the VSC-HVDC system to improve the dynamic frequency stability, two VSC-HVDC operation modes are investigated:

1- The VSC-HVDC systems in Fig. 7.4 are equipped with a frequency controller. This means that both the VSC converters and generation units contribute to frequency stabilization.

2- The VSC-HVDC systems in Fig. 7.4 are not equipped with a frequency controller. This means that only the generation units provide frequency stabilization.

I- Under-frequency case

First, the VSC-HVDC systems operate with frequency controllers. It can be observed that when the additional load is connected the Scotland network frequency decreases, indicating that the generation becomes less than the network demand (see Fig. 7.6a). The frequency controllers in the VSC converters in the Scotland network (VSC_1 and VSC_2) sense the decrease in the Scotland network frequency and generate a negative correction signal in order to reduce the power transmitted to the England network by an amount exactly enough to stabilize the network frequency. The VSC_1 and VSC_2 active power controllers received the correction signals and reduced the transmitted power as shown in Fig. 7.6b and Fig 7.6c. The VSC converters respond immediately after the connection of the additional load with a high response to restore the frequency. VSC_1 and VSC_2 adjust the transmitted power from 2150MW to 1970MW and from 2400MW to 2200MW respectively. This represents 72% of the additional load, and the remaining 28% is covered by the generation units in Scotland (SG_1-to-SG_5). The fast time response of the VSC converters to adjust their transmitted power and to provide most of the power required to stabilize the frequency is due to their small inertia compared to that of conventional synchronous generators.

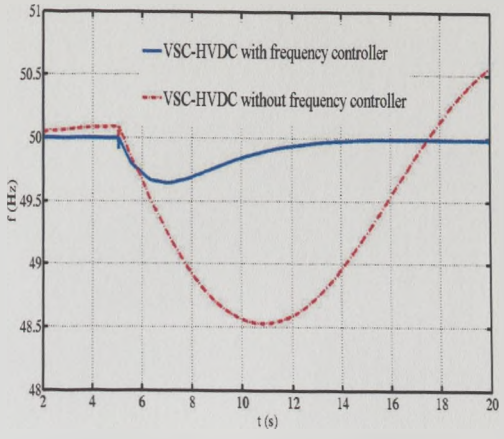
To asses the benefits of the VSC converters in frequency stabilization, the VSC-HVDC systems in Fig. 7.4 are now operated without frequency controllers with the same operating conditions, the simulation results are shown in the same Figures along with the first operation mode to facilitate the comparisons. At the same time (t=5s), the additional load is connected to the Scotland network, in this case the conventional synchronous generators in the Scotland network respond alone to stabilize the network by speeding-up their turbines to increase the output power in order to restore the generation-demand balance and stabilize the network frequency with a slow time response as shown in Fig. 7.6a. Referring to Fig. 7.6a, the frequency dynamic stability, the time required to return to the nominal frequency, the frequency overshoot, and the deviation in frequency magnitude are better when the VSC-HVDC system is equipped with frequency controllers.

II-Over-frequency case

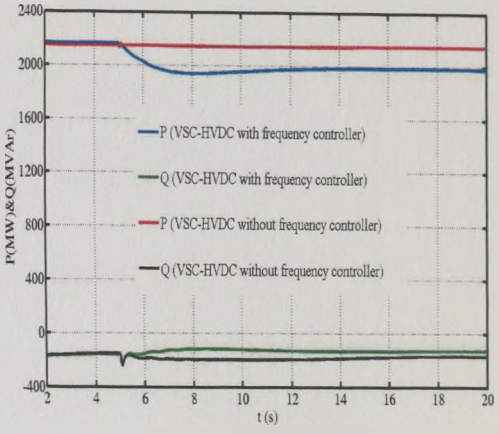
Similarly, the system behavior during over-frequency cases resulting from increases in wind farm generation, or removal of major load is studied with the sudden removal of a (400+j150) MVA load at time t=5s from the Scotland network. Same operation modes are considered for the investigation. Fig. 7.7 shows the simulation results obtained during system over-frequency events initiated by the load disconnection at time t=5s in the Scotland network when the VSC-HVDC system is operated with frequency controller. The frequency at the Scotland side is slightly increased as shown in Fig. 7.7a, and the frequency controllers equipped in VSC_1 and VSC_2 converters sense the increase in the frequency and generate positive correction signals to adjust the active power setting point. VSC_1 and VSC_2 received the correction signals and increased the power transmitted to the England network with the required amount to stabilize the network frequency, as shown in Fig. 7.7b and Fig. 7.7c. VSC_1 and VSC_2 adjust the transmitted power from 2150MW to 2305MW and from 2400MW to 2575MW respectively, this represents 82.5% of the disconnected load, and the remaining 17.5% is covered by the generation units in Scotland (SG_1-to-SG_5).

The system dynamic behavior during an over-frequency event when the VSC-HVDC system is not equipped with a frequency controller is shown also in Fig. 7.7 to facilitate the comparison of the two modes of operation. The frequency stabilization is better when the VSC-HVDC system operates with a frequency controller considering the time required to returns to the nominal frequency, and the overshoot and deviation in the frequency magnitude.

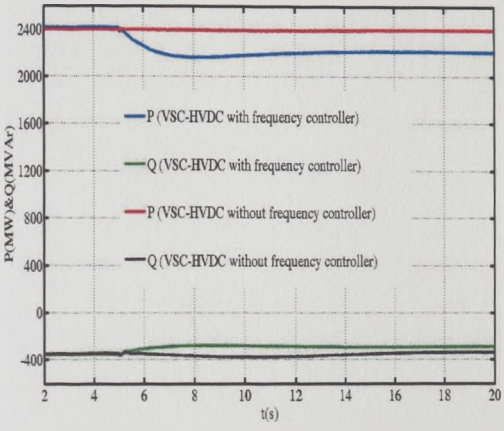
The capability of the VSC-HVDC systems to provide voltage control at the points of common coupling (Busses B_1-B_4) is explained with the aid of Figures 7.5d and 7.6d. The voltages at the PCCs are kept within the nominal value in both over- and under-frequency events. The reactive power exchange in VSC converters (VSC_1-to-VSC_4) is changed simultaneously with the change in the transmitted active power in order to regulate the voltage at the PCCs. This is clear in simulation results, which show the converters active and reactive power (Figures 7.6b to Fig. 7.6d, and Figures 7.7b to Fig. 7.7d).



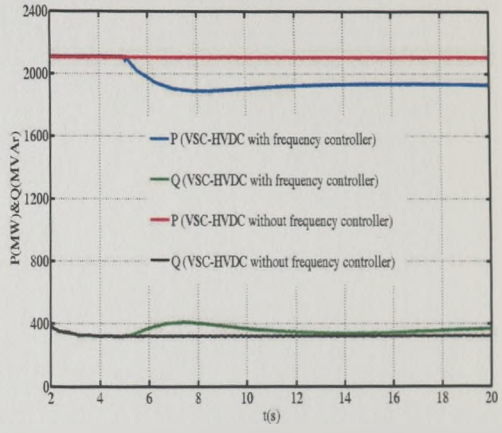
(a) Frequency in the Scotland network



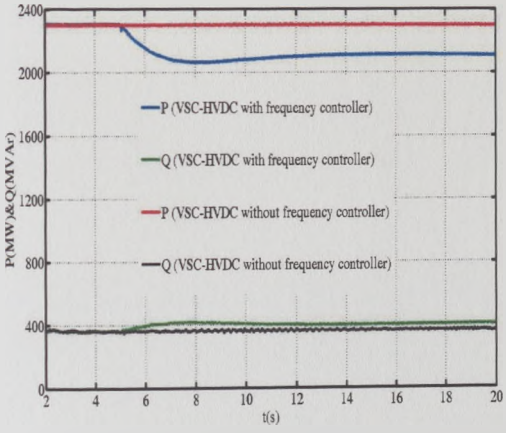
(b) Active power at B_1 (transmitted power by VSC-HVDC$_1$)



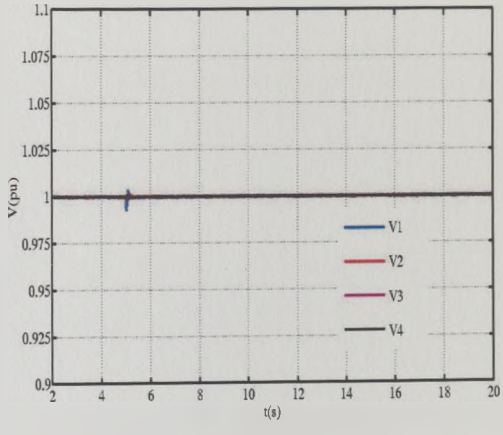
(c) Active power at B_2 (transmitted power by VSC-HVDC$_2$)



(d) Active power at B_3 (received power by VSC-HVDC$_1$)

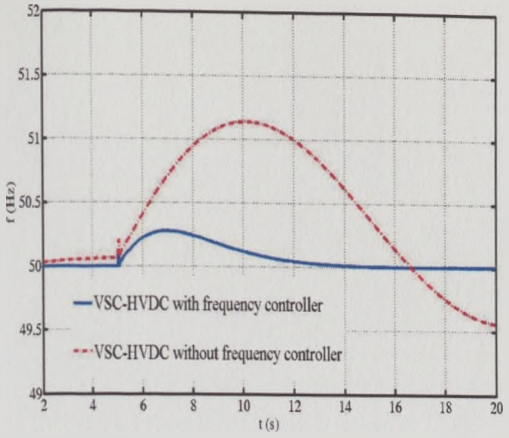


(e) Active power at B_4 (received power by VSC-HVDC$_2$)

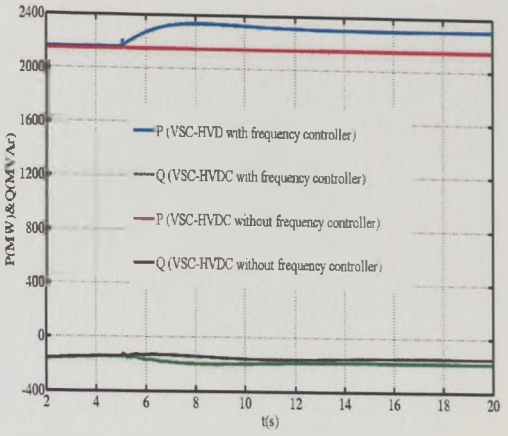


(f) The voltages at busses B_1-B_4

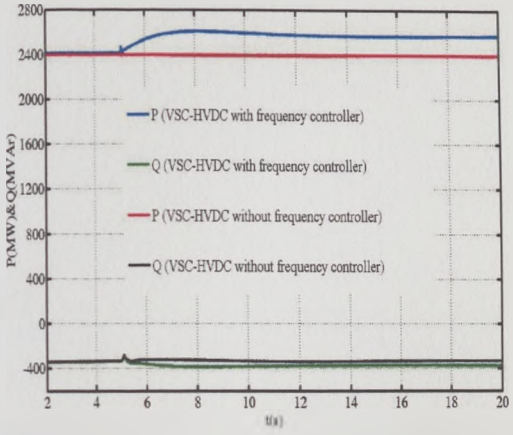
Fig. 7.6: Simulation results explaining the role of VSC-HVDC systems to participate in frequency regulation in the Scotland network after connection of (500+j100) MVA into the Scotland network



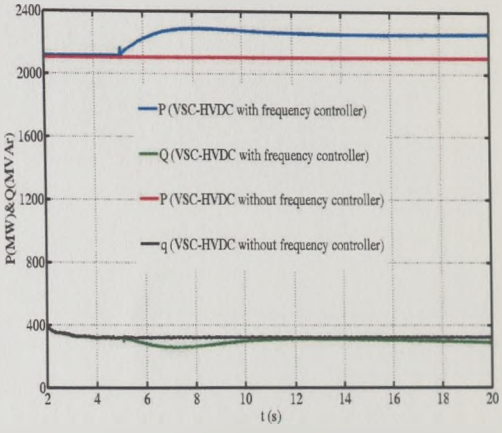
(a) Frequency in the Scotland network



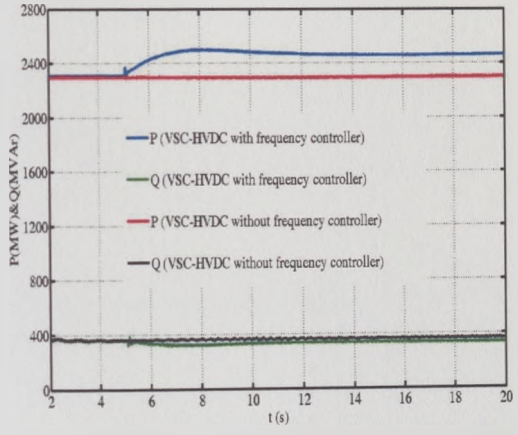
(b) Active power at B_1 (transmitted power by VSC-HVDC$_1$)



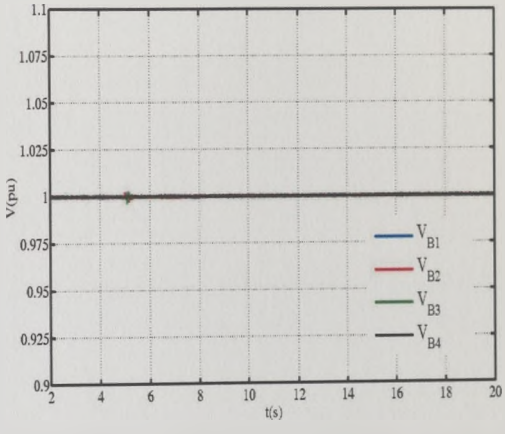
(c) Active power at B_2 (transmitted power by VSC-HVDC$_2$)



(d) Active power at B_3 (received power by VSC-HVDC$_1$)



(e) Active power at B_4 (received power by VSC-HVDC$_2$)



(f) The voltages at busses B_1-B_4

Fig. 7.7: Simulation results explaining the role of VSC-HVDC systems to participate in frequency regulation in the Scotland network after disconnection of (500+j100) MVA from the Scotland network

7-5-3 Isolating the Scottish network from disturbances in the English network

In interconnected networks based on HVAC transmission, the automatic generation control of the individual units is coordinated using tie-line power and frequency signals [18]. One of the disadvantages of tie-line operation is the possibility of disturbance propagation from one network to the remaining networks. For example, if a short circuit occurs somewhere in any network, the voltage becomes zero in the faulted phases, and due to the low impedance of the transmission line the voltage depression extends across the whole system until the fault is terminated by circuit breakers [16]. Another disadvantage of tie-line operation is the propagation of frequency instability due to connection/disconnection of generation units or major load change events.

In the GB interconnected network case, any abnormal conditions in the England or Scotland networks propagate and affect the whole network and this could increase the black-out risk. The use of VSC-HVDC as transmission medium eliminates these problems because in asynchronous connection (decoupled operation), there is no need for coordinated control [18]. By decoupling the operation of the Scotland-England networks through VSC-HVDC transmission, the two networks are operated separately without any control coordination; this may improve the fault-ride through capability and prevent the propagation of disturbances.

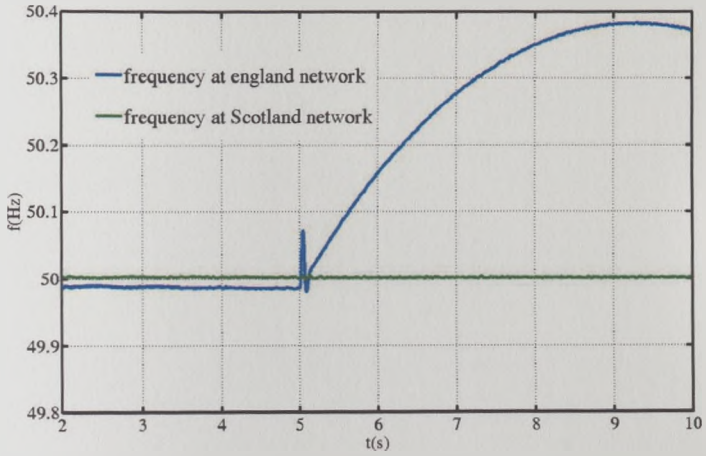
The ability of VSC-HVDC to act as firewall and prevent the transmission of disturbances is investigated considering the following scenarios:

- Sudden loss of major load in the England network and its effect in the Scotland network (frequency instability propagation).
- Three-phase fault at one of the point of common coupling in the England network (fault propagation).

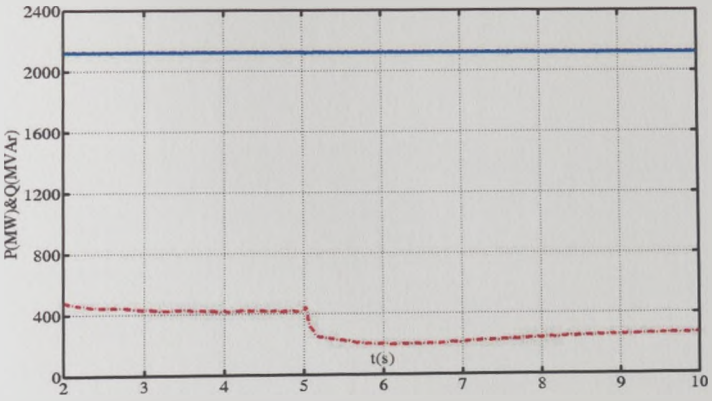
The frequency instability event is investigated by removing a load of 500+180MVA from B_3 in the England network at t=5s (this is also equivalent to connecting a 500MW generation unit). Fig. 7.8 shows the key simulation waveforms explaining the system behaviour in both networks after the sudden removal of the load from England. As expected the English network frequency is affected due to the active power imbalance that results from the removal of the load, whilst the Scotland network frequency remains unaffected as shown in Fig. 7.8a due to the decoupled operation. The reactive power exchange of converter VSC_3 is adjusted after the removal of the load to maintain the voltage magnitude at B_3 as shown in Fig. 7.8b.

AC line faults in the England network and their effects in the Scotland network is investigated by subjecting the English network to a solid three-phase fault at bus B_4. Fig. 7.9 shows the networks behaviour after the application of a three-phase fault at bus B_4 with duration of 100ms at t=3.5s. It can be observed that the active powers and voltages in the England network (B_3 and B_4) are significantly affected by the short-circuit fault as shown in Fig. 7.9a and Fig. 7.9b. The active power and voltage at the faulted bus phases (bus B_4) collapses to zero and recovers again after circuit breakers remove the fault. On the other hand, the active power and voltage in the Scotland network (buses B_1 and B_2) remain less sensitive to the ac fault occurring in the English network as shown in Fig. 7.9c and Fig. 7.9d.

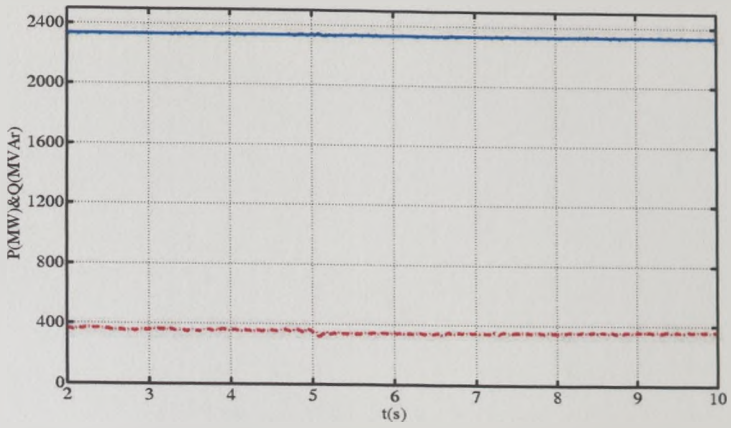
The simulation results in Fig. 7.8 and Fig. 7.9 illustrate the advantages of the decoupled operation to prevent disturbance propagation from the England network to the Scotland network.



(a) Active frequency in the Scotland and England networks

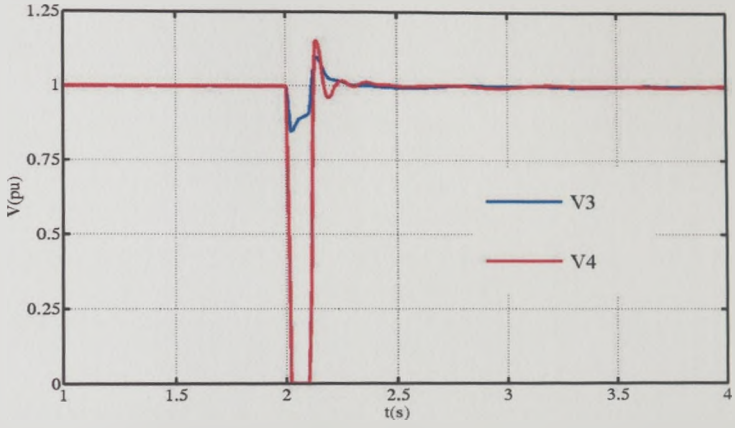


(b) Active power at B_3 (received power by VSC-HVDC$_3$)

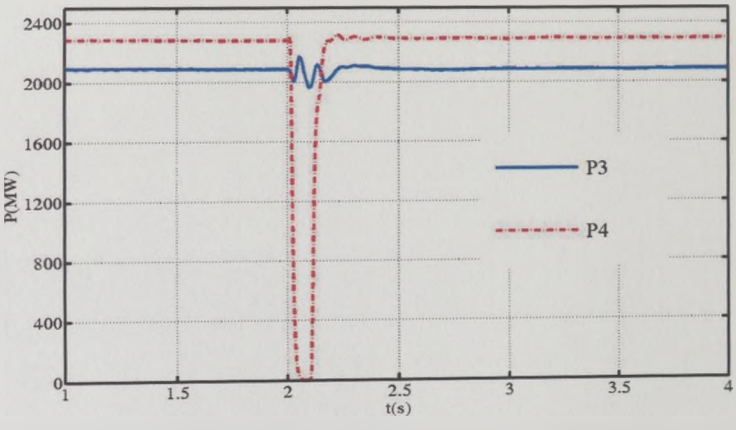


(c) Active power at B_4 (received power by VSC-HVDC$_4$)

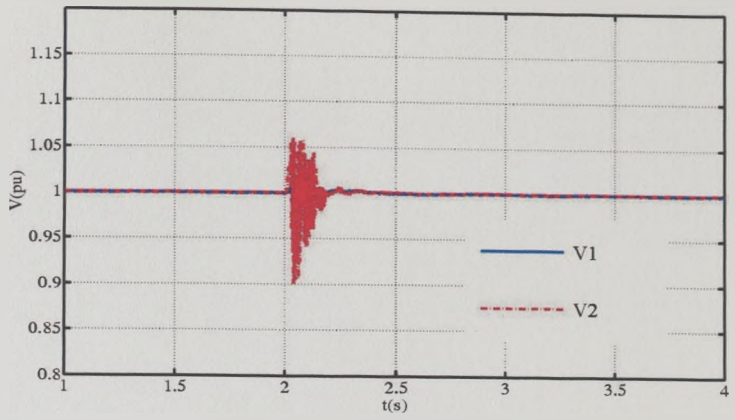
Fig. 7.8: Simulation results illustrating the decoupling operation of Scotland-England networks after the disconnection of (500+100) MVA from the England network.



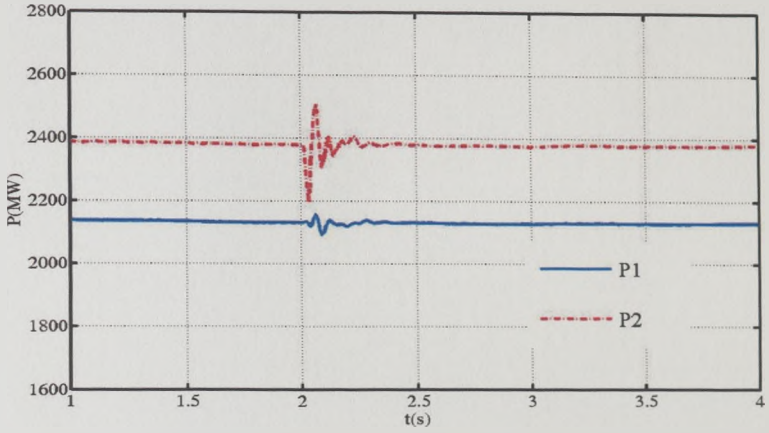
(a) Voltages at B_3 and B_4 (England side)



(b) Active power at B_3 and B_4 (England side)



(c) Voltages at B_1 and B_2 (Scotland side)



(b) Active power at B_1 and B_2 (Scotland side)

Fig. 7.9 Simulation results explains the decoupling operation of Scotland-England networks during three-phase fault at B_4 at England network.

7-6 Scotland-England interconnectors reinforcement using parallel HVAC-HVDC links

The capacity and controllability of the interconnectors could be increased by addition of a point-to-point VSC-HVDC system in parallel with the existing HVAC lines. The main task of the added VSC-HVDC system is to enhance the interconnectors and to increase the transmission capacity from Scotland to England. The VSC-HVDC system converters are used to provide voltage control at the ends of the HVAC systems by generating or absorbing the required reactive power to keep the voltage at the rated value. The single-line diagram in Fig. 7.10 shows the use of the parallel VSC-HVDC and HVAC system to transmit the power from Scotland to England. The VSC-HVDC systems are label VSC-HVDC1 and VSC-HVDC2 while the HVAC are labeled HVAC1 and HVAC2.

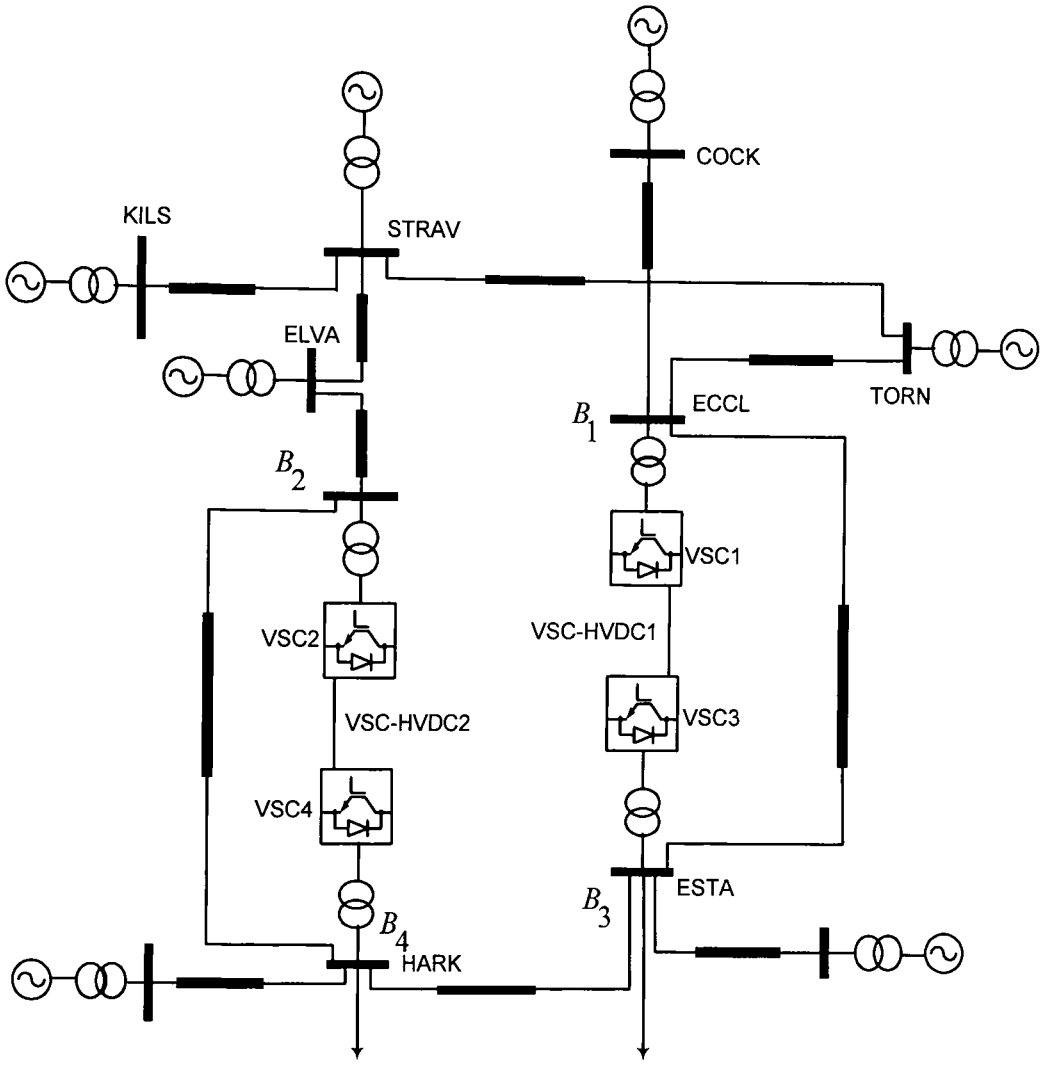
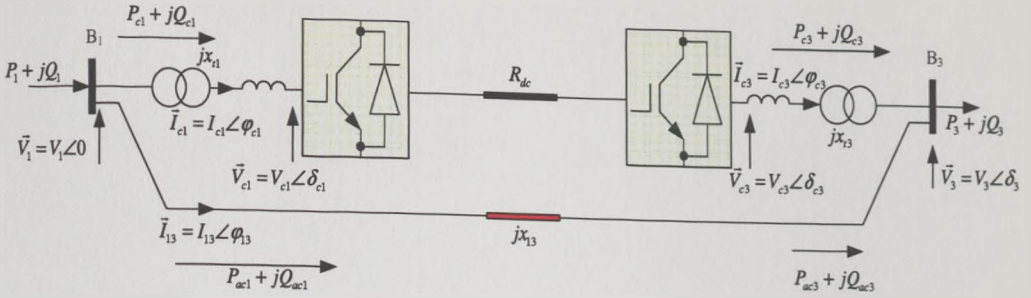
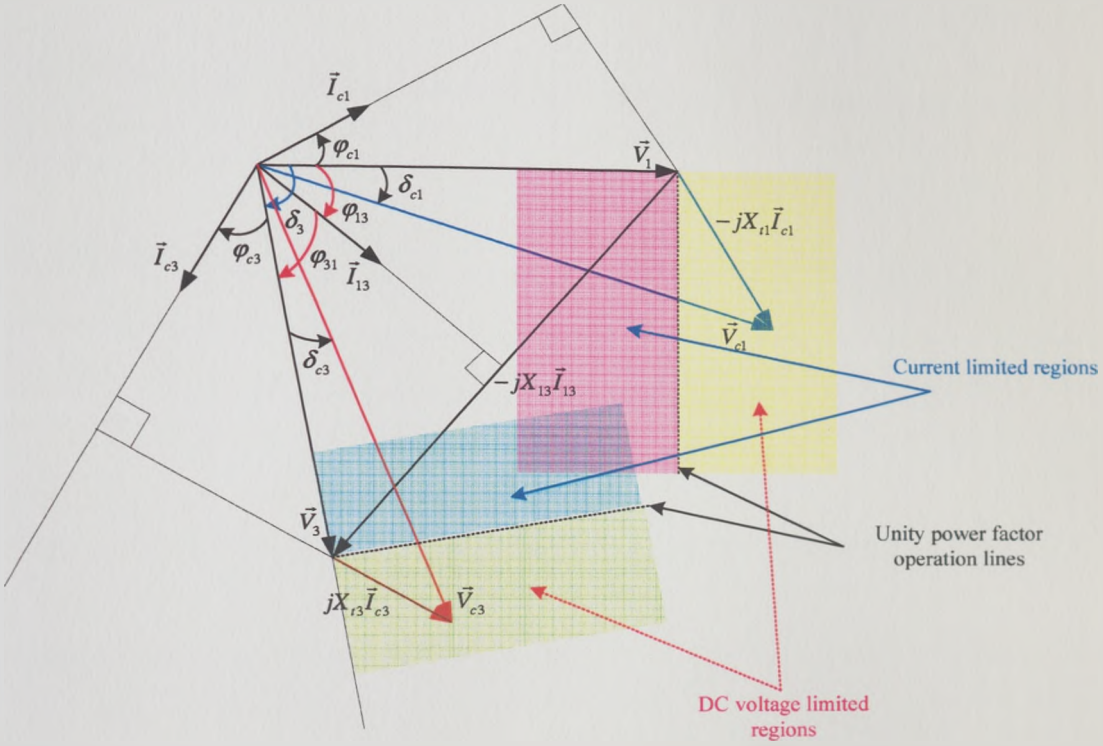


Fig. 7.10: Use of VSC-HVDC in parallel with HVAC system to interconnect Scotland and England networks.

Fig. 7.11 shows the schematic diagram for the hybrid parallel connection between ECCL4 and STEW4 substations and its overall vector diagram. The vector diagram in Fig. 7.11b is drawn under the following assumptions: ac line connecting buses B1 and B2 is highly inductive, therefore its resistance has been neglected; ac side filters are neglected; leakage inductances of transformers and that of interfacing reactors are added together; power flows in ac and HVDC lines are from B1 to B3; voltage vector $\vec{V}_1$ is the reference for the whole system; and converter stations VSC1 and VSC3 regulate the voltage at buses B1 and B3.



(a) Single-line diagram of VSC-HVDC1 and HVAC1 lines connecting buses B1 and B3.



(b) Phasor diagram of hybrid connection of two ac systems

Fig. 7.11: Simplified model of the hybrid parallel interconnector between ECCL4 and STWE4.

The steady-state equations describing the power exchange in the parallel system are as follow:

$$\vec{I}_{c1}=\frac{\vec{V}_1-\vec{V}_{c1}}{jX_{t1}}=\frac{1}{X_{t1}}\left[V_1 e^{-\frac{1}{2}\pi j}-V_{c1}e^{j(\delta_{c1}-\frac{1}{2}\pi)}\right] \tag{7-3}$$

The active and reactive power that converter VSC1 exchanges with B1 are:

$$P_{c1}+jQ_{c1}=\vec{V}_1\vec{I}_{c1}^{*}=\frac{V_1^2}{X_{t1}}e^{j\frac{1}{2}\pi}-\frac{V_1V_{c1}}{X_{t1}}e^{j(\frac{1}{2}\pi-\delta_{c1})} \tag{7-4}$$

$$P_{c1}=-\frac{V_1V_{c1}}{X_{t1}}\sin\delta_{c1} \tag{7-5}$$

$$Q_{c1} = \frac{V_1^2}{X_{t1}} - \frac{V_1 V_{c1}}{X_{t1}} \cos \delta_{c1} \tag{7-6}$$

Similarly, the active and reactive power that converter VSC3 exchanges with B3 are:

$$P_{c3} = \frac{V_3 V_{c3}}{X_{t3}} \sin(\delta_{c2} - \delta_3) \tag{7-7}$$

$$Q_{c3} = \frac{V_3 V_{c3}}{X_{t3}} \cos(\delta_{c3} - \delta_3) - \frac{V_3^2}{X_{t3}} \tag{7-8}$$

The active and reactive powers at the sending end of the HVAC1 line in parallel with VSC-HVDC1 link that connects B1 and B3 are:

$$P_{ac1} = -\frac{V_1 V_3}{X_{13}} \sin \delta_3 \tag{7-9}$$

$$Q_{ac1} = \frac{V_1^2}{X_{13}} - \frac{V_1 V_3}{X_{13}} \cos \delta_3 \tag{7-10}$$

When converters VSC1 and VSC3 regulate the voltage magnitude at B1 and B3, such that $|\vec{V}_1| = |\vec{V}_3| = V_1$, by adjusting the reactive power exchange between VSC_1 and VSC_3 and the coupling point with the ends of HVAC1 line, may force the power factor at both ends of the HVAC1 line connecting B1 and B3 to be equal, $\cos\varphi_{ac1} = \cos\varphi_{ac3} = \cos\frac{1}{2}\delta_3$, see Fig. 7.11b. This case is identical to that when the line is fully compensated with an SVC or a STATCOM at the middle [19]. This demonstrates the technical and economical value of the parallel scheme especially in the context of network reinforcement and offshore wind farm connection.

Since the VSC converters keep V_1 and V_3 at equal values (1.0pu), then $\frac{1}{2} I_{13} X_{13} = V_1 \sin\varphi_{ac13} = V_3 \sin\varphi_{ac31} = V_1 \sin\frac{1}{2}\delta_3$, and the active and reactive power at the sending end of HVAC can be expressed as:

$$P_{ac1} = -\frac{V_1^2}{X_{12}} \sin \delta_3 \tag{7-11}$$

$$Q_{ac1} = \frac{2V_1^2}{X_{13}} \sin^2 \tfrac{1}{2}\delta_3 = \tfrac{1}{2} X_{13} I_{ac1}^2 \tag{7-12}$$

A similar expression can be obtained for the receiving end.

The vector diagram in Fig. 7.11b also illustrates the operating regions of both converter stations during power transmission from B1 to B3, including the unity power factor boundary, the region where converter operation is limited by available dc link voltage, and

the region where operation is limited by converter switching device current rating. The mirror of this vector diagram represents the reversed power flow. It can be observed from Fig. 7.11b that changing VSC1 operation from over-excitation (when converter releases VAr to bus B1), to under-excitation (where VSC absorbs VAr from B1), the voltage vector $\vec{V}_{c1}$ moves from the yellow region, through the unity power factor boundary line, into the pink region.

It is not possible for the VSC-HVDC system to enhance the HVAC line and provide reactive power support when it reaches its maximum reactive power limit. The reactive power capability of the VSC-HVDC system is limited according to the converter rating and the dc link voltage. Therefore, any attempt to increase the power flow after the converters have reached their reactive power limit require more reactive power from an external source to keep the ac voltage at the end of the HVAC system at the rated value. In the parallel connection, the VSC-HVDC systems could not be used to provide frequency stabilization or used as firewall to prevent disturbances propagation as in the decoupling operation, because the two network generation plants are still coordinated via HVAC lines power and frequency signals.

7-7 Simulation results of using parallel operation

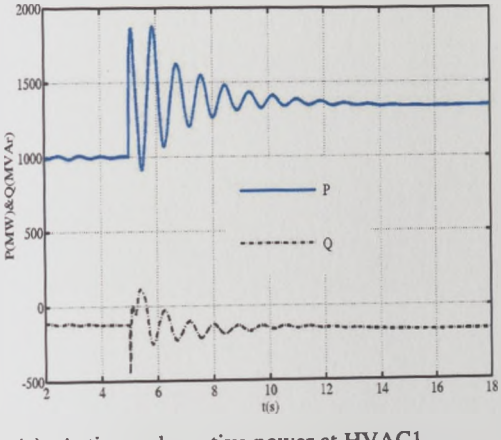
Fig. 7.12 shows the simulation results that demonstrate the capability of VSC-HVDC system to enhance the HVAC transmission system and provide the required reactive power control at the end of the HVAC lines. First, the hybrid parallel interconnectors operate at steady-state and transmit the power into the England network. VSC-HVDC1 and VSC-HVDC2 are controlled to transmit the rated powers 1100MW, 1000MW respectively, while HVAC1 and HVAC2 lines are accommodating the rest of power delivered to England which is 1000MW, 1500MW respectively. The reactive power exchange between the VSC converters and the coupling points with the HVAC systems is regulated such that the voltages at the ends of the HVAC line (buses B_1-to-B_4) are kept within 1.0pu. According to Fig. 7.12a and Fig. 7.12b, the reactive power exchange is not the same for all VSC converters (VSC1-to-VSC4) due to the difference in ac systems strength. The power factor of the current flowing in the HVAC lines are kept close to unity (really it is 0.993) at both ends of the line as shown in Fig. 7.12f.

To demonstrate the ability of the VSC-HVDC system to provide the reactive power support, the power transmission to England is increased by 1000 MW. At t=5s, a 1000MW generation plant is connected to the Scotland network and the additional power is delivered to England

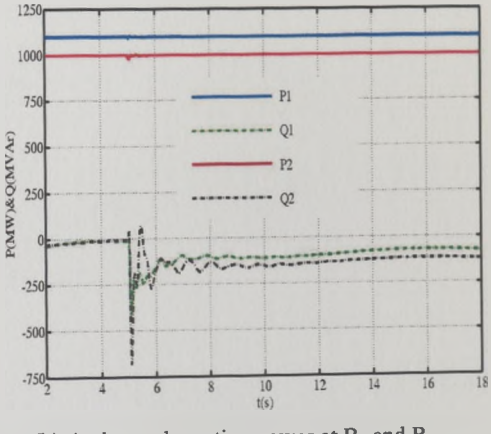
through the parallel interconnectors. Since the VSC-HVDC systems are operated with constant active power, therefore the additional power flows through the HVAC lines.

The VSC converters adjust their reactive power exchange with the buses at t=5s to maintain the voltages at the rated value as shown in Fig. 7.12a and Fig. 7.12b. The PWM-technique implemented in the VSC converters changes the voltages at converters terminals in order to regulate the reactive power flow between the converters and the buses as shown in Fig. 7.12g and Fig. 7.12h. The power factor of the current flowing in HVAC1 after the increase of transmission power is kept at the same value (0.993), as shown in Fig. 7.12f; this indicates that the lines are not affected by the increase in transmission capacities. The responses shown in Fig. 7.12 explain the ability of the VSC-HVDC system to provide the reactive power support to the HAVC system in order to maintain voltage stability during change in transmission capacity.

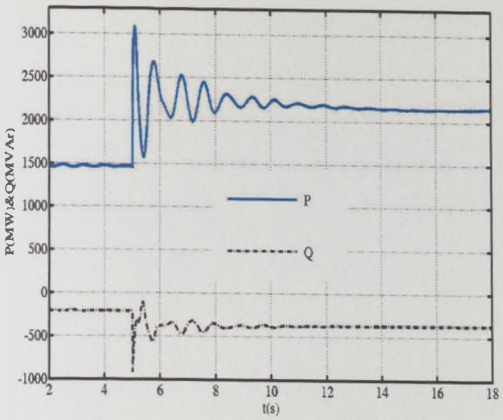
Figures 7.13 show the possibility of propagation of disturbances from England into Scotland due to synchronous connection of the network. A three-phase-to-ground fault occurs in the England network at the middle of the transmission line connecting STWE4 and HARK4 at t=6s and cleared after 140ms. As expected the fault affects the voltage and powers at B_3 and B_4 at the England side and then propagates to affect the voltages and power at buses B_1 and B_2 in the Scotland network.



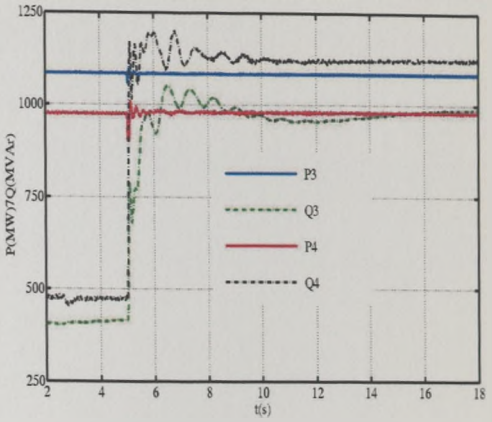
(a) Active and reactive power at HVAC1



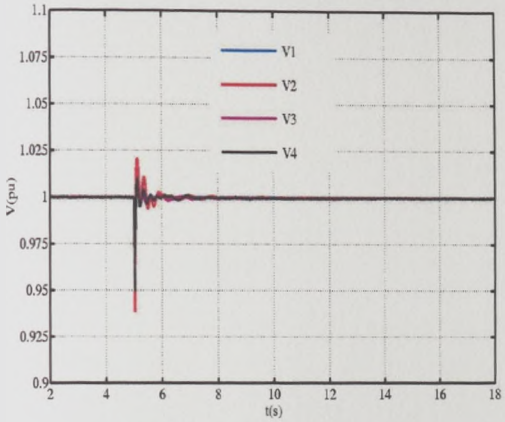
(b) Active and reactive power at B_1 and B_2



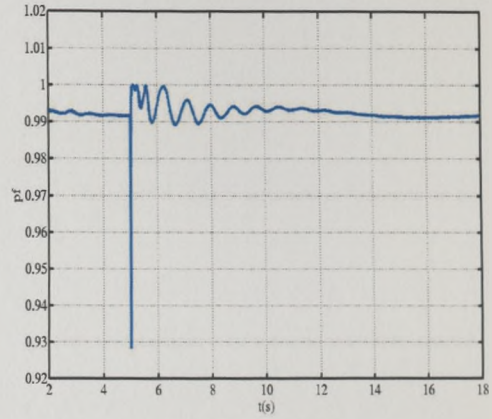
(c) Active and reactive power at HVAC2



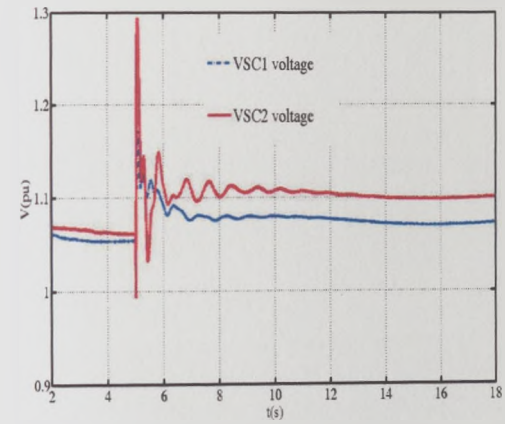
(d) Active and reactive power at B_3 and B_4



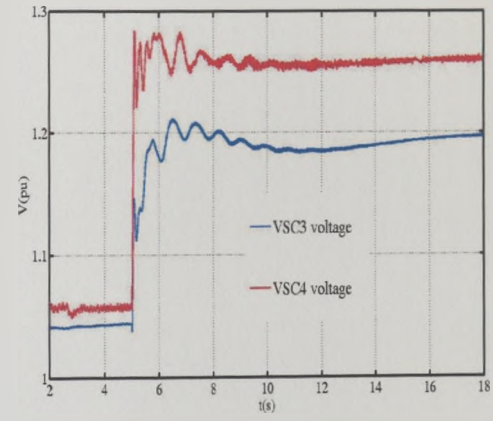
(e) Voltages at B_1 to B_4



(f) Voltages at VSC1 and VSC2 terminals

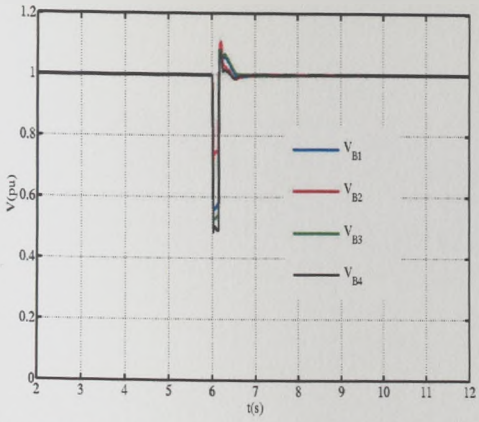


(g) Voltages at VSC1 and VSC2 terminals

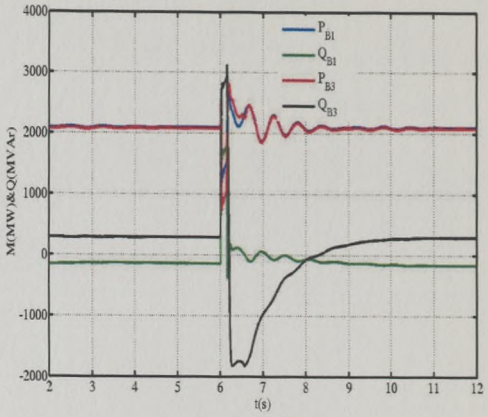


(h) Voltages at VSC3 and VSC4 terminals

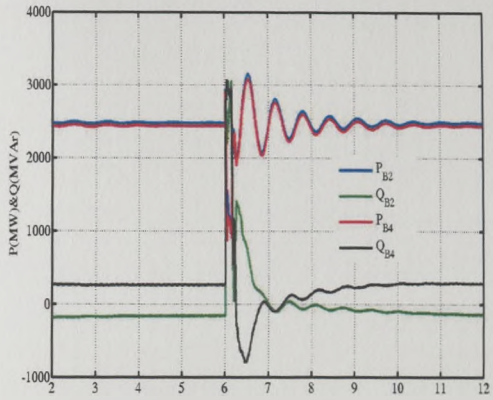
Fig. 7.12: Simulation results explaining the hybrid parallel operation of Scotland-England networks during sudden change in HVAC line transmission capacity and three-phase fault at England side.



(a) Voltages at B_1 to B_4 (when ac fault occur at England side)



(b) Voltages at B_1 to B_4 (when ac fault occur at England side)



(c) Voltages at B_1 to B_4 (when ac fault occur at England side)

Fig. 7.13: Simulation results explaining the hybrid parallel operation of Scotland-England networks during three-phase fault at England side.

7-7 Summary

This chapter investigates the use of VSC-HVDC system to enhance and increase the transmission capacity of the interconnectors between Scotland and England. Two options are used for interconnector enhancement: The first option is to replace the HVAC links with point-to-point VSC-HVDC systems, and the second option is to connect HVDC system in parallel with the existing HVAC lines. The first option represents the decoupling operation of the Scotland-England networks without coordination control. The two networks are isolated and operated separately without any coordination. In this option, the VSC-HVDC system transmits large-scale power and provides additional functionalities. The VSC converter at the Scotland network is equipped with a frequency controller in order to improve the dynamic frequency stability in the Scotland network during active power imbalance events. When the

power balance in the Scotland network is affected, the converters at the Scotland side adjust the transmitted power to England with sufficient amount to stabilize the network frequency. The VSC converter also provides voltage control at the point of common coupling and maintains the voltages at 1.0pu. This helps in maintaining the voltage stability at both sides of the HVDC system. In the decoupled operation, the VSC-HVDC system acts as firewall to prevent the propagation of disturbances from the England network to the Scotland network, and this reduces the risk of black-out in the Scotland network. Simulation results were used to demonstrate the advantage of the decoupled operation including frequency stabilization in the Scottish network, improving of voltage stability at the end of the HVDC system and prevent of fault transmission. The English network in this case suffers during the change in transmitted power but it handles these power variations because it is a strong network (with enough generation reserve). Energy storage may be required to be installed if the wind power penetration is increased further.

The third option is to use a parallel HVAC/VSC-HVDC connection to increase the interconnector's capacity and controllability. The VSC-HVDC is used to transmit the power into the England network and to enhance the HVAC system by regulating the voltage at the ends of the HVAC lines. In this option, the VSC-HVDC system improves system voltage stability when the transmission capacity is increased, but the system still suffers from synchronous operation problems. The network is operated in synchronism due to the existence of the HVAC links, for this reason the VSC-HVDC cannot be used to provide additional functionalities similar to that obtained in the decoupled operation.

References

[1] "OUR ELECTRICITY TRANSMISSION NETWORK: A VISION FOR 2020," *A Report by the Electricity Networks Strategy Group, avialable at webarchive.nationalarchives.gov.uk/...uk/.../1696-01-ensg_vision2020.pdf, March 2009*.

[2] C. Bayfield, *et al.*, "Planning for the integration of on-shore renewable generation for the GB transmission system," *CIGRÉ 2006 Session in Paris, avialable at http://www.labplan.ufsc.br/congressos/cigre06/DATA/C1_114.PDF*.

[3] *The Grid Code, Issue 3, Revision 12,* vol. National Grid Electricity Transmission plc, available at, http://www.nationalgrid.com/uk/Electricity/Codes/gridcode/gridcodedocs/.

[4] O. A. Giddani, *et al.*, "Potential benefits of decoupling the Scotland-England network using VSC-HVDC," in *AC and DC Power Transmission, 2010. ACDC. 9th IET International Conference on*, 2010, pp. 1-5.

[5] E. M. Yap, *et al.*, "HVDC and FACTS for improved power delivery through long transmission lines," in *Power Engineering Society Inaugural Conference and Exposition in Africa, 2005 IEEE*, 2005, pp. 299-304.

[6] L. Kirschner, *et al.*, "Benefits of FACTS for Power System Enhancement," in *Transmission and Distribution Conference and Exhibition: Asia and Pacific, 2005 IEEE/PES*, 2005, pp. 1-7.

[7] N. G. Hingorani, "FACTS Technology - State of the Art, Current Challenges and the Future Prospects," in *Power Engineering Society General Meeting, 2007. IEEE*, 2007, pp. 1-4.

[8] Xiao-Ping Zhang, *et al.*, *Flexible AC Transmission Systems: Modelling and Control*: Springer, **Germany,** 2006.

[9] Xiao-Ping Zhang, *et al.*, *Flexible AC Transmission Systems: Modelling and Control*. New York: Springer, 2006.

[10] B. R. Andersen, *et al.*, "Topologies for VSC transmission," in *AC-DC Power Transmission, 2001. Seventh International Conference on (Conf. Publ. No. 485)*, 2001, pp. 298-304.

[11] C. A. Canizaresa, *et al.*, "STATCOM modeling for voltage and angle stability studies," *International Journal of Electrical Power and Energy Systems, Volume 25, Number 6, July 2003 , pp. 431-441(11).*

[12] J. Arrillaga, *et al.*, *Flexible Power Transmission Systems-The HVDC Options*: John Wiley & Sons, Publication, 2007.

[13] N. Flourentzou, *et al.*, "VSC-Based HVDC Power Transmission Systems: An Overview," *IEEE Trans on Power Electronics,*, vol. 24, pp. 592-602, 2009.

[14] S. Galli, *et al.*, "For the Grid and Through the Grid: The Role of Power Line Communications in the Smart Grid," *Proceedings of the IEEE,* vol. 99, pp. 998-1027, 2011.

[15] A. Yakout, *et al.*, "Improving the transient frequency response of unintentional islands via local optimal controllers," in *Advances in Power System Control, Operation and Management (APSCOM 2009), 8th International Conference on*, 2009, pp. 1-6.

[16] I. M. d. Alegri, *et al.*, "Connection requirements for wind farms: A survey on technical requirements and regulation," *Renewable and Sustainable Energy Reviews Volume 11, Issue 8, October 2007, Pages 1858-1872.*

[17] *Review of HVDC Link Technology Issues, Electricity Network Investment (ENI), March 2009.*

[18] K. R. Padiyar, *HVDC power transmission systems: technology and system interactions*. New Delhi: New Age International (P) Limited, Publishers, 2005.

[19] N. Hingorani and L. Gyugyi, *Concepts and Technology of Flexible AC Transmission Systems*, 1999.

Chapter Eight

Conclusions and Recommendations for Further Research

8-1 General conclusions

This thesis investigated the use of HVDC transmission systems for the large-scale integration of offshore wind farms into mainland power networks and for reinforcement of the HVAC links between Scotland and England in order to increase their transmission capacities without affecting the power and voltage stability. Due to limitations of conventional current source converter-based HVDC systems, such as commutation failures, and inability to operate in weak or dead ac systems with no generation, voltage source converter-based HVDC systems were selected and discussed in detail in this thesis.

A detailed model for VSC-HVDC converters based on the neutral-point clamped converter was developed as a modelling platform in Simulink and used throughout the thesis to conduct the various studies presented. Design of multi-tasking control systems for voltage source converter HVDC systems was conducted to ensure robust dynamic performance and to enhance disturbance rejection. This improved VSC-HVDC performance was achieved by including feed-forward terms in the current signal controllers and neglecting those of the dc voltage controllers. The basic VSC-HVDC controllers incorporated are active power, frequency, dc voltage, ac voltage and ac current controllers. However, the choice between these controllers was application dependent (for example, the wind farm-side converter is equipped with ac controller when the wind farm is operated without power command to maintain the voltage at the wind farm network, while active power controller is incorporated when the wind farm is operated with power command).

The steady-state and transient performance of the developed VSC-HVDC systems was investigated in the context of point-to-point and multi-terminal VSC-HVDC networks. This included the dynamic assessment in the event of step changes in the active power command, power reversal, and ac and dc side faults. Further investigations were carried out on the hybrid connection 'VSC-HVDC in parallel with HVAC line' for connection of two network areas, and in the integration of offshore wind farms using point-to-point and multi-terminal VSC-HVDC networks.

In multi-terminal dc operation, active power-dc voltage droop control was included in the control systems of the converters that regulate the dc voltage in order to facilitate power sharing (dispatch) between grid-side converters. This thesis also investigated the use of

multi-terminal VSC-HVDC networks for the development of a transnational grid for power trading, network reinforcement, and voltage support at individual ac regions. Furthermore, power management during loss of ac grid at one converter station was investigated. The vulnerabilities of the voltage source converter in HVDC networks were identified during various types of disturbances such as loss of dc-side slack bus, loss of an ac grid converter station, and exposure of the multi-terminal dc network to dc- and ac-side faults.

Regarding offshore wind farm integration using VSC-HVDC transmission, wind turbine generators based on fixed-speed induction generators (FSIGs) were selected in this thesis to represent the more demanding case scenario. Here, the purpose of the VSC-HVDC link was to facilitate GB Grid Code compliance, to improve ac fault ride-through capability by decoupling the FSIG dynamics from the onshore grid during ac faults in the grid side, and to provide reactive power support at both ends. Two control approaches for the offshore converter of the VSC-HVDC system were investigated.

In the first approach, the VSC-HVDC injects the wind power into the dc link without assigning a direct power command, and establishes a stiff ac bus at the wind farm network supplying the reactive power required by individual FSIGs. This control approach does not allow the wind farm to contribute to ancillary services to the mainland grid such as power levelling and frequency stabilization. Nonetheless, this approach allows operation of the wind farm with a maximum power tracking strategy and is independent of the wind turbine technology being used (i.e. FSIG, DFIG or full-converter with synchronous generators).

In the second control approach, the wind farm-side converter of the VSC-HVDC link was used to inject the offshore wind power into the dc link with an assigned active power command, while the wind turbines use their pitch control to regulate the active power injection. Also, an additional frequency control loop was included to enable the wind farm to provide frequency support to the onshore network. In this approach, the wind farms were not allowed to operate with a maximum power tracking; at average wind speed (11m/s) the blade angle position is at 4° to limit the wind generation to 350MW while this is the maximum power tracking with 8m/s wind speed. This feature enables the wind farms to increase/or decrease the transmitted power into the mainland network by adjusting turbine blades positions. For example, with 11/ms the wind generation may increased to 400MW or reduced to 300MW by reposition the blades at 1.6° or 8° respectively. The wind farm contribution to frequency regulation is limited to 20% of the converter rating (this means 80MW maximum penetration in frequency regulation).

The frequency support from wind farms is valuable to power system operators but not preferred by the wind farm owners due to economical reasons. Both approaches can be used with point-to-point and multi-terminal VSC-HVDC systems in order to improve the overall power system reliability and stability.

Additionally, the small-signal stability of a generic four-terminal VSC-HVDC network connected to two independent offshore wind farms and synchronous machine in the mainland grid was investigated. In this investigation all the controllers of the VSC-HVDC converters and conventional power plants were fully modeled and represented. The wind farm was assumed to operate with constant input mechanical torque for simplicity in the analysis. The eigenvalues and corresponding participation factors were calculated to evaluate the small-signal stability of the overall system. The impact of the controllers of the grid-side converters on small-signal stability was investigated thoroughly, by observing the impact of variations in the controllers' gains in the oscillations frequencies and damping times of each individual mode. For further validation, time-domain simulations with the obtained controller's gains were carried out when the system was exposed to small perturbations.

For reinforcement of the existing interconnectors between the Scottish and English networks using VSC-HVDC transmission, two connection scenarios were investigated.

The first scenario was to replace both existing HVAC links with point-to-point VSC-HVDC links. This connection option may result in complete decoupling operation of the Scottish power network from the English one. The benefits of the decoupling feature facilitated by the VSC-HVDC connection with regards to power system transient and voltage stability were investigated and are summarized as follows:

- The proposed VSC-HVDC links may increase the amount of power that could be exchanged between Scotland and England by 2.5 times compared to that achievable with the existing HVAC lines (using the same power corridors). Also, the VSC-HVDC links can provide reactive power support to both ac networks without additional cost, improving transient and voltage stability at both networks.
- The VSC-HVDC converters located in the Scottish network may provide frequency support to the Scottish network by adjusting the amount of power exchanged between the Scottish and English networks.
- The proposed VSC-HVDC links act as a firewall that could prevent any propagation of ac network disturbances from one network to the other. This reduces the risk of black-out in the in both networks.

In the second scenario, two hybrid connections were proposed to increase the interconnectors' transmission capacity. This required installation of two new VSC-HVDC links in parallel with the existing HVAC links between Scotland and England. In this configuration the VSC-HVDC converters at both ends of the links may enhance the utilization and voltage profile of the existing HVAC links. The VSC converters at both ends of the HVAC links can regulate the reactive power at the PCCs in order to maintain the voltages at 1.0pu. The main shortcoming of this approach is that the VSC-HVDC links cannot be used to provide frequency support or prevent disturbance propagation. This is because the two networks are still operating in synchronism due to the existence of the HVAC links.

8-2 Research Findings

The main findings of the thesis are summarized as follow:

1- VSC-HVDC systems address most of the shortcomings associated with HVAC and LCC-HVDC systems, and represent an attractive solution for various applications in power systems such as wind farms connection, multi-terminal dc operation, and reinforcement of electrical power systems.

2- VSC-HVDC systems are a suitable option for wind farm connection in order to meet all Grid Code requirements issued by GB national electricity network (regardless of the wind turbine technology being used).

3- Integration of large offshore wind farms via VSC-HVDC systems enables them to contribute to frequency stabilization in the onshore power network (at the expense of operating slightly off the maximum power tracking curve). The wind farms are able to provide 71.4% of the power required to stabilize the frequency in the event of 70MW difference in power balance of the network. The high response of the VSC-HVDC compared to conventional synchronous generation enables the wind farm to provide 50MW by changing the turbine blades position and machine speed (the position is adjusted from 4 to 8°/ or 1.6° and the machine speed is changed from 1.03pu to 1.02/ or 1.006 to increase / or decrease the injected power into the mainland network) . This percentage increases if the power variation is less than 70MW and vice versa.

4- The use of VSC-HVDC systems to replace the HVAC links between Scotland and England increases the transmission capacity of the links, improves system voltage stability, prevents faults propagation, and could provide frequency support to the Scotland network in the event of power mismatches. VSC_1 and VSC_2 provide 72% / or 82% of the required power

to stabilize the frequency during sudden increase of 500MW/ or losing of 400MW and this speeds-up the time required for network frequency stabilization compared to the time required when the conventional machines adjust their outputs and reduce the frequency deviation. When the 500MW is added to the system it took 9s for the frequency to recover back to the nominal with less than -0.5Hz deviation, while the same action took the conventional machine more than 20s with frequency deviation of -1.5Hz to recover.

5- A hybrid connection increases the transmission capacity of the links between England and Scotland and improves the voltage stability of the system, but cannot help in frequency stabilization or prevent faults propagation.

8-3 Suggestions for future research

The main drawbacks of the VSC-HVDC system used in this thesis for wind farms integration and transmission line reinforcement are the high conversion losses and the absence of reliable protection systems at the dc side. In addition to that, the power leveling in the English network during wind farm power output variations is a serious issue since the VSC converters achieve the power leveling only at the Scottish side. Therefore, suggestions for further investigation are as follows:

- Development of reliable dc system protection systems to protect the converters during dc-side faults. The research will focus in new generation of hybrid multi-level converters introduced recently with ability to riding through both ac and dc faults.
- Investigate the possibility of installation of energy storage systems (ESS) in the English network to achieve power leveling during wind power variations. The main question here is what is the optimal location of ESS and their affect in the dynamic performance of the network.
- Investigate the possible scenarios to connect the GB network with the countries in the North Sea to create a transnational super grid. This will help to maximize the utilization of the wind power in the North Sea. The study focuses on finding the optimal option for the creation of the network and stability assessment of overall system under different circumstances. In these scenarios the ESS mentioned above can be used to achieve the power leveling in the North Sea network.
- Optimization of the design in order to reduce the overall conversion losses in VSC converters.

Appendix A

Fourier analysis of an LCC converter ac input current

Any regular time-domain waveform can be represented by an infinite sum of sinusoidal terms. The general expression of the Fourier series is [1]:

$$f(\omega t)=\frac{a_0}{2}+a_1\cos\omega t+a_2\cos 2\omega t+a_3\cos 3\omega t+...+b_1\sin\omega t+b_2\sin 2\omega t+b_3\sin 3\omega t+... \quad \text{(A-1)}$$

where

$$a_n=\frac{1}{\pi}\int_0^{2\pi} f(\omega t)\cos n\omega t\ d\omega t \qquad n=0,1,2,3..... \quad \text{(A-2)}$$

$$b_n=\frac{1}{\pi}\int_0^{2\pi} f(\omega t)\sin n\omega t\ d\omega t \qquad n=1,2,3..... \quad \text{(A-3)}$$

If $f(-\omega t)=f(\omega t)$ then the function is even and $b_n=0$.

If $f(-\omega t)=-f(\omega t)$ then the function is odd and $a_n=0$.

If $f(\omega t+\pi)=-f(\omega t)$ then the Fourier series contains only odd harmonics

A-1 Harmonic analysis of a 6-pulse converter with star/star transformer

The ac input line current waveform of an LCC converter with transformer winding connected as star/star is shown in Fig. A. It can be seen that the waveform has zero average value in a complete periodic cycle, therefore $a_0=0$. Since $f(-\omega t)=-f(\omega t)$ then the function is odd which means $a_n=0$.

The current waveform over the range (0-to-2π) is described as follow [2]:

$$\begin{cases} i=I_{dc}, & \text{(0-to-}\pi/6\text{)} \quad i=0, \ (\pi/6\text{-to-}5\pi/6) \\ i=-I_{dc}, & (7\pi/6\text{-to-}11\pi/6) \quad i=0, \ (11\pi/6\text{-to-}2\pi) \end{cases}$$

The value of b_n is calculated as follow:

$$b_n=\frac{2}{\pi}\int_{\frac{\pi}{6}}^{\frac{5\pi}{6}}\sin n\omega t\ d\omega t=\frac{-2}{n\pi}\left(\cos\frac{5n\pi}{6}-\cos\frac{n\pi}{6}\right) \quad \text{(A-4)}$$

$$b_n=\frac{4}{n\pi}\left(\sin\frac{n\pi}{2}\sin\frac{n\pi}{3}\right)$$

And the Fourier analysis for the ac input line current waveform is

$$f(\omega t)=\frac{2\sqrt{3}I_{dc}}{\pi}\left(\sin\omega t-\frac{1}{5}\sin 5\omega t-\frac{1}{7}\sin 7\omega t+\frac{1}{11}\sin 11\omega t+\frac{1}{13}\sin 13\omega t+.....\right) \quad \text{(A-5)}$$

A-2 Harmonic analysis of a 6-pulse converter with star/delta transformer

The ac input line current waveform of an LCC converter with transformer winding connected as star/star is shown in Fig. A. Similarly, a_0=zero, the function is odd and a_n=zero.

The current waveform is described as follow [2]:

$$\begin{cases} i = I_{dc}/\sqrt{3} \quad (0 < \omega t < \pi/3) \quad i = 2I_{dc}/\sqrt{3} \quad (\pi/3 < \omega t < 2\pi/3) \quad i = I_{dc}/\sqrt{3} \quad (2\pi/3 < \omega t < \pi) \\ i = -I_{dc}/\sqrt{3} (\pi < \omega t < 4\pi/3) \quad i = -2I_{dc}/\sqrt{3}, (4\pi/3 < \omega t < 5\pi/3) \quad i = -I_{dc}/\sqrt{3}, \ (0 < \omega t < \pi/6) \end{cases}$$

The value of b_n is calculated as follow:

$$b_n = \frac{2}{\pi}\left(\int_0^{\frac{\pi}{3}} \sin n\omega t \, d\omega t + \int_{\frac{\pi}{3}}^{\frac{2\pi}{3}} \sin n\omega t \, d\omega t + \int_{\frac{2\pi}{3}}^{\pi} \sin n\omega t \, d\omega t \right) \tag{A-6}$$

$$b_n = \frac{4}{n\pi\sqrt{3}} \sin\frac{n\pi}{6}\left(\sin\frac{n\pi}{6} + 2\sin\frac{n\pi}{2} + \sin\frac{5n\pi}{6} \right)$$

And the Fourier analysis for the ac input line current waveform is

$$f(\omega t) = \frac{2\sqrt{3}I_{dc}}{\pi}\left(\sin\omega t + \frac{1}{5}\sin 5\omega t + \frac{1}{7}\sin 7\omega t + \frac{1}{11}\sin 11\omega t + \frac{1}{13}\sin 13\omega t + ... \right) \tag{A-7}$$

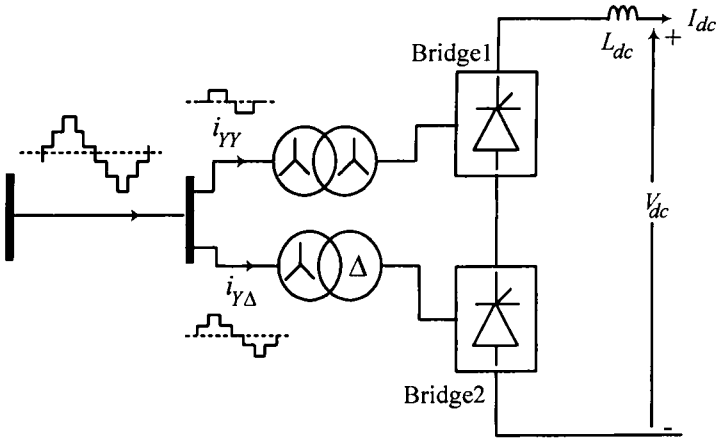


Fig. A: The 12-pulse converter bridge.

A-3 Harmonic analysis of a 12-pulse converter

The 12-pulse converter comprises of two parallel 6-pulse converters. The first one is connected via a star/star transformer while the second one is connected via a star/delta transformer as shown in Fig. A. Due to the phase relationships some of the currents components in one bridge are in anti-phase with those in the other converter [3-4]. This means some harmonic components are eliminated.

The Fourier analysis of the ac input line current of a 12-pulse converter is the sum of the individual currents of the 6-pulse converters. The 5^{th}, 7^{th}, 17^{th}, 19^{th}….are cancelled and the harmonic series contains only harmonics of order 12k ±1. The Fourier analysis for the ac input line current waveform is

$$f(\omega t)=\frac{4\sqrt{3}I_{dc}}{\pi}\left(\sin\omega t+\frac{1}{11}\sin 11\omega t+\frac{1}{13}\sin 13\omega t+\frac{1}{23}\sin 23\omega t+\frac{1}{25}\sin 25\omega t+.....\right) \quad \text{(A-6)}$$

References

[1] G. Holmes and T. A. Lio, *Pulse Width Modulation for Power Converters:principles and practice*: IEEE Press, John Wiley & Sons, Publication, 2003.

[2] D. E. Rice, "A detailed analysis of six-pulse converter harmonic currents," *Industry Applications, IEEE Transactions on,* vol. 30, pp. 294-304, 1994.

[3] D. Paice, *Multipulse Methods for Clean Power*: IEEE PRESS, 1999, 1999.

[4] P. Kundur, *Power System Stability and Control*: Electric Power Research Institute, Power System Engineering Series, 1994.

Appendix B

Pulse Width Modulation (PWM)

Pulse width modulation is one of most common strategies to control the ac output of a VSC converter. PWM varies the duty cycle of the converter switches at a high switching frequency; the output waveform is then averaged to produce the low-frequency output voltage (or current). The main advantage of PWM is the elimination of low-order harmonics in the output waveform. The only conflict comes from the energy losses due to the frequent switching of the converter reducing its efficiency.

B-1 Sinusoidal PWM Modulation

The most straightforward PWM modulation scheme is the sinusoidal pulse width modulation (SPWM) in which a low-frequency sinusoidal reference waveform is compared against a high-frequency carrier waveform [1-2]. Fig. B1 shows one-phase leg of a VSC driven by a triangle-wave carrier, the phase leg can switch either to the upper dc rail when the reference waveform is greater than the carrier waveform and supply a positive output voltage, or to the lower dc rail when the carrier waveform is greater than the reference waveform and supply a negative output voltage.

The phase leg voltage is defined as [2], [3]:

$$v_{az} = V_{dc} M \sin\omega t \tag{B-1}$$

Where M is the modulation index, V_{dc} is the dc voltage, and ω the angular frequency.

The modulation index is defined as:

$$M_a = \frac{V_{\max(a)}}{V_{\max(cr)}} \tag{B-2}$$

Where $V_{max(z)}$ and $V_{max(cr)}$ are the peak values of the reference waveform and carrier waveforms, respectively.

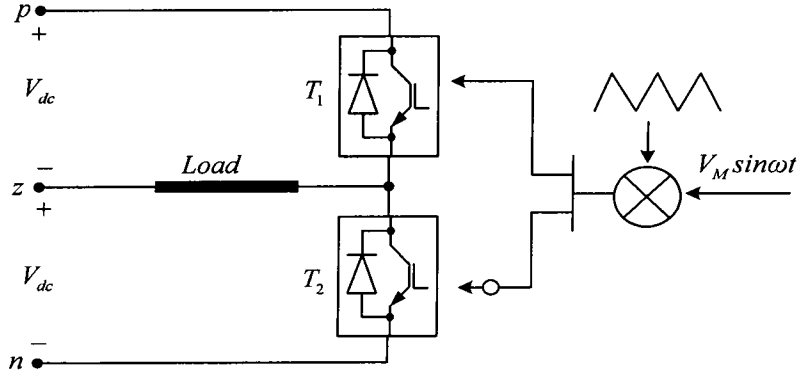


Fig. B1: One-phase leg of a voltage source converter driven by triangle-wave carrier.

In Fig. B1, the converter switches T_1 and T_2 are controlled based on the comparison of the reference waveform $V_{max(z)}$ and the carrier waveform $V_{max(cr)}$. The result is shown in Fig. B2:

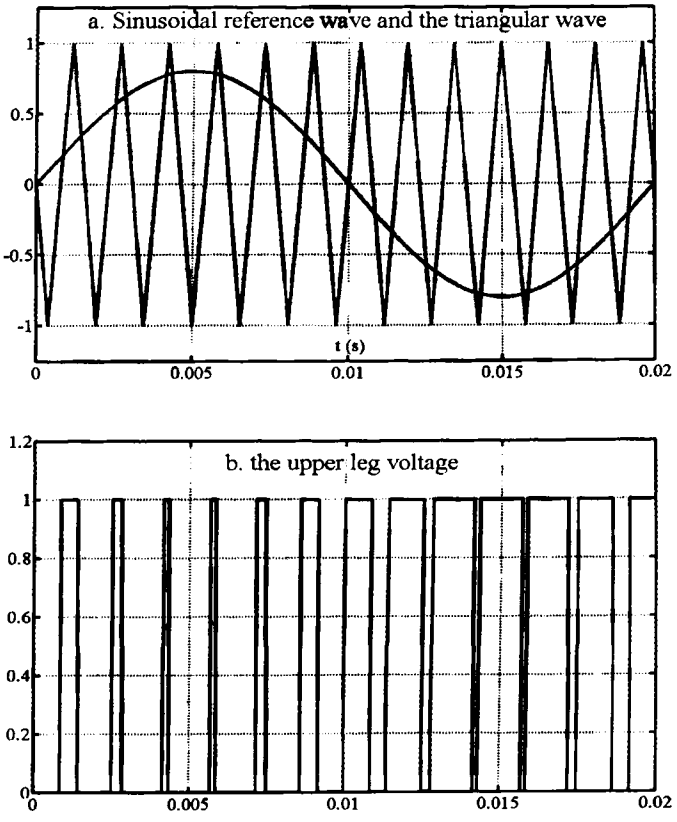
- T_1 is ON when $V_{max(az)} > V_{max(cr)}$ and the output voltage is $V_{dc}/2$
- T_2 is ON when $V_{max(az)} < V_{max(cr)}$ and the output voltage is $-V_{dc}/2$
- The output voltage is varied between $V_{dc}/2$ and $-V_{dc}/2$.

The harmonic spectrum of the output voltage waveform shows that it is composed of:

1- Fundamental frequency component.

2- Harmonic components of order $A*f_{cr} \pm B*f_1$ around the fundamental frequency component, where f_{cr} is the carrier frequency, f_1 is the fundamental frequency, A and B are integers. B is 1 if A is an even number, otherwise it is 2.

The selection of the frequency modulation index ($m_f = f_{cr}/f_1$) is very important since this ratio determines the harmonic spectrum of the output waveform. A higher value of the frequency modulation index produces the lowest harmonic amount but at the same time increases the VSC losses. Fig. B3 illustrates the harmonic spectrum of a two-level converter with: f_1=60Hz, f_{cr}=1080, and m_f= 18.



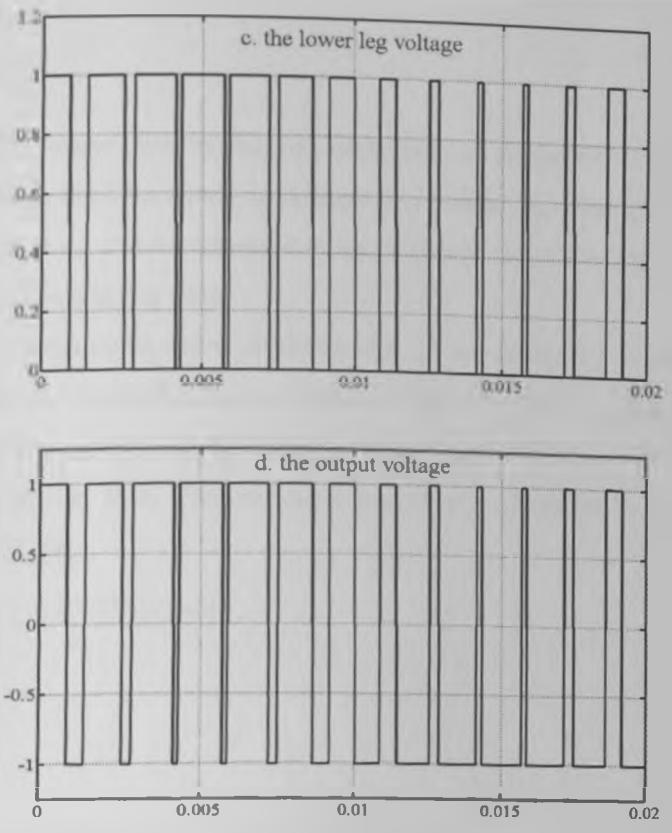


Fig. B2: Sinusoidal pulse-width modulation (SPWM).

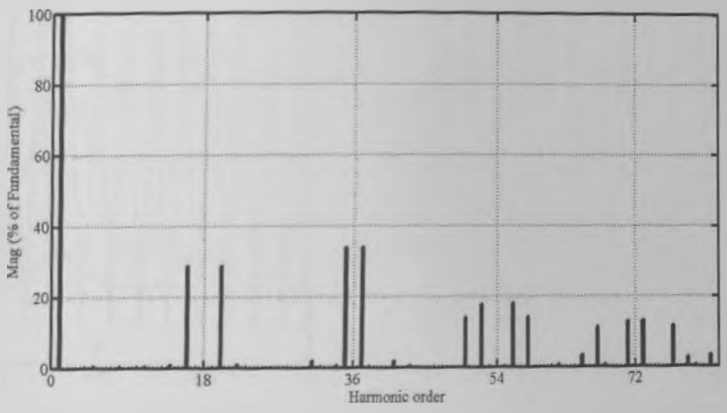


Fig. B3: Harmonic spectrum of the voltage waveform of a two level-converter

B-2 Third-harmonic injection and Switching Frequency Optimal PWM techniques

When the amplitude modulation index M_a is greater than unity then over-modulation occurs. The over-modulation causes a reduction in the number of pulses in the line-to-line voltage waveform, leading to the generation of low-order harmonics such as the 5^{th} and 11^{th}. The fundamental voltage v_{ab} can be increased by adding a third-harmonic component to the three-phase sinusoidal modulating waveform without causing over-modulation and generating unwanted low-order harmonics. This modulation technique is known as third-harmonic

injection PWM [4], where the modulation waveform is composed of the fundamental component v_{ab1} and a third-harmonic component v_{ab3} making v_{ab} flattened at the top. The maximum amount that v_{ab} can be increased by this technique is 15.5%. The principle of this PWM technique is shown in Fig. B4a.

Anther option to overcome the over-modulation is to use Switching Frequency Optimal PWM (SFO-PWM). In this method a zero-sequence voltage is added to each of the reference waveforms. The reference voltage for SFO-PWM is described by equation (B.3) and the principle is shown in Fig. B4b. The maximum amount of v_{ab} that can be increased by this scheme is 15.5% [2], [4].

$$
\begin{aligned}
v_{offset} &= \frac{max(v_a, v_b, v_c) + min(v_a, v_b, v_c)}{2} \\
v_a^* &= v_a - v_{offset} \\
v_b^* &= v_b - v_{offset} \\
v_c^* &= v_c - v_{offset}
\end{aligned}
\qquad \text{(B-3)}
$$

Where v_a, v_b, and v_c are the original reference signals.

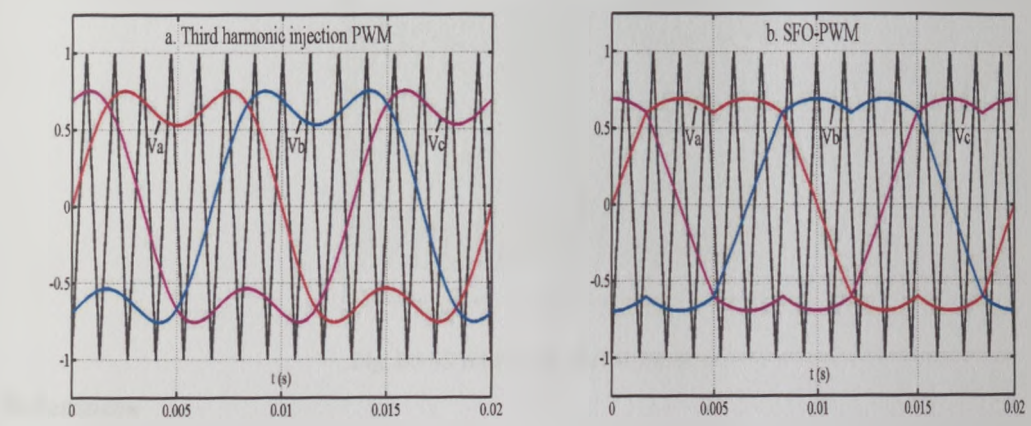


Fig. B4: Third harmonic injection and Switching Frequency Optimal PWM techniques

B-3 Multilevel carrier-based PWM

Several multilevel carrier-based PWM schemes have been developed as a means for controlling the active devices in a multilevel converter. The most popular and easiest technique uses several triangle carrier signals and one reference. The number of carriers is *N-1* where *N* is the number of converter levels, the carriers are arranged to cover continuing bands in the range of $-(N-1)V_{dc}/2$ to $+(N-1)V_{dc}/2$. There are three different SPWM techniques for multilevel converters (with different phase relationships) [2, 5].

• Alternative Phase Opposition Disposition (APOD), all carriers' signals are phase shifted by 180°, Fig. B5a.

• Phase Opposition Disposition (POD) all carriers above the zero reference are out of phase with those below zero reference 180°, Fig. B5b.

• Phase Disposition (PD), all the carriers are in phase with each other, Fig. B5c.

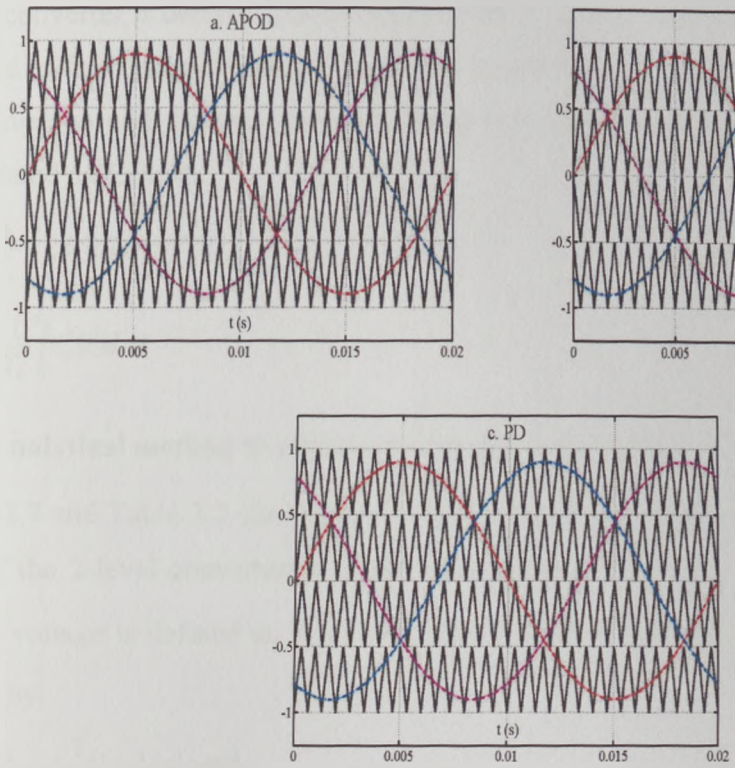


Fig. B5 SPWM of multilevel converters.

References

[1] M. P. Bahrman and B. K. Johnson, "The ABCs of HVDC transmission technologies," *Power and Energy Magazine, IEEE,* vol. 5, pp. 32-44, 2007.

[2] G. Holmes and T. A. Lio, *Pulse Width Modulation for Power Converters:principles and practice*: IEEE Press, John Wiley & Sons, Publication, 2003.

[3] B. Wu, *High-Power Converters and ac Drives*: The Institute of Electrical and Electronics Engineers, Inc., 2006.

[4] M. H. Rashid, *Power Electronics Handbook*: Academic Press, 2001.

[5] J. Arrillaga, *et al.*, *Flexible Power Transmission Systems-The HVDC Options*: John Wiley & Sons, Publication, 2007.

Appendix C

Analytical method to calculate the VSC converter conversion losses

The analytical method is one of the approaches for evaluating the conversion losses in the VSC converter. It is used in the earlier stage of converter design in order to estimate the losses and the heat-sinking devices requirements.

In this Appendix the analytical method is used to calculate the losses in two-level and three-level neutral-point clamped converters. The equation to calculate the conversion losses of the VSC converter is derived based on sinusoidal pulse modulation; the datasheet of IGBT/diode is used to find the converter devices characteristics.

The average and the *rms* current flowing through the device in the conduction period are calculated as follow:

$$i_{av} = \frac{1}{T_s}\int_0^{T_s} i_a(t)d\omega t \tag{C-1}$$

$$i_{rms}^2 = \frac{1}{T_s}\int_0^{T_s} i_a^2(t)d\omega t \tag{C-2}$$

C-1 Analytical method to calculate conversion losses in two-level converters

Figs. 3.7 and Table 3.2 (in chapter 3) show the current path and switching condition of one leg of the 2-level converter, i_a is the load current defined as $i_a(t) = I_m \sin(\omega t - \theta)$, the leg phase voltage is defined as $V_a(t) = V_m \sin \omega t$ while the duty cycle for the device switches is given by:

$$d_{T1} = d_{D2} = \frac{1}{2}[1 + M \sin \omega t] \tag{C-3a}$$

$$d_{T2} = d_{D1} = 1 - d_{T1} = \frac{1}{2}[1 - M \sin \omega t] \tag{C-3b}$$

The average and rms currents for IGBTs T_1 and T_2 are calculated using equations (C-1, C-2) and the duty cycle defined by (C-3) as:

$$I_{T1,av} = \frac{1}{2\pi}\int_{\theta}^{\pi+\theta} \delta_{T1} i_a d\omega = I_m[\frac{1}{2\pi} + \frac{M\cos\theta}{8}] \tag{C.4}$$

$$I_{T2,av} = I_m[\frac{1}{2\pi} - \frac{M\cos\theta}{8}] \tag{C-5}$$

$$I_{T1,rms}^2 = \frac{1}{2\pi}\int_{\theta}^{\pi+\theta} \delta_{sa1} i_a^2 d\omega t = I_m^2[\frac{1}{8} + \frac{M\cos\theta}{3\pi}] \tag{C-6}$$

$$I_{T2,rms}^2 = I_m^2[\frac{1}{8} - \frac{M\cos\theta}{3\pi}] \tag{C-7}$$

The average current for the lower free-wheeling diode is similar to that of the upper IGBT device but in the opposite direction, therefore:

$$I_{D1,av} = -I_{T2,av} \tag{C-8}$$

$$I_{D2,av} = -I_{T1,av} \tag{C-9}$$

$$I^2_{D1,rms} = I^2_{T2,rms} \tag{C-10}$$

$$I^2_{D2,rms} = I^2_{T1,rms} \tag{C-11}$$

After the calculation of the average and the *rms* currents through the devices the conduction losses are calculated as follow:

$$P_C = V_f I_{av} + r_f I^2_{rms} \tag{C-12}$$

where V_f is the device forward voltage and r_f is the device forward resistance.

The free-wheeling diode is switched ON/OFF very fast compared to the IGBT so its switching losses are relatively small compared to that in the IGBT, therefore they are neglected. The switching losses for the IGBT are calculated using equation:

$$P_{sw} = \frac{6k_1 f_S}{2\pi} \int_{\theta}^{\pi+\theta} I_m \sin(\omega t - \theta) d\omega t = \frac{6k_1 f_S I_m}{\pi} \tag{C-13}$$

C-2 Analytical method to calculate conversion losses in three-level converters

Figs. 3.10 and Table 3.3 (in chapter 3) show the current path and switching condition for one leg of the 3-level diode-clamped converter system. The load current is $i_a(t) = I_m \sin(\omega t - \theta)$ and the phase leg voltage is $V_a(t) = V_m \sin \omega t$. The duty cycle of the switching devices is:

$$\delta_{sa1} = \begin{cases} M \sin \omega t & 0 \le \omega t \le \pi \\ 0 & \pi \le \omega t \le 2\pi \end{cases} \qquad \delta_{sa2} = \begin{cases} 1 & 0 \le \omega t \le \pi \\ 1 + M \sin \omega t & \pi \le \omega t \le 2\pi \end{cases} \tag{C-14}$$

$$\delta_{sa3} = 1 - \delta_{sa1} \qquad \delta_{sa4} = 1 - \delta_{sa2}$$

The average and root-mean-square currents in the IGBTs are calculated as follow:

$$I_{sa1,av} = I_{sa4,av} = \frac{1}{2\pi} \int_{\theta}^{\pi} \delta_{sa1} i_a d\omega = \frac{MI_m}{4\pi} [(\pi - \theta)\cos\theta + \sin\theta] \tag{C-15}$$

$$I_{sa2,av} = I_{sa3,av} = \frac{1}{2\pi} [\int_{\theta}^{\pi} i_a d\omega t + \int_{\pi}^{\pi+\theta} \delta_{sa2} i_a d\omega t] = \frac{I_m}{4\pi} [4 + \theta M \cos\theta - M \sin\theta] \tag{C-16}$$

$$I^2_{sa1,av} = I^2_{sa4,av} = \frac{1}{2\pi} \int_{\theta}^{\pi} \delta_{sa1} i_a^2 d\omega = \frac{MI_m^2}{12\pi} [3 + 4\cos\theta + \cos 2\theta] \tag{C-17}$$

$$I^2_{sa2,rms} = I^2_{sa3,rms} = \frac{1}{2\pi} [\int_{\theta}^{\pi} i_a^2 d\omega t + \int_{\pi}^{\pi+\theta} \delta_{sa2} i_a^2 d\omega t] = \frac{I_m^2}{12\pi} [3(\pi - M) + 4M\cos\theta - M\cos 2\theta] \tag{C-18}$$

The average and root-mean-square currents in the free-wheeling diodes are:

$$I_{Da1,av} = \frac{1}{2\pi}\int_0^{\theta} \delta_{sa1} i_a d\omega = \frac{MI_m}{4\pi}[\theta\cos\theta - \sin\theta]$$
$$I_{Da4,av} = I_{Da3,av} = I_{Da2,av} = I_{Da1,av} \tag{C-19}$$

$$I^2_{Da1,rms} = \frac{1}{2\pi}\int_0^{\theta} \delta_{sa1} i_a^2 d\omega = \frac{MI_m^2}{4\pi}[3 - 4\cos\theta + \cos 2\theta]$$
$$I^2_{Da4,rms} = I^2_{Da3,rms} = I^2_{Da2,rms} = I^2_{Da1,rms} \tag{C-20}$$

The average and root-mean-square currents in the clamping diodes are:

$$I_{sa5,av} = I_{sa6,av} = \frac{1}{2\pi}[\int_{\theta}^{\pi} \delta_{sa3} i_a d\omega t + \int_{\pi}^{\pi+\theta} \delta_{sa2} i_a d\omega t] = \frac{I_m}{\pi} - \frac{MI_m}{4\pi}[(\pi - 2\theta)\cos\theta + 2\sin\theta] \tag{C-21}$$

$$I^2_{sa5,rms} = I^2_{sa6,rms} = \frac{1}{2\pi}[\int_{\theta}^{\pi} \delta_{sa3} i_a^2 d\omega t + \int_{\pi}^{\pi+\theta} \delta_{sa2} i_a^2 d\omega t] = \frac{I_m^2}{12\pi}[3\pi - 6M - 2M\cos 2\theta] \tag{C-22}$$

After calculation of the average and the *rms* currents through the devices, equation (C-12) is used to estimate the conduction losses.

For a three-level NPC converter, the switching losses in the IGBTs T_1 and T_2 are:

$$P_{sa1,sw} = P_{sa4,sw} = \frac{f_s}{2\pi}\int_{\theta}^{\pi} k_1 I_m \sin(\omega t - \theta) d\omega t = \frac{k_1 f_s I_m}{2\pi}[1 + \cos\theta]$$
$$P_{sa2,sw} = P_{sa3,sw} = \frac{f_s}{2\pi}\int_{\pi}^{\pi+\theta} k_1 I_m \sin(\omega t - \theta) d\omega t = \frac{k_1 f_s I_m}{2\pi}[1 - \cos\theta] \tag{C-23}$$

Appendix D

Fixed-Speed Wind Turbine Model

Fixed-speed wind turbines use a squirrel-cage induction generator to convert the mechanical power to electrical power. A gearbox is required on the drive shaft to match the difference on operation speed between wind turbines and drive generator.

The fixed-speed term comes from the fact that the rotor speed remains constant despite the change on generation power level. In general, the basic components of a fixed-speed wind turbine as illustrated in Fig. D1 are [1]:

- The aerodynamic rotor (converts the wind power into mechanical power).
- Mechanical system (connects the aerodynamic rotor to the electrical generator using shafts and gearbox).
- Squirrel-cage induction generator (converts the mechanical power to electrical power).
- Blade angle controls (control and optimize the wind turbine operation).
- Reactive power compensation (generate the magnetizing current for the squirrel-cage induction generator).

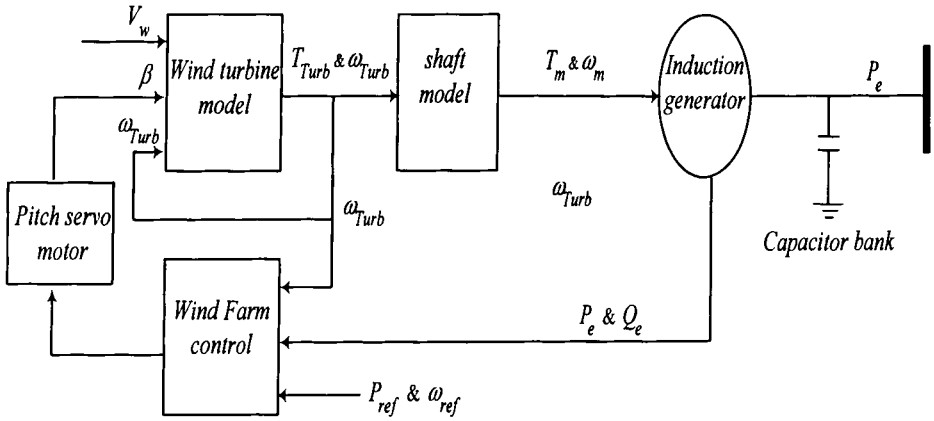


Fig. D1: Fixed-speed wind turbine structure

To simplify the derivation of the mathematical model of a fixed-speed wind turbine, the following assumptions are take into account:

1- Magnetic saturation is neglected.

2- Flux distribution is sinusoidal.

3- Any losses, apart from copper losses, are neglected.

4- Stator voltages and currents are sinusoidal at the fundamental frequency.

5- Stator transients are neglected.

D-1 Wind Turbine Aerodynamic System

The wind turbine rotor transforms the absorbed kinetic energy of the air into mechanical power. The mechanical produced by the wind turbine is expressed as [2]:

$$P_m = \frac{1}{2}\rho_{air} c_p \pi R^2 V_w^3 \tag{D-1}$$

Where ρ_{air} is the air density (1.225Kg/m^3), R is the rotor radius (m) and V_w is the wind speed (m/s) and c_p is the power efficiency coefficient. The wind turbine just extracts a fraction of the power in the wind, and this fraction depends on the power efficiency coefficient. The Betz's limit defines the maximum limit for the power efficiency coefficient (c_p) as 0.59% of the kinetic energy on the moving wind. The power efficiency coefficient is a function of the turbine tip-speed ration (λ) and turbine blade angle in degrees (β). The general expression to describe the power efficiency coefficient is:

$$c_p = c_1\left(\frac{c_2}{\lambda_i} - c_3\beta - c_4\right)e^{\left(\frac{-c_5}{\lambda_i}\right)} + c_6\lambda \tag{D-2}$$

Where the value of λ_i and λ are calculated as:

$$\frac{1}{\lambda_i} = \frac{1}{\lambda + 0.08\beta} - \frac{0.035}{\beta + 1} \tag{D-3}$$

$$\lambda = \frac{\omega_{Turb}}{V_w} \tag{D-4}$$

where ω_{Turb} is the turbine rotational speed, the value of constant c_1-c_6 is varying due to manufacturer data, the constant value used in this research is given in the table below:

Table D.1: Approximation of power curve constant values used in fixed speed wind turbine

c_1	c_2	c_3	c_4	c_5	c_6
0.5176	116	0.4	5	21	0.0068

The optimal operational point of a wind turbine at a given speed for extracting maximum power from the prevailing wind can be found from the wind turbine characteristics shown in Fig. D2. Fixed-speed wind turbines have to be designed with rotational speed to match the most likely wind speed in the area of installation.

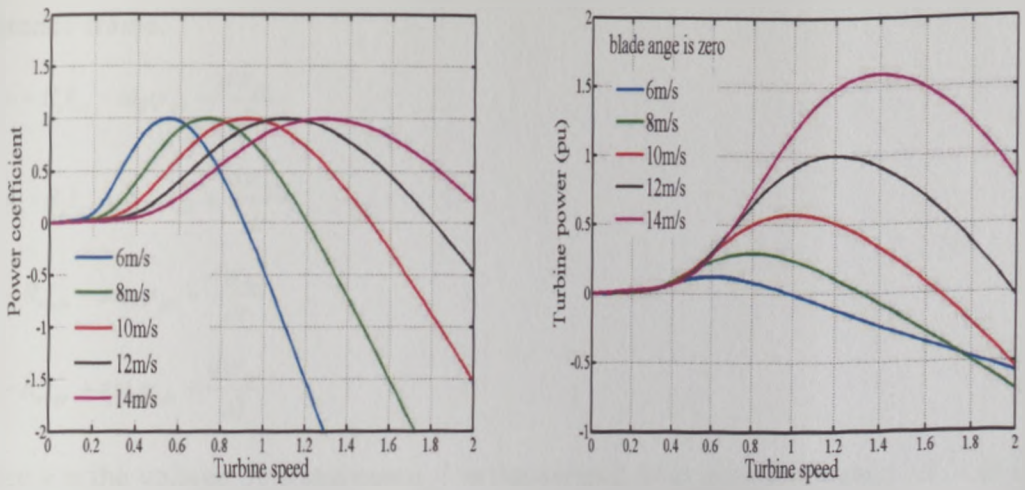


Fig. D2: C_P and P_m as a function of rotational speed for various wind speeds.

D-2 Mechanical System

The drive-train of the wind turbine is represented by a two-mass model as shown in Fig. D3, the first mass stand for blade, hub and low-speed shaft, while the second mass stands for the high-speed shaft [1, 3]. The relationship between the torques supplied by the wind turbine T_{wt}, mechanical torque T_m and the electrical torque from generator T_e is defined as:

$$2H_{wt}\frac{d\omega_r}{dt} = T_{wt} - T_m \tag{D-5}$$

$$2H_e\frac{d\omega_e}{dt} = T_m - T_e \tag{D-6}$$

$$T_m = D_m(\omega_r - \omega_e) + K_m\int(\omega_r - \omega_e)dt \tag{D-7}$$

Where H_{wt}, H_e, ω_r, ω_e, D_m, and K_m are wind turbine inertia, generator inertia, wind turbine rotational speed, generator rotational speed, mechanical system damping constant and mechanical system stiffness respectively.

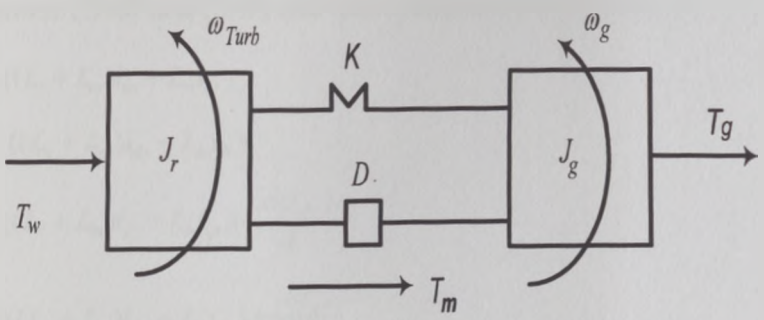


Fig. D3: Drive-train two-mass model.

D-3 Squirrel-cage induction generator model

The mathematical model of the squirrel-cage induction generator is well-documented in the literature [1, 4]. The following equations describe both stator and rotor voltages in the dq reference frame.

$$v_{ds} = -R_s i_{ds} - \omega_S \psi_{qs} + \frac{d\psi_{ds}}{dt} \tag{D-8a}$$

$$v_{qs} = -R_s i_{qs} + \omega_S \psi_{ds} + \frac{d\psi_{qs}}{dt} \tag{D-8b}$$

$$0 = -R_r i_{dr} - s\omega_s \psi_{qr} + \frac{d\psi_{dr}}{dt} \tag{D-8c}$$

$$0 = -R_r i_{qr} + s\omega_s \psi_{dr} + \frac{d\psi_{qr}}{dt} \tag{D-8d}$$

where v is the voltage, R is resistance, i is the current, ω_s is stator frequency, S is the machine slip, and ψ is the flux linkage. The subscripts d and q indicate the direct and quadrature axes frame respectively, and subscripts r and s stand for rotor and stator quantities. The induction machine can operate as generator or motor, when the machine operate as generator the current leaving the machine is positive whilst the current leaving the machine is negative in motor convention. The flux linkage in equation (D-8) can be calculated using the following equations:

$$\psi_{ds} = -(L_s + L_m) i_{ds} - L_m i_{dr} \tag{D-9a}$$

$$\psi_{qs} = -(L_s + L_m) i_{qs} - L_m i_{qr} \tag{D-9b}$$

$$\psi_{dr} = -(L_r + L_m) i_{dr} - L_m i_{dr} \tag{D-9c}$$

$$\psi_{qr} = -(L_r + L_m) i_{qr} - L_m i_{qs} \tag{D-9d}$$

Where L_s , L_r , L_m are stator leakage inductance, rotor leakage inductance, and mutual inductance respectively. The voltage equation can be rewritten as in equation (D-10) by re-arranging equations (D-8) and (D-9) and neglecting stator transients as:

$$v_{ds} = -R_s i_{ds} + \omega_s ((L_s + L_m) i_{qs} + L_m i_{qr}) \tag{D-10a}$$

$$v_{qs} = -R_s i_{qs} - \omega_s ((L_s + L_m) i_{ds} + L_m i_{dr}) \tag{D-10b}$$

$$0 = -R_r i_{dr} + S\omega_s ((L_r + L_m) i_{qr} + L_m i_{qs}) + \frac{d\psi_{dr}}{dt} \tag{D-10c}$$

$$0 = -R_r i_{qr} - S\omega_s ((L_r + L_m) i_{dr} + L_m i_{ds}) + \frac{d\psi_{qr}}{dt} \tag{D-10d}$$

The rotor slip equation is defined as:

$$s = 1 - \frac{p}{2}\frac{\omega_m}{\omega_s} \tag{D-11}$$

Where p is the number of machine poles, ω_m is the mechanical frequency of generator.

The electrical torque T_e is given by:

$$T_e = \psi_{qr} i_{dr} - \psi_{dr} i_{qr} \tag{D-12}$$

The equation of motion of the generator is defined as:

$$\frac{d\omega_m}{dt} = \frac{1}{2H_m}(T_m - T_e) \tag{D-13}$$

And the active and reactive power (P_s, Q_s) are given as:

$$P_s = v_{ds} i_{ds} + v_{qs} i_{qs} \tag{D-14}$$

$$Q_s = v_{qs} i_{ds} - v_{ds} i_{qs} \tag{D-15}$$

The power exchange in a fixed-speed wind turbine is only through the stator terminal because just the stator terminal is connected to the grid, while the rotor is short circuited.

References

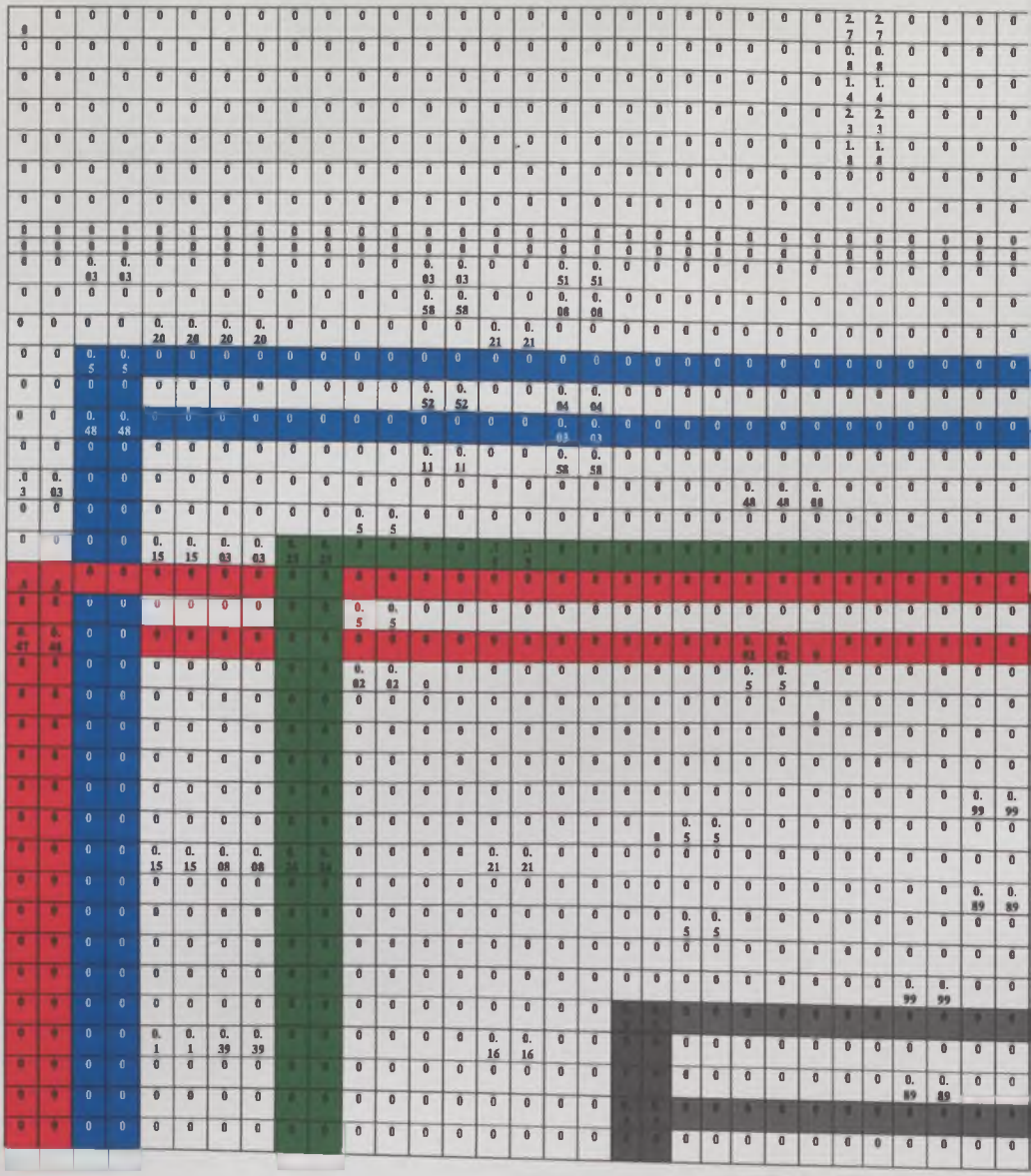
[1] T. Ackermann, *Wind Power in Power System*: John Wiley & Sons. Ltd, 2005.

[2] L. M. Fernández, *et al.*, "Dynamic models of wind farms with fixed speed wind turbines" *Renewable Energy, Volume 31, Issue 8, July 2006, Pages 1203-1230.*

[3] P. Ledesma, *et al.*, "Transient stability of a fixed speed wind farm," *Renewable Energy, Volume 28, Issue 9, July 2003, Pages 1341-1355.*

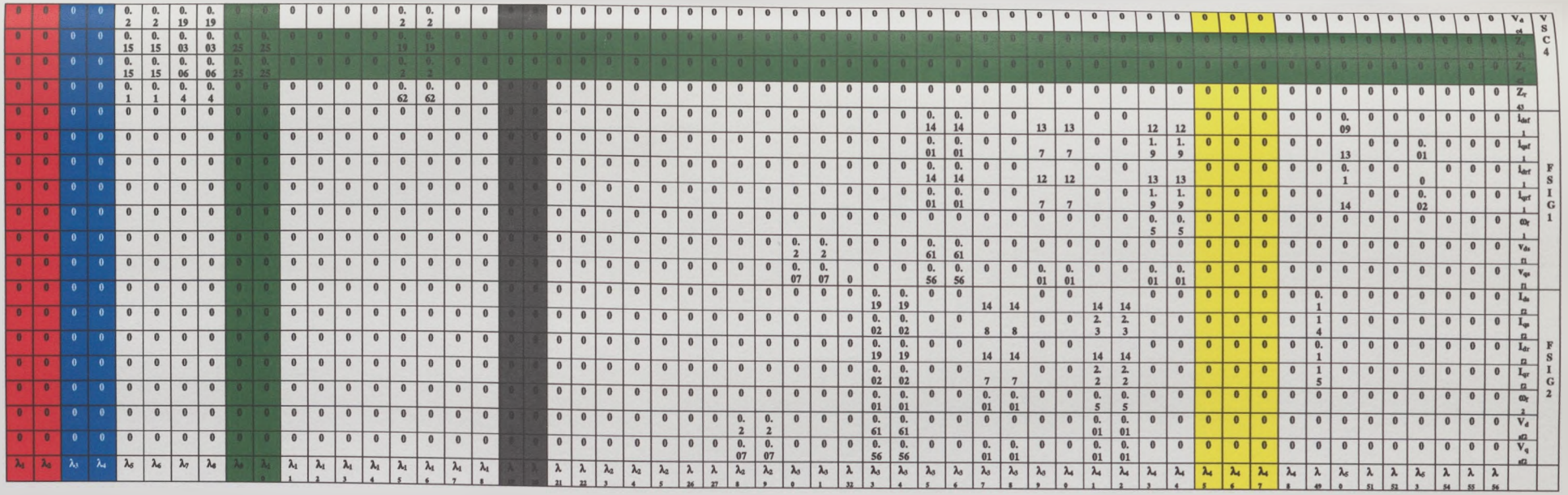
[4] P. Kundur, *Power System Stability and Control*: Electric Power Research Institute, Power System Engineering Series, 1994.

Participation factor



matrix

0.3	0	0	0	0	0	0	0	0	0	0	0	0	0.6	0.6	2.1	0.7	0	0	0	0	0	0	0	0	i_d	SG
2.2	0	0	0	0	0	0	0	0	0	0	0	0	1.2	1.2	4.4	0.3	0	0	0	0	0	0	0	0	i_F	
3.6	0	0	0	0	0	0	0	0	0	0	0	0	1.2	1.2	0.05	0.13	0	0	0	0	0	0	0	0	i_D	
0	0	0	0	0	0	0	0	0	0	0	0	0	0.83	0.83	0	1.97	0	0	0	0	0	0	0	0	i_q	
0	0	0	0	0	0	0	0	0	0	0	0	0	0.84	0.84	0.00	2.97	0	0	0	0	0	0	0	0	i_Q	
0	0	0	0	0	0	0	0	0	0	0	0	0	0.51	0.51	0.00	0.00	0	0	0	0	0	0	0	0	ω	
0	0	0	0	0	0	0	0	0	0	0	0	0	0.93	0.93	1.37	0.52	0	0	0	0	0	0	0	0	δ	
0	0	0	0	0	0	0	0	0	0	0	0	0	0	0	0	0	0	0	1	0	0	0	0	0	v_F	
0	0	0	0	0	0	0	0	0	0	0	0	0	0	0	0	0	0	0	0	0	0	0	0	0	v_A	
0	0	0	0	0	0	0	0	0	0	0	0	0	0	0	0	0	0	0	0	0	0	0	0	0	i_{sd1}	VSC1
0	0	0	0	0	0	0	0	0	0	0	0	0	0	0	0	0	0	0	0	0	0	0	0	0	i_{sq1}	
0	0	0	0	0	0	0	0	0	0	0	0	0	0	0	0	0	0	0	0	0	0	0	0	0	V_{dc1}	
0	0	0	0	0	0	0	0	0	0	0	0	0	0	0	0	0	0	0	0	0	0	0	0	0	Z_{11}	
0	0	0	0	0	0	0	0	0	0	0	0	0	0	0	0	0	0	0	0	0	0	0	0	0	Z_{12}	
0	0	0	0	0	0	0	0	0	0	0	0	0	0	0	0	0	0	0	0	0	0	0	0	0	Z_{13}	
0	0	0	0	0	0	0	0	0	0	0	0	0	0	0	0	0	0	0	0	0	0	0	0	0	Z_{14}	
0	0	0	0	0	0	0	0	0	0	0	0	0	0	0	0	0	0	0	0	0	0	0	0	0	I_{sd2}	VSC2
0	0	0	0	0	0	0	0	0	0	0	0	0	0	0	0	0	0	0	0	0	0	0	0	0	I_{sq2}	
0	0	0	0	0	0	0	0	0	0	0	0	0	0	0	0	0	0	0	0	0	0	0	0	0	V_{dc2}	
0	0	0	0	0	0	0	0	0	0	0	0	0	0	0	0	0	0	0	0	0	0	0	0	0	Z_{21}	
0	0	0	0	0	0	0	0	0	0	0	0	0	0	0	0	0	0	0	0	0	0	0	0	0	Z_{22}	
0	0	0	0	0	0	0	0	0	0	0	0	0	0	0	0	0	0	0	0	0	0	0	0	0	Z_{23}	
0	0	0	0	0	0	0	0	0	0	0	0	0	0	0	0	0	0	0	0	0	0	0	0	0	Z_{24}	
0	0	0	0	0	0	0	0	0	0	0	0	0	0	0	0	0	0	0	0	0	0	0	0	1	I_{dc31}	DC SIDe
0	0	0	0	0	0	0	0	0	0	0	0	0	0	0	0	0	0	0	0	0	0	0	1	0	I_{dc42}	
0	0	0	0	0	0	0	0	0	0	0	0	0	0	0	0	0	0	0	0	0	1	0	0	0	I_{dc34}	
0	0	0	0	0	0	0	0	0	0	0	0	0	0	0	0	0	0	0	0	0	0	0	0	0	I_{dc21}	
0	0	0	0	0	0	0	0	0	0	0	0	0	0	0	0	0	0	0	0	0	0	0	0	0	Y_1	
0	0	0	0	0	0	0	0	0	0	0	0	0	0	0	0	0	0	0	0	0	0	0	0	0	Y_2	
0	0	0.00	0.08	0.08	0	0	0	0	0	0	0	0	0	0	0	0	0	0	0	0	0	0	0	0	P_m	
0	0	0	0	0	0	0	0	0	0	0	0	0	0	0	0	0	0	0	0	0	0	0	0	0	I_{sd3}	VSC3
0	0	0	0.01	0.01	0	0	0	0	0	0	0	0	0	0	0	0	0	0	0	0	0	1	0	0	I_{sq3}	
0	0.1	0.1	0	0	0	0	0	0	0	0	0	0	0	0	0	0	0	0	0	0	0	0	0	0	V_{dc3}	
0	0	0	0	0	0	0	0	0	0	0	0	0	0	0	0	0	0	0	0	0	0	0	0	0	Z_{31}	
0	0	0	0	0	0	0	0	0	0	0	0	0	0	0	0	0	0	0	0	0	0	0	0	0	Z_{32}	
0	0.08	0.08	0	0	0	0	0	0	0	0	0	0	0	0	0	0	0	0	0	0	0	0	0	0	Z_{33}	
0	0	0	0	0	0	0	0	0	0	0	0	0	0	0	0	0	0	0	0	0	0	0	0	0	I_{sd4}	
0	0.01	0.01	0	0	0	0	0	0	0	0	0	0	0	0	0	0	0	0	0	1	0	0	0	0	I_{sq4}	



Appendix F

List of Figures and Tables

F-1 List of Figures

Figure Number	Figure caption	Page number
2-1	HVAC and HVDC transmission cost versus distance	11
2-2	Schematic diagrams of different HVDC circuit arrangements	16
2-3	Line-commutated converter stations	17
2-4	capacitor-commutated converter stations	18
2-5	Converter arrangements: (a) six-pulse connection, (b) twelve-pulse connection	18
2-6	Rectifier operation without commutation angle	21
2-7	Rectifier operation with commutation angle	22
2-8	Inverter operation without commutation angle	23
2-9	ac Harmonic analysis of a 6-pulse converter	26
2-10	ac Harmonic analysis of a 12-pulse converter	27
2-11	Harmonic spectrum of the dc voltage for 6-pulse and 12-pulse converters	28
2-12	V_{dc}-I_{dc} characteristics for a two terminal LCC-HVDC system	29
2-13	Rectifier control system layout	31
2-14	Inverter control system layout	32
2-15	12-pulse LCC-HVDC connecting two ac networks	33
2-16	LCC-HVDC behavior during current step (power step up).	34
2-17	LCC-HVDC behavior during a dc fault	36
2-18	LCC-HVDC behavior during three phase fault at B2	38
3-1	(a) VSC connected to an ac system; (b) equivalent ac and dc circuits	45
3-2	PQ diagram of VSC converter	46
3-3	Schematic of a typical VSC-HVDC system	46
3-4	VSC converter: (a) two-level converter; (b) three-level converter	47
3-5	Equivalent circuit of a VSC-HVDC transmission system	49
3-6	Vector diagram representation of a VSC-HVDC System: (a) sending end (b) receiving end	50

3-7	Two-level voltage source converter and the possible conduction current paths in one leg	51
3-8	SPWM of a three-phase two-level converter	53
3-9	Three-level Neutral-Point Clamped (NPC) voltage source converter	54
3-10	Power paths in one leg of a three-level NPC converter	55
3-11	SPWM of the three-level NPC converter	56
3-12	IGBT datasheet	58
3-13	VSC-HVDC Transmission System	60
3-14	Overall Control of a VSC-HVDC	62
3-15	Block diagram of the current control loop	63
3-16	Block diagram of the active and reactive power controller	65
3-17	Block diagram of the dc and ac voltage controllers	66
3-18	VSC-HVDC layout	67
3-19	Overall schematic control block diagram of a 3-level VSC-HVDC system.	68
3-20	Key simulation results during active power variations	69
3-21	AC voltage waveform at B_1 and B2 with/without ac filter in VSC converter stations	70
3-22	Key simulation results during a three-phase fault at B_2	71
3-23	Key simulation results for a dc fault at the midpoint of the dc cable	72
4-1	Examples of possible multi-terminal configurations for wind farm integration	79
4-2	Four-terminal transnational dc network system	80
4-3	Multi-terminal HVDC system for an urban area distribution network	81
4-4	Multi-terminal HVDC system for offshore wind farms, oil/gas platform and onshore network	81
4-5	Voltage-current characteristic of the dc droop controller	83
4-6	Four-terminal dc transmission system based on voltage source connecting two different grids	83
4-7	Voltage-current droop controller	84
4-8	Control system of VSC_2 for power sharing	84
4-9	Key simulation results during power management between VSC_1 and VSC_2	86

4-10	Key simulation results during loss of VSC_1	87
4-11	Key simulation results during loss of dc link $cable_1$	88
4-12	Four-terminal HVDC network used as a test system for grid integration of offshore wind farms, and implementation of a transnational dc grid for power trading with real-time dispatch capability	92
4-13	dc fault in the VSC-HVDC system	93
4-14	IGBT-circuit breakers	94
4-15	Multi-terminal dc system behavior during loss of one converter	95
4-16	Key results of the multi-terminal dc system power system	97
4-17	Key results for the multi-terminal dc system behavior during loss of converter stations	99
5-1	String cluster layout configuration	103
5-2	Reactive power requirement for wind farm integration in UK	106
5-3	AC Fault Ride-Through capability requirement for wind farm integration in the UK	107
5-4	Frequency requirement for wind farm integration in UK	108
5-5	Basic configuration for HVAC system used for wind farm connection	108
5-6	Basic configuration for LCC-HVDC system used for wind farm connection	110
5-7	Basic configuration for VSC-HVDC system used for wind farm connection	111
5-8	Schematic control diagram of a VSC-HVDC connecting an FSIG wind farm	114
5-9	VSC-HVDC connecting offshore wind farms to an ac network	115
5-10	Simulation results of FSIG and VSC-HVDC operated without power command during wind speed variation	118
5-11	Key simulation results of FSIG and VSC-HVDC system operated without power command during three-phase fault at ac side (at B_2)	119
5-12	Control scheme of pitch-regulated wind turbine	121
5-13	c_p-λ characteristics for wind turbine β=0	121
5-14	Wind farm-side converter control system	123
5-15	Key simulation results of FSIG and VSC-HVDC system operated with power command during wind speed variation	124

5-16	FSIG and VSC-HVDC system operated with power command response during load demand change at the ac system network	126
5-17	Key simulation results of FSIG and VSC-HVDC system operating with power command during three-phase fault at the ac side (at B_2)	127
5-18	Four multi-terminal VSC-HVDC system connecting FSIG wind farms	129
5-19	Grid-side converters active power sharing (between VSC_1 and VSC_2)	129
5-20	Multi-terminal VSC-HVDC system behavior during sudden loss of VSC_1 and dc $link_1$	130
5-21	VSC-HVDC system for DFIG wind farm integration	131
5-22	VSC-HVDC system for SG-based wind farm integration	132
5-23	VSC-HVDC system for PMSG wind farm integration	133
6-1	Multi-terminal VSC-HVDC for offshore wind farm integration	141
6-2	Control system of the grid-side converters	143
6-3	Excitation system block diagram	146
6-4	Steam turbine-governor system block diagram	146
6-5	Single-line diagram of the dc link circuit	147
6-6	Control system of the wind farm-side converters	149
6-7	Methodology to obtain the complete state space model of the test system	
6-8	Effect of the grid-side VSC current controllers on system stability	158
6-9	Effect of the grid-side VSC ac voltage control parameters on system stability	160
6-10	Effect of the grid-side VSC dc voltage controller on system stability	162
7-1	Reinforcement projects in Scotland network to transmit the large-scale wind power to England	167
7-2	Generic model of Scotland network, the interconnectors and England networks.	170
7-3	Single-line diagram of VSC converter and phasor diagrams for leading and lagging modes of operation	173
7-4	Using VSC-HVDC system to interconnect Scotland and England networks	174
7-5	Typical frequency response under the event of loss of generation	176
7-6	Simulation results explaining the role of VSC-HVDC systems to participate in frequency regulation in the Scotland network after	180

	connection of (500+j100) MVA into the Scotland network	
7-7	Simulation results explaining the role of VSC-HVDC systems to participate in frequency regulation in the Scotland network after disconnection of (500+j100) MVA from the Scotland network	181
7-8	Simulation results illustrating the decoupling operation of Scotland-England networks after the disconnection of (500+100) MVA from the England network	184
7-9	Simulation results explains the decoupling operation of Scotland-England networks during three-phase fault at B_4 at England network	185
7-10	Use of VSC-HVDC in parallel with HVAC system to interconnect Scotland and England networks	186
7-11	Simplified model of the hybrid parallel interconnector between ECCL4 and STWE4	187
7-12	Simulation results explains the hybrid parallel operation of Scotland-England networks during sudden change in HVAC line transmission capacity	191
7-13	Simulation results explains the hybrid parallel operation of Scotland-England networks during three-phase fault at England side	192

F-2 List of Tables

Table Number	Table caption	Table number
2-1	Examples of existing (and under construction) HVDC transmission systems using current source converter technology	14
2-2	LCC-HVDC parameters	32
3-1	Voltage source converter (VSC) and current source converter (CSC) comparison	44
3-2	Switching states of a 2-level voltage source converter	51
3-3	Switching states of a 3-level diode-clamped voltage source converter	55
3-4	VSC-HVDC parameters.	66
4-1	System parameters	84
5-1	Examples of current offshore wind farms connected via HVAC in Europe	109

5-2	Examples of the VSC-HVDC transmission systems for wind farm integration	111
5-3	system parameters	115
5-4	Comparison of the FSIG wind farm integration via VSC-HVDC system	128
5-5	Compassion of the different wind turbine technologies	134
6-1	Initial operating conditions of the interconnected system	154
6-2	Eigenvalues for the test system	155
6-3	(a) Effect of changing k_{ii} of the grid-side VSC dc voltage controller (b)	157
	Effect of changing k_{pi} of the grid-side VSC dc voltage controller	158
6-4	(a) Effect of changing k_{iac} of the grid-side VSC dc voltage controller (b)	159
	Effect of changing k_{pac} of the grid-side VSC dc voltage controller	159
6-5	(a) Effect of changing k_{idc} of the grid-side VSC dc voltage controller (b)	161
	Effect of changing k_{pdc} of the grid-side VSC dc voltage controller	161
6-6	Eigenvalues for different loading scenarios	163
7-1	Amount of the transmitted power from Scotland to England in MW [3](2011-to-2018)	170
7-2	Summary of flexible ac transmission system (FACTS) devices	172